Aus dem Walther-Straub-Institut für Pharmakologie und Toxikologie
Institut der Ludwig-Maximilians-Universität München
Vorstand: Prof. Dr. med. Thomas Gudermann

Identification and Characterization of Two Distinct Activator Binding Sites in the TRPC5 Channel

Dissertation
zum Erwerb des Doktorgrades der Naturwissenschaften
an der Medizinischen Fakultät der
Ludwig-Maximilians-Universität zu München

vorgelegt von

Aaron Treder

aus

Berlin

2022

Mit Genehmigung der Medizinischen Fakultät
der Universität München

Betreuerin:	PD Dr. rer. nat. Ursula Storch
Zweitgutachter:	Prof. Dr. rer. nat. Andreas G. Ladurner
Dekan:	Prof. Dr. med. Thomas Gudermann
Tag der mündlichen Prüfung:	20.03.2023

Contents

Zusammenfassung

Der transient receptor potential canonical (TRPC) 5-Kanal ist ein nicht-selektiver Kationenkanal, welcher für Na^+, K^+ sowie Ca^{2+} Ionen durchlässig ist. Des Weiteren ist er in viele pathophysiologisch relevante Vorgänge involviert und spielt eine Rolle bei psychischen und nephrologischen Erkrankungen, sowie bei der Vermittlung von Resistenzen gegen Zytostatika. Aus diesem Grund ist eine ausführliche Kenntnis über potentielle Liganden-Bindestellen und über die generelle Funktionsweise dieses Kanals von großem Interesse, um in Zukunft neue Therapiemöglichkeiten zu entwickeln.

Das Ziel der vorliegenden Arbeit ist deshalb die Identifizierung und Charakterisierung der Bindestellen der beiden TRPC5-Kanalaktivatoren Riluzol und (-)-Englerin A.

Potentielle, an der möglichen Bindung der Aktivatoren beteiligte Aminosäuren wurden mittels molekularem Docking identifiziert und anschließend mit Hilfe ortspezifischer Mutagenesen ausgetauscht. Die mutierten TRPC5-Kanäle wurden in HEK293T-Zellen überexprimiert und mittels konventioneller Ganzzellableitungen und aufeinanderfolger Applikation beider Aktivatoren elektrophysiologisch charakterisiert. Die Oberflächenexpression der mutierten Kanäle wurde durch eine Biotinylierung der Oberflächenproteine und anschließende immunchemische Detektion durch Westernblot ermittelt. Bestimmte Aminosäureaustausche führten zu verringerten Stromantworten durch jeweils einen der beiden Aktivatoren im Vergleich zum unveränderten Wildtyp-TRPC5-Kanal.

Entscheidende Aminosäuren, deren Austausche zu verringerten Riluzol-induzierten Stromantworten führten, sind: Tryptophan 435, Arginin 492, Aspartat 439, Leucin 496, Glutamat 418, Histidin 370 und Isoleucin 368. Der Austausch von Phenylalanin 576, Tyrosin 524, Leucin 521 und Glutamin 573 führte zu verringerten (-)-Englerin A-induzierten Stromantworten. Diese Ergebnisse deuten auf zwei unterschiedliche Bindestellen für die Aktivatoren Riluzol und (-)-Englerin A hin. Wichtige, diese Aminosäuren betreffenden Austausche waren an der Zelloberfläche exprimiert. Mutanten, welche die Riluzol Bindung verhindern, aber unverändert an der Oberfläche exprimiert sind verglichen mit dem Wildtyp-TRPC5-Kanal, lauten Arginin 492 mutiert zu Lysin, Glutamat 418 mutiert zu Alanin, Histidin 370 mutiert zu Tryptophan und Isoleucin 368 mutiert zu Threonin. Dagegen sind die Mutanten Tryptophan 435 mutiert zu Alanin, Arginin 492 mutiert zu Alanin, Aspartat 439 mutiert zu Alanin und Leucin 496 mutiert zu Alanin signifikant niedriger auf der Zelloberfläche exprimiert. Mutanten, welche die (-)-Englerin A Bindung verhindern, aber unverändert an der Oberfläche exprimiert sind verglichen mit dem Wildtyp-TRPC5-Kanal, lauten Tyrosin 524 mutiert zu Alanin und Glutamin 573 mutiert zu Alanin. Dagegen ist die Mutante Phenylalanin 576 mutiert zu Alanin signifikant niedriger und die Mutante Leucin 521 mutiert zu Alanin signifikant höher als der Wildtyp-TRPC5-Kanal an der Zelloberfläche exprimiert.

Die identifizierte Riluzol-Bindestelle ist monomerisch und wird durch die TRP-

Box sowie den unteren Teil der Transmembrandomänen (TM)1, TM2, TM3 und TM4, welcher auch voltage-sensor-like domain (VSLD) genannt wird, gebildet. Im Gegensatz dazu wird die (-)-Englerin A Bindestelle durch zwei Monomere gebildet und befindet sich zwischen der Porenhelix und der TM5 des einen sowie der TM6 des benachbarten Monomers. Beide Bindestellen sind bereits in der Literatur beschrieben. Die Riluzol-Bindestelle ist zusätzlich auch die Bindestelle einiger Inhibitoren wie des TRPC5-Inhibitors Clemizol und der TRPC4-Inhibitoren GFB-9289, GFB-8438 sowie GFB-8749. Bisher wurde jedoch noch keine Bindung eines TRPC4 oder 5-Aktivators an dieser Position beschrieben. Die identifizierte (-)-Englerin A Bindestelle ist bereits als Diacylglycerol (DAG) sowie als Bindestelle für die TRPC5-Kanalinhibitoren Pico-145 und HC-070 bekannt.

Zusammenfassend lässt sich sagen, dass die vorliegende Arbeit zwei unterschiedliche TRPC5-Aktivatorbindestellen beschreibt, die regulatorische Knotenpunkte des Kanals darstellen und vorher nur als Bindestellen für TRPC5-Kanalinhibitoren bekannt waren. Diese Erkenntnisse ermöglichen ein besseres Verständnis des Aktivierungsmechanismus von TRPC5-Kanälen im Speziellen und von rezeptorgesteuerten TRPC-Kanälen im Allgemeinen. Zudem führt die Identifikation und Charakterisierung dieser Ligandenbindestellen zu neuen Möglichkeiten für virtuelle Medikamentenscreenings.

Abstract

The transient receptor potential (TRPC)5 channel is a non-selective cation channel conducting Na^+, K^+ and Ca^{2+}. TRPC5 is involved in several pathophysiological conditions like mental disorders and nephrological diseases and mediates cytostatic drug resistance. Therefore, an extensive knowledge of potential ligand binding sites and of the general functionality of the channel is essential to develop new treatment options in the future.

The aim of this study is to identify and characterize the potential binding sites of the two TRPC5 channel activators riluzole and (-)-englerin A.

To achieve this, amino acids that might participate in activator binding were identified via molecular docking and thereafter exchanged via site directed mutagenesis. The mutant TRPC5 channels were overexpressed in HEK293T cells and characterized by whole-cell patch clamp experiments with consecutive application of both activators. The surface expression of the mutant channels was confirmed by surface biotinylation and subsequent detection using the immunoblot technique. Distinct amino acid exchanges resulted in a significant current density reduction of either of the two activators compared to the wildtype TRPC5 channel.

Crucial amino acids where exchanges resulted in a significant reduction of the riluzole evoked current densities are: tryptophane 435, arginine 492, aspartate 439, leucine 496, glutamate 418, histidine 370 and isoleucine 368. However, key amino acids where exchanges resulted in a significant reduction of the (-)-englerin A-induced current densities are: phenylalanine 576, tyrosine 524, leucine 521 and glutamine 573. These findings suggest that riluzole and (-)-englerin A bind in two distinct binding sites. Important amino acid exchanges were still expressed at the cell surface. Mutants negating a riluzole binding but showing a similar surface expression as the wildtype were: arginine 492 mutated to lysine, glutamate 418 mutated to alanine, histidine 370 mutated to tryptophane and isoleucine 368 mutated to threonine. However, the mutants tryptophane 435 mutated to alanine, leucine 496 mutated to alanine and arginine 492 mutated to alanine are significantly lower expressed at the cell surface compared with the wildtype TRPC5 channel. Mutants which show an impaired (-)-englerin A binding but are still similarly expressed at the cell surface as the wildtype TRPC5 channel are: tyrosine 524 mutated to alanine and glutamine 573 mutated to alanine. However, the mutant phenylalanine 576 mutated to alanine is significantly lower and the mutant leucine 521 mutated to alanine is significantly higher expressed at the cell surface compared with the wildtype TRPC5 channel.

The identified riluzole binding site is monomeric and is located between the TRP-box and the transmembrane domain (TM)1, TM2, TM3 and TM4 which is commonly known as the voltage-sensor-like domain (VSLD). The (-)-englerin A binding site is located between two monomers and is built by the pore helix and TM5 of one and TM6 of the adjacent monomer. The riluzole binding site is additionally described as the binding site of several inhibitors like the TRPC5

inhibitor clemizole and the TRPC4 inhibitors GFB-9289, GFB-8438 and GFB-8749. However, no TRPC4 or TRPC5 activator has been described to bind in this site so far. The identified (-)-englerin A binding site is already known to bind diacylglycerol (DAG) and the TRPC5 channel inhibitors Pico-145 and HC-070.

To summarize, this study describes two distinct activator binding sites and therefore regulatory hot-spots of the TRPC5 channel which were previously described to bind inhibitors. These findings may provide a better understanding of the activation mechanism of TRPC5 channels in particular and of receptor-operated TRPC channels in general. In addition, the identification and characterization of these ligand binding sites will lead to new opportunities for virtual drug screenings.

List of Tables

List of Figures

List of Abbreviations

AMPKα AMP-activated protein kinase alpha

ARC Arachidonic acid-regulated calcium-selective

ATP Adenosine triphosphate

ALS Amyotrophic lateral sclerosis

BSA Bovine serum albumin

BAPTA 1,2-bis(o-aminophenoxy)ethane-N,N,N',N'-tetraacetic acid

BME 2-mercaptoethanol

BTD N-[3-(adamantan-2-yloxy)propyl]-3-(6-methyl-1,1-dioxo-2H-1λ^6,2,4-benzothiadiazin-3-yl)propanamide

BTDM (2-(benzo[d][1,3]dioxol-5-ylamino)thiazol-4-yl)((3S,5R)-3,5-dimethylpiperidin-1-yl)methanone

CaM Calmodulin

CaMKKβ Calcium/calmodulin-dependent protein kinase kinase β

Ca^{2+}/NFAT Ca^{2+}/nuclear factor of activated T-cells

CCK_2 Cholecystokinin B receptor

CDV Current density voltage

CFTR Cystic fibrosis transmembrane conductance regulator

CHS Cholesteryl hemisuccinate

CIRB Calmodulin-inositol receptor binding

CRAC Ca^{2+} release-activated Ca^{2+}

Cryo-EM Cryogenic electron microscopy

DAG Diacylglycerol

DMSO Dimethyl sulfoxide

DTT Dithiothreitol

CMV Cytomegalovirus

DPBS Dulbecco's phosphate buffered saline

EC_{50} Half maximal effective concentration

ECL Enhanced chemoluminescence

EGFP Enhanced green flourescent protein

EMEM Eagle's minimum essential medium

ENaC Epithelial Na^+ channel

ER Endoplasmatic reticulum

ERM Ezrin, radixin, moesin

FCS Fetal calf serum

FSGS Focal segmental glomerulosclerosis

GABA Gamma-aminobutyric acid

mGluR Metabotropic glutamate receptor

GPCR G-protein coupled receptor

HEK293T Human embryonic kidney 293T

HEPES 4-(2-hydroxyethyl)-1-piperazineethanesulfonic acid

HRP Horseraddish peroxidase

I_{CRAC} Ca^{2+} release-activated Ca^{2+} current

IQR Interquartile range

4-IPBA 4-iodophenylboronic acid

IP_3 Inositol trisphosphate

IP3R Inositol 1,4,5-trisphosphate receptor

IRES Internal ribosomal entry site

I_{SOC} Store operated Ca^{2+} current

IV Current-voltage

KLD Kinase, ligase, DpnI

KO Knock-out

LB Lysogeny broth

MDR1 Multidrug resistance protein 1

MeOH Methanol

NaK-ATPase Sodium potassium ATPase

NEB New england biolabs

NFATC3 Nuclear factor of activated T-cells, cytoplasmic 3

NHERF Na^+/H^+ exchanger regulatory factor

NMDA N-methyl-D-aspartate

NOS Nitric oxide synthase

NSC Normalized slope conductance

OAG 1-oleoyl-2-acetyl-sn-glycerol

Orai Calcium release-activated calcium channel protein

PBS Phosphate buffered saline

PCR Polymerase chain reaction

PDB Protein data bank

PDZB PDZ-binding

PDZ PSD-95/Discs-large/ZO-1

p-gp Permeability glycoprotein

PIP_2 Phosphatidylinositol 4,5-bisphosphate

PIP4K Phosphatidylinositol-5-phosphate 4-kinase

PKC Proteinkinase C

PLC Phospholipase C

Pen/Strep Penicillin/streptomycin

PVDF Polyvinyliden flouride

qPCR Real-time quantitative polymerase chain reaction

Rac1 Ras-related C3 botulinum toxin substrate 1

RTX Resiniferatoxin

RhoA Ras homolog family member A

ROC Receptor-operated channel

S-A Detection solution A

S-B Detection solution B

SDM Side directed mutagenesis

SDS Sodium dodecyl sulfate

SDS-PAGE Sodium dodecyl sulphate–polyacrylamide gel electrophoresis

SESTD SEC14 and spectrin domain 1

SOC Super optimal broth with catabolite repression

soc Store operated Ca^{2+}

SOCE Store-operated calcium entry

Stim Stromal interaction molecule

Sulfo-NHS-SS-Biotin Sulfo-succinimidyl-2-(biotinamido)ethyl-1,3-dithiopropionate

SV40 Simian virus 40

TOR Target of rapamycin

TBS Tris buffered saline

TBST Tris buffered saline + Tween 20

TG Tris-glycine

TGS Tris-glycine SDS

TGM Tris-glycine methanol

TM Transmembrane helix

Tris 2-amino-2-(hydroxymethyl)propane-1,3-diol

TRP Transient receptor potential

TRPA1 Transient receptor potential ankyrin 1

TRPC Transient receptor potential canonical

TRPM Transient receptor potential melastatin

TRPML Transient receptor potential mucolipin

TRPV Transient receptor potential vanilloid

TRPP Transient receptor potential polycystin

UCSF University of California, San Francisco

VSD Voltage-sensor domain

VSLD Voltage-sensor-like domain

WHO World health organisation

1. Introduction

1.1. Historical Overview and Expression Profile of TRPC Channels

The term transient receptor potential (TRP) was first introduced by Minke et al. (1975) and describes a spontaneous mutation of *Drosophila melanogaster*. The mutant behaved as blind in bright light and the electroretinogram exhibited a transient instead of a long lasting voltage response to continuous light exposure (Cosens & Manning, 1969). The corresponding gene locus was therefore referred to as the *trp* gene (Wong et al., 1985) which encodes a light sensitive, Ca^{2+} conductive ion channel (Hardie & Minke, 1992). Due to sequential similarities in mammalian systems the first TRP channel found in humans was TRPC1 (Zhu et al., 1995; Wes et al., 1995). Today, 28 members of the TRP channel superfamily are known, divided into six families, namely TRPC ("canonical"), TRPM ("melastatin"), TRPML ("mucolipin"), TRPV ("vanilloid"), TRPP ("polycystin") and TRPA1 ("ankyrin") channels. Most of the TRP channels are non-selective cation channels, but some have a high selectivity for Ca^{2+} ions and some are permeable for Mg^{2+} (Nilius & Owsianik, 2011). TRPC channels are permeable for monovalent cations like Na^{+}, K^{+} and for divalent cations like Ca^{2+}.

In the beginning of TRP channel research, TRPC channels were often discussed as being store-operated. Store-operated in this context means that depletion of the endoplasmatic reticulum (ER) Ca^{2+}-stores is sufficient to trigger a Ca^{2+} inward current over the plasma membrane. This process is called store-operated calcium entry (SOCE) and was first described by Putney (1986). The SOCE is then subsequently able to refill the intracellular Ca^{2+}-ER-stores to restore the equilibrium. The initial signal for a Ca^{2+} efflux of the ER can be diverse, but in non-excitable cells the predominant transduction system and second messenger for Ca^{2+} signal generation is inositol trisphosphate (IP_3) (Verkhratsky & Parpura, 2014). To summarize the originally described pathway (Putney, 1986; Smani et al., 2016; Stanzione et al., 2022), a $G\alpha_{q/11}$-coupled receptor at the plasma membrane gets activated by an extracellular stimulus and tranduces the signal by activating the phospholipase C (PLC) which produces IP_3 and diacylglycerol (DAG) from phosphatidylinositol 4,5-bisphosphate (PIP_2) cleavage. Then, IP_3 activates a receptor in the endoplasmatic reticulum and Ca^{2+} gets released from the store. This store depletion causes a Ca^{2+} influx from the extracellular space into the cytosole which is called SOCE. Ultimately, Ca^{2+} gets pumped back into the ER to refill the stores. The key players mediating store-operated Ca^{2+} inward currents over the plasmamembrane and sensing a store-depletion in the pathway were unknown at that time.

Only Ca^{2+} currents were observed and measured (Ca^{2+} release-activated Ca^{2+} current (I_{CRAC}) and store operated Ca^{2+} current (I_{SOC})) produced by unknown Ca^{2+} channels in the plasmamembrane (Hoth & Penner, 1992; Krause et al.,

1996; Vaca & Kunze, 1994). TRPC channels were discovered at roughly the same time. However, their function was unknown (Wes et al., 1995; Zhu et al., 1995). Because they were identified as being Ca^{2+} conductant, it was speculated that they might play a major role in SOCE (Zhu et al., 1995; Wes et al., 1995). A big scientific controversy about the role of TRPC channels in SOCE started and did not calm down until the description of the calcium release-activated calcium channel protein (Orai) and the stromal interaction molecule (Stim) (Roos et al., 2005; Liou et al., 2005; Luik et al., 2006; Yeromin et al., 2006; Vig et al., 2006). Stim functions as as a Ca^{2+} sensor located in the ER membrane, which can bind to and activate Orai protein subunits that represent the channel pore. Orai subunits are further involved in a similar, non-store-operated channel called arachidonic acid-regulated calcium-selective (ARC) channel (Mignen et al., 2008). In contrast to the Ca^{2+} release-activated Ca^{2+} (CRAC) channel, the ARC channel is composed of two different Orai subunits (Orai1 and 3), it represents a pentameric channel, it is non-store-operated and it interacts with plasma membrane-bound Stim1 (Thompson et al., 2013). Currently, TRPC channels and in particular TRPC1 are regarded as being involved in SOCE, but the mechanism is not fully understood until now (Bird & Putney, 2018). Besides TRPC1, all other TRPC channels, namely TRPC2, 3, 4, 5, 6, 7 are regarded as being receptor-operated which is described in more detail in section 1.3.

TRPC channels are widely expressed in numerous cell types and organs, including the cardiovascular system, kidney, lung, reproductive organs, liver, immune cells and brain tissue. According to the human protein atlas TRPC5 is mainly expressed in the brain, the adrenal gland, liver, kidney and bone marrow (Uhlén et al., 2005, 2015). Because TRPC5 is the main focus of this thesis, the following sections will discuss the expression profile of TRPC5 and its contribution to pathophysiologic phenotypes.

TRPC5 in the Brain

In the brain TRPC5 expression is widespread, and includes the cerebral cortex, hippocampus, amygdala and cerebellum (Morelli et al., 2013). TRPC5 knock-out (KO) in mice is involved in dendritic morphogenesis (Puram et al., 2011), contributes to seizures and excitotoxicity (Phelan et al., 2013) and regulates growth cone length and morphology (Greka et al., 2003; Kaczmarek et al., 2012).

Furthermore, TRPC5 and 4 were linked to amygdala function and mental disorders like anxiety and fear-related behavior. Due to the close relation and ability to form heterotetramers, the influence of TRPC4, 5 and 1 channels is often linked. TRPC4 and 5 gene-deficient mice, respectively, show less innate fear behavior then the wildtype mice in a open-field test and in a maze test (Riccio et al., 2009, 2014). The same group further hypothesized the changes in fear behavior could be due to abrogation of cholecystokinin B receptor (CCK_2) and/or glutamate-mediated potentiation of TRPC5 channels via G_q-coupled group I metabotropic glutamate receptors (mGluRs). These findings could lead to blcokers of TRPC4 and TRPC5 channels as a new class of anxiolytic and antidepressant drugs. In fact, there is first evidence that the TRPC4 and 5 antagonists ML084 and HC-070 may have anxiolytic and antidepressant effects in mice by reducing the immobility time in a forced swim test and tail suspension test (Yang et al.,

2015b; Just et al., 2018). Currently, a TRPC4 and 5 blocker, BI1358894 is in the phase II clinical trials (Boehringer Ingelheim) to potentially treat major depression disorder, borderline personality disorder as well as post-traumatic stress disorder.

TRPC5 in the Kidney

In the kidney, TRPC5 channels play a role in calcium homeostasis and are linked to focal segmental glomerulosclerosis (FSGS) and progressive chronic kidney diseases, similar to TRPC6. But the exact role and underlying mechanism of disease development and involvement of TRPC channels is yet not fully understood. It has been shown that inhibition of TRPC5 leads to podocyte protection and prevents proteinuria, a common symptom of kidney malfunction. The current role of TRPC5 is based on first experiments by Tian et al. (2010) linking TRPC5 and TRPC6 in an antagonistic regulation mechanism of actin remodeling in podocytes. The authors of this study suggest, TRPC5 activation leads to ras-related C3 botulinum toxin substrate 1 (Rac1) activation, followed by a promotion of cell migration. Rac1 activation then results in proteinuric kidney disease (Shibata et al., 2008). In contrast, a TRPC6 activation leads to increased ras homolog family member A (RhoA) activity, inhibiting cell migration. Increased Rac1 activation further leads to a positive feedback loop, because increased Ca^{2+} concentrations promote further Rac1 activation (Tian et al., 2010; Yu et al., 2013; Schaldecker et al., 2013).

In addition, similar results were obtained in animal models. Schaldecker et al. (2013), Yu et al. (2019) and Zhou et al. (2021) showed that animals treated with TRPC5 inhibitors were protected against progressive kidney diseases. These findings even resulted in a clinical trial with patients obtaining GFB-887, a TRPC4 and 5 inhibitor, as a treatment against FSGS, treatment-resistant minimal change disease and diabetic nephropathy (Walsh et al., 2021). There is still an ongoing debate about the role of TRPC5 in the community as authors of Wang et al. (2018b) and Polat et al. (2021) contest the involvement of TRPC5 in glomerular disease and proteinuria, even though first clinical trials have started.

TRPC5 in the Cardiovascular System

According to the world health organisation (WHO), cardiovascular diseases are the leading cause of deaths world-wide, accounting for approximately 32 % of all deaths in 2019. This makes research regarding cardiovascular diseases very relevant and underlines the significance to identify risk factors and causes, cellular markers and new therapeutic intervention strategies of cardiovascular diseases.

Several studies show similar expression patterns for TRPC channels in different tissues and mammalian cell lines quite early in the research history (Garcia & Schilling, 1997; Chang et al., 1997; Groschner et al., 1998; Freichel et al., 2001; Inoue et al., 2001; Walker et al., 2001; McDaniel et al., 2001; Xu & Beech, 2001). Similarly, TRPC channels are expressed in human vessels of any caliber (Yip et al., 2004). Therefore, an ubiquitous role of TRPCs in the cardiovascular system is very likely.

However, TRPC5 seems to play a minor role in the cardiovascular system, as expression seems low, whereas all other TRPC channels are expressed sig-

nificantly higher (Inoue et al., 2006). On the other hand receptor-operated channels (ROCs) like TRPCs may indirectly contribute to chloride and or potassium channel activation by depolarization of the membrane and therefore induce L-type Ca^{2+} channel activation, one of the key players in the cardiovascular system (House et al., 2008). Even though the expression is low, TRPC5 however could contribute to this cascade. Like all other TRPC channels, TRPC5 is involved in calcium homeostasis and is able to conduct Ca^{2+} ions and therefore be a potential candidate to influence cellular function in smooth muscle cells in the cardiovascular system. TRPC5 is up-regulated in failing and pathologically hypertrophied human heart (Bush et al., 2006) which still raises the question of the exact role of TRPC5 in the cardiovascular system and the involvement in cardiac diseases. Inhibition of TRPC5 in cardiomyocytes results in adenosine triphosphate (ATP)-induced activation of Ca^{2+}/nuclear factor of activated T-cells (Ca^{2+}/NFAT) dependent signaling and nitric oxide synthase (NOS) activation (Sunggip et al., 2018). This signaling pathway plays a significant role in cardiac hypertrophy. Additionally, TRPC5 is up-regulated in cardiac injury related to obscure sleep apnea-hyponea syndrome in rats (Wen et al., 2020). To some extent, these studies represent an involvement of TRPC5 in various cell types and pathological phenotypes in the cardiovascular system. However, it is obvious that the exact role of TRPC5 in the cardiovascular system is not finally clarified and should be investigated in more detail.

1.1.1. TRPC Channels Associated with Cancer

According to the WHO, cancer is the leading cause of death wordwide and accounts for nearly 10 million deaths in 2020. Therefore, investigation of cancer predispositions, of the leading pathways to develop cancer, of new therapeutic approaches and of the development of resistance mechanisms are of global concern. TRPC5 might be involved in a few cancer related topics, which are discussed in this paragraph. One of them being angiogenesis. In the transition from a quiescent to an invasive phenotype of tumors, the acquisition of angiogenic properties plays a crucial role (Hanahan & Weinberg, 2000, 2011; Folkman, 2002). Therefore, understanding angiogenesis and the regulating pathways are of utmost importance. Mutations in the TRPC5 channel can lead to dysregulation of Ca^{2+} homeostasis and therefore promote cancer progression (He & Ma, 2016).

TRPC3, 4 and 5 as well as Stim1 and Orai1 are expressed in umbilical vein-derived endothelial cells. The knockdown of the TRPC3, 4 and 5 channels results in a prevention of tubulogenesis, i.e. the formation of tubular structures in the organism, but not the knockdown of Stim1 and Orai1, suggesting a cooperative effect of the channel types or an exclusive effect of the TRPC channel knockdown (Antigny et al., 2012). Furthermore, the same study showed that cell proliferation is reduced by silencing TRPC3, 5 and Orai1, but not Stim1. In long-term drug-treated breast cancer cells, TRPC5 is highly expressed and promotes tumor angiogenesis by indirectly activating the transcription of vascular endothelial growth factor (Zhu et al., 2015b).

Another cancer-related topic where TRPC5 may be involved, is chemoresistance and its transmission. TRPC5 was found to be overexpressed in permeability glycoprotein (p-gp)(alternatively called multidrug resistance protein 1 (MDR1))-rich chemoresistant breast cancer cells (Ma et al., 2012). The overexpression

of TRPC5 in cancer cells can generate high Ca^{2+} channel activity, resulting in activation of nuclear factor of activated T-cells, cytoplasmic 3 (NFATC3) which is part of a T-cell DNA-binding transcription complex and therefore the transcription initiation of p-gp, which plays a crucial role in chemoresistance. p-gp serves as an ATP-dependent efflux pump with low substrate specifity. It is able to pump xenobiotics back across the cell membrane and is therefore involved in defense mechanisms of cancer cells (Bell et al., 1985). Its function has now been linked to TRPC5 in several cancer cell types (Ma et al., 2012; Wang et al., 2015, 2017; Zhou et al., 2021). Interestingly, TRPC5 inhibition even results in reversion of the resistance to 5-fluorouracil in human colorectal cancer cells (Wang et al., 2015) and to temozolomide in glioblastoma cells (Zou et al., 2021). Another group showed a similar result for the autophagy- and calcium/calmodulin-dependent protein kinase kinase β (CaMKKβ)/AMP-activated protein kinase alpha (AMPKα)/target of rapamycin (TOR)-mediated drug resistance of breast carcinoma cells against adriamycin. They figured out that TRPC5 induced the resistance pathway whereas silencing of TRPC5 reduces the drug resistance (Zhang et al., 2017).

Remarkably, TRPC5 mediated drug resistance has been shown to not only be vertically transferred between cell-generations but horizontally within a cell population. Drug-resistant cells produce extracellular vesicles, containing membrane-bound TRPC5 protein and mRNA and transfer them to drug-sensitive cells (Ma et al., 2014; Dong et al., 2014; Wang et al., 2017). This newly gained amount of TRPC5 channel proteins in the membrane is sufficient to develop NFATC3-p-gp-mediated chemoresistance in the acceptor cell.

More research regarding the exact role of TRPC5 in cancer development is needed, but it can be already concluded, that TRPC5 may serve as a potential drug target to prevent p-gp-mediated chemoresistance. Furthermore, TRPC5 expression in (breast cancer)-cells could serve as a biomarker for chemoresistance to indentify resistant cells and adjust treatment options (He & Ma, 2016; Wang et al., 2017, 2018a).

1.2. Structure of TRPC Channels

TRPC channels share a tetrameric superstructure, which can consist of homomers as well as heteromers (Strübing et al., 2001; Schaefer, 2005; Fischer & Edwardson, 2014). Heteromeric channels can comprise monomers of the same subfamily like TRPC4/5, TRPC1/3, TRPC3/4 and TRPC1/5, respecively (Plant & Schaefer, 2005; Liu et al., 2005; Poteser et al., 2006; Strübing et al., 2001) but they can also be built between different TRP families, resulting in even more complex channel superstructures like TRPC1 and TRPP2 heteromers (Bai et al., 2008; Kobori et al., 2009), TRPV4 and TRPP2 heteromers (Köttgen et al., 2008; Stewart et al., 2010) and other combinations including TRPC1/C6/V4 or TRPA1/V1 (Alessandri-Haber et al., 2009; Salas et al., 2009; Du et al., 2014), to name a few.

These channel heteromers can form in vitro, but they are also found to be expressed natively (Poteser et al., 2006; Strübing et al., 2001; Zergane et al., 2021). Due to this heteromerization, channel functionality is altered which could lead to fine-tuning of cellular processes. For example, the activation pathway and even the general functionality of TRPC1 homotetramers is very

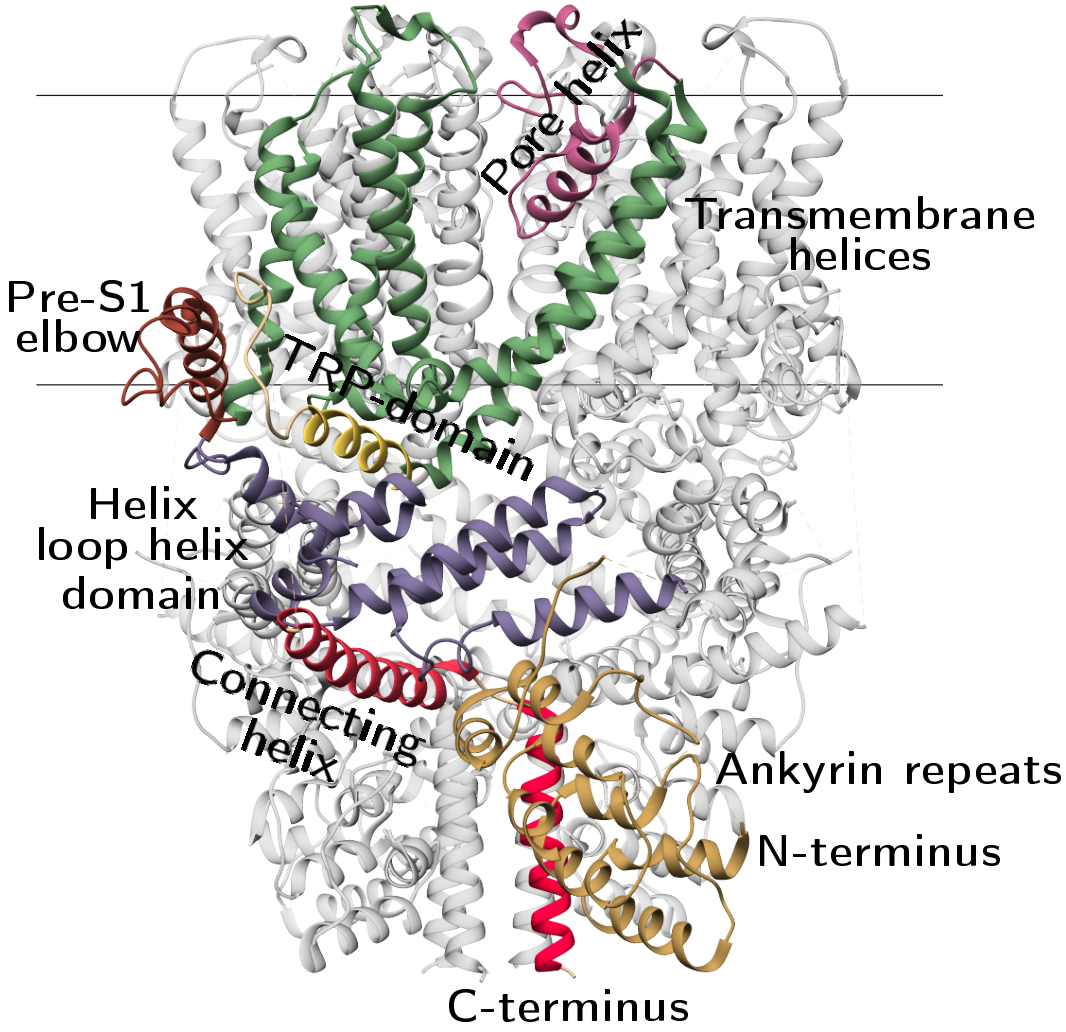

Figure 1.1.: **Structure of the mTRPC5 channel.** In this figure mTRPC5 (protein data bank (PDB): 6AEI) is shown as a tetrameric ribbon structure. The structural elements of one monomer are labelled according to Duan et al. (2018a). The cell membrane is indicated by two black horizontal lines.

controversially discussed. In contrast to that, it is widely accepted that TRPC1 can built heterotetrameric channel complexes with other TRPC subunits like TRPC4 or TRPC5, which leads to a uniquely shaped I-V course (Strübing et al., 2001) and thereby modifies channel properties like the Ca^{2+} conductance (Storch et al., 2012; Minard et al., 2018).

With the advantages in the cryogenic electron microscopy (cryo-EM) technique, more and more structures of TRPC channels and co-crystallized ligands got published since 2018 (Duan et al., 2018a,b; Fan et al., 2018; Tang et al., 2018; Vinayagam et al., 2020; Wright et al., 2020; Bai et al., 2020; Song et al., 2021). The TRPC channels share a typical architecture as shown in Figure 1.1 based on mTRPC5. In the next sections the structural properties and their functionality are presented.

1.2.1. Ankyrin-Like Repeats

Starting with the N-terminus, the first structural feature commonly found in TRPC channels are the ankyrin-like repeats. They are conserved in transient receptor potential melastatin (TRPM), TRPC, transient receptor potential vanilloid (TRPV) and transient receptor potential ankyrin 1 (TRPA1) channels but vary in number between the families (Huffer et al., 2020). Ankyrin repeats are protein-interacting motifs found in many proteins from all three domains of life (Mosavi et al., 2004). But they are likely more important in multicellular organisms, even though they are found in bacteria and viruses (Marcotte et al., 1999; Bork, 1993). Historically the ankyrin repeat is a sequence motif consisting of 33 residues which was first described in a yeast cell-cycle regulator and notch protein (Breeden & Nasmyth, 1987). It was later named after the cytoskeletal protein ankyrin which consists of 24 copies of the motif (Lux et al., 1990).

In the case of TRPC channels one monomer has four ankyrin-like repeats and particularly the first one might play a major role in channel homo- and hetero-tetramerization of TRPC4 and 5 channel complexes. Expressing one channel monomer without the first ankyrin-like repeat resulted in non-functional channels which no longer integrate into the plasma membrane (Schindl et al., 2008). Authors of Vinayagam et al. (2018) published the 3D-structure of TRPC4 and state that the ankyrin-like repeat domain interacts with the rib helix (connecting helix) and the C-terminus of the adjacent monomer and thereby increasing the stability of the tetramer. This underlines the hypothesis made by Schindl et al. (2008).

Not much is known about the ankyrin-like repeats in TRPC channels and if additional interaction proteins are needed for channel tetramerization which may stabilize the channel structure through the ankyrin-like repeat domain. Extensive studies were done using the related channels TRPV4 and 6 to figure out the exact function of the ankyrin-repeat domain. For TRPV6 it was shown that especially ankyrin-like repeat three is important for assembly of tetramers (Erler et al., 2004). Mutations in critical parts or deletion of the whole repeat resulted in non-functional channels that do not form tetramers. Authors of Chang et al. (2004) further showed that both, C- and N-terminus are important for subunit assembly and plasma membrane trafficking. Nevertheless, deleting both termini resulted in functional, plasma membrane expressed channels. Other studies agree that the N-terminus of TRPC1, TRPV4 and 6 plays an important role for channel oligomerization (Engelke et al., 2002; Arniges et al., 2006; Kahr et al., 2004). Arniges et al. (2006) demonstrate the importance of the N-terminus in trafficking and oligomerization using the example of TRPV4 splice variants lacking parts of the N-terminus as they accumulate in the endoplasmatic reticulum.

1.2.2. Transmembrane Helices

The transmembrane helices mainly stabilize the channel in the cell membrane due to their hydrophobic nature. One TRP channel monomer typically consits of six transmembrane helices with the pore helix between transmembrane helix (TM)5 and TM6. The ion conducting pathway is surrounded by the transmembrane helices domain and thereby stabilized through their rigid structure. The central gating elements are located in TM6 (Beck et al., 2013). During gating and

channel activation, the transmembrane helices most likely perform the critical movements, which are responsible for a channel opening as suggested by the 3D-structure of an activator-bound TRPC6 channel (Bai et al., 2020). Probably, TM6 relaxes and moves downwards, thereby widening the restriction point at the lower gate at residue Leu^{723}, Ile^{727} and Phe^{731} (translates to Ile^{621}, N^{625} and Gln^{629} in TRPC5). This movement is accompanied by a downward bending of TM5. Vinayagam et al. (2020) suggest a slightly different central mechanistic pathway during gating, where the voltage-sensor-like domain (VSLD) between TM1, 2, 3, 4 and the TRP-box plays a central role. They suggest that the TRP-box can move in and out towards the central ion pathway and therefore bend TM6 to widen or narrow the lower gate. During inhibitor binding this movement gets locked and the channel is held in a closed conformation (Vinayagam et al., 2020).

1.2.3. Pore Region

With the availability of more structural insights in TRPC channels due to advances in the cryo-EM technique the overall channel architecture and structural details become more obvious. The ion conducting pathway is mainly formed by TM5, 6 and the pore domain with the pore helix, turret and pore loop. Noteworthy, TRPC4 and 5 share 100 % amino acid identity in TM5, 6 and the selectivity filter (Duan et al., 2019) so that the structure of their pore region is almost identical.

The selectivity filter is built by the pore loop and divides the outer, more hydrophilic area from the hydrophobic central cavity (Vinayagam et al., 2018). The extracellular opening of the pore is negatively charged and slightly different between TRPC4 and TRPC5. TRPC5 possesses three more amino acids compared to TRPC4, one of them being negatively charged. Duan et al. (2019) state that this may attract more cations around the pore and might explain the higher single channel conductance of TRPC5 compared to TRPC4 (Schaefer et al., 2000).

Vinayagam et al. (2018) found no parameter in the ion conducting pathway itself (pore diameter, type of residues in the selectivity filter) which might explain differences in the ion conductance of TRP channels. Therefore they state the ion selectivity of the channel has to be defined by other structural elements, too, besides just the selectivity filter. The whole extracellular region around the pore mouth might be involved in ion selectivity. Other groups reported similar findings. Mutations in the outer pore regions could alter channel properties suggesting that the stability of this region may be important for ion selectivity and conductivity. However, this part of the channel is located slightly above the selectivity filter which is mainly built by residue G^{577} (in TRPC4). For TRPC5 it was observed that residue N^{584} alters the Ca^{2+} conductivity (Chen et al., 2017) like the analogous amino acid does in TRPV1 (Cao et al., 2013).

Yoshida et al. (2006) stated that modification of the two cysteines C^{549} and C^{554} has a direct effect on the channel gate by affecting TM6 which leads to a channel opening. However, according to Vinayagam et al. (2018) C^{549} and C^{554} do not locate close enough to TM6 to have a direct effect. They propose that residue E^{555} might be kept in place by the disulfide bond formed by C^{549} and C^{554} (Vinayagam et al., 2018).

Taken together these results suggest that the selectivity filter is not only built by residue G^{577}. Other amino acids located more towards the pore mouth are involved in stabilizing the structure or they might even directly participate in ion selection.

The lower gate defines the narrowest diameter in the ion conducting pore which is formed by three amino acids (isoleucine, asparagine, glutamine, short INQ). The motif is conserved between TRPC4 and 5 (Freichel et al., 2014). The minimal constriction of the lower gate has a radius of 0.7 A by using van-der-Waals surfaces and is defined by the asparagine residue (residue N^{621} in TRPC4 and N^{625} in TRPC5). Without van-der-Waals surfaces, the radius would be estimated to 4.2 Å for TRPC4 (Vinayagam et al., 2018, 2020). TRPC5 has a comparable constriction radius of 5 Å formed by the residue N^{625} (Duan et al., 2019). It has to be kept in mind that at present even though the resolution of cryo-EM can reach a stunning 1.25 Å in the best case (Yip et al., 2020), the resolutions for TRPC channels are 2.7 Å in the best case (Song et al., 2021), but often lower. Therefore small differences in atomic locations between structures might be a result of different resolutions and calculations. Recently, the first TRPC structures with co-crystallized ligands have been published, but even though channels were occupied by activator molecules, the channel pore was closed (Vinayagam et al., 2020; Bai et al., 2020). This may be due to very low opening probabilities and/or small channel open times (Hofmann et al., 1999; Jung et al., 2003; Schaefer et al., 2000). These limitations in the time resolution of the cryo-EM technique highlights the need of additional in-depth electrophysiological studies which are of utmost importance for a better understanding of the published cryo-EM data.

1.2.4. TRP Domain

The TRP domain is a helical structure which lies directly under the level of the cell membrane. In the case of TRPC5 it ranged from residues His^{634} to Phe^{651}. Until now, the function of the highly conserved TRP domain is not completely understood. In TRPC channels a few publications targeted the role of the TRP domain. Authors of Beck et al. (2013) suggest a crucial role of G^{503} by indirectly affecting the gating of TRPC4/5 because exchanges resulted in uncontrolled open channels. Structural details where unknown to this timepoint, but the hypothesis was confirmed by Vinayagam et al. (2018) publishing the molecular structure of TRPC4. They found that the interaction between amino acid W^{635} of the TRP domain and G^{503} is crucial for the stabilization of TM6 which forms the lower gate. The residues E^{648} and E^{649} (in TRPC4) which are located at the peripheral loop of the TRP domain are thought to interact with two lysine residues in Stim1 proteins (Zeng et al., 2008; Lee et al., 2010). According to Vinayagam et al. (2018) this would be possible due to peripheral exposure of the residues. From other related channels like TRPM5, TRPM8 and TRPV5 it is assumed, that the TRP domain interacts with PIP_2, because amino acid exchanges in the region resulted in a reduction of PIP_2 sensitivity and in an increased channel inhibition mediated by PIP_2 depletion (Rohács et al., 2005). Later, Yin et al. (2018) partly agreed with Rohács et al. (2005), as they published a cryo-EM structure of TRPM8. However, they suggest some indirect interactions of the TRP domain amino acids and they propose that only

one residue actually interacts with PIP_2. Only one year later, this was confirmed by the same group by co-crystallizing PIP_2 with TRPM8 (Yin et al., 2019).

For TRPV1 it has been implicated that the TRP domain has an allosteric impact on the activation and gating mechanism of the channel (García-Sanz et al., 2007; Valente et al., 2008; Gregorio-Teruel et al., 2014). Conservative mutations in the TRP domain sequence result in decreases of the current amplitudes or even in non-functional channels (Gregorio-Teruel et al., 2015). The TRP domain is conserved between TRP channels but even chimeras of TRPV1 channels where the TRP domain is replaced with a TRP domain of TRPV2 results in non-functional channels (Gregorio-Teruel et al., 2015; García-Sanz et al., 2007). This experiment impressively outlines the highly specific role of the TRP domain in the channel (sub)families.

Later, the TRPV1 cryo-EM structure unveiled stabilizing effects of the TRP domain on the TM region (Liao et al., 2013a). This further highlights the versatile impact of the TRP domain on the upper channel structure.

Taken together, these results reveal a very pivotal role of the TRP domain on the whole channel. Even though the sequence itself is very conserved in the TRP channel super-family, the very exact sequence of the motif seems important for structural stabilization, allosteric gating manipulation and co-factor assembly.

1.2.5. Protein Binding Sites and Interacting Proteins

Several different proteins are interacting with TRPC5 channels and regulate the channel functionality either directly or indirectly. Important interacting proteins are presented in the following section.

NHERF, EBP50 and PDZB Domain

TRPC4 and 5 have a C-terminal PDZ-binding (PDZB) motif (amino acid sequence "VTTRL") which can bind PSD-95/Discs-large/ZO-1 (PDZ) domains of scaffolding proteins like Na^+/H^+ exchanger regulatory factor (NHERF)1 and NHERF2 (Tang et al., 2000; Obukhov & Nowycky, 2004). NHERF proteins can also interact with PLCβ (Tang et al., 2000). In addition, NHERF binds to members of the ezrin, radixin, moesin (ERM) protein family (Murthy et al., 1998; Yun et al., 1998; Terawaki et al., 2006) that anchors the multi-protein complex to the actin skeleton (Tang et al., 2000; Constantin, 2016). Later, it was shown that the calmodulin-inositol receptor binding (CIRB) domain additionally binds to the SEC14 and spectrin domain 1 (SESTD)1, which may act in a similar fashion as NHERF. SESTD1 is able to bind phospholipids including PIP_2 and spectrins, thereby anchoring TRPC4 and 5 to the cell membrane and/or the cytoskeleton (Miehe et al., 2010).

The PDZB domain further displays a proteinkinase C (PKC) phosphorylation site involved in the desensitization of TRPC4 and 5 (Zhu et al., 2005). $G\alpha_{i/o}$ may also interact at this site (Jeon et al., 2012).

The PDZB domain does not only serve as a membrane anchoring point, but it also has a regulatory function. Storch et al. (2017) showed that the PDZB motif is involved in the DAG sensitivity of TRPC4 and 5 channels. NHERF dissociation e.g. by PIP_2 depletion or by prevention of PKC-mediated channel phosphorylation in the PDZB motif resulted in direct DAG-mediated chan-

nel activation which was previously only reported for TRPC3, 6 and 7 channels (Hofmann et al., 1999).

CaM, IP3R and CaM-binding Domain

Calmodulin (CaM) is an EF-hand, low-molecular-weight Ca^{2+} binding protein that is highly conserved in eukaryotes (Clapham, 2007). CaM was discovered in 1970 as a calcium-dependent regulator for the nucleotide phophodiesterase in the brain (Kakiuchi & Yamazaki, 1970). CaM regulates a lot of different proteins such as: CaM kinases, membrane protein receptors and ion channels (e. g. N-methyl-D-aspartate (NMDA) glutamate receptors, voltage-gated potassium, sodium and calcium channels, inositol 1,4,5-trisphosphate receptor (IP3R)) but also ER membrane associated Stim and Orai proteins (Marshall et al., 2015). CaM therefore is a very versatile and essential regulatory protein in Ca^{2+} homeostasis (Carafoli & Krebs, 2016; Junho et al., 2020).

Every TRPC channel has at least one CaM-binding domain per monomer (Zhu, 2005), however TRPC5 even has three CaM-binding sites per monomer (two exclusive CaM-binding domains and one CIRB domain) (Eder et al., 2007; Zholos, 2014). The CaM-binding domains exclusively bind CaM, whereas the CIRB domain is a competitive binding site for CaM and IP3R (Zhang et al., 2001; Tang et al., 2001; Zhu & Tang, 2004). Vinayagam et al. (2020) were the first who co-crystallized CaM with TRPC4 and therefore the first TRPC channel in complex with CaM. They could show that up to four CaM molecules bind to the CIRB domains of the homotetrameric channel, meaning one CaM molecule per monomer. However, the respective sites are not always occupied by one molecules of CaM, but a state of two or three bound CaM molecules per tetramer is favored and any bound CaM seems to stabilize the channel in an inactive state.

The binding of CaM or IP3R to the CIRB is Ca^{2+} dependent, meaning that at low Ca^{2+} concentrations an IP3R binding is preferred, whereas at high Ca^{2+} concentrations a CaM binding is preferred. In this scenario, CaM is stabilizing an inactive channel state, whereas the IP3R binding is needed for an active channel conformation (Vinayagam et al., 2020; Berridge, 2004; Kanki et al., 2001). This is at least debatable and there is an ongoing discussion about the role of CaM and especially the need for an IP3R binding for the channel activity.

There are groups showing a dependence or at least an involvement of the IP3R in the activation mechanism of TRPC3 channels (Kiselyov et al., 1998; Yuan et al., 2003), but others showing that the channel activation is independent of IP3R (Venkatachalam et al., 2001; Ma et al., 2001; Vazquez et al., 2001). But nonetheless the IP3R co-immunoprecipitates and is pulled-down together with TRPC channels (Kiselyov et al., 1999). This shows that the role of the IP3R for the activation mechanism of TRPC channels is not fully understood and needs more systematic research.

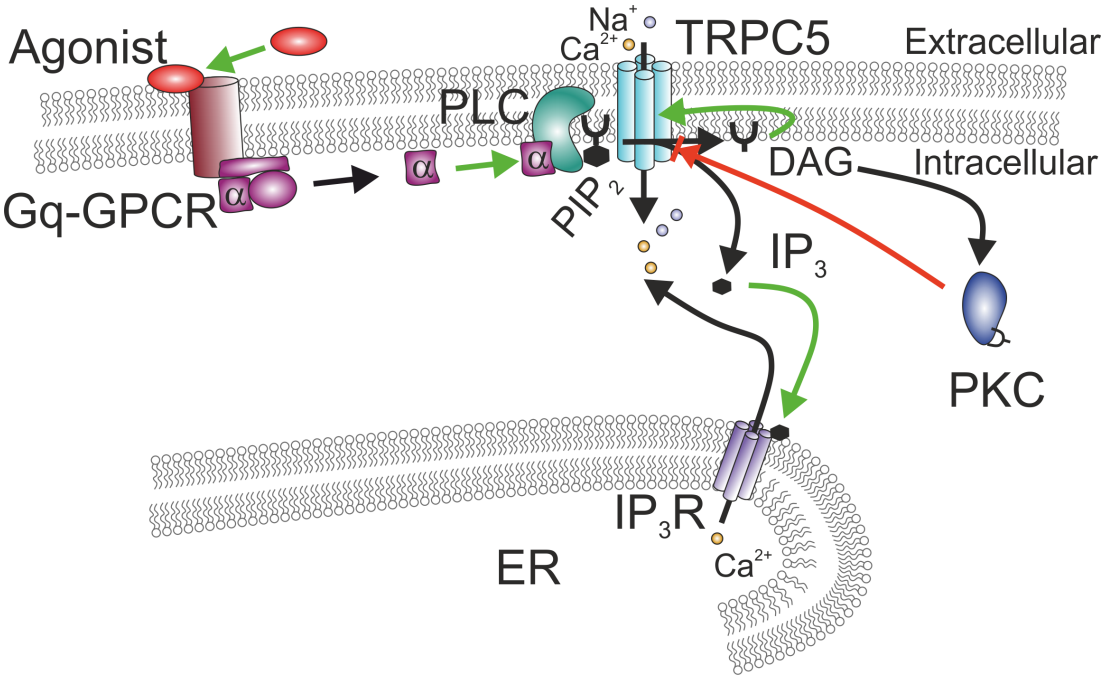

Figure 1.2.: **PLC pathway.** The figure shows the proposed receptor-operated activation mechanism of TRPC5 that involves PLC activation. An agonist activates a G_q-coupled receptor (green arrow) leading to G-protein activation. Subsequently, the alpha subunit of the G-protein activates the PLC. The PLC then cleaves membrane-bound PIP_2 into the two second messengers DAG, which stays in the membrane and IP_3, which is released into the cytosole. IP_3 then activates the ER-bound IP3R, leading to a Ca^{2+} release into the cytosole. DAG directly activates the TRPC5 channel under certain circumstances that require NHERF dissociation from the C-terminus (Storch et al., 2017). Cleavage of PIP_2 also results in a channel activation. This channel activation leads to a Na^+ and Ca^{2+} influx into the cytosole. DAG can activate the PKC, which in turn inactivates TRPC5 (red arrow).

1.3. The Endogenous Activation Pathways of TRPCs

The activation mechanism of TRPC channels in general and of TRPC5 in particular are not fully understood until now. At first, as described in section 1.1, TRPC channels were thought to be store-operated. Meaning a Ca^{2+} lack in the ER is perceived that activates TRPC channels in the plasma membrane (Zhu et al., 1995, 1996; Philipp et al., 1996, 1998; Vannier et al., 1999; Riccio et al., 2002; Zitt et al., 1996). Only TRPC6 was traditionally described as being receptor-operated or -activated (Boulay et al., 1997). Later, TRPC3 was also declared as being receptor-activatable in a PLC-dependent, but store-independent manner (Zitt et al., 1997). For TRPC4 and 5 first doubts arose whether they are really store-operated since a receptor-operated channel activation via G-protein coupled receptor (GPCR) or receptor tyrosine kinases downstream of PLC was shown (Okada et al., 1998; Schaefer et al., 2000).

Kiselyov et al. (1998) showed that TRPC3 can be activated via store-depletion or directly via IP_3 bound IP3R. Three years later, the description of the C-terminal CIRB domain of TRPC channels led to another controversial discussion (Tang et al., 2001; Zhang et al., 2001). As described in the previous section, the CIRB domain is able to bind CaM, a regulatory protein inhibiting the channel activity, which can get displaced by the IP3R and thus may indirectly activate the channel, as shown for TRPC3 (Tang et al., 2001; Zhang et al., 2001). Contrary to that, it was shown that TRPC3 and 5 can be activated in a PLC dependent manner, independent of the expression of IP3R, indicating that the IP3R is at least not necessary to activate TRPC3 or 5 (Venkatachalam et al., 2003).

At present, it is commonly accepted, that TRPC channels are receptor-operated and are activated via $G_{q/11}$-protein coupled receptors or by receeptor tyrosine kinases downstream of PLCβ or PLCγ, respectively (see Figure 1.2, Montell (2005); Venkatachalam & Montell (2007); Chen et al. (2020)). In this scenario, a GPCR gets activated via agonist binding leading to $G_{q/11}$-protein activation. The $G_{q/11}$-protein then activates PLCβ, which leads to cleavage of PIP_2 into IP_3 and DAG. DAG can then directly activate TRPC3, 6 and 7 channels (Hofmann et al., 1999). Until recently, only TRPC3, 6 and 7 were thought to be DAG sensitive, but Storch et al. (2017) could show that under specific conditions, namely C-terminal NHERF dissociation, TRPC4 and 5 are also directly DAG sensitive. This means that all TRPC channels are regulated in a similar fashion, namely through the second messenger molecule DAG.

The other product of PIP_2 cleavage, IP_3, is able to activate IP_3 receptors in the ER membrane and thus causing a Ca^{2+} release and store depletion. The Ca^{2+} release could recruit regulatory proteins like CaM and PKC and therefore negatively regulate TRPC channels. Additionally, DAG is able to activate PKC directly, resulting in a negative feedback inhibition of TRPC currents.

TRPC4 and TRPC1 may be an exception of the above described activation mechanism. TRPC1 could be store-operated, either on its own or in complex with Orai1 (Jardin et al., 2008; Kim et al., 2009; Guéguinou et al., 2016; Shi et al., 2017; Ambudkar et al., 2017). Alternatively, TRPC1 might be receptor-operated with a store-depletion dependent receptor activation mechanism (Shi et al., 2016), meaning a combination of both. For the activation of TRPC4 however, the signaling via $G_{i/o}$ and PLCδ1 may be more important for the receptor-activation than the signaling via $G_{q/11}$ and PLCβ (Jeon et al., 2008, 2012; Thakur et al., 2016).

Altogether, the research community is in disagreement about the activation mechanism of TRPC channels. Since TRPC5 channels evolved as potential new drug targets, a detailed biophysical characterization of the structure-function relations of the channel and in particular of the ligand binding regions are of utmost importance to further improve drug development.

PIP_2 and TRPC Channels

Another piece in the puzzle is PIP_2 and its role in TRPC channel regulation. PIP_2 seems to play a very versatile role in the TRPC activation pathway. One of the challenges in examining the role of PIP_2 in the activation mechanism is, that PIP_2 as a second messenger affects a lot of other cellular processes, including organization of the cytoskeleton and membrane trafficking (Saarikangas et al., 2010;

Shewan et al., 2011; DiNitto et al., 2003). These processes likely influence ion channel activity (Hilgemann & Ball, 1996; Rohacs, 2009; Logothetis et al., 2015) and therefore different results are obtained by using different patch clamp configurations like inside-out or whole-cell configuration. In inside-out patches a lot of cellular cofactors and proteins get lost during the measurement (run-down) and cytosolic cofactors are not present. Therefore it is a more artificial approach but the extra- and intracelluar conditions are more controlled. Lemonnier et al. (2008) and Trebak et al. (2009) showed that heterologously expressed TRPC5 and TRPC3, 6 and 7, are activated by PIP_2 in inside-out patches. On the other hand, studies with endogenously expressed TRPC5 channel show the contrary: PIP_2 inhibits the channel in inside-out patches (Shi et al., 2012). The same phenomenon was observed for TRPC6 (Albert et al., 2008; Ju et al., 2010) indicating the inhibition is not limited to TRPC5 in the channel family. For whole-cell patch clamp measurements with heterologously expressed TRPC5, the channel can be activated by limiting PIP_2 production through inhibition of phosphatidylinositol-5-phosphate 4-kinase (PIP4K) (Storch et al., 2017; Trebak et al., 2009). Applying PIP_2 through the patch-pipette inhibited the channel (Trebak et al., 2009). Similar results were obtained with TRPC4, where PIP_2 inhibited the channel isoform-specific by interacting with the the C-terminus (Otsuguro et al., 2008). Another group showed an attenuating effect on TRPC5 desensitation by directly applied PIP_2, but a current potentiation with PIP4K inhibition (Kim et al., 2008). Storch et al. (2017) demonstrated that PIP_2-depletion induces a conformational change resulting in a NHERF dissociation from the channel and a direct DAG sensitivity of TRPC5. Ningoo et al. (2021) further attributes a very pivotal role to PIP_2 in the activation pathway of TRPC5. They showed that trivalent cations and DAG allosterically modulates the PIP_2-binding of TRPC5 and that PIP_2 is an important factor in the channel activation and inactivation process.

1.3.1. Small Molecule Activators of TRPC5

In order to investigate the TRPC channel function *in vivo* or *in vitro*, potent and selective channel activators and blockers are extremely valuable.

More and more small molecule activators and modulators of TRPC5 channels are available at present. They are important to study channel activation mechanisms on the molecular level, to get insights in channel gating mechanisms and might be applicable as therapeutic drugs for TRPC5 associated diseases. Because of the limitation of the cryo-EM approaches, particularly that no TRPC channel 3D-structure is resolved in an activated channel state so far (Vinayagam et al., 2020), other techniques should be applied to investigate the channel properties on the molecular level. Furthermore, using cryo-EM not all parts of the channel structure are resolved until now and some attempts to co-cristallize specific ligands failed.

Englerins

In 1988 the NCI-60 screening program for natural compounds regarding their effectiveness against 60 different tumor cell lines started (Alley et al., 1988; Shoemaker, 2006). One of the top scoring extracts regarding the effectiveness

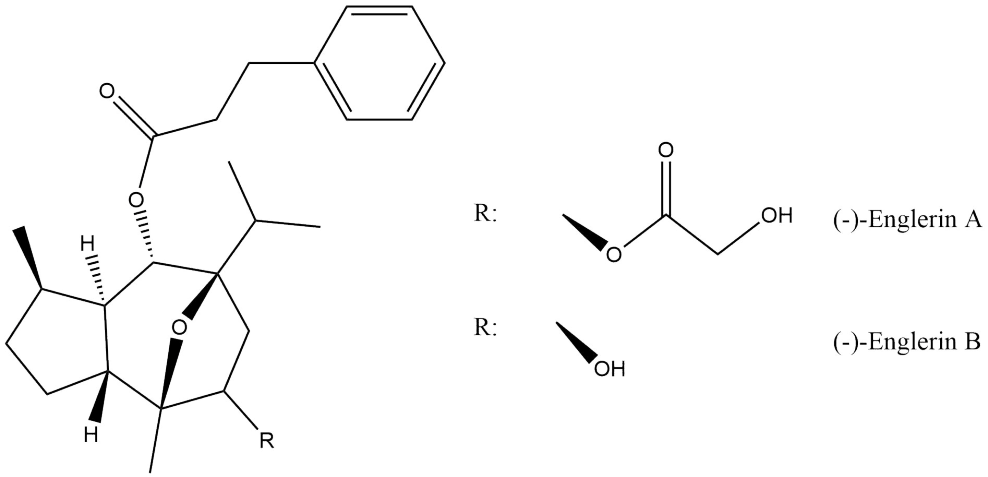

Figure 1.3.: **Chemical structure of englerins.** This figure shows the chemical structure of englerin A and englerin B. The difference in the structure is indicated by a variable residue R.

was the bark extract of *Phyllanthus engleri*, a Tanzanian tree from the genus Euphorbiazeae (Wu et al., 2017). The most bioactive compounds of the extract were seven chlorinated sesquiterpenes with the strongest activity against the renal cancer cell line A498 (Akee et al., 2012). Later, this result was partly withdrawn because an extraction error yielded chlorinated englerin derivatives. This happened due to the fact that the used chloroform apparently generated Cl_2 on standing, reacting with the compounds. Nonetheless, englerin A was identified as the leading compound (but not chlorinated), responsible for the cytostatic effect. Thereupon, different stereoisomers of englerin were synthesized: (+)-englerin A was the first synthesized englerin A (Willot et al., 2009), followed by (-)-englerin A and englerin B (Figure 1.3) through different routes by independent groups (Zhou et al., 2010; Molawi et al., 2010; Nicolaou et al., 2010; Radtke et al., 2011). Interestingly, (+)-englerin A was identified as non-reactive against A498 cells at 1 µM, whereas (-)-englerin A was highly effective with an IC_{50} of 45 nM. Later, Akbulut et al. (2015) linked the cell death of A498 cells to a Ca^{2+} inward current through TRPC4 and TRPC5 channels with an EC_{50} of 11 nM and 7 nM, respectively. However, in 2017 the actual cell toxicity was linked to the TRPC4/5 mediated sodium instead of the calcium inward current (Ludlow et al., 2017). Carson et al. (2015) confirmed the involvement of TRPC4 and 5 in (-)-englerin A mediated cytotoxicity by heterologous expression in human embryonic kidney 293T (HEK293T) cells where the (-)-englerin A-induced cell toxicity could be reproduced. Furthermore, (-)-englerin A also activates TRPC4/1 and TRPC5/1 heteromers and weakly inhibits TRPA1, TRPV3, TRPV4, and TRPM8 with an IC_{50} in the 3–4 µM range (Carson et al., 2015). However, it did not show activity against the non-TRP channels epithelial Na^+ channel (ENaC), gamma-aminobutyric acid (GABA)-receptor, cystic fibrosis transmembrane conductance regulator (CFTR), $Na_V1.5$, $Ca_V1.2$ and $K_V7.1$ in functional essays (Carson et al., 2015). Additionally, (-)-englerin A is reported to affect PKCθ (Sourbier et al., 2013) and L-type calcium channels (Rodrigues et al., 2016), but in much higher and even micromolar concentrations. In canine and human serum, (-)-englerin A is stable, whereas it is hydrolyzed to (-)-englerin B in rodent serum. Oral doses of 5 mg kg^{-1} resulted in

low (-)-englerin A serum concentrations of <12 nM, but in high serum concentrations of the inactive metabolite (-)-englerin B of >50 nM (Carson et al., 2015). Additionally, (-)-englerin A is toxic for rodents when applied intravenously or intraperitoneally and only tolerated up to a dose of <1.5 mg kg^{-1} (Carson et al., 2015). Unfortunately, Carson et al. (2015) could not detect any (-)-englerin A in the serum after subcutaneous application. Nonetheless, Fash et al. (2016) reported that aza-englerin A analogues are bioavailable after oral application. In 2018, Rubaiy et al. (2018b) described A54, a (-)-englerin A analogue with inhibitory effects on TRPC4 and 5, although it lacks just one oxygen atom compared to (-)-englerin A. So far, (-)-englerin A represents the most efficacious and potent activator of TRPC4 and 5 homomers as well as TRPC1/4 and 1/5 channel heteromers. Although (-)-englerin A is the most potent TRPC4 and 5 channel activator known so far, co-crystallization efforts with TRPC4 or TRPC5 channels failed. A detailed biophysical characterization of the (-)-englerin A binding site might help to get new insights into the activation and regulation mechanisms of TRPC4 and TRPC5 channels which lays the basis for further drug development.

Riluzole

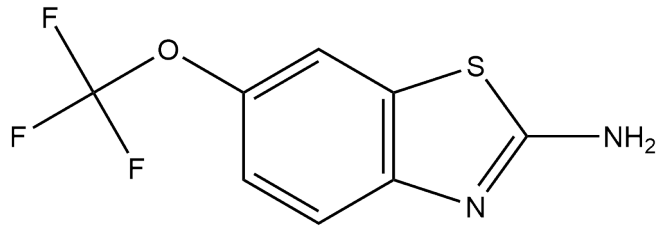

Figure 1.4.: **Chemical structure of riluzole.** This figure shows the chemical structure of riluzole

Riluzole (Figure 1.4) is a benzothiazole derivative and an approved drug for the use in amyotrophic lateral sclerosis (ALS)-patients and can prolong the survival by approximately 2 to 4 months (Bensimon et al., 1994; Lacomblez et al., 1996; Traynor et al., 2003). The drug is also used in off label treatments of psychiatric disorders in adults and children (Grant et al., 2010). In a screening approach for TRPC5 the activator riluzole was found to be active against heterologously expressed TRPC5 in HEK293T cells with an EC_{50} of 9.2 µM (Richter et al., 2014b). Interestingly, riluzole is a specific TRPC5 and TRPC1/5 activator with no activity against TRPC4 or TRPC1/4 channels (Richter et al., 2014b). Because riluzole is only activating TRPC5 and not TRPC4 channels, it can be speculated that it has a distinct activation mechanism compared with (-)-englerin A. Therefore riluzole was used as a control in the present thesis to study the (-)-englerin A mediated TRPC5 activation and vice versa.

BTD and Methylprednisolone

In another drug screening, the benzothiadiazine BTD (Figure 1.5a) as well as the glucocorticoid methylprednisolone (Figure 1.5b) were discovered as both being TRPC5 specific activators with an EC_{50} of 1.4 µM and 12 µM, respectively (Beckmann et al., 2017). Due to the lower EC_{50}, BTD was studied in more

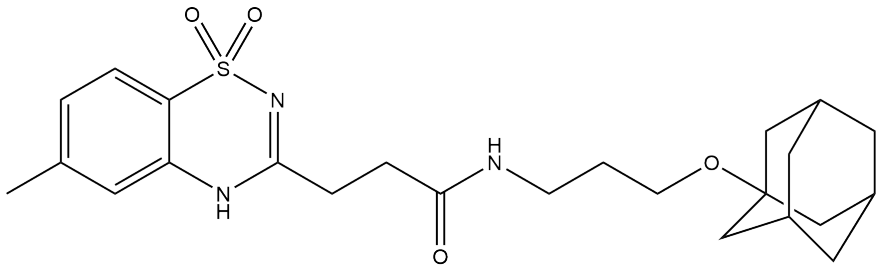

(a) BTD

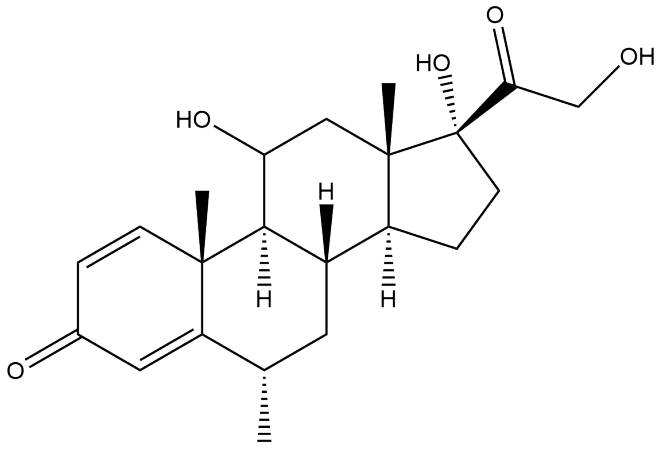

(b) Methylprednisolone

Figure 1.5.: **Chemical structures of BTD and methylprednisolone.** This figure shows the chemical structure of BTD **(a)** and methylprednisolone **(b)**.

detail and showed no effect against other TRP channels, like TRPC3, 4, 6, 7, TRPA1, TRPV1, 2, 3, 4, TRPM2 and 3. Therefore, BTD was characterized as a very specific TRPC5 activator with an EC_{50} in the low micro-molar range. Additionally, a photoswitchable BTD analogue was designed in 2022 named BTDAzo with an EC_{50} similar to the parental substance of 1.5 µM (Müller et al., 2022). Photoswitchable ligands can be converted from a non-active (trans) state to an active (cis) state using light of a specific wavelength. Using those photoswitchable ligands, high precision measurements like channel inactivation kinetics or other time-dependent aspects can be resolved.

Thiazolidinediones and Isoflavones

Rosigitazone (Figure 1.6a) is one representative of the thiazolidinediones and is able to activate TRPC5 with an EC_{50} of 31 µM (Majeed et al., 2011). It is an approved drug for the treatment of type-2 diabetes and therefore widely available. The chemically related compounds pioglitazone and troglitazone were not active against TRPC5, but all three compounds inhibited TRPM3.

Isoflavones (Figure 1.6b) are phytochemicals which naturally occur e. g. in soy like genistein and daidzein. The isoflavone genistein activates TRPC5 with an EC_{50} of 93 µM and La^{3+} is able to further potentiate the activating effect of genistein when applied simultaneously (Wong et al., 2010). Daidzein, a genistein analogue acts similarly on TRPC5 (Wong et al., 2010).

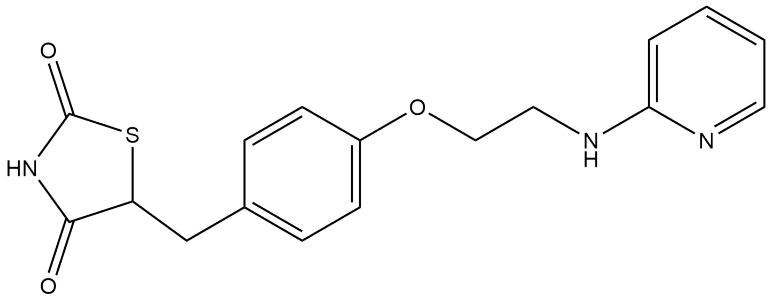

(a) Rosiglitazone

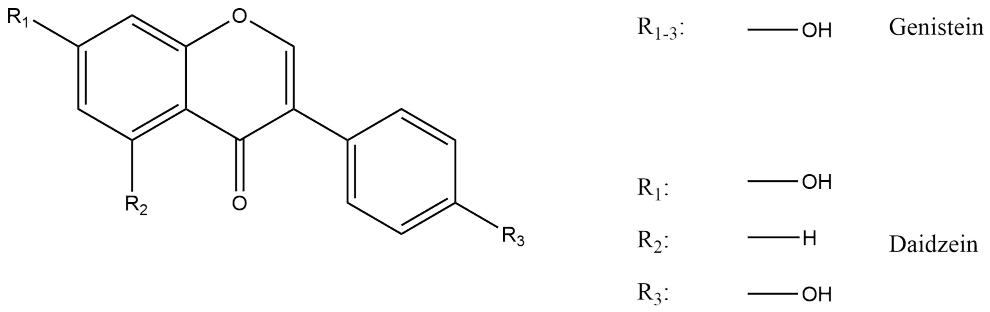

(b) Isoflavones

Figure 1.6.: **Chemical structure of rosiglitazone and the isoflavones.** This figure shows the chemical structure of rosiglitazone **(a)** and the isoflavones using the examples of genistein and daidzein **(b)**.

Tontantzitlolone

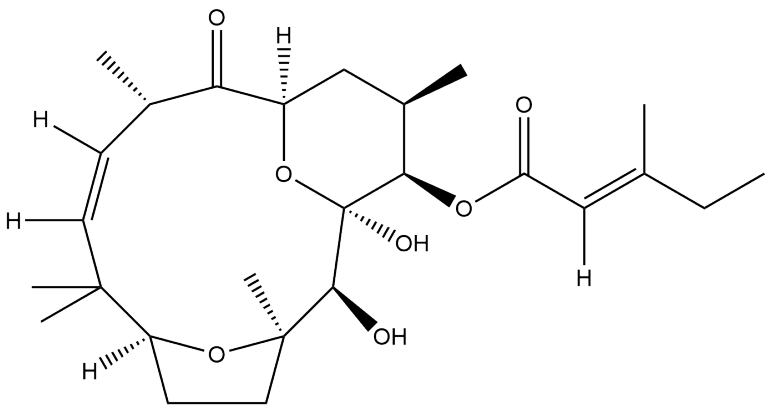

Figure 1.7.: **Chemical structure of tonantzitlolone.** This figure shows the chemical structure of tonantzitlolone.

Tontantzitlolone (Figure 1.7) is a rather unique representative of the diterpene ester group of TRPC5 activators. It is worth mentioning because of its similar effect on A498 renal cancer cells as (-)-englerin A (Rubaiy et al., 2018a). The activation profile of tonantzitlolone includes TRPC5 (EC_{50} = 83 nM) and TRPC4 monomers (EC_{50} = 123 nM) as well as TRPC1/4 (EC_{50} = 140 nM) (Rubaiy et al., 2018a).

1.3.2. Small Molecule Inhibitors of TRPC5

Xanthines

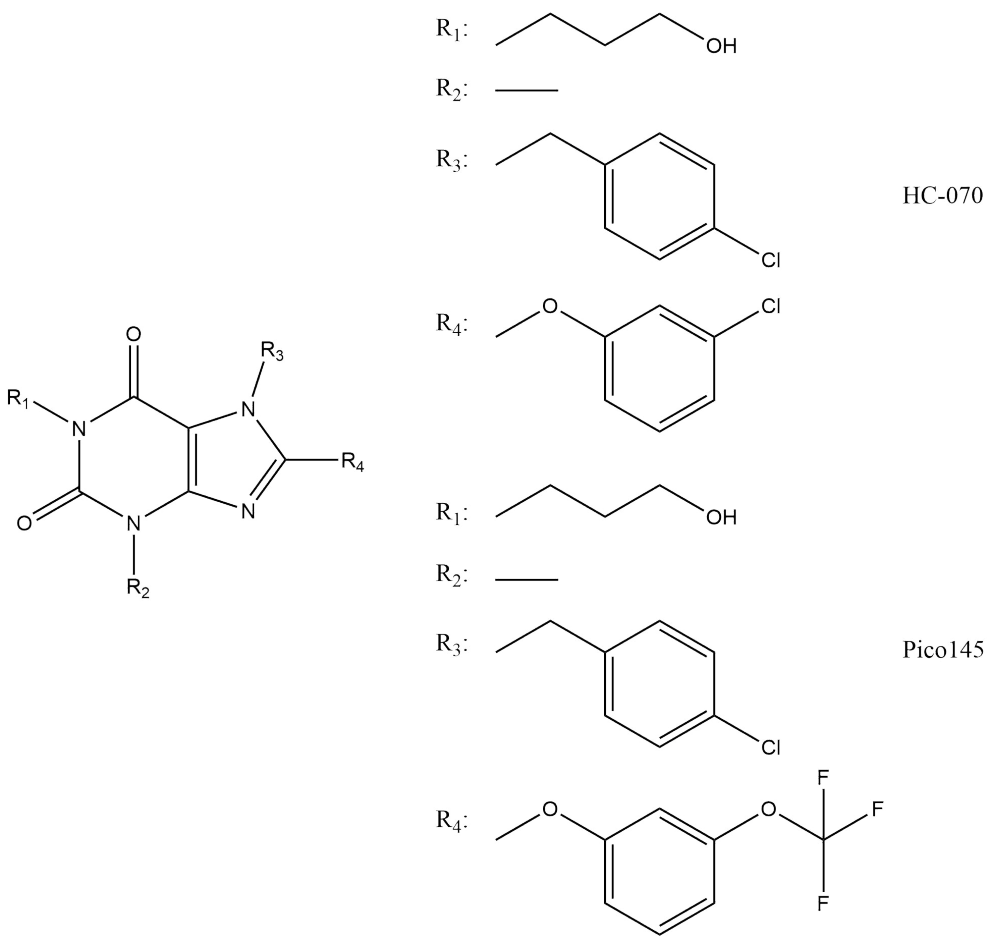

Figure 1.8.: **Chemical structure of the xanthine class.** This figure shows the chemical structure of the xanthines and their representatives HC-070 and Pico145. The differences in the structure are indicated by a variable residue R.

The xanthine class of TRPC5 ligands (Figure 1.8) is one of the most considerable and important classes of TRPC5 inhibitors. More than 600 substances of the group are patented by the pharmaceutical companies Hydra Biosciences Inc. and Boehringer Ingelheim, including several candidates with an IC_{50} of <100 nM (Chenard & Gallaschun, 2014). Two of the most promising compounds, HC-070 (Just et al., 2018) and Pico145 (also referred to as HC-608) (Rubaiy et al., 2017) were further characterized. Pico145 is the most potent inhibitor known so far that inhibits TRPC5 currents with an IC_{50} of 1.3 pM, TRPC4 with an IC_{50} of 349 pM, TRPC1/5 and TRPC1/4 heteromers with an IC_{50} of 199 pM and 33 pM, respectively. The same patent also contained an activator of TRPC5 which is called AM237 (Minard et al., 2019). Strikingly, AM237 specifically activates TRPC5 homomers with an EC_{50} of 15–20 nM, but inhibits (-)-englerin A evoked TRPC5 or TRPC4 channels and TRPC1/4, 1/5 or 4/5 heteromers with an IC_{50} of 0.9–13 nM (Minard et al., 2019). This suggests a very specific xanthine binding site distinguishing between closely related substances that induce distinct transduction pathways.

Benzimidazoles and ML204

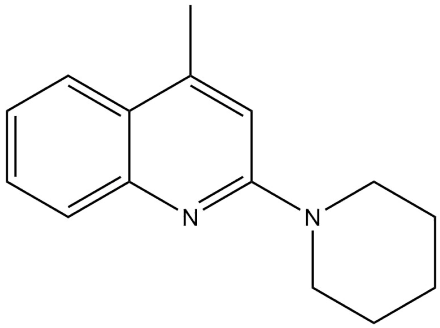

Figure 1.9.: **Chemical structure of ML204.** This figure shows the chemical structure of ML204.

ML204, a quinoline (Figure 1.9), was one of the first described inhibitors of TRPC4 and TRPC5 channels with an IC_{50} of 0.99 µM and 13.6 µM, respectively (Miller et al., 2011; Zhou et al., 2017). Rubaiy et al. (2017) further tested the activity of ML204 against heteromeric TRPC1/4 channels resulting in an IC_{50} of 58 µM. Clemizole is a member of the benzimidazole class of TRPC channel inhibitors and was originally designed as a histamine receptor antagonist. However, Richter et al. (2014a) described clemizole as an inhibitor of TRPC5 currents with an IC_{50} of 1.1 µM. Notably, clemizole is a rather unspecific TRPC channel inhibitor that also inhibits TRPC4, TRPC3 and TRPC6 with an IC_{50} of 6.4 µM, 9.1 µM and 11.3 µM, respectively (Richter et al., 2014a). M084 was another hit of the same screening approach as ML204. M084 is also a benzimidazole-based compound which inhibits TRPC4 and 5 channels, as well as heteromeric TRPC1/4 channels. However, M084 has a lower IC_{50} of 8.3 µM inhibiting TRPC1/4 channels compared to ML204 and a higher IC_{50} regarding the inhibition of TRPC4 (10.3 µM) and 5 (8.2 µM) homomers (Zhu et al., 2015a). M084 also inhibits TRPC3 and 6 currents with an IC_{50} of 48.6 µM and 59.6 µM, respectively (Zhu et al., 2015a). However, other M084 derivatives with a comparable IC_{50}, named compound 16, 17, 27 or 28 are more specific inhibitors (Zhu et al., 2015a). M084 was further suggested to have an antidepressant and an anxiolytic-like effect in mice (Yang et al., 2015a). AC1903 represents a later synthesized compound which is based on the benzimidazole structure of M084 and ML204 (Sharma et al., 2019). AC1903 is able to inhibit riluzole evoked TRPC5 currents with a similar IC_{50} of 14.7 µM compared to ML204 or M084. Strikingly, AC1903 seems to be a selective inhibitor of TRPC5, as it does not inhibit carbachol-induced TRPC4 currents or 1-oleoyl-2-acetyl-sn-glycerol (OAG)-induced TRPC6 currents (Zhou et al., 2017). Furthermore, AC1903 has been shown to suppress progressive kidney disease in rats (Zhou et al., 2017). This underlines the importance of TRPC channel inhibitors and their mode of action to potentially treat TRPC channel associated diseases like mental disorders and FSGS.

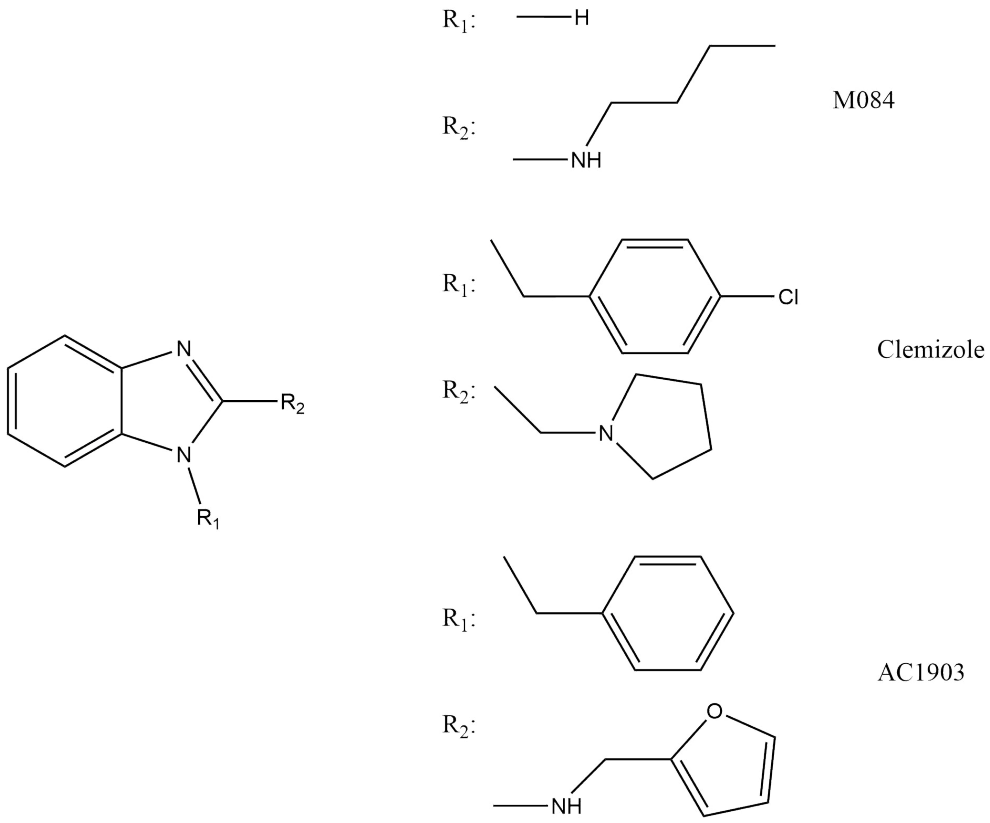

Figure 1.10.: **Chemical structure of the benzimidazole class.** This figure shows the chemical structure of the benzimidazoles and their representatives M084, clemizole and AC1903. The differences in the structures are indicated by a variable residue R.

Flavonoles

The flavonoles are another subgroup of the flavonoids like the isoflavones mentioned in subsection 1.3.1. One representative is galangin (Figure 1.11), a phytochemical compound from the ginger family. Galangin has been shown to inhibit La^{3+} induced TRPC5 currents with an IC_{50} of 0.45 µM (Naylor et al., 2016). The related compounds kaempferol and quercetin also inhibited Gd^{3+} induced TRPC5 currents with an IC_{50} of 3.9 µM and 6.5 µM, respectively (Naylor et al., 2016). A structure-activity-relationship approach led to the synthetic flavonole compound AM12 which inhibits Gd^{3+}-induced TRPC5 currents with an IC_{50} of 0.28 µM. (-)-englerin A-evoked TRPC4 and TRPC5 currents were also inhibited showing 65 % inhibition at a concentration of 5 µM applied AM12. However, on TRPC1/4 and TRPC1/5 heteromers the inhibitory effect was lower, reaching only 20 % inhibition at a concentration of 5 µM AM12 (Naylor et al., 2016).

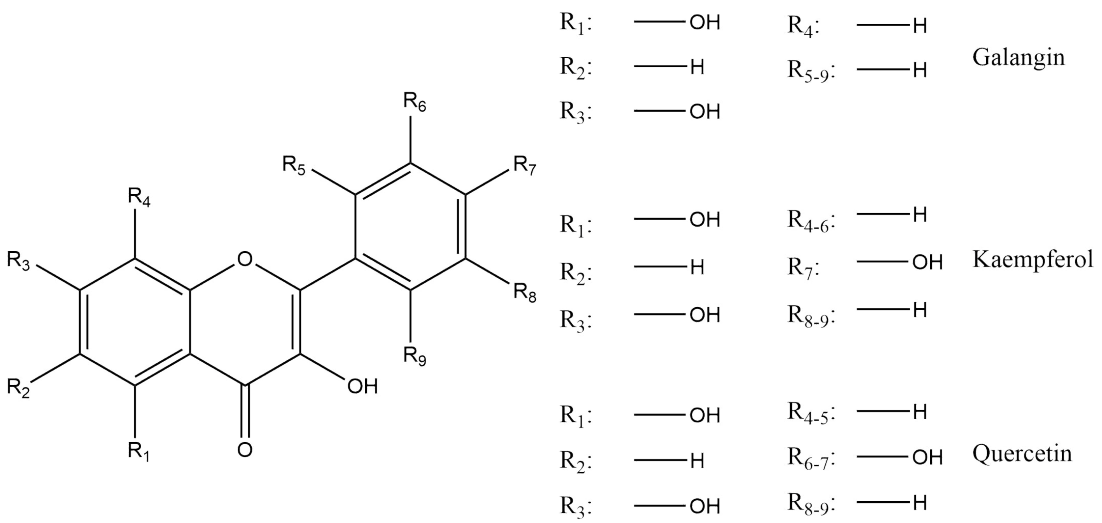

Figure 1.11.: **Chemical structure of the flavonol class.** This figure shows the chemical structure of the flavonols and their representatives Galangin, Kaempferol and Quercetin. The differences in the structure are indicated by a variable residue R.

1.4. Aim of the Study

TRPC5 channels are essentially involved in several physiological and pathophysiological processes and they recently emerged as novel drug targets for the treatment of mental and kidney disorders. However, the activation mechanism of TRPC5 channels is not fully understood until now. Although recent advances in the cryo-EM technique resulted in the elucidation of the first 3D-protein structures of TRPC5 channels, the information remains static and the open pore conformation of the channel is still missing. A deeper knowledge of the exact ligand binding sites and of regulatory regions in the channel structure is essential for novel drug design and it will open new opportunities for virtual drug screening.

The aim of this study is to identify and characterize the binding sites of the two TRPC5 channel activators riluzole and (-)-englerin A in order to get deeper insights into the activation and transduction mechanism of TRPC5 channels.

2. Materials and Methods

2.1. Docking

Molecular docking was carried out using the AutoDock vina plugin (Trott & Olson, 2010) for UCSF Chimera 1.13.1 (Pettersen et al., 2004). The possible binding sites used for the docking runs were selected using qualitative criteria, e.g. size, accessibility, proximity to the membrane and to important channel regions like the gate, TRP helix and VSLD. Furthermore, information from the literature regarding published ligand interaction sites and high quality 3D-protein structures were considered. Since distinct ligand interaction sites and higher quality 3D-structures were continuously published, higher resolved PDB files were used during the progress of the thesis.

All possible options for the docking runs were set to default (see Table 2.1, Table 2.2 and Table 2.3) except "Number of binding modes" which was set to 10 (default=9, see Table 2.3). More detailed information on the settings can be received from the Chimera AutoDock vina Plugin website (Chimera website).

Table 2.1.: **AutoDock vina receptor options.**

Option	Value
Add hydrogens in Chimera	TRUE
Merge charges and remove non-polar hydrogens	TRUE
Merge charges and remove lone pairs	TRUE
Ignore waters	TRUE
Ignore cains of non-standard residues	TRUE
Ignore all non-standard residues	FALSE

Table 2.2.: **AutoDock vina ligand options.**

Option	Value
Merge charges and remove non-polar hydrogens	TRUE
Merge charges and remove lone pairs	TRUE

Table 2.3.: **AutoDock vina advanced options.**

Option	Value
Number of binding modes	10
Exhaustiveness of search	8
Maximum energy difference (kcal/mol)	3

2.1.1. Analysis of Docking Results

The docking results were analyzed using the software LigPlot+ v.2.2 (Wallace et al. (1995) and Laskowski & Swindells (2011)). The criteria for selecting amino acids that possibly interact with the ligand were as follows: how often the exact amino acids appears in the ten docking positions and the quality of the interaction, i. e. the binding energy and type of interaction. The selected amino acids were subsequently exchanged performing site directed mutagenesis (see subsection 2.2.2).

2.2. Molecular Biology

2.2.1. Material and Media

Table 2.4.: **Materials and regents for molecular biology.**

Kit	Catalogue No., Manufacturer
Q5 SDM Kit	E0552S, New England Biolabs, Ipswich, Massachusetts, USA
HiYield Plasmid Mini Kit	30 HYPD100, Süd-Laborbedarf GmbH, Gauting, Germany
NucleoBond Xtra Midi Kit	740410.50, Machery-Nagel GmbH & Co. KG, Düren, Germany

Table 2.5.: **Super optimal broth with catabolite repression (SOC) Medium.** The table shows the composition of the SOC medium.

Substance	Weigh-in quantity [g]
Tryptone	20
Yeast extract	5
NaCl	0.584
KCl	0.186
ad 1000 mL ddH_2O After autoclaving the following was added	
2 M $MgSO_4$, sterile solution	10 mL
2 M Glucose, sterile solution	10 mL

Table 2.6.: **Lysogeny broth (LB) medium**. In the following table the composition of the LB medium is displayed.

Substance	Weigh-in quantity [g]
Tryptone	10
Yeast extract	5
NaCl	10
ad 1000 mL ddH_2O	

2.2.2. Mutagenesis PCR

Table 2.7.: **New england biolabs (NEB) side directed mutagenesis (SDM) kit protocol.**

Reagent	Volume [µL]	Final concentration
Q5 Hot Start High-Fidelity 2X Master Mix	12.5	1X
10 µM forward primer	1.25	0.5 µM
10 µM reverse primer	1.25	0.5 µM
mTRPC5 pIRES2 EGFP plasmid DNA (20 ng μL^{-1})	1	20 ng
ddH_2O	9	

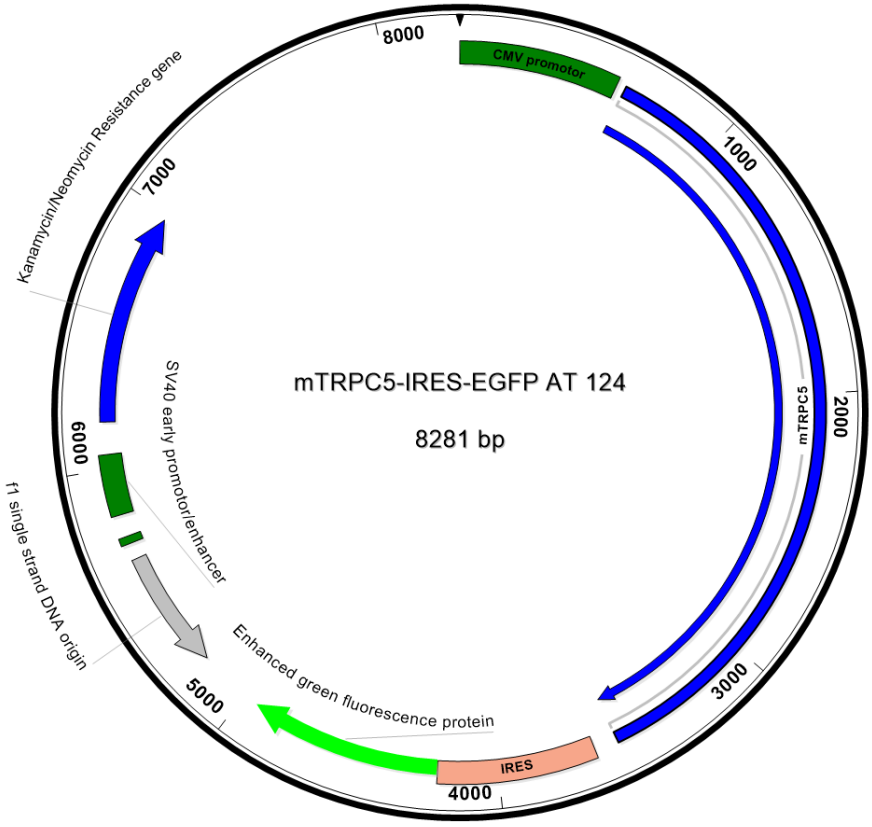

Figure 2.1.: **Vector map of mTRPC5 in a pIRES2-EGFP vector.** The figure displays the vector map of mTRPC5 in the pIRES2-EGFP vector with the respective name and number in the internal database. The plasmid consists of a CMV promotor, the gene of interest mTRPC5, an IRES-sequence, a reporter gene, in this case EGFP, the f1 origin of replication for bacterial plasmid replication, the SV40 early promotor, which enables and improves DNA replication in mammalian systems (Wildeman, 1988) and lastly the resistance gene (in this case Kanamycin/Neomycin).

Table 2.8.: **Polymerase chain reaction (PCR)-program of the SDM.** The primer specific annealing temperatures are listed in Table A.1

Temperature in °C	Time [min:sec]	Cycles
98	0:30	
98	0:10	
Primer specific annealing temperature	0:30	X25
72	5:00	
72	2:00	
8	2:00	

Table 2.9.: **Kinase, ligase, DpnI (KLD) reaction protocol.**

Substance	Volume [µL]
SDM PCR product	1
2X KLD reaction buffer	5
10X KLD enzyme mix	1
ddH_2O	3

The primers were automatically designed using the NEBaseChanger for optimal functionality (NEBaseChanger). Their sequence and annealing temperatures are listed in Table A.1.

The first step in analyzing the mutant TRPC5 channels was to generate a mutant channel in a mammalian expression plasmid (for a vector map see Figure 2.1). The used plasmid was a pIRES2-EGFP vector with a mTRPC5 cDNA. Amino acid exchanges in the mTRPC5 channel were introduced by side directed mutagenesis (SDM) using the Q5 SDM Kit (see Table 2.4) according to the manufacturer's protocol with slight changes (Table 2.7, Table 2.8 and Table 2.9). In brief, a mutagenesis PCR was designed (Table 2.7 and Table 2.8) and an aliquot of the reaction product was simultaneously digested, phosphorylated and ligated in a second experiment, called Kinase, ligase, DpnI (KLD) reaction (part of the SDM kit, see Table 2.9). 5 µL of the KLD reaction product was directly added to 50 µL of chemically competent *E. coli* DH5α cells (according to Inoue et al. (1990)) and incubated on ice for 30 min. After this incubation period, the cells were heat-shocked at 42 °C for 30 s and incubated on ice for another 5 min. Then 950 µL of SOC Medium (see Table 2.5) was added and the cells were incubated at 37 °C for 1 h with gentle shaking. 100 µL of the suspension were plated out on a $LB_{Kanamycin}$ agar plate (50 µg mL^{-1}; see Table 2.6) and incubated for 12–16 h at 37 °C.

2.2.3. Mini Plasmid Preparation

3 mL of $LB_{Kanamycin}$ (50 µg mL^{-1}) were inoculated with one bacterial colony of the selection plates (see subsection 2.2.2) and incubated at 37 °C and 300 rpm for 12–16 h. The overnight culture was then spun at 16 000 ×g for 1 min and the plasmid DNA was prepared with the Hi Yield Plasmid Mini Kit (see Table 2.4) according to the manufacturer's protocol. The plasmid was eluted from the column using 30 µL ddH_2O.

2.2.4. Sequencing

The correct mutation was validated via Sanger sequencing, which was carried out by Eurofins Genomics (Luxembourg). Sequencing primers were designed using the online Sequencing Primer Design Tool by Eurofins Genomics and ordered from Sigma Aldrich (St. Louis, Missouri, USA). For the reaction 300–500 µg of plasmid DNA was mixed with 5 µL of 10 µM sequencing primer in ddH_2O and filled up to 10 µL with ddH_2O.

2.2.5. Midi Plasmid Preparation

To receive higher DNA quality and yield of the mutated plasmid DNA, plasmid preparations which carried the validated mutation were retransformed. 200 mL $LB_{Kanamycin}$ were inoculated with a retransformed *E. coli* colony and incubated at 37 °C and 300 rpm for 12–16 h. The bacterial suspension was then spun at 6000 rpm for 10 min. The plasmid DNA was then prepared with the NuleoBond Xtra Midi Kit (see Table 2.4) according to the manufacturer's protocol.

2.3. Cell Culture

2.3.1. Material, Media and Supplements

Table 2.10.: **Materials and reagents used for cell culture.**

Substance/Material	Catalogue No., Manufacturer
Dishes (10 cm)	83.3902, Sarstedt, Nümbrecht, Germany
Dishes (35 mm)	153066, Thermo Fisher Scientific, Waltham, Massachusetts, USA
	Media and Supplements
Genejuice	70967, Merck KGaA, Darmstadt, Germany
EMEM	M4655, Sigma-Aldrich, St. Louis, Missouri, USA
Pen/Strep	P4333, Sigma-Aldrich, St. Louis, Missouri, USA
FCS	10270-106, Life Technologies/Gibco, Carlsbad, California, USA
DPBS	D8537, Sigma-Aldrich, St. Louis, Missouri, USA
Trypsin-EDTA	T3924, Sigma-Aldrich, St. Louis, Missouri, USA

2.3.2. Media and Supplements

2.3.3. General Procedure

HEK293T cells (ACC635; German Collection of Microorganisms and Cell Cultures GmbH, Braunschweig, Germany) were always cultivated in T75 flasks in eagle's minimum essential medium (EMEM) completed with 10 % fetal calf serum (FCS) and 1 % penicillin/streptomycin (Pen/Strep) (in the following just named EMEM) and incubated at 37 °C and 5 % CO_2. For subculturing HEK293T cells, they were split (see subsection 2.3.4) 1:5 or 1:10 to be confluent after 2 d or 3 d, respectively. For the use in patch clamp experiments cells were seeded at densities of 600 000, 300 000 or 200 000 cells per well in a six well plate, depending if they were transfected (see subsection 2.3.5) the next day, after 2 d or 3 d, respectively. Patch clamp experiments were always carried out 24–30 h post transfection.

2.3.4. Splitting and Seeding

The cell culture medium was aspirated and cells were washed with 10 mL of dulbecco's phosphate buffered saline (DPBS). The DPBS was likewise aspirated

and 2 mL of Trypsin-EDTA was added to the cells. After gentle tapping of the cell culture flask to loosen the adhering cells, 10 mL EMEM was added to stop the trypsin reaction. The cell suspension was then spun at 1200 rpm for 1 min and the supernatant was aspirated. The cell pellet was resuspended in 10 mL EMEM and aliquoted in T75 culture flasks with 20 mL prewarmed EMEM or seeded in 6-well plates with 2 mL prewarmed EMEM.

2.3.5. Transfection

HEK293T cells were transfected using Genejuice (Table 2.10), a non-lipid based chemical transfection reagent, according to the manufacturer's instructions. In brief, 100 µL FCS free EMEM was preincubated with 6 µL Genejuice for 5 min at room temperature. Then 2 µg plasmid DNA were added to the solution and incubated for another 20 min. After incubation, the mixture was applied dropwise to the cells in a 6-well plate.

2.3.6. Transfer in Dishes for Electrophysiological Measurements

For the actual electrophysiological experiments, the cells were transferred from the 6-well plate (see subsection 2.3.4) to single plastic dishes (35 mm, see Table 2.10). The medium was aspirated and the cells were washed with 2 mL DPBS. Subsequently, the DPBS was aspirated, then 300 µL Trypsin-EDTA was applied to the cells and the reaction was stopped by adding 1.5 mL EMEM to the well. The cells were resuspended by pipetting up and down ten times. 300 µL of the cell suspension was added to 2 mL of prewarmed EMEM in the 35 mm dishes.

2.4. Electrophysiology

2.4.1. Material

Table 2.11.: **Materials and reagents used for electrophysiological experiments.**

Substance/Material	Catalogue No., Manufacturer
Reference electrode	E-205, Science Products, Hofheim am Taunus, Germany
Patch pipette capillaries	GB150TF-8P, Science Products, Hofheim am Taunus, Germany
(-)-Englerin A	6492.1, Carl Roth, Karlruhe, Germany
Riluzole hydrochloride	0768/25, Tocris Bioscience, Bristol, United Kingdom

2.4.2. General Procedure

Table 2.12.: **Composition of bath solution B1 with the corresponding concentrations.** The measured osmolality for the solution was accepted in the range of 290–300 mosmol kg^{-1}

Substance	Concentration [mM]
NaCl	140
CsCl	5
$CaCl_2 \cdot 2\,H_2O$	2
HEPES	10
Glucose	10
$MgCl_2 \cdot 6\,H_2O$	1
pH adjusted to 7.4 with NaOH	

Table 2.13.: **Composition of pipette solution P16.** The measured osmolality for the solution was accepted in the range of 290–300 mosmol kg^{-1}. The free Ca^{2+} concentration amounts to 100 nM.

Substance	Concentration [mM]
CsCl	120
$CaCl_2 \cdot 2\,H_2O$	3.949
HEPES	10
BAPTA	10
$MgCl_2 \cdot 6\,H_2O$	1
Na_3-GTP	0.2
NaCl	9.4
pH adjusted to 7.2 with CsOH	

Whole-cell patch clamp recordings were carried out using an EPC 10 USB amplifier (HEKA Elektronik GmbH, Lambrecht, Germany). Patch-clamp micropipettes (see Table 2.11) were pulled using a DMZ-Universal Puller (Zeitz-Instrumente Vertriebs GmbH, Martinsried, Germany) resulting in pipette resistances of 2.0–3.5 MΩ. The measuring electrode consisted of a silver wire which was regularly covered with AgCl using electrochemical oxidation. Reference electrodes were selfmade using silver wires attached to a sintered AgCl pellet (see Table 2.11).

To start a whole-cell patch clamp measurement first the cell-attached configuration was established and the seal quality was evaluated by checking the seal resistance (>1 GΩ). To further record the seal quality, a sealpulse was applied (see Figure 2.3a). The membrane patch beneath the pipette was removed to get access to the cytosol (see Figure 2.2b) in order to establish a whole-cell configuration. The actual measurement was started by applying continuous voltage up-ramps with potentials of −100 to 100 mV with a total duration of 500 ms (Figure 2.3b). The holding potential was −60 mV and the liquid junction potential was set to 4.0 mV. The sample interval was 5 kHz and two bessel filters were

applied subsequently to filter the signal (filter 1 = 10 kHz, filter 2 = 2.9 kHz). The resulting signal was then analyzed according to subsection 2.4.3.

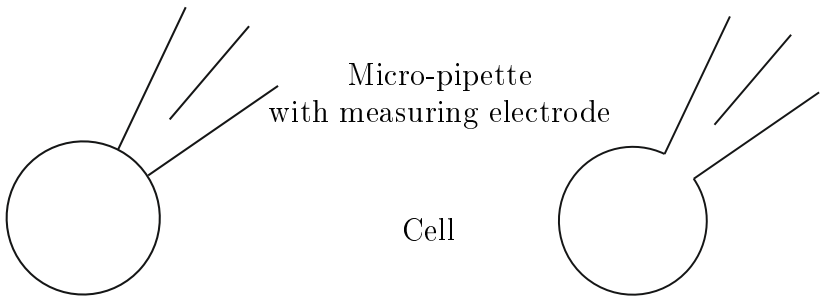

(a) Cell-attached configuration (b) Whole-cell configuration

Figure 2.2.: **Cell-attached and whole-cell configuration.** In this figure, the two configurations cell-attached (a) and whole-cell (b) are shown. The cell-attached configuration was used to evaluate the quality of the gigaohm seal by applying a test pulse (see Figure 2.3a).

2.4.3. Data Analysis

Generally, obtained data of patch clamp measurements are displayed as single current-voltage (IV) or current density voltage (CDV) curves as well as current time courses.

The recorded data is structured like the following: One sweep is defined as one up-ramp (Figure 2.3b) applied at a given timepoint in the experiment resulting in an IV curve. That means sweep 200 is the 200^{th} applied voltage-ramp (Figure 2.3b) in the experiment at the given timepoint, resulting in the 200^{th} IV curve of the experiment.

From these subsequently applied up-ramps and their corresponding injected current values the current time course is constructed. For the inward current I_{min}, the corresponding mean current at the holding potential of -100 mV (see Figure 2.3b, time range in the up-ramp: 15.5–42.8 ms) was plotted againt the timepoint of the sweep. For the outward current I_{max}, the corresponding mean current at the holding potential of 100 mV (see Figure 2.3b, time range in the up-ramp: 409.4–444.6 ms) was plotted against the timepoint of the sweep. This results in a current time course. To generate a current density time course from this, I_{min} and I_{max} were then divided by the cell size expressed by the membrane capacity of the cell C_M, respectively. This results in the current densities CD_{min} and CD_{max}. Those were subtracted by the IV offset before stimulus application and plotted against the time-point of the sweep to result in a current density time course.

As follows, three CDV curves were extracted and displayed. One CDV curve was extracted before stimulus application and one during stimulus application of riluzole and (-)-englerin A, respectively. First, the basal current level in the current time course was estimated by choosing a representative value before application of a stimulus and the respective IV curve was exported. Then the peak current in the presence of the applied stimuli were defined as the maximum outward-current value. For the following analysis an R-script written by Christian Hermann was used.

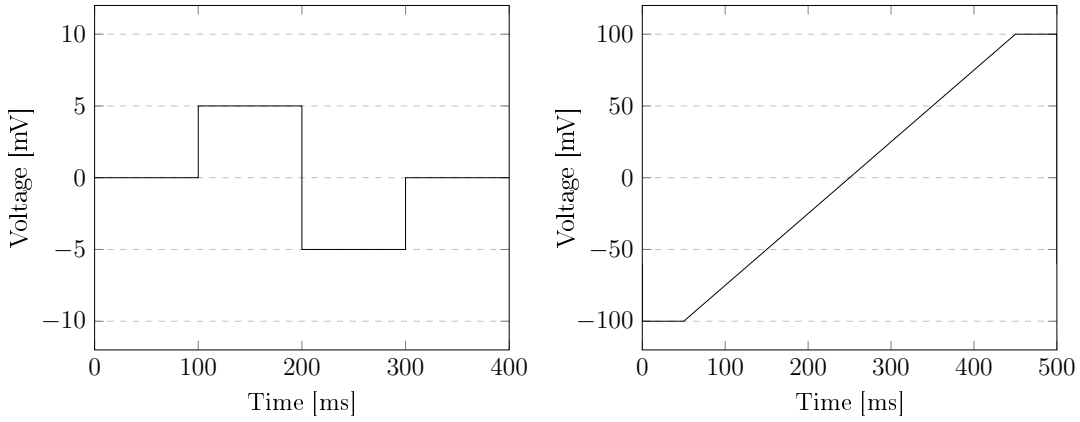

(a) Sealpulse

(b) Up-ramp protocol

Figure 2.3.: **Sealpulse and up-ramp protocol.** In this figure, the two command voltage protocols sealpulse (a) and up-ramp (b) are displayed. The sealpulse was used to record the seal quality in the cell-attached configuration (see Figure 2.2a). The up-ramp protocol was continuously applied in the whole-cell configuration (Figure 2.2b).

First, the IV-curves were offset corrected by subtracting the current value at 0 mV. In the next step current density values were calculated by dividing the current response by the cell capacity to normalize for the cell size. The resulting CDV curves are displayed from −100 to 100 mV which corresponds to the time-range from 48–452 ms of the applied voltage up-ramp.

2.5. Surface Expression of mTRPC5

Unless otherwise mentioned, all chemicals were obtained from Sigma-Aldrich (St. Louis, Missouri, USA) or Carl Roth (Karlsruhe, Germany).

2.5.1. Material

Table 2.14.: **Materials and reagents used for western blot experiments.**

Substance/Material	Catalogue No., Manufacturer
Pierce™ Cell Surface Biotinylation and Isolation Kit	A44390, Thermo Fisher Scientific, Waltham, Massachusetts, USA
HALT Protease Inhibitors	87786, Thermo Fisher Scientific, Waltham, Massachusetts, USA
Bradford reagent	K015.1, Carl-Roth, Karlsruhe, Germany
BSA	A7030, Sigma-Aldrich, St. Louis, Missouri, USA
Methanol, blotting grade	0082.3, Carl Roth, Karlsruhe, Germany
SDS gels (Mini Protean TGX 4–15 %)	45610884, Bio-Rad, Hercules, California, USA
PVDF membrane 0.45 µm	T830.1, Carl-Roth, Karlsruhe, Germany
Gel chamber	1703930, Bio-Rad, Hercules, California, USA
Marker Spectra BroadRange	26634, Thermo Fisher Scientific, Waltham, Massachusetts, USA
Antibodies used	
Rabbit anti TRPC5 777	Kindly provided by Veit Flockerzi
Anti NaK-ATPase HRP	ab185065, Abcam, Cambridge, UK
Goat anti rabbit IgG, HRP-linked	7074S, Proteintech, Rosemont, Illinois, USA

Table 2.15.: **Composition of the 10X tris-glycine (TG) buffer.**

Substance	Amount [g]	Final concentration [M]
Tris base	30.3	0.25
Glycine	144.2	1.92
Ad 1000 mL ddH_2O		

Table 2.16.: **Composition of the tris-glycine methanol (TGM) buffer.**

Substance	Amount [mL]	Final concentration
10X TG buffer	100	0.025 M Tris, 0.192 M glycine
Methanol	200	20 %
Ad 1000 mL ddH_2O		

Table 2.17.: **Composition of the 10X tris buffered saline (TBS) buffer.**

Substance	Amount [g]	Final concentration [M]
Tris	24.23	0.2
NaCl	80.06	1.37
Ad 1000 mL ddH_2O		

Table 2.18.: **Composition of the 1X TBS buffer.**

Substance	Amount [mL]	Final concentration
10X TBS	100	20 mM; 137 mM NaCl
Ad 1000 mL ddH_2O		

Table 2.19.: **Composition of the buffer tris buffered saline + Tween 20 (TBST).**

Substance	Amount [mL]	Final concentration
10X TBS	100	20 mM; 137 mM NaCl
Tween 20	1	0.1 %
Ad 1000 mL ddH_2O		

Table 2.20.: **"Mild" stripping buffer.** The protocol was taken from the Thermo Fisher website (Link to the website).

Substance	Amount
Glycine	15 g
SDS	1 g
Tween 20	10 mL
ddH_2O	800 mL
adjust pH to 2.2 with HCl	
Ad 1000 mL ddH_2O	

Table 2.21.: **Detection enhanced chemoluminescence (ECL) reagent buffer S-B.** The protocol was obtained from the Schwer laboratory at University of California, San Francisco (UCSF) (unpublished data) and modified from Haan & Behrmann (2007) and Kricka et al. (1996)

Substance	Amount [mL]	Final concentration [mM]
30 % (9.8 M) H_2O_2	0.0433	10.6
1 M Tris-HCl, pH 8.8	4	100
Ad 40 mL ddH_2O		

Table 2.22.: **Detection substrate buffer S-A.** The protocol was obtained from the Schwer laboratory at UCSF (unpublished data) and modified from Haan & Behrmann (2007) and Kricka et al. (1996). Luminol was prepared as a 250 mM stock solution by dissolving 1 g in 22.57 mL dimethyl sulfoxide (DMSO). 4-iodophenylboronic acid (4-IPBA) was prepared as a 100 mM stock solution by dissolving 1 g in 40.35 mL DMSO.

Substance	Amount [mL]	Final concentration [mM]
250 mM Luminol	0.4	2.5
100 mM 4-IPBA	1.6	4
1 M Tris-HCl, pH 8.8	4	100
Ad 40 mL ddH_2O		

2.5.2. Surface Biotinylation

Biotinylation of Surface Proteins

HEK293T cells were cultivated as mentioned in subsection 2.3.3 and subsection 2.3.4 and were seeded to a density of 2 500 000 cells per 10 cm dish (see Table 2.10) with 10 mL of prewarmed EMEM. The day after seeding, the cells were transfected as mentioned before (see subsection 2.3.5), using 500 µL FCS free EMEM, 30 µL Genejuice and 10 µg plasmid DNA. 24–30 h post transfection the medium was aspirated and the cells were washed with 10 mL room temperature phosphate buffered saline (PBS) (part of the Pierce™ Surface expression kit, see Table 2.14). After aspirating the PBS, cells were covered with 10 mL of sulfo-succinimidyl-2-(biotinamido)ethyl-1,3-dithiopropionate (Sulfo-NHS-SS-Biotin) in PBS (according to the manufacturer) and incubated for 30 min at 4 °C. In the next step, the PBS got aspirated and the cells were washed with 10 mL of ice-cold TBS. After washing, the TBS got aspirated and another 10 mL of ice-cold TBS were added and the cells were scraped off the plate using a cell-scraper. The scraped cells were collected in a tube and a 1 mL sample was taken for possible future real-time quantitative polymerase chain reaction (qPCR) analysis. The scraped plates were rinsed with another 10 mL ice-cold TBS which were then added to the collection tube. The cell suspension was then spun at 500 xg for 3 min at 4 °C and the supernatant was discarded.

Cell Lysis

500 µL lysis buffer of the Pierce™ Surface expression kit were completed with the addition of 5 µL protease inhibitor cocktail (see Table 2.14) and 500 µL were added to the cell pellet. The suspension was well mixed 20 times and transferred to a 1.5 mL reaction tube. Afterwards, the suspension was incubated on ice for 30 min with thorough mixing for 5 s at the beginning and end of the incubation period. Then the cell lysate was centrifuged at 15 000 xg for 5 min at 4 °C. The supernatant was used for the further experiments and the cell pellet was discarded.

Bradford Assay

For every assay a new standard curve was measured using bovine serum albumin (BSA) concentrations of 0, 20, 40, 60, 80 and 100 µg mL^{-1}. 50 µL of the standard and sample were pipetted in a 96-well plate and 200 µL of 1X Roti-Quant (see Table 2.14) was added, respectively (resulting in BSA concentrations of 0–20 µg mL^{-1}). After 5 min of incubation the absorption at 595 nm was measured using a ClarioStar micro-plate reader (BMG Labtech, Ortenberg, Germany).

Isolation of Labeled Proteins

After measuring the protein content of the samples (see subsection Bradford Assay), all sample volumes were equalized to the least amount of protein found in all samples. Therefore all NeutrAvidin™ columns were loaded with an equal amount of protein. 250 µL of NeutrAvidin™ agarose slurry was added to a column and centrifuged at 1000 xg for 1 min. Equal amounts of protein were added to the columns and they were incubated for 30 min on an end-over-end rotator. After the incubation step, the columns were centrifuged at 1000 xg for 1 min and the flowthrough was kept for potential further experiments. Afterwards the columns were washed 4 times with 500 µL wash buffer each and subsequent centrifugation at 1000 xg for 1 min. 25 µL dithiothreitol (DTT) stock solution were added to 225 µL of elution buffer resulting in a 10 mM concentration of DTT. 200 µL elution buffer were added to the column which was then incubated for 30 min on an end-over-end rotator at room temperature. To elute the protein, the columns were centrifuged at 1000 xg for 2 min.

2.5.3. SDS-PAGE

Table 2.23.: 1 M **Tris-HCl buffer pH 6.8.**

Substance	Amount [g]	Final concentration [M]
Tris base	12.114	1
Adjust pH to 6.8 with HCl		
Ad 100 mL ddH_2O		

Table 2.24.: **4X Laemmli buffer.** The protocol is taken from LAEMMLI (1970). The buffer got aliquoted before addition of 2-mercaptoethanol (BME) and stored. Just prior to use, the BME was added.

Substance	Amount	Final concentration
Bromphenol Blue	2 mg	0.004 %
SDS	4 g	8 %
Glycerol	20 mL	40 %
1 M Tris-HCl pH 6.8	12.5 mL	0.25 mM
Ad 40 mL ddH_2O		
Add just prior to use		
BME	10 mL	20 %

Table 2.25.: **Buffer tris-glycine SDS (TGS).**

Substance	Amount [mL]	Final concentration
10X TG buffer	100	0.025 M Tris; 0.192 M glycine
10 % SDS solution	10	0.1 %
Ad 1000 mL ddH_2O		

5 µL of 4X Laemmli buffer (see Table 2.24) were added to 15 µL of the eluted protein sample (see subsubsection Isolation of Labeled Proteins) and incubated at 70 °C for 10 min. The loaded sample volume was kept equal between the pockets because the protein content got normalized before the column was loaded (see subsubsection 2.5.2). 20 µL sample and 10 µL marker (Table 2.14) were loaded onto the sodium dodecyl sulfate (SDS)-Gel (Table 2.14). The gel chamber (Bio-Rad Trans Blot Cell, Table 2.14) was filled with TGS-buffer (Table 2.25) and the run was performed using a BioRad PowerPac HC Power Supply (Bio-Rad, Hercules, California, USA) at 100 V for about 1.5 h.

2.5.4. Western Blot

The western blot experiments were executed in a wet tank setup in the same electrophoresis system (Table 2.14) as the sodium dodecyl sulphate–polyacrylamide gel electrophoresis (SDS-PAGE). For the transfer itself TGM (Table 2.16) buffer was used. A polyvinyliden flouride (PVDF) membrane with a pore size of 0.45 µm (Table 2.14) was selected for blotting due to the better protein binding capability and the better suitability for low abundance proteins. Before transfer, the membrane was activated with methanol (MeOH) for 30 s, and equilibrated with TGM buffer. For the transfer a constant voltage of 100 V for 1 h was set. To prevent overheating, the transfer chamber was cooled with cooling packs and placed into an ice-box. Overheating may occur with a high voltage and low time transfer protocol. After transfer, the membrane was cut to size and submerged in TBS. The membrane was then blocked in TBST containing 5 % (w/w) skim milk powder for 2 h at room temperature with gentle agitation. After blocking, the membrane was washed once with TBST and incubated with the primary antibody (anti TRPC5

1:200; anti sodium potassium ATPase (NaK-ATPase) 1:5000; see Table 2.14) in TBST containing 5 % (w/w) BSA for 12–18 h at 4 °C with gentle agitation. The antibody was used up to 2 times within one week. The membrane was washed three times with TBST for 5 min with gentle agitation at room temperature. After washing, the membrane was incubated with the secondary antibody (1:2000; goat anti rabbit antibody, Table 2.14) in TBST containing 5 % (w/w) BSA for 1 h at room temperature with gentle agitation. This step was unnecessary for the anti NaK-ATPase antibody because it is directly conjugated to horseraddish peroxidase (HRP). After incubation with the secondary antibody, the membrane was washed three times with TBST for 5 min with gentle agitation at room temperature and stored in TBS until detection. For the detection of bands on the blot, the membrane was covered with equal volumes of detection solution A (S-A) and detection solution B (S-B) (Table 2.22), covered with a plastic foil and detected using a BioRad ChemiDoc Imaging System (Bio-Rad Laboratories, Inc., Hercules, California, USA). After detection of the TRPC5 antibody the membrane was stripped. Due to roughly the same molecular mass of TRPC5 and NaK-ATPase, it was not possible to detect both proteins either simultaneously or to cut the blot and work with two separate blots. For the stripping, the membrane was washed three times with TBST after the detection to wash off any excess detection reagent. After that, the membrane was incubated at room temperature for 20 min in stripping buffer (Table 2.20) with gentle agitation. Thereafter, the membrane was washed with TBST to equilibrate the pH-value. The membrane was then re-blocked according to the above mentioned blocking step and incubated in the anti-NaK-ATPase antibody in 5 % BSA-TBST over night for 12–18 h at 4 °C with gentle agitation. The detection step was carried out as mentioned above.

2.5.5. Quantification of the Surface Expression Results

The western blot bands were quantificated using the .raw tiff format. The used software was ImageStudio Lite v5.2.5. The defined square-size to measure the intensity was hold equal between the bands of the same blot and were automatically background subtracted. The background was defined automatically as a small margin around the boarder of the actual quantification-square (local background). Due to differences in the observed intensity of the expression control bands, the signal was normalized to the internal expression control and subsequently to the normalized wildtype expression, resulting in a normalized expression of the given mutant compared to the wildtype.

3. Results

3.1. Two Activators as an Expression Estimation

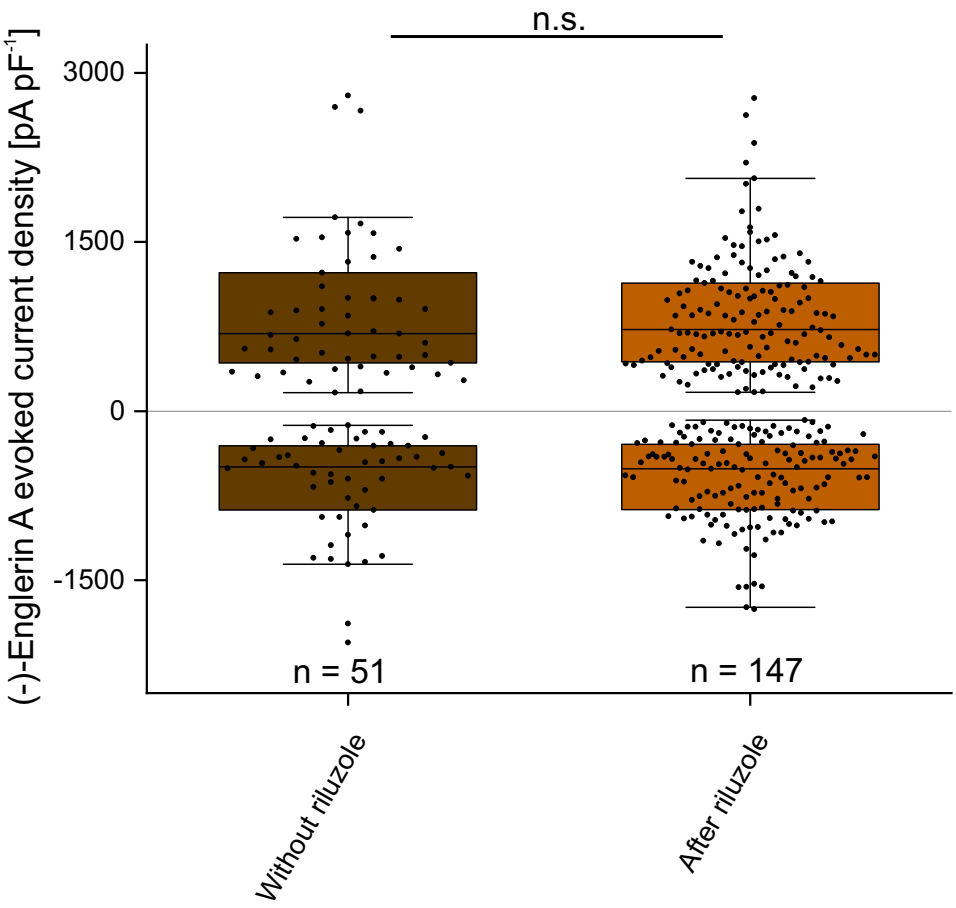

Figure 3.1.: **Difference between (-)-englerin A evoked current densities after a prior or no riluzole activation.** In this figure the difference in the (-)-englerin A evoked current densities are shown, depending on a prior activation with riluzole or no prior activation stimulus. The used statistical test was the Mann-Whitney-U-Test, n stands for the number of independent experiments.

The TRPC5 channel activators riluzole and (-)-englerin A both have distinct chemical structures and belong to different chemical classes. Furthermore, riluzole selectively activates TRPC, whereas (-)-englerin A activates TRPC4 and TRPC5. Therefore one hypothesis was that the TRPC5 channel activators riluzole and (-)-englerin A have different activation mechanisms and act on different

independent ligand binding sites. Thus, riluzole was used as an expression control for the functional expression of potential (-)-englerin A binding mutants and vice versa. Without such an internal control, non-functional channels could be mistaken for binding mutants. Performing whole-cell patch-clamp measurements with TRPC5 overexpressing HEK293T cells no significant changes in (-)-englerin A-induced current densities before and after riluzole application were found (Figure 3.1). This suggests that the application of riluzole before (-)-englerin A does not change the maximal induced (-)-englerin A evoked current density. Therefore this application order can be used as a control for functional channel expression of riluzole and (-)-englerin A binding mutants, respectively.

3.2. Docking Project I

3.2.1. Membrane-Close Cytosolic Channel Regions

The interface between membrane and cytosol is an interesting channel region, because of the close proximity to important channel features like the TRP-domain, the VSLD and the lower gate. The VSLD is named after the voltage-sensor domain (VSD) of voltage-gated ion channels. In voltage-gated ion channels the VSD senses membrane depolarization and mediates channel gating (Hille, 2001; Tao et al., 2010). Even though TRPC channels are ligand-gated and not voltage-gated, they posses a similar structure. In the TRPC5 protein structure the region around the VSLD offers different cavities and possible binding pockets. This includes the biggest monomeric cavity of the channel. Because of the numerous possibilities of potential ligand interactions, in total seven dockings were carried out regarding this channel part. Before a TRPC5 protein structure was published, only the cryo-EM structures of TRPC3, 4 and 6 were available (Tang et al., 2018; Fan et al., 2018; Vinayagam et al., 2018; Duan et al., 2018b). Because (-)-englerin A serves as an activiator of TRPC4 and 5, it led to the assumption, that both channels possess a similarly located (-)-englerin A binding site. Furthermore, due to their structural and highest sequential similarity in the TRPC family (Clapham et al., 2001; Plant & Schaefer, 2005), TRPC4 and 5 were regarded as equal in the dockings. Therefore the first docking project was carried out using the TRPC4 PDB file with the accession number 5Z96 (Duan et al., 2018b). The resulting interacting amino acids were translated from TRPC4 to TRPC5 and the actual measurements very conducted in TRPC5 overexpressing cells.

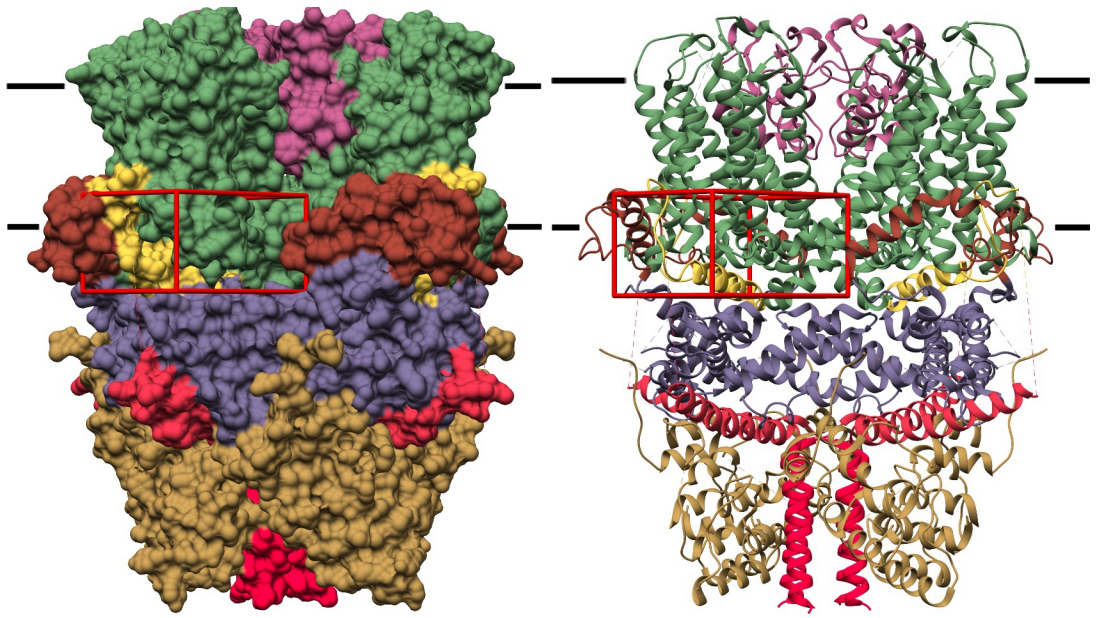

(a) TRPC5 surface structure with the docking cube at position I.

(b) TRPC5 ribbon structure with the docking cube at position I.

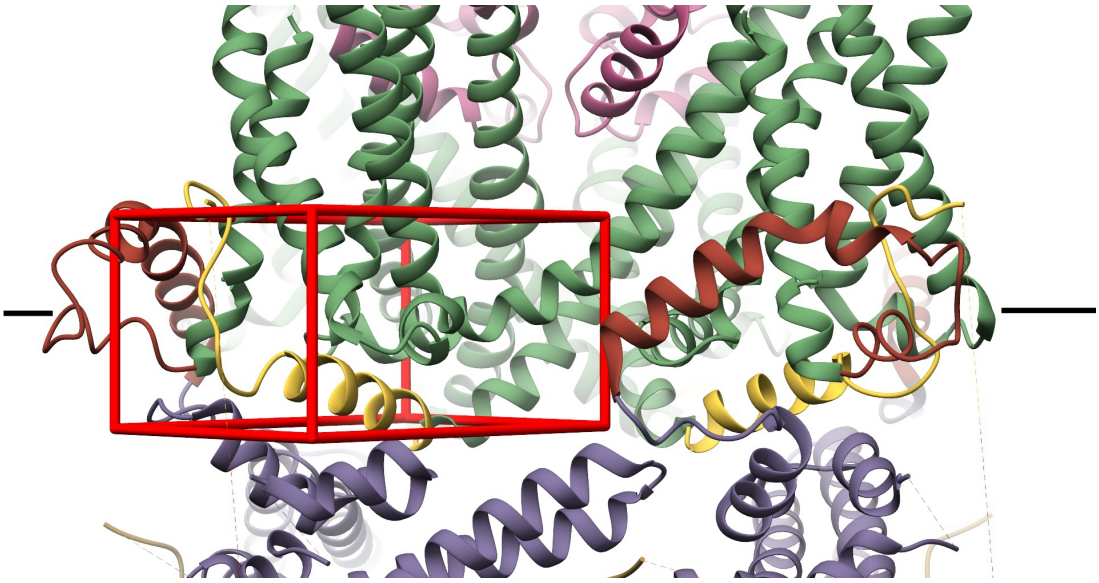

(c) TRPC5 ribbon structure with a detailed view of docking cube I.

Figure 3.2.: **Docking area in cavity I.** In this figure, Cavity I is shown using the 3D-structure of TRPC5 (PDB: 6AEI, Duan et al. (2019)). The 3D structure is either presented with its surface structure **(a)**, or ribbon structure **(b)** and colored according to Figure 1.1. Subfigure **(c)** is a close-up view of (b) for better visualization of the docking area. Horizontal black lines indicate the cell membrane.

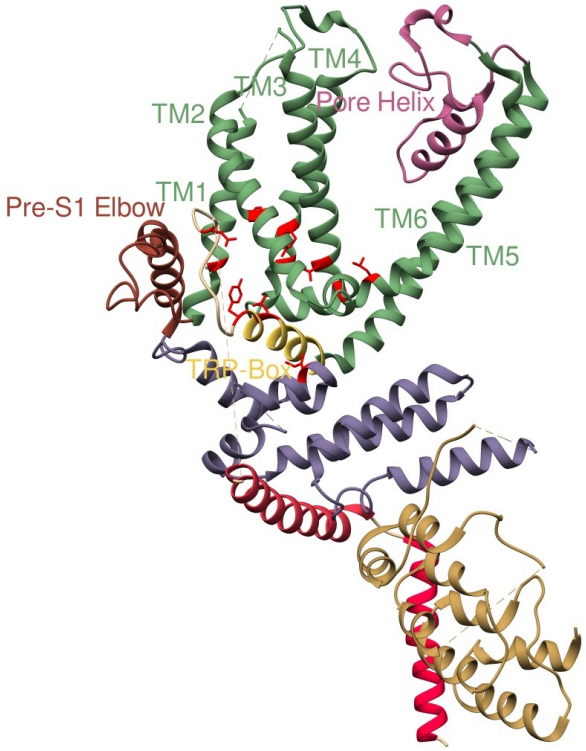

(a) Overview of the amino acids potentially involved in a binding of riluzole or (-)-englerin A and their respective orientation and position (red residues).

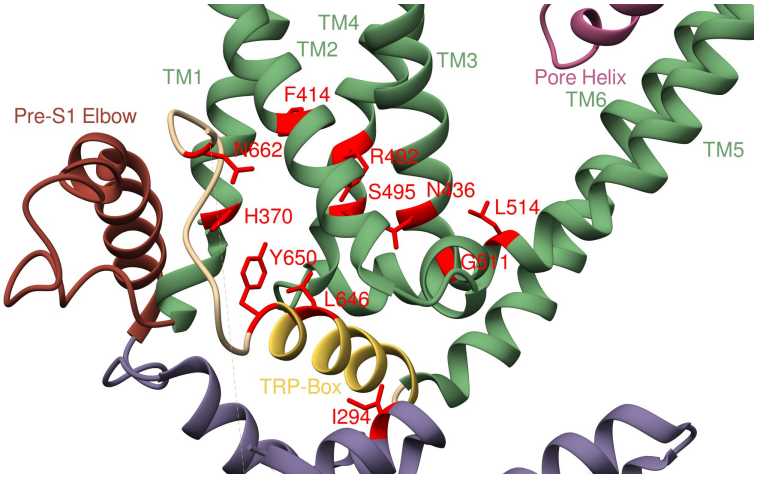

(b) Detailed view of the amino acids potentially involved in binding of riluzole or (-)-englerin A and their respective orientation and position (red residues).

Figure 3.3.: **Potential ligand binding amino acids of cavity I.** In this figure, TRPC5 (PDB: 6AEI) and amino acids which are potentially involved in a binding of riluzole or (-)-englerin A are displayed with their respective orientation and position (red residues). Channel elements are colored according to Figure 1.1.

The first three dockings were carried out with (-)-englerin A, A54 and englerin B in the same docking area (docking project I, see Figure 3.2). A54 is a (-)-englerin A analogue with minimal structural changes which has a competitive antagonistic effect on the (-)-englerin A induced TRPC5 currents (Rubaiy et al., 2018b). Englerin B is showing a much lower toxic effect on renal cancer cell lines (Ratnayake et al., 2009). Therefore it binds TRPC5 not as effectively as (-)-englerin A.

All three substances were used for the docking and the positions were compared. Amino acids, which were interacting with the glycolic acid group of (-)-englerin A but did not show up in the dockings of A54 and englerin B were especially interesting hits, because englerin B as well as A54 do not possess this functional group. Secondly, amino acids which appeared most often were considered. Thirdly, amino acids which could play a gatekeeper role for the pocket entrance were considered. The docking area was defined as shown in Figure 3.2. This cavity was chosen because of the size of the pocket, the proximity to the plasma membrane and the previously described channel features. The cavity is easily accessible from the interface between the inner membrane leaflet and cytosolic side. The docking run was realized in the whole cavity, but because of the cavity dimensions the results were split into four subcavities. In Figure 3.2 the docking cube is shown using the example of TRPC5, for better comparison between the dockings.

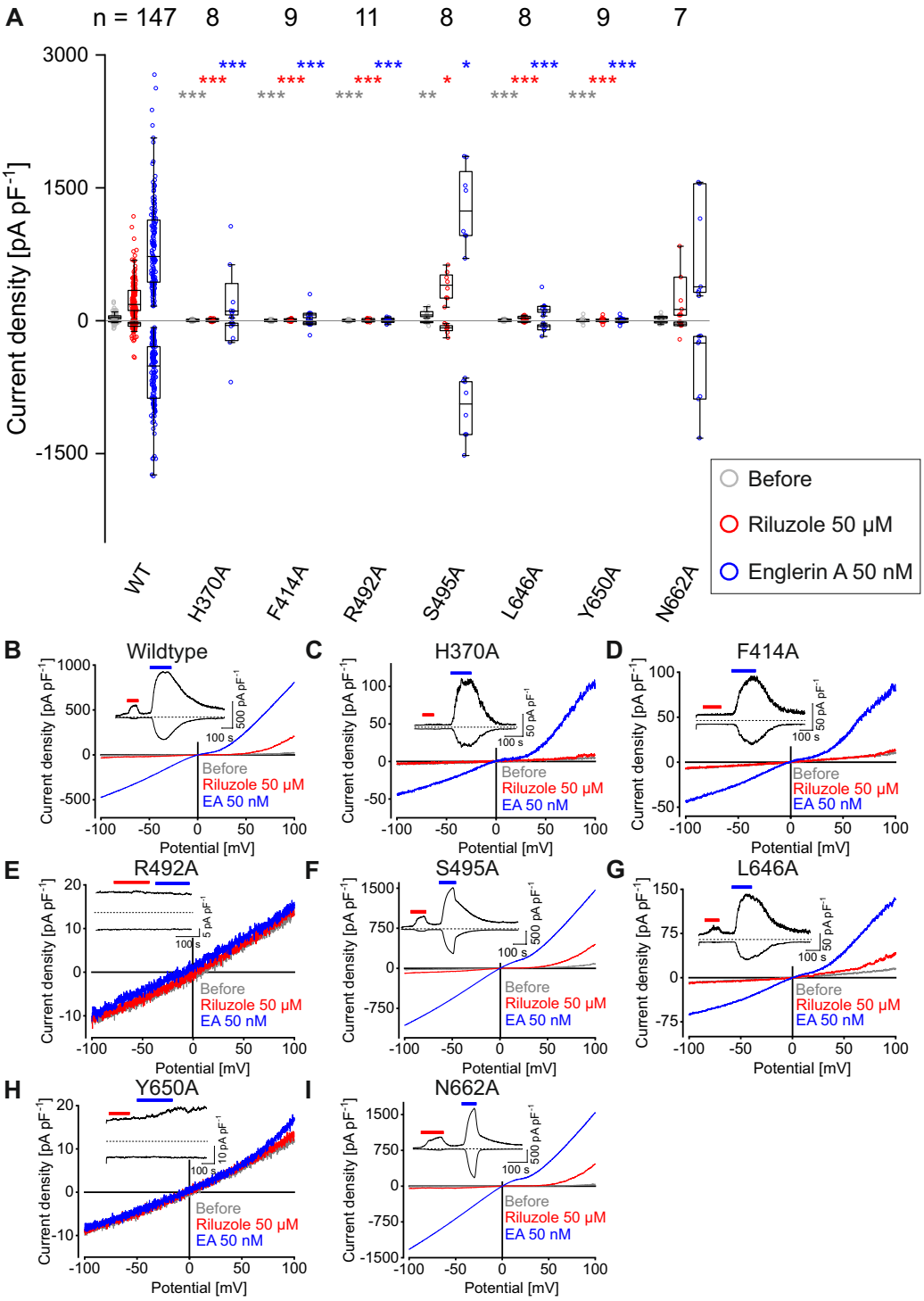

Figure 3.4.: **Whole-cell measurements of potential ligand binding amino acids in cavity I. (A)** shows the maximal and minimal current density at the potentials 100 mV and −100 mV evoked by the given treatment, respectively. Their respective distribution is indicated by the median (horizontal line) and 50 % of the data points (box) as well as the 1.5 × interquartile range (IQR) (whiskers). The number of independent experiments is indicated by numbers over the plot. * $P < 0.05$, ** $P < 0.01$, *** $P < 0.001$ (Tested against Wildtype (WT); Mann-Whitney-U). **(B-I)** show representative single CDV curves during the given treatments selected at maximal current responses. The insets show the corresponding current density time course of the same measurement.

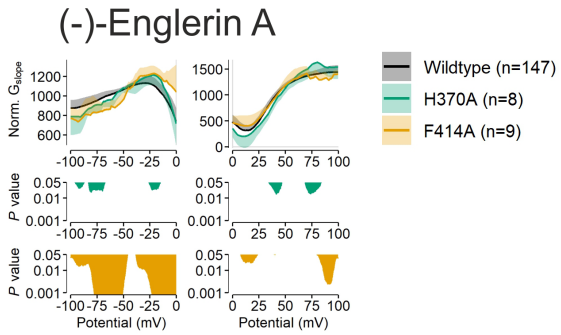

Figure 3.5.: **Normalized slope conductance (NSC) of potential ligand binding amino acids in cavity I.** This figure shows the calculated NSC (Hermann et al., 2022) of the given mutation (top) $\pm SD$ compared to the wildtype NSC during the given treatment (bottom). Statistical significance was analyzed using the Mann-Whitney-U-test. n indicates the number of independent experiments.

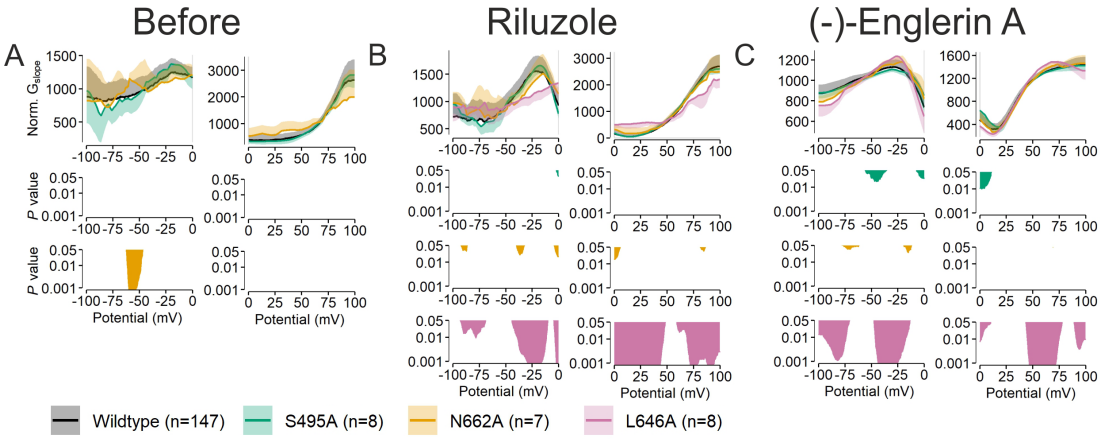

Figure 3.6.: **NSC of potential ligand binding amino acids in cavity I.** This figure shows the calculated NSC (Hermann et al., 2022) of the given mutation (top) $\pm SD$ compared to the wildtype NSC during the given treatment (bottom). Statistical significance was analyzed using the Mann-Whitney-U-test. n indicates the number of independent experiments.

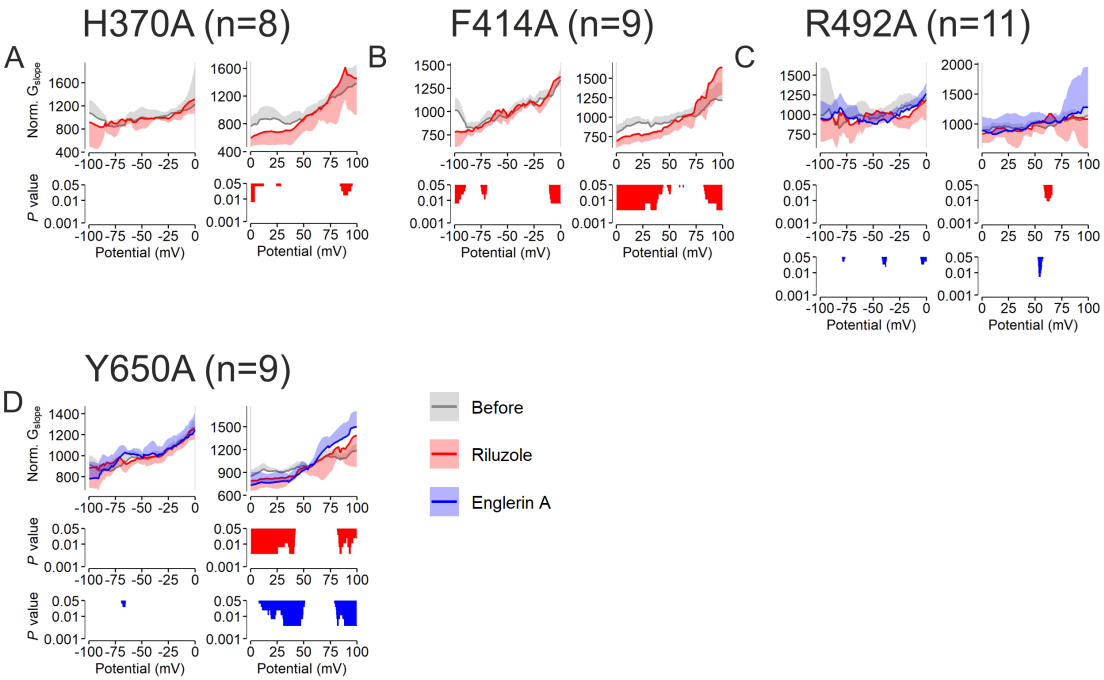

Figure 3.7.: **NSC of potential ligand binding amino acids in cavity I.** This figure shows the calculated NSC (Hermann et al., 2022) of the given mutation (top) $\pm SD$. The given treatment is compared with no treatment (bottom). Statistical significance was analyzed using the Wilcoxon signed-rank test. n indicates the number of independent experiments.

Next, amino acids that might be involved in the (-)-englerin A-binding were selected based on the previously described criteria and exchanged to alanine by site directed mutagenesis. After the exchange and heterologous expression in HEK293T cells, the mutant channels were characterized via whole-cell patch-clamp measurements. The potential (-)-englerin A binding amino acids which were chosen for mutagenesis are displayed in Figure 3.3 for better visualization of their position and orientation. Amino acids His^{370}, F^{414}, L^{646}, Tyr^{650} and Arg^{492} show frequent interactions in different docking poses (see Appendix B) and were therefore considered as candidates for exchanges. Amino acids Ser^{495} and Asn^{662} were chosen because they might interact with the glycolic acid group of (-)-englerin A.

The amino acid exchanges histidine at position 370 and phenylalanine at position 414 for alanine show a strong significant overall current density reduction (Figure 3.4A). But the CDV curves (Figure 3.4C and D) still show TRPC5 characteristics during (-)-englerin A application indicating a still functional channel. The NSC, which is a tool for quantitative analysis of current-voltage relations (Hermann et al., 2022), suggests a very similar course during the (-)-englerin A application of mutant H370A and a very similar course of the outward current during the (-)-englerin A application of mutant F414A compared to the wildtype, respectively (Figure 3.5). However, the (-)-englerin A evoked inward NSC is significantly changed over the whole course (Figure 3.5, bottom left). Surprisingly, the riluzole activation peaks in the current density time courses (Figure 3.4C and D, embedded figure) are completely abolished and the corresponding CDV curve (Figure 3.4C and D, red) is congruent with the CDV curve before activator application (Figure 3.4D, gray). The NSC comparing H370A before activator application and during riluzole application are very similar with only a few significant changes in the outward current, suggesting that this mutant is not sensitive to riluzole (Figure 3.7A).

The mutant F414A shows a similar NSC in the inward current when comparing the riluzole evoked currents with the basal currents before application of any activator, but in the outward current, the NSC is slightly different (Figure 3.7B). Taken together, the two amino acids Phe^{414} and His^{370} likely represent riluzole binding candidates.

Amino acid exchanges arginine at position 492 and tyrosine at position 650 for alanine result in nonfunctional channels as indicated by a strong, significant reduction of current densities before and after subsequent application of 50 µM riluzole and 50 nM (-)-englerin A (see Figure 3.4A). The CDV curve similarly shows a nonfunctional channel with no changes in the current density during application of 50 µM riluzole and 50 nM (-)-englerin A (Figure 3.4E and H). For R492A, the NSC shows that the riluzole and (-)-englerin A evoked currents have a similar course as the basal currents before activator application (Figure 3.7C), suggesting a non-functional channel.

However, Y650A shows significant changes in the NSC of the outward current between 0–40 mV and 80–100 mV comparing the basal NSC before application of a activator with the NSC during riluzole and (-)-englerin A application, respectively (Figure 3.7D). This suggests at least some channel response to both activator stimuli.

The amino acid exchanges serine at position 495 and arginine at position 662 for alanine show no significant reductions in the activator evoked current densities

(Figure 3.4A), no changes in the CDV curves (Figure 3.4F and I) and no changes in the current density time courses (Figure 3.4F and I, embedded figures), indicating a functional channel and suggesting that the mutations have no effect on activator binding. The NSC similarly shows only very few significant changes for these two mutants comparing the NSC before and during activator application with the wildtype, respectively (Figure 3.6 green and yellow).

The exchange leucine at position 646 for alanine on the other hand shows a significant reduction in current densities before and after application of both activators, respectively (Figure 3.4A), but the current density time course (Figure 3.4G, embedded figure), as well as the CDV curve (Figure 3.4G) show a similar picture like the wildtype channel with a roughly four times lower riluzole evoked current density than the (-)-englerin A evoked current density. However, the NSC shows significant changes when comparing the riluzole and (-)-englerin A evoked IV curves with the wildtype.

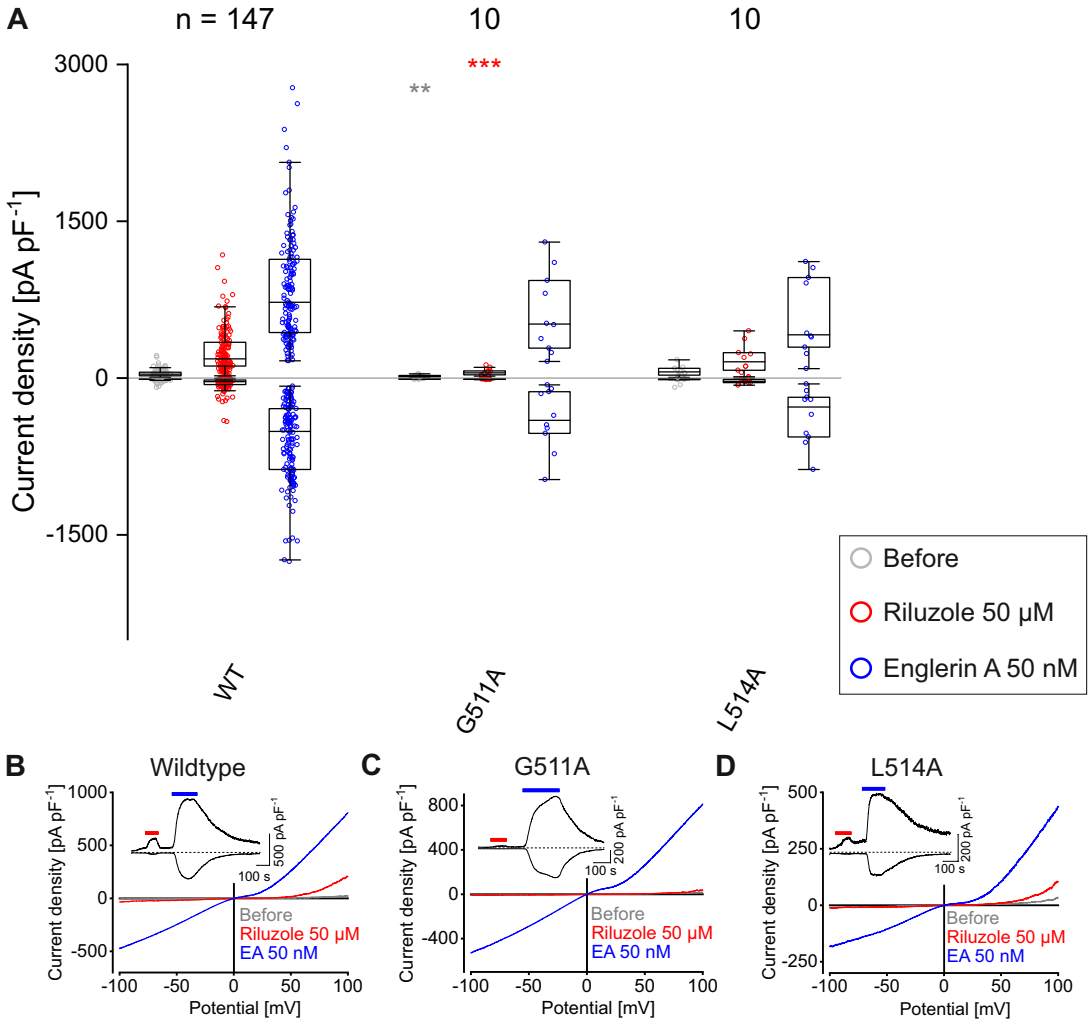

Figure 3.8.: **Whole-cell measurements of potential ligand binding amino acids in cavity I. (A)** shows the maximal and minimal current density at the potentials 100 mV and −100 mV evoked by the given treatment, respectively. Their respective distribution is indicated by the median (horizontal line) and 50 % of the data points (box) as well as the 1.5 × IQR (whiskers). The number of independent experiments is indicated by numbers over the plot. * $P < 0.05$, ** $P < 0.01$, *** $P < 0.001$ (Tested against Wildtype (WT); Mann-Whitney-U). **(B-D)** show representative single CDV curves during the given treatments selected at maximal current responses. The insets show the corresponding current density time course of the same measurement.

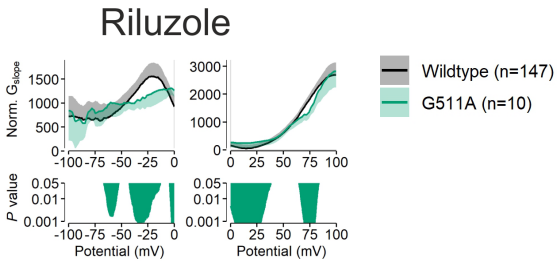

Figure 3.9.: **NSC of potential ligand binding amino acids in cavity I.** This figure shows the calculated NSC (Hermann et al., 2022) of the mutation G511A (top) $\pm SD$ compared to the wildtype NSC during riluzole activation (bottom). Statistical significance was analyzed using the Mann-Whitney-U-test. n indicates the number of independent experiments.

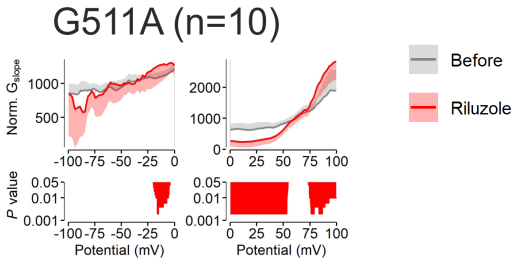

Figure 3.10.: **NSC of potential ligand binding amino acids in cavity I.** This figure shows the calculated NSC (Hermann et al., 2022) of mutation G511A (top) $\pm SD$. The riluzole evoked NSC is compared with the basal NSC before applcation of riluzole (bottom). Statistical significance was analyzed using the Wilcoxon signed-rank test. n indicates the number of independent experiments.

Gly^{511} and L^{514} show a lot of interactions in the different docking positions and were therefore chosen as potential candidates for ligand binding. Their respective position and orientation is shown in Figure 3.3. The exchange glycine at position 511 for alanine shows a strong significant reduction in the riluzole evoked current density, but not in the (-)-englerin A evoked current density (Figure 3.8). This again suggests a riluzole specific effect of the mutation G511A. In the current density time course (Figure 3.8C, embedded figure) as well as in the CDV curve (Figure 3.8C) a similar result can be observed. The riluzole evoked peak in the current-density time course is nonexistent (Figure 3.8C, embedded figure) and the CDV curve shows a nearly congruent course before (Figure 3.8C, grey) and after riluzole application (Figure 3.8C, red). Interestingly, the NSC of the riluzole evoked IV curve of G511A is significantly changed when compared to the wildtype (Figure 3.9), especially in the characteristic notch-region of the IV-curve around 0 mV and it is also changed when compared to the NSC before the application of riluzole (especially in the outward current, Figure 3.10). This means, G511A produces some residual current especially in the outward direction with a slightly different course when compared the the wildtype. Glycine inherently takes a unique role in protein structures. It is the only proteinogenic amino acid with an achiral α-carbon atom, i. e. the peptide bond is rotatable. Changing glycine to alanine denies this rotatability. Due to the distance to other amino acids which are important for the riluzole binding, a direct interaction of riluzole with Gly^{511} seems unlikely. Nonetheless, the rotatability of amino acid Gly^{511} seems to be very important for the riluzole dependent TRPC5 activation, but interestingly not for the (-)-englerin A dependent activation.

The exchange leucine at position 514 for alanine shows no significant reduction in any current density value, suggesting it is not involved in ligand binding of either riluzole or (-)-englerin A (Figure 3.8A).

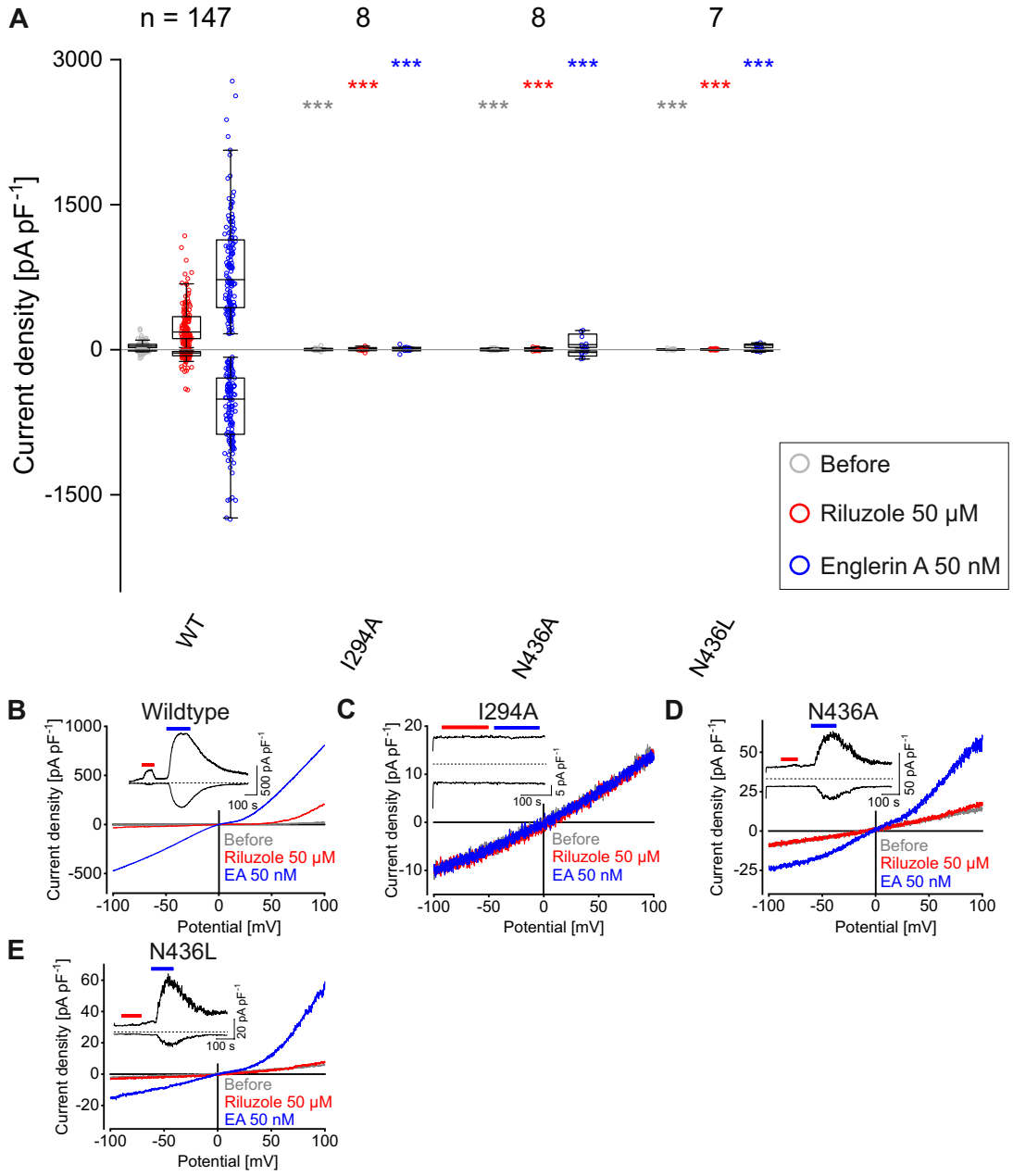

Figure 3.11.: **Whole-cell measurements of potential ligand binding amino acids in cavity I. (A)** shows the maximal and minimal current density at the potentials 100 mV and −100 mV evoked by the given treatment, respectively. Their respective distribution is indicated by the median (horizontal line) and 50 % of the data points (box) as well as the 1.5 × IQR (whiskers). The number of independent experiments is indicated by numbers over the plot. * $P < 0.05$, ** $P < 0.01$, *** $P < 0.001$ (Tested against Wildtype (WT); Mann-Whitney-U). **(B-E)** show representative single CDV curves during the given treatments selected at maximal current responses. The insets show the corresponding current density time course of the same measurement.

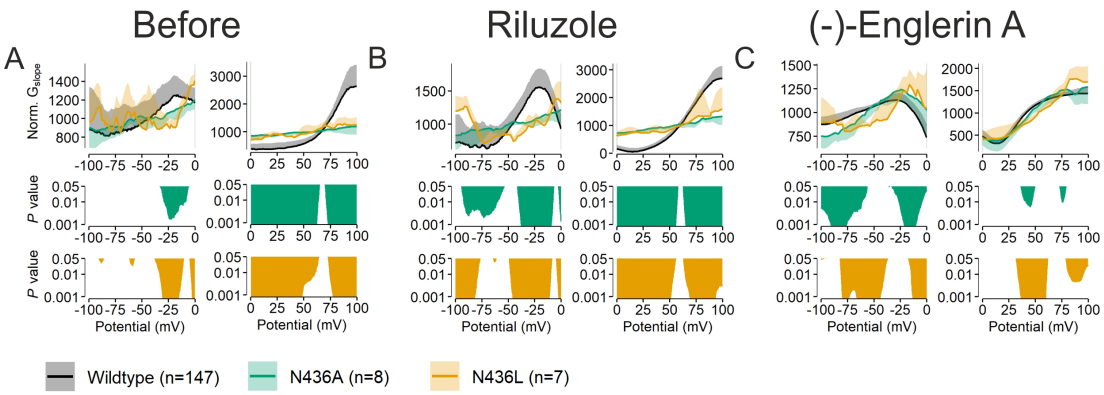

Figure 3.12.: **NSC of potential ligand binding amino acids in cavity I.** This figure shows the calculated NSC (Hermann et al., 2022) of the given mutation (top) $\pm SD$ compared to the wildtype NSC during the given treatment (bottom). Statistical significance was analyzed using the Mann-Whitney-U-test. n indicates the number of independent experiments.

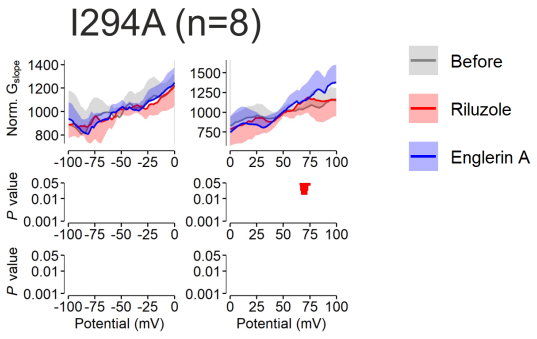

Figure 3.13.: **NSC of potential ligand binding amino acids in cavity I.** This figure shows the calculated NSC (Hermann et al., 2022) of the given mutation (top) $\pm SD$. The given treatment is compared with the basal NSC before application of any activator (bottom). Statistical significance was analyzed using the Wilcoxon signed-rank test. n indicates the number of independent experiments.

Amino acids Ile^{294} and N^{436} originate from the first docking as well and represent candidates with many potential interactions. Their respective location is shown in Figure 3.3. Unfortunately, the amino acid exchange isoleucine at position 294 for alanine results in strong significant reductions in all current density values (Figure 3.11A). This observation is confirmed by a nearly straight baseline current in the current-density time course (Figure 3.11C, embedded figure). The CDV curves show three congruent graphs (Figure 3.11C), supporting the suggestion of a non functional or non expressed variant. The NSC likewise shows nearly no significant changes when comparing the course before and during application of riluzole or (-)-englerin A (Figure 3.13). The exchange asparagine at position 436 for alanine and the less drastic exchange asparagine at position 436 for leucine result in strong significant reductions in current density values before and after subsequent riluzole and (-)-englerin A application (Figure 3.11A). No riluzole-induced current responses are observed in the current density time courses (Figure 3.11C, D embedded figures). Even though (-)-englerin A is still able to evoke currents, the overall generated current density of the mutant is low. The NSC shows significant changes before and during riluzole and (-)-englerin A application in comparison to the wildtype NSC as well (Figure 3.12). Especially when comparing the course of the NSC before and during riluzole application with the wildtype, strong significant changes can be observed (Figure 3.12A, B). To determine if this effect is riluzole specific, due to an overall reduction of the channel function or might be caused by a reduced surface expression, a western blot analysis of the surface expression was performed (see section 3.4).

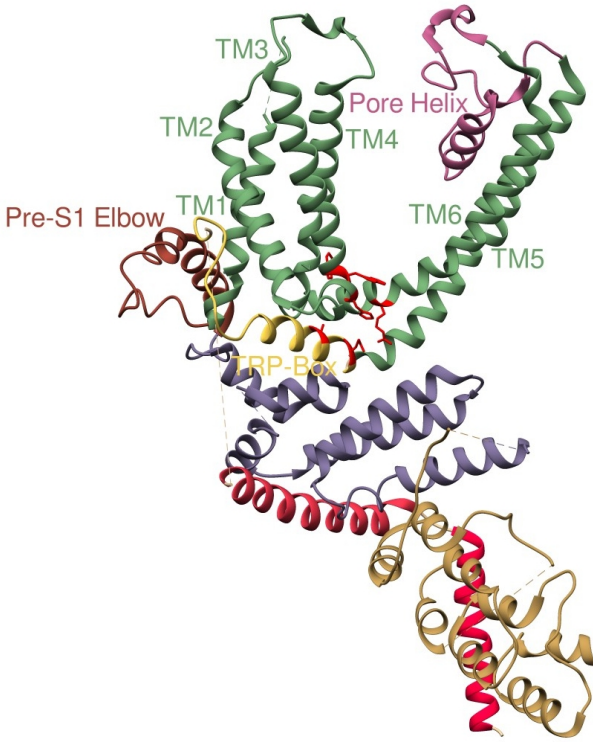

(a) Overview of the amino acids potentially involved in binding of riluzole or (-)-englerin A and their respective orientation and position (red residues).

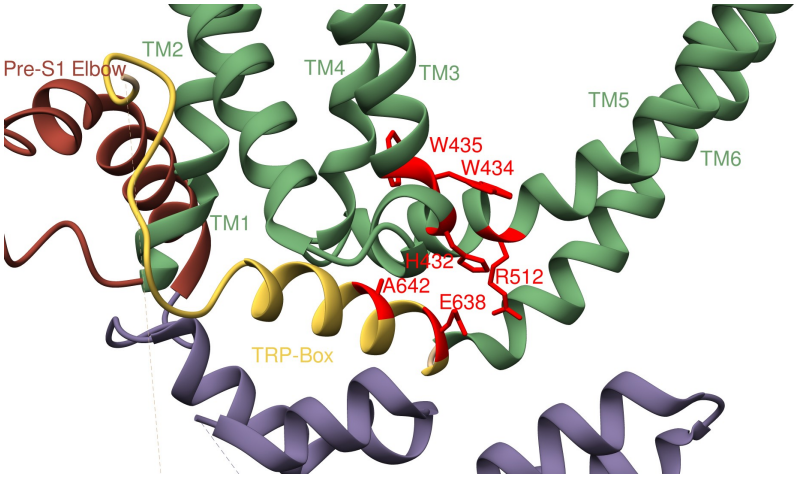

(b) Detailed view of the amino acids potentially involved in binding of riluzole or (-)-englerin A and their respective orientation and position (red residues).

Figure 3.14.: **Potential ligand binding amino acids of cavity I.** In this figure, TRPC5 (PDB: 6AEI) and amino acids which are potentially involved in binding of riluzole or (-)-englerin A are displayed with their respective orientation and position (red residues). Channel elements are colored according to Figure 1.1.

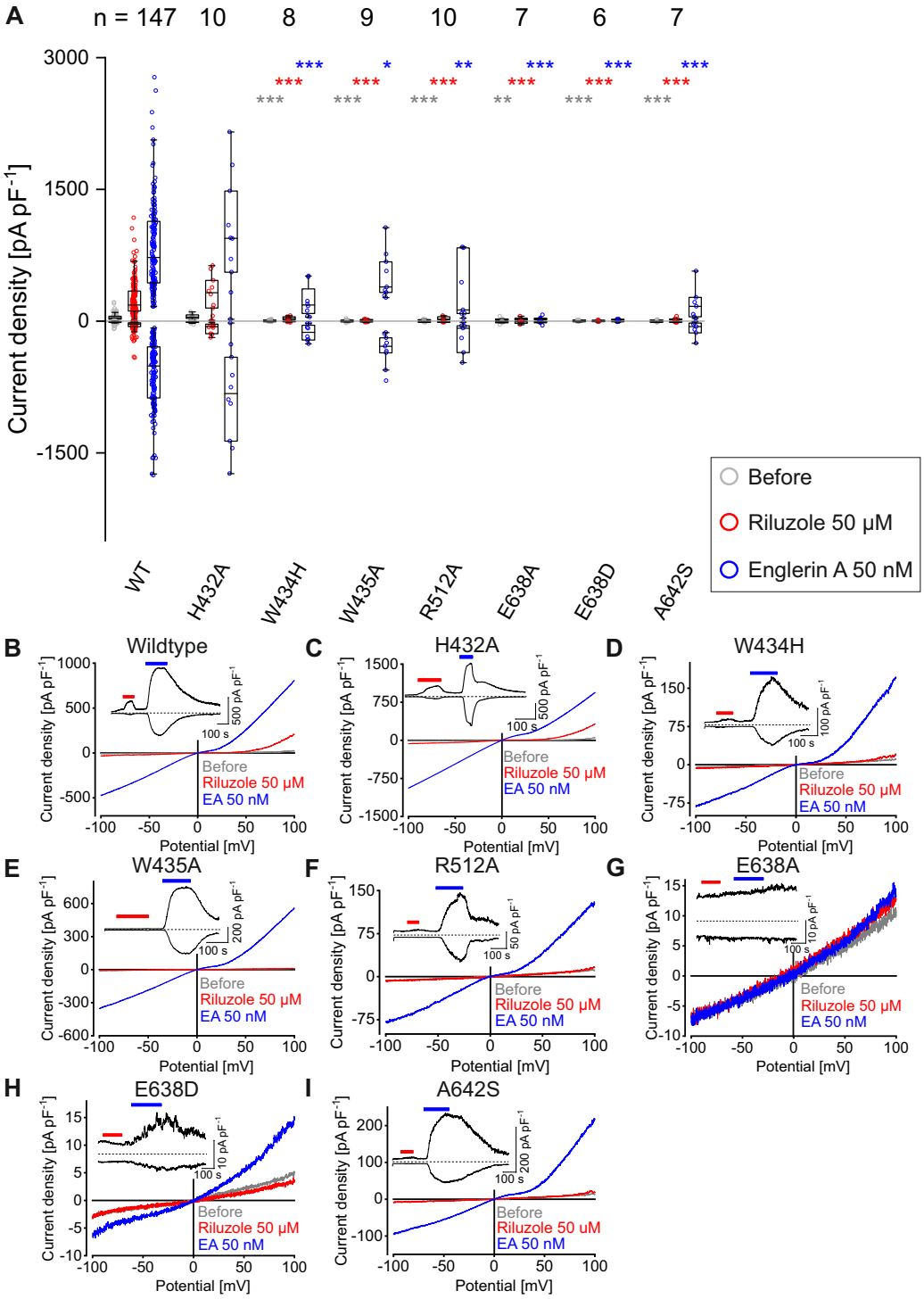

Figure 3.15.: **Whole-cell measurements of potential ligand binding amino acids in cavity I. (A)** shows the maximal and minimal current density at the potentials 100 mV and −100 mV evoked by the given treatment, respectively. Their respective distribution is indicated by the median (horizontal line) and 50 % of the data points (box) as well as the 1.5 × IQR (whiskers). The number of independent experiments is indicated by numbers over the plot. * $P < 0.05$, ** $P < 0.01$, *** $P < 0.001$ (Tested against Wildtype (WT); Mann-Whitney-U). **(B-I)** show representative single CDV curves during the given treatments selected at maximal current responses. The insets show the corresponding current density time course of the same measurement.

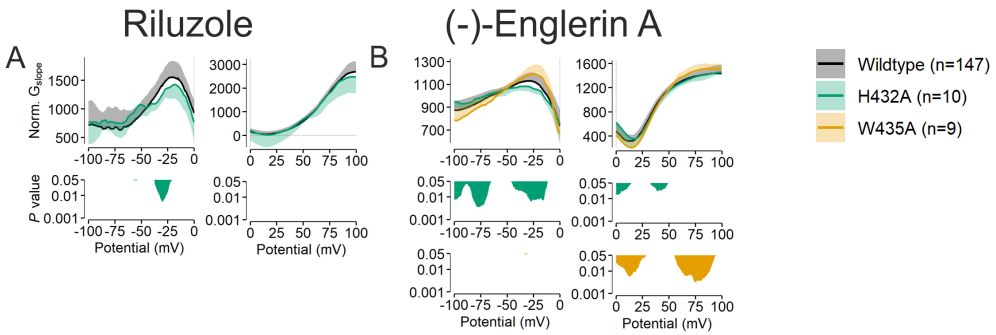

Figure 3.16.: **NSC of potential ligand binding amino acids in cavity I.** This figure shows the calculated NSC (Hermann et al., 2022) of the given mutation (top) $\pm SD$ compared to the wildtype NSC during the given treatment (bottom). Statistical significance was analyzed using the Mann-Whitney-U-test. n indicates the number of independent experiments.

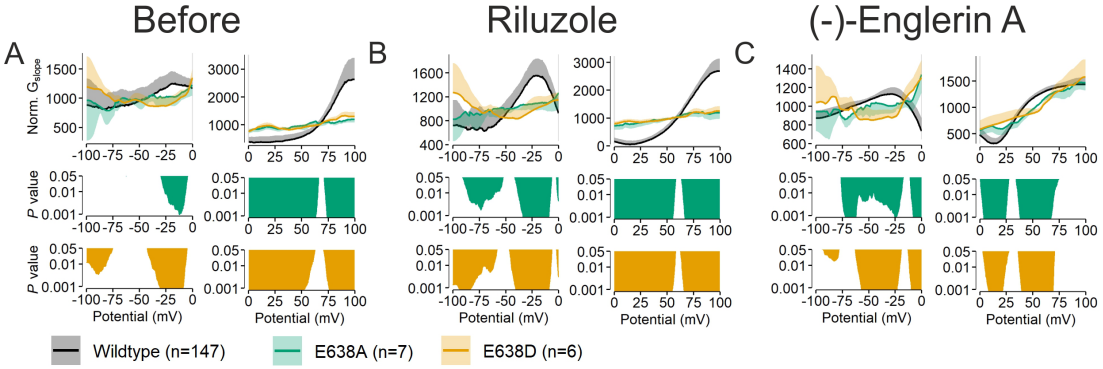

Figure 3.17.: **NSC of potential ligand binding amino acids in cavity I.** This figure shows the calculated NSC (Hermann et al., 2022) of the given mutation (top) $\pm SD$ compared to the wildtype NSC during the given treatment (bottom). Statistical significance was analyzed using the Mann-Whitney-U-test. n indicates the number of independent experiments.

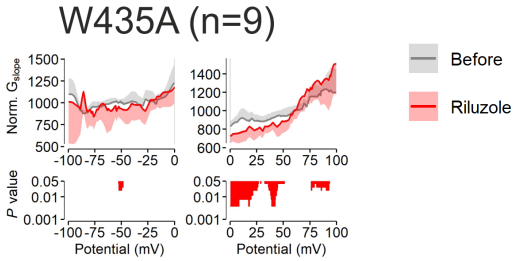

Figure 3.18.: **NSC of potential ligand binding amino acids in cavity I.** This figure shows the calculated NSC (Hermann et al., 2022) of the given mutation (top) $\pm SD$. The given treatment is compared with no treatment (bottom). Statistical significance was analyzed using the Wilcoxon signed-rank test. n indicates the number of independent experiments.

All mutations displayed in Figure 3.15 are derived from docking project I as well and are presented in Figure 3.14.

The exchange of histidine at position 432 for alanine shows no significant reduction of the current densities (Figure 3.15A) and the CDV curves represent wildtype similar courses, too (Figure 3.15A). The NSC of mutant H432A likewise shows only a few and no strong significant changes in the NSC during riluzole and (-)-englerin A treatment when compared to the wildtype, respectively (Figure 3.16A, B, green plot). Therefore, this amino acid is presumably not involved in ligand binding.

Exchanges tryptophane at position 434 for histidine, arginine at position 512 for alanine and alanine at position 642 for serine all show significantly reduced current densities before and after consecutive activator application (Figure 3.15A, D, F, I). The riluzole peak in the current density time courses (Figure 3.15D, F, I, embedded figures) is still present, but very low compared with the wildtype current density time course (Figure 3.15B). However, the (-)-englerin A evoked current density peak is still prominent compared with the riluzole evoked peak, which implies a riluzole specific effect.

The exchange tryptophane at position 435 for alanine produces a mutant channel, which shows no riluzole evoked current (Figure 3.15A, E, embedded figure), whereas the (-)-englerin A evoked current density peak is only weakly, but significantly reduced (Figure 3.15A). As seen in the current density time course (Figure 3.15E, embedded figure) the (-)-englerin A evoked current is still very prominent, but the riluzole peak is lacking. The (-)-englerin A evoked CDV curve (blue) shows wildtype TRPC5 specific characteristics, whereas the riluzole evoked CDV curve (red) is congruent with the CDV curve before activator application (gray). When comparing the NSC of the (-)-englerin A evoked current of W435A with the (-)-englerin A evoked wildtype current, no strongly significant changes can be observed (Figure 3.16B). When comparing the NSC of the IV curves before and after riluzole application of mutant W435A, there are only a few significant changes observed beween 0–50 mV, meaning the course of the riluzole evoked IV curve is very similar to the course of the IV curve before riluzole activation.

Taken together, the CDV curves and their corresponding NSC support the previous observation (Figure 3.15E) of a riluzole specific effect of the mutant W435A.

Mutations of Glu^{638}, namely the exchange glutamate at position 638 to alanine and aspartate result in very low channel overall functionality and/or low channel surface-expression levels. Current density time courses as well as CDV curves (Figure 3.15G, H) show very small current density amplitudes during application of riluzole and (-)-englerin A as well as overall significant current density reduction before and after application of the channel activators (Figure 3.15A). The NSC supports this observation by showing strongly significant differences comparing the courses of the NSC before and during riluzole and (-)-englerin A application of mutants E638A and D with the wildtype, respectively (Figure 3.17). The differences in the NSC indicate a non-functional channel or an impaired trafficking of the channel to the membrane.

Glu^{638} is part of the TRP-box, a very important and delicate channel structure (see subsection 1.2.4), which may explain the drastic effect of mutations introduced in this region.

Taken together, these results suggest that mutations of the amino acids Trp^{434}, Arg^{512}, Ala^{642} and Trp^{435} all produce still functional TRPC5 channels. They show specific reductions of riluzole evoked current densities and therefore may contribute to a riluzole binding.

3.2.2. Non-Docking Derived Mutations

The amino acids Thr^{371}, Asp^{424} and Phe^{497} do not represent possible amino acids involved in ligand interactions that were derived from dockings. In Figure 3.19 their respective position and orientation is presented. They were chosen because of their potential role as "gatekeepers" and they are located at the entrance to a potential ligand binding cavity. The hypothesis was on the one hand by introducing large amino acids like aromatic residues, the access to the potential ligand binding site gets blocked and therefore the ligand can't diffuse into the pocket. On the other hand, even though these mutated amino acids may not be directly involved in ligand binding, they might cause a deformation of the potential ligand binding pocket. With introduction of aromatic residues the ligand might be "pushed" out of its binding position making a binding impossible.

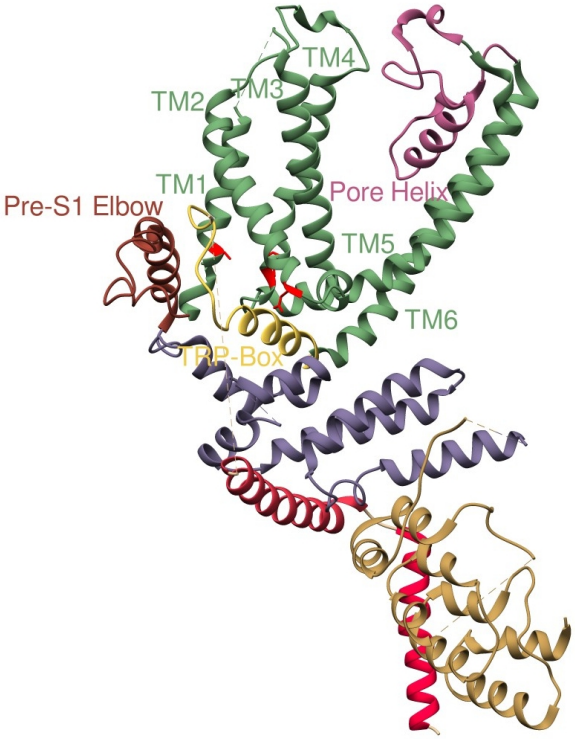

(a) Overview of the amino acids potentially involved in binding of riluzole or (-)-englerin A and their respective orientation and position (red residues).

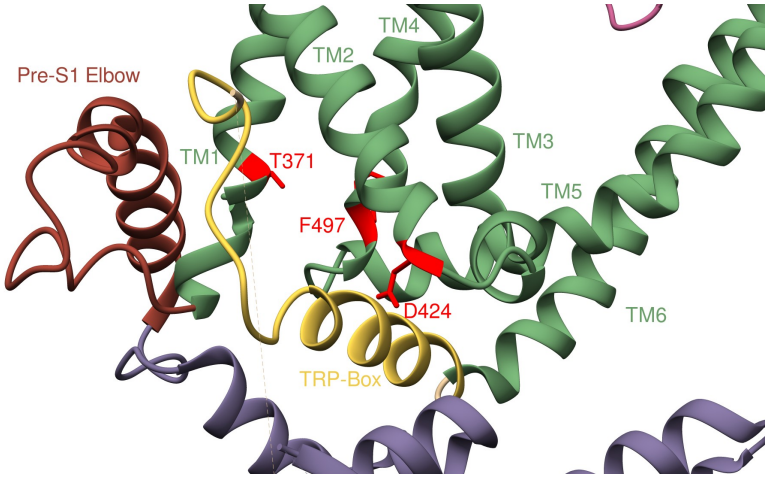

(b) Detailed view of the amino acids potentially involved in binding of riluzole or (-)-englerin A and their respective orientation and position (red residues).

Figure 3.19.: **Potential ligand binding amino acids of cavity I.** In this figure, TRPC5 (PDB: 6AEI) and amino acids which are potentially involved in binding of riluzole or (-)-englerin A are displayed with their respective orientation and position (red residues). Channel elements are colored according to Figure 1.1.

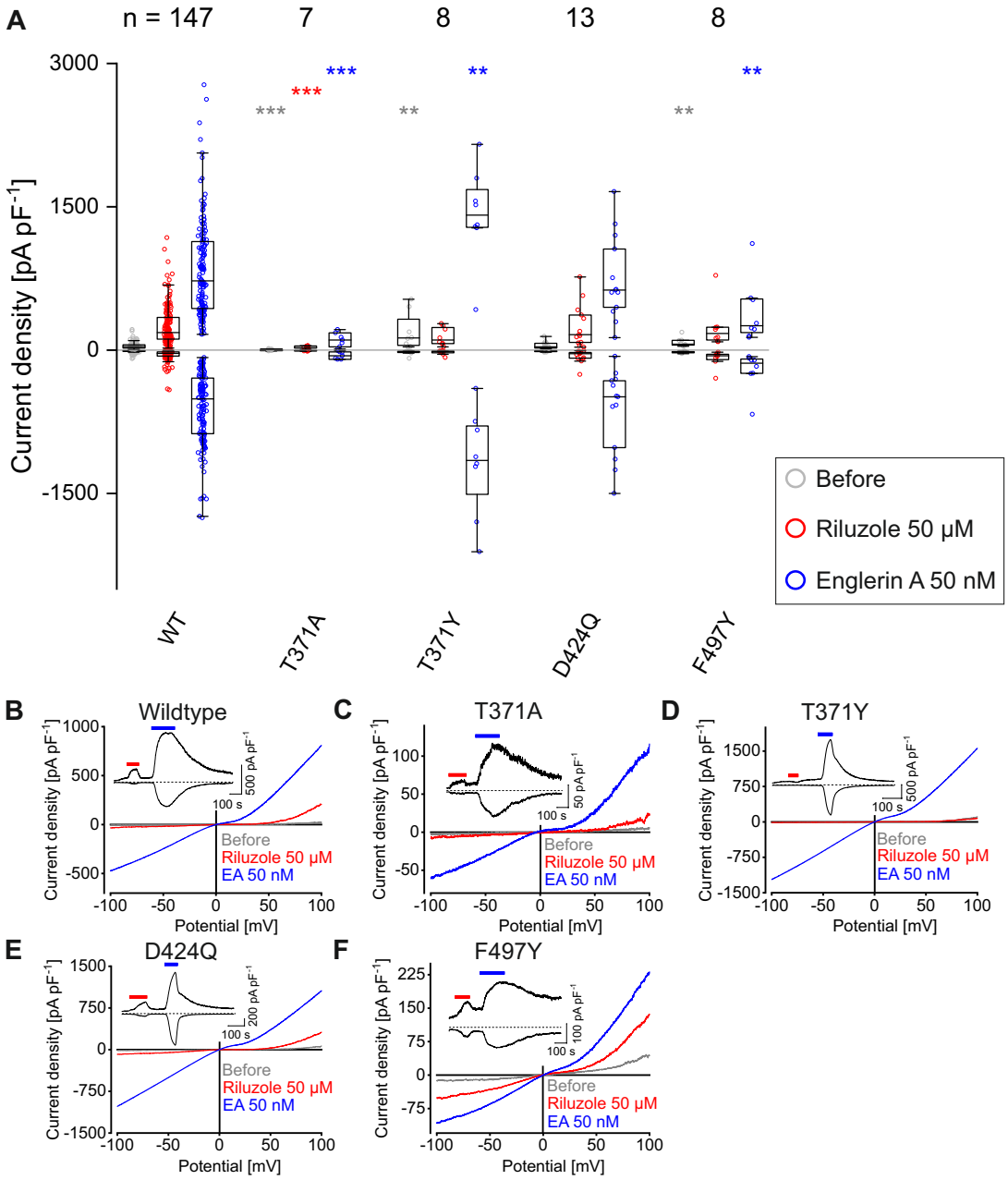

Figure 3.20.: **Whole-cell measurements of potential ligand binding amino acids in cavity I. (A)** shows the maximal and minimal current density at the potentials 100 mV and −100 mV evoked by the given treatment, respectively. Their respective distribution is indicated by the median (horizontal line) and 50 % of the data points (box) as well as the 1.5 × IQR (whiskers). The number of independent experiments is indicated by numbers over the plot. * $P < 0.05$, ** $P < 0.01$, *** $P < 0.001$ (Tested against Wildtype (WT); Mann-Whitney-U). **(B-F)** show representative single CDV curves during the given treatments selected at maximal current responses. The insets show the corresponding current density time course of the same measurement.

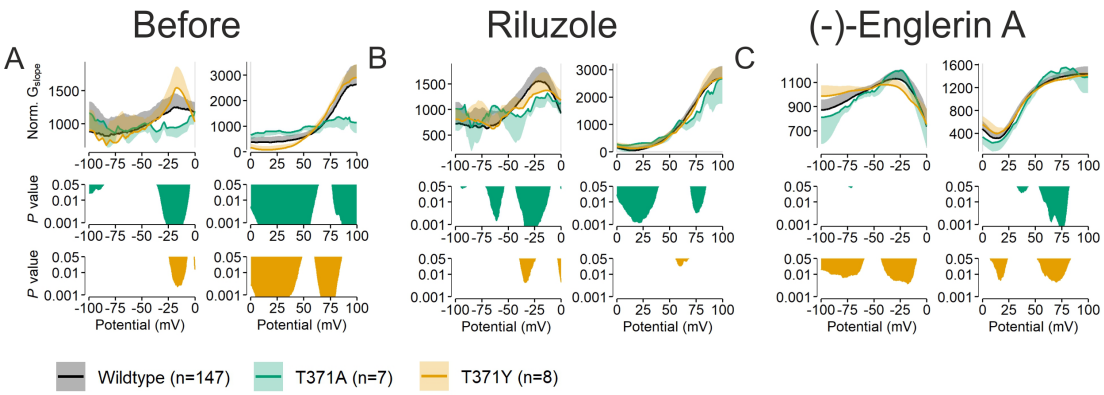

Figure 3.21.: **NSC of potential ligand binding amino acids in cavity I.** This figure shows the calculated NSC (Hermann et al., 2022) of the given mutation (top) $\pm SD$ compared to the wildtype NSC during the given treatment (bottom). Statistical significance was analyzed using the Mann-Whitney-U-test. n indicates the number of independent experiments.

The replacement of threonine at position 371 with alanine shows a significant current density reduction before and during consecutive application of the activators riluzole and (-)-englerin A. However, the riluzole evoked CDV curve (Figure 3.20C, red) and the riluzole evoked maximal current density peak (Figure 3.20C, embedded figure) are similar in their height and shape compared to the wildtype. The NSC shows significant differences in the IV shape, especially before application of any ligand and in the outward current (Figure 3.21, green plot). The least differences in the NSC can be observed in in the (-)-englerin A evoked current. Even though the riluzole evoked current of T371A is very low, the NSC shows only moderate differences compared to the wildtype (Figure 3.21, green plot). These findings suggest that it is unlikely that Thr^{371} contributes to a ligand binding of either riluzole or (-)-englerin A. The replacement of threonine at position 371 with tyrosine however shows a significant increase in basal current density (Figure 3.20A and D). Interestingly, the riluzole-induced current densities were slightly inhibited compared to the current densities before application of riluzole (Figure 3.20A and D, red). In addition, the (-)-englerin A-induced maximal current densities were significantly increased compared with the wildtype (Figure 3.20A, blue). The NSC illustrates even further the significant difference between the basal IV slope before application of any activators and the wildype NSC (Figure 3.21, yellow plot). Interestingly, the riluzole evoked IV curve and the corresponding NSCs are very similar compared to the wildtype NSC, even though the current gets slightly inhibited by the application of riluzole (Figure 3.21, yellow plot). Taken together, this may indicate a pivotal role of Thr^{371} in the recognition of TRPC5 ligands, deciding between agonist and antagonist. Another possible explanation is, that the channel is already in an open state due to the high basal current and the agonist binding leads to the inactivation of the channel. Furthermore, these findings suggest that the amino acid Thr^{371} is not involved in direct ligand binding but might be important for ligand recognition or for channel transduction.

In addition, the replacement of aspartate at position 424 with glutamine does not lead to any significant changes in current densities evoked by riluzole or (-)-englerin A (Figure 3.20A). Thus, the expected blockade of the cavity was not observed.

Interestingly, the mutation phenylalanine at position 497 to tyrosine shows significant current density reductions of the basal current densities and the (-)-englerin A evoked current densities. However, the riluzole evoked maximal current densities were unchanged (Figure 3.20A). Mutations of amino acids His^{370}, Phe^{414}, W^{435} and Asn^{436} already suggest a riluzole binding in this pocket and not an (-)-englerin A binding (see Figure 3.4A, C, Figure 3.11E and Figure 3.8D, E). Therefore the (-)-englerin A specific current density reduction of F497Y is surprising and discussed later in more detail (chapter 4).

3.2.3. Refinement of the Potential Riluzole Binding Position

Since His^{370} emerged as a possible amino acid that might directly interact with riluzole, additional functional amino acid exchanges were performed. Functional exchanges in this context means that the amino acid was substituted with different, less severe and more precise amino acid exchanges compared with the

complete loss of any functional group in the case of the exchange to alanine. The resulting exchanges were the following: H370L does not possess the imidazole moiety which is replaced by a non-polar, non-aromatic isopropyl group. Therefore, polar interactions between the amino acid residue and the ligand are prevented.

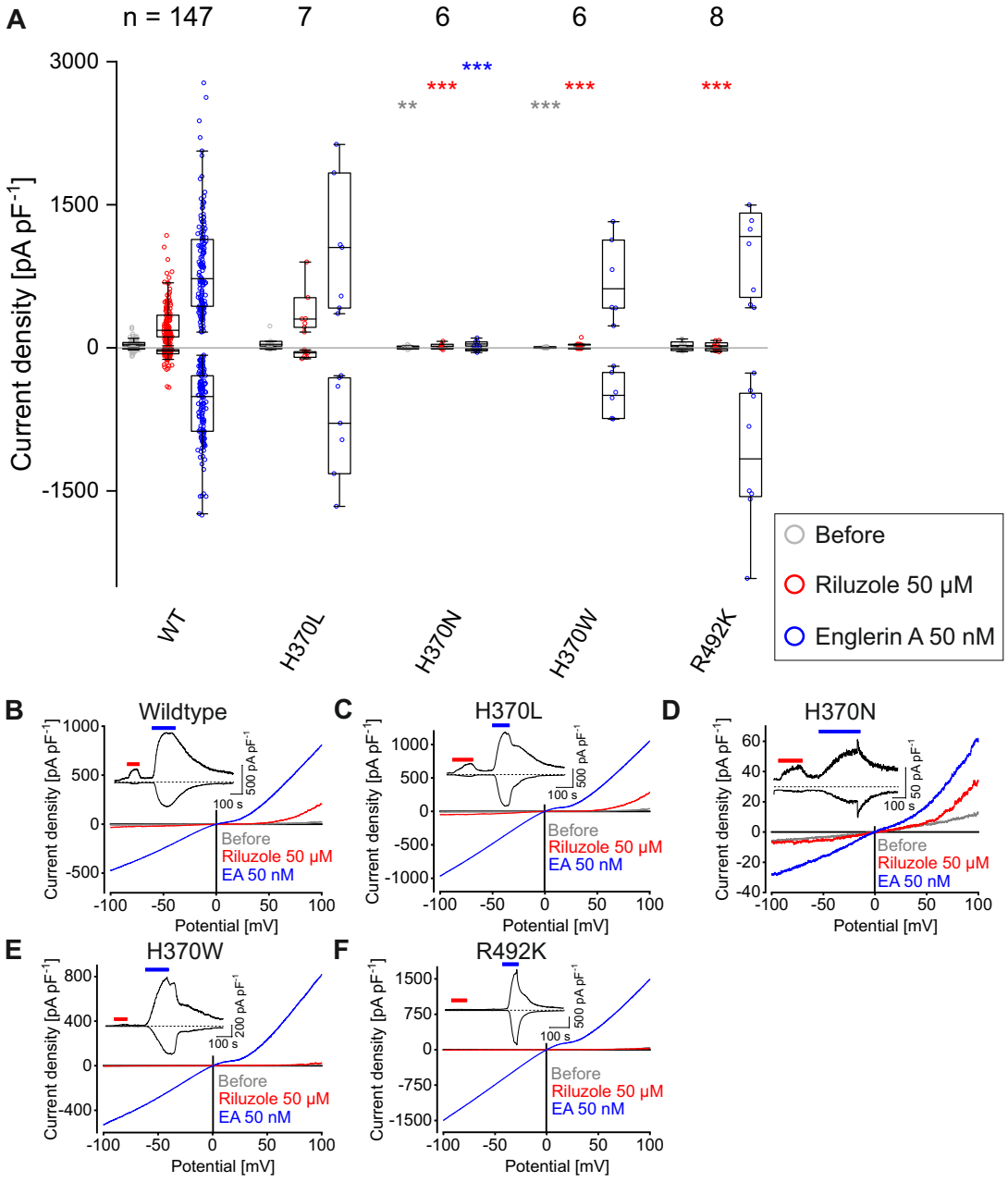

Figure 3.22.: **Whole-cell measurements of potential ligand binding amino acids in cavity I. (A)** shows the maximal and minimal current density at the potentials 100 mV and −100 mV evoked by the given treatment, respectively. Their respective distribution is indicated by the median (horizontal line) and 50 % of the data points (box) as well as the 1.5 × IQR (whiskers). The number of independent experiments is indicated by numbers over the plot. * $P < 0.05$, ** $P < 0.01$, *** $P < 0.001$ (Tested against Wildtype (WT); Mann-Whitney-U). **(B-F)** show representative single CDV curves during the given treatments selected at maximal current responses. The insets show the corresponding current density time course of the same measurement.

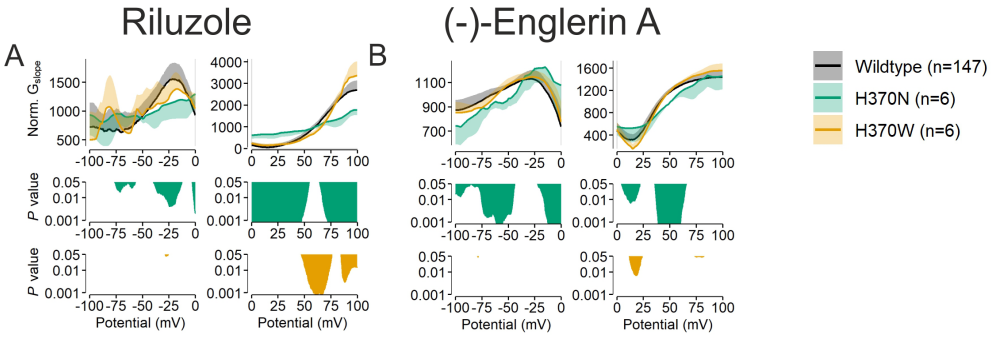

Figure 3.23.: **NSC of potential ligand binding amino acids in cavity I.** This figure shows the calculated NSC (Hermann et al., 2022) of the given mutation (top) $\pm SD$ compared to the wildtype NSC during the given treatment (bottom). Statistical significance was analyzed using the Mann-Whitney-U-test. n indicates the number of independent experiments.

As shown in Figure 3.22A the mutation H370L has no significant effect on any current density value, and therefore no effect on the riluzole binding. The mutation H370N significantly reduces the evoked current densities before and during subsequent riluzole and (-)-englerin A application (Figure 3.22A), therefore no riluzole specific effect can be observed (Figure 3.22D and D, embedded figure). The CDV curves show a similar result with the (-)-englerin A stimulated CDV relation having the highest and the CDV relation before application of the drugs having the lowest amplitude (Figure 3.22D). The NSC similarly shows a significant difference comparing the riluzole and the (-)-englerin A application with the wildtype, respectively Figure 3.23.

Surprisingly, the H370W exchange shows the most specific effect. The riluzole elicited current density is significantly reduced, whereas the (-)-englerin A induced current densities are unchanged (Figure 3.22A). Riluzole was not able to evoke any current increase as seen in the current density time course (Figure 3.22E, embedded figure). The riluzole evoked CDV curve is congruent with the CDV curve before value (Figure 3.22E), whereas the (-)-englerin A stimulated CDV curve has a wildtype comparable course. The NSC of the riluzole evoked IV curve exhibit only a few significant differences compared to the wildtype, especially in the outward current. The NSC of the (-)-englerin A evoked IV curve however shows nearly no differences when compared to the wildtype (Figure 3.23, yellow plot).

Taken together these results suggest an indirect effect of the mutations on the riluzole binding rather than a binding directly to these amino acids. One could speculate that riluzole binds near His^{370} and an exchange to tryptophane, due to the size, pushes riluzole out of the exact binding position. A mutation to alanine on the other hand modifies the original surface structure of the binding pocket in an opposite way. Leucine and asparagine, which are big enough to mimic the size of histidine, which might rebuild a similar surface structure of the pocket as the wildtype channel has. Because the amino acid exchange arginine at position 492 for alanine caused a complete loss of channel function (Figure 3.4), arginine was in the next step exchanged for lysine. The lysine exchange eliminates the guanidino group and replaces it by a primary amino group, meaning only one nitrogen can still potentially interact with the ligand and the chain length is slightly reduced. This exchange is not as drastic as an alanine exchange, but nonetheless produced a very specific reaction. The mutant R492K shows a highly significant reduction only in the the riluzole evoked current densities (Figure 3.22A), with no visible riluzole evoked peak in the current density time course (Figure 3.22F, embedded figure). However, the (-)-englerin A-induced maximal current densities were comparable to the wildtype current densities. This leads to the assumption that riluzole might directly bind to Arg^{492}.

3.3. Docking Project II

In docking project II the aim was to refine the previously assumed riluzole binding position. Positive hits from the first docking run, which were already electrophyiologically confirmed were used as a starting point for a more detailed characterization. Interestingly, the first docking project was actually carried out using (-)-englerin A and (-)-englerin A derivatives in order to identify a potential (-)-englerin A binding site. However, the biophysical characterization of the

TRPC5 mutants performing whole-cell measurements supports the notion that this cavity is rather important for the riluzole binding. Therefore a second docking was necessary using riluzole as the ligand. Riluzole was docked in cavity I and mutations that cause reduced riluzole induced current densities were taken into account (Figure 3.2). Additionally, a second docking was carried out in this project, aiming at cavity II (Figure 3.24). Cavity II is located at the backside of cavity I and the aim was to exclude riluzole binding at this location. Only two amino acids of the docking with riluzole in cavity II were regarded as potential binding partners: Cys^{334} and Ile^{368}. Their respective position and orientation is presented in Figure 3.25.

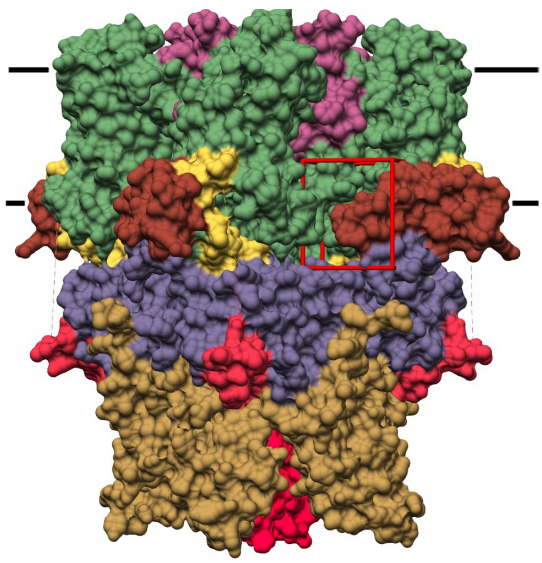

(a) TRPC5 surface structure with docking cube at position II.

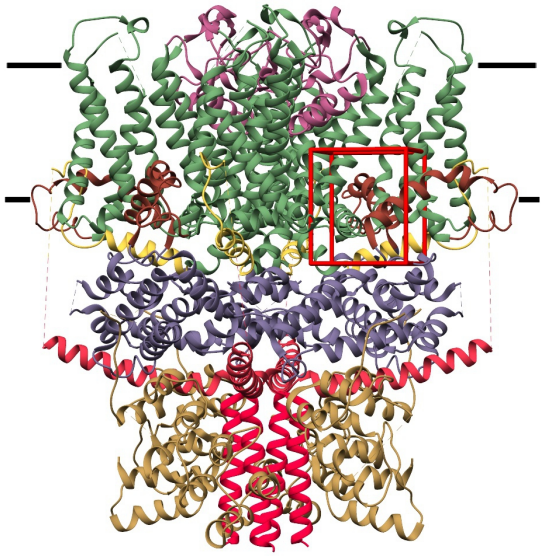

(b) TRPC5 ribbon structure with docking cube at position II.

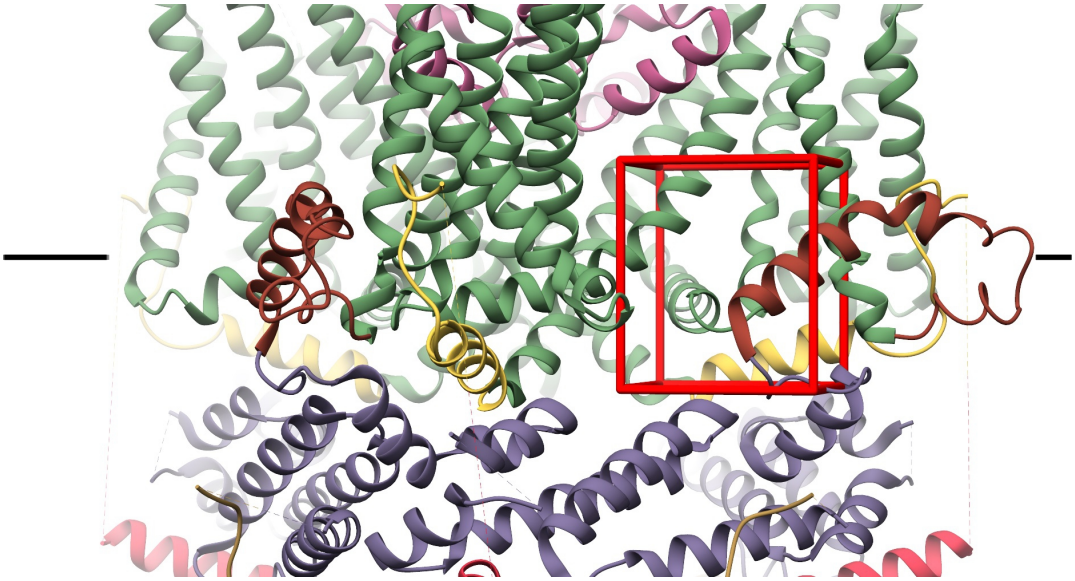

(c) TRPC5 ribbon structure with a detailed view of docking cube II.

Figure 3.24.: **Docking area in cavity II.** In this figure, cavity II is shown. Due to the size it was split in two parts for the actual docking, an upper and a lower part. TRPC5 (PDB: 6AEI, Duan et al. (2018a)) is presented either with its surface structure (a), or ribbon structure (b) and colored according to Figure 1.1 but independently of their related protein chain. Subfigure c is a closeup of (b) for better visualization of the cube.

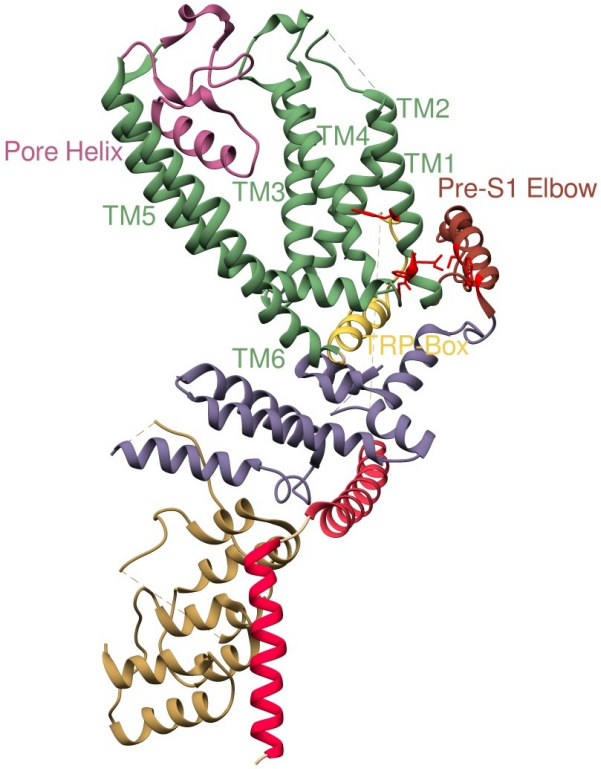

(a) Overview of the amino acids potentially involved in binding of riluzole or (-)-englerin A and their respective orientation and position (red residues).

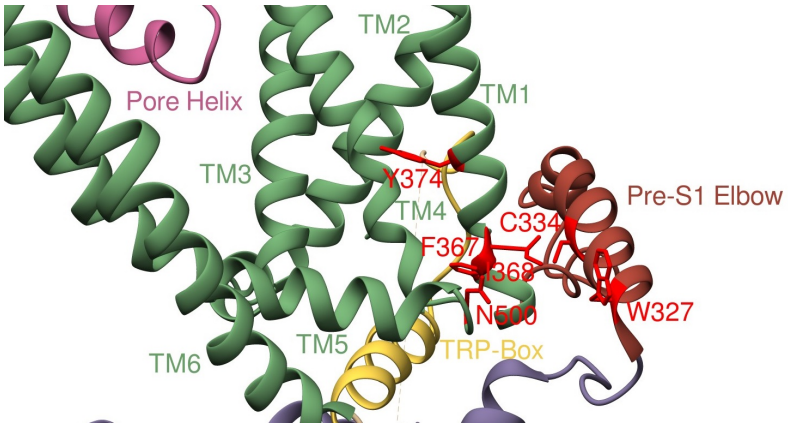

(b) Detailed view of the amino acids potentially involved in binding of riluzole or (-)-englerin A and their respective orientation and position (red residues).

Figure 3.25.: **Potential ligand binding amino acids of cavity II.** In this figure, TRPC5 (PDB: 6AEI) and amino acids which are potentially involved in binding of riluzole or (-)-englerin A in cavity II are displayed with their respective orientation and position (red residues). Channel elements are colored according to Figure 1.1.

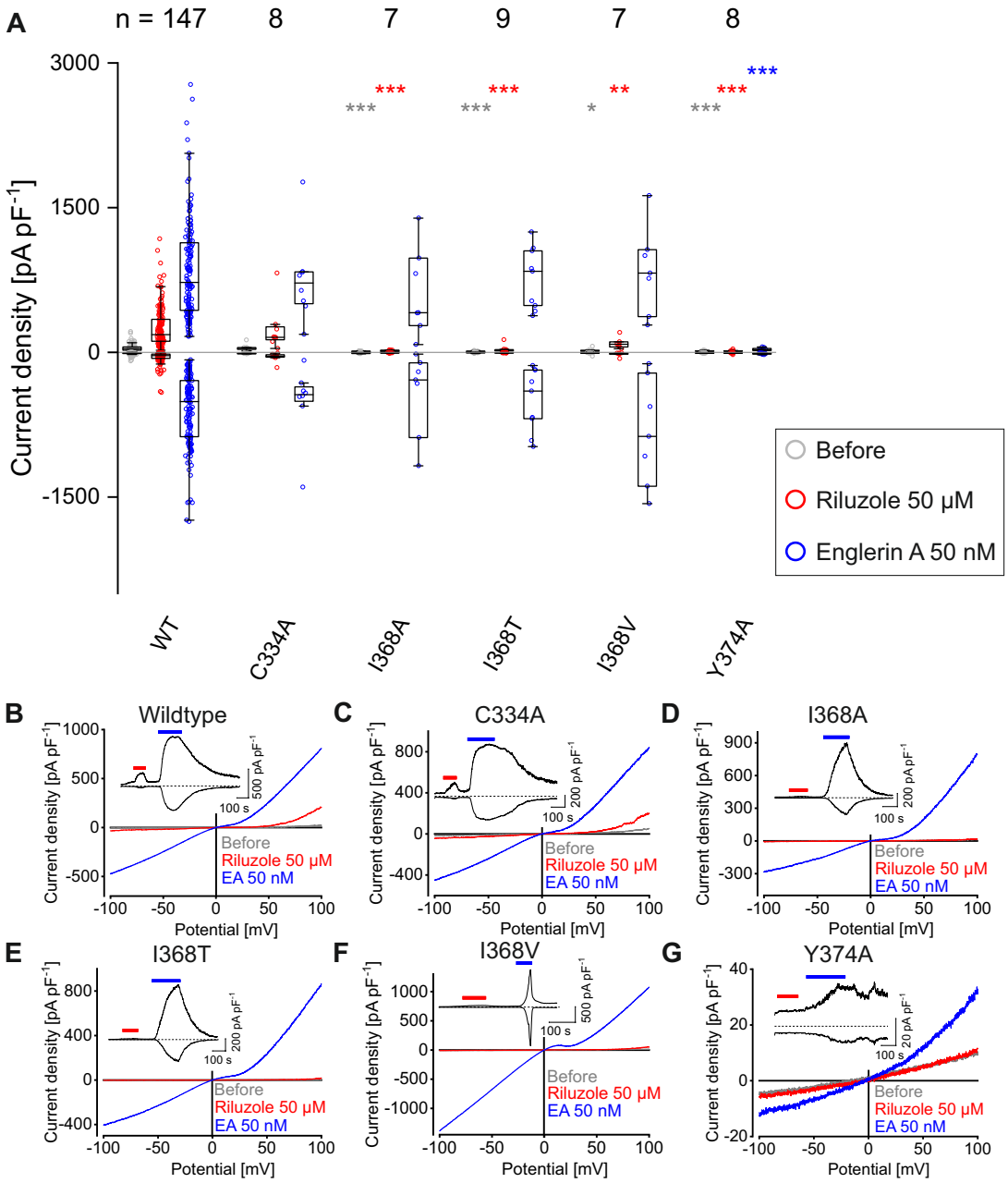

Figure 3.26.: **Whole-cell measurements of potential ligand binding amino acids in cavity II. (A)** shows the maximal and minimal current density at the potentials 100 mV and −100 mV evoked by the given treatment, respectively. Their respective distribution is indicated by the median (horizontal line) and 50 % of the data points (box) as well as the 1.5 × IQR (whiskers). The number of independent experiments is indicated by numbers over the plot. * $P < 0.05$, ** $P < 0.01$, *** $P < 0.001$ (Tested against Wildtype (WT); Mann-Whitney-U). **(B-G)** show representative single CDV curves during the given treatments selected at maximal current responses. The insets show the corresponding current density time course of the same measurement.

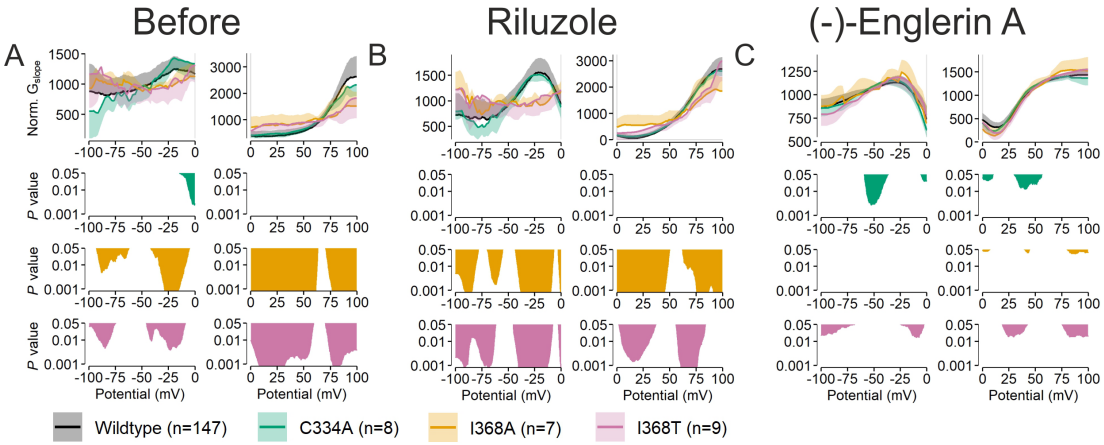

Figure 3.27.: **NSC of potential ligand binding amino acids in cavity II.** This figure shows the calculated NSC (Hermann et al., 2022) of the given mutation (top) $\pm SD$ compared to the wildtype NSC during the given treatment (bottom). Statistical significance was analyzed using the Mann-Whitney-U-test. n indicates the number of independent experiments.

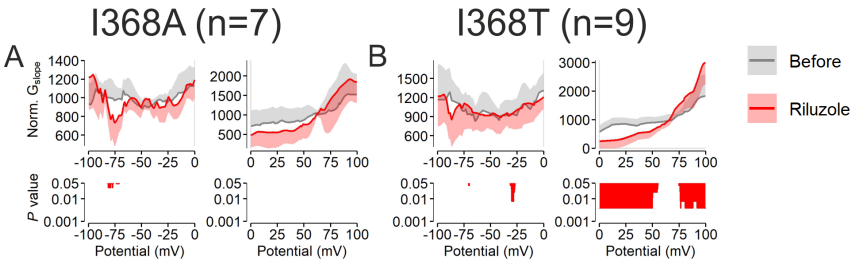

Figure 3.28.: **NSC of potential ligand binding amino acids in cavity II.** This figure shows the calculated NSC (Hermann et al., 2022) of the given mutation (top) $\pm SD$. The NSC under riluzole treatment is compared with no treatment (bottom). Statistical significance was analyzed using the Wilcoxon signed-rank test. n indicates the number of independent experiments.

Mutation of residue cysteine at position 334 to alanine caused no significant changes in maximal current densities evoked by riluzole and (-)-englerin A compared to the wildtype (Figure 3.26A). Furthermore, no changes in current density time courses (Figure 3.26C, embedded figure) or in the CDV curves were observed (Figure 3.26C) compared to the wildtype, respectively. The NSC does not show many significant differences compared to the wildtype, either (Figure 3.27, green plot). Therefore the possible binding in cavity II at the backside of cavity I becomes more unlikely.

The mutations of isoleucine at position 368 to either alanine or threonine both show strong significant current density reductions before and during application of riluzole (Figure 3.26A). The riluzole peak in the current density time course is completely abolished (Figure 3.26D, E, embedded figure) and the CDV curve (Figure 3.26D, E) is congruent before and during application of riluzole. However, (-)-englerin A evoked current densities are not significantly changed compared to the wildtype(Figure 3.26A). Analysis of the NSC clearly show strong differences before application of the activators and during the riluzole application (Figure 3.27A, B, yellow and magenta plot). The NSC of the (-)-englerin A evoked IV curve however shows less significant differences, indicating no changes in the (-)-englerin A provoked response (Figure 3.27C). When comparing the NSC of the riluzole evoked IV curve of I368A with the NSC of the IV curve before the activation no significant difference can be observed Figure 3.28. Therefore riluzole is not able to provoke any current response of the TRPC5 mutant I368A. The NSC of the IV curve of the mutant I368T under riluzole stimulation however shows some, but low residual current in the outward direction, indicated by a significant difference between the NSC before and during the riluzole application (Figure 3.28B, right plot).

These findings support the notion that Ile^{368} is involved in a direct riluzole binding or has a strong indirect effect on the binding. When Ile^{368} is substituted by valine, the riluzole evoked current densities (Figure 3.26A) are also significantly reduced, but not as strong as compared with I368A or I368T. However, the (-)-englerin A evoked current densities are not significantly changed (Figure 3.26A). The current density time-course (Figure 3.26F) shows a hardly noticeable riluzole evoked current increase, but a wildtype comparable (-)-englerin A elicited peak (Figure 3.26F, embedded figure). Taken together, the exchange of Ile^{368} to alanine and even to threonine and valine which are comparable to isoleucine in size, all result in specific reductions of riluzole evoked current densities. Hence, Ile^{368} represents a likely candidate for a riluzole binding. Ile^{368} was originally thought to be contributing to cavity II, but the position of its residue might be miscalculated in the PDB file 6AEI. The helix torsion at this position seems unnaturally bent. Therefore the exact residue position is not certain. Cavity I and II are sharing the same back wall where Ile^{368} is participating in building both surface areas. Consequently, the residue could point more towards cavity I, where other binding mutants were already found.

The purpose of mutation Y374A, which is located in cavity I (illustrated in Figure 3.25), was to determine how the binding of riluzole takes place in TM1. Unfortunately, the amino acid exchange from tyrosine at position 374 to alanine results in a non-functional channel. Neither riluzole nor (-)-englerin A could induce any current responses (Figure 3.26A).

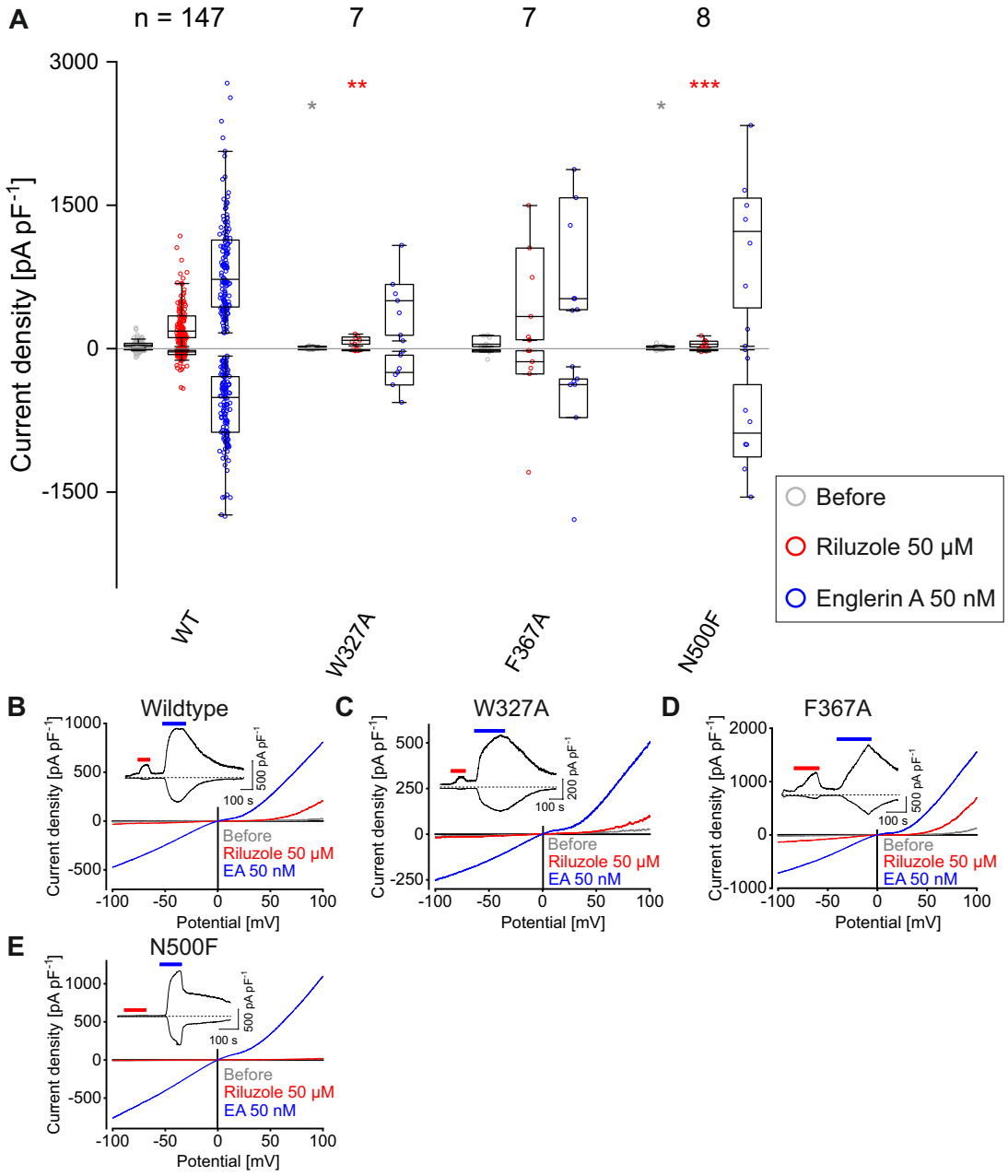

Figure 3.29.: **Whole-cell measurements of potential ligand binding amino acids in cavity II. (A)** shows the maximal and minimal current density at the potentials 100 mV and −100 mV evoked by the given treatment, respectively. Their respective distribution is indicated by the median (horizontal line) and 50 % of the data points (box) as well as the 1.5 × IQR (whiskers). The number of independent experiments is indicated by numbers over the plot. * $P < 0.05$, ** $P < 0.01$, *** $P < 0.001$ (Tested against Wildtype (WT); Mann-Whitney-U). **(B-E)** show representative single CDV curves during the given treatments selected at maximal current responses. The insets show the corresponding current density time course of the same measurement.

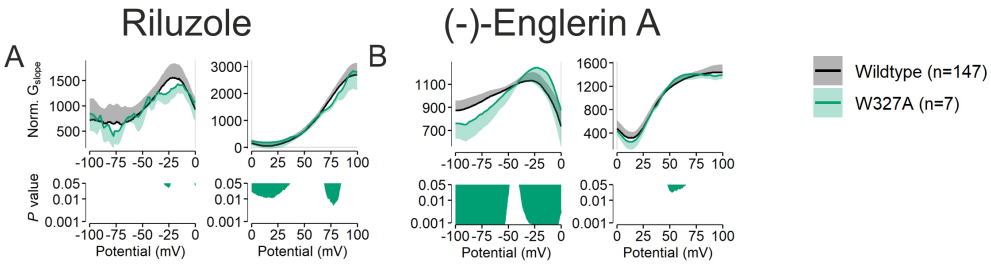

Figure 3.30.: **NSC of potential ligand binding amino acids in cavity II.** This figure shows the calculated NSC (Hermann et al., 2022) of the mutation W327A (top) $\pm SD$ compared to the wildtype NSC during the given treatment (bottom). Statistical significance was analyzed using the Mann-Whitney-U-test. n indicates the number of independent experiments.

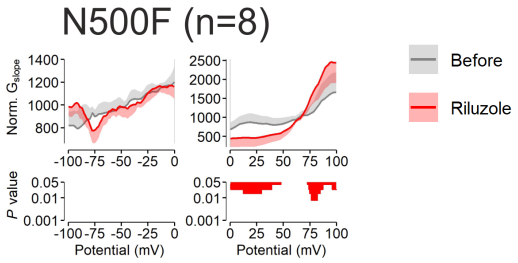

Figure 3.31.: **NSC of potential ligand binding amino acids in cavity II.** This figure shows the calculated NSC (Hermann et al., 2022) of the mutation N500F (top) $\pm SD$. The given treatment is compared with no treatment (bottom). Statistical significance was analyzed using the Wilcoxon signed-rank test. n indicates the number of independent experiments.

The amino acids Trp^{327}, Phe^{367} and Asn^{500} which are presented in Figure 3.29 are located in cavity II at the backside of cavity I (see Figure 3.24 for the location of cavity II and Figure 3.25 for the exact locations of the amino acids). The hypotheses are, that Trp^{327} and Phe^{367} are potential riluzole or (-)-englerin A binding partners in cavity II. The substitution asparagine at position 500 by phenylalanine on the other hand deforms the entrance of the potential binding pocket and therefore prevents the access to cavity II.

Interestingly, W327A shows a significant reduction in the riluzole evoked current densities but the (-)-englerin A elicited current densities are unchanged (Figure 3.29A). The current density time course similarly shows a reduction of the peak height during riluzole application compared to the wildtype and the peak during (-)-englerin A application is comparable to the (-)-englerin A evoked peak of the wildtype (Figure 3.29C, embedded figure). The CDV curves show only slight differences in the amplitude. The NSC of the IV curve mainly shows significant differences comparing the inward current in the presence of (-)-englerin A with the wildtype NSC (Figure 3.30). The NSC of the (-)-englerin A evoked outward current as well as the NSC of the riluzole evoked current show only minor significant differences compared with the wildtype (Figure 3.30).

The amino exchange phenylalanine at position 367 for alanine produces no significant effects on the current density values. The mutant N500F on the other hand again shows no riluzole evoked current densities at all, whereas the (-)-englerin A evoked current densities are unchanged compared to the wildtype (Figure 3.29A). The current density time course shows no riluzole elicited peak, but a prominent (-)-englerin A evoked peak (Figure 3.29E, embedded figure). The IV curves similarly show a congruent course for the IV curve before and during riluzole application (Figure 3.29E). The NSC of the IV curve during riluzole application shows only small significant differences in the outward current when compared with the wildtype (Figure 3.31).

Altogether, even though exchanges in cavity II show significant current density reductions, like N500F and W327A, which show a reduced riluzole response, it is more likely that these amino acids are involved in the riluzole mediated transduction of the activation which will be discussed in chapter 4.

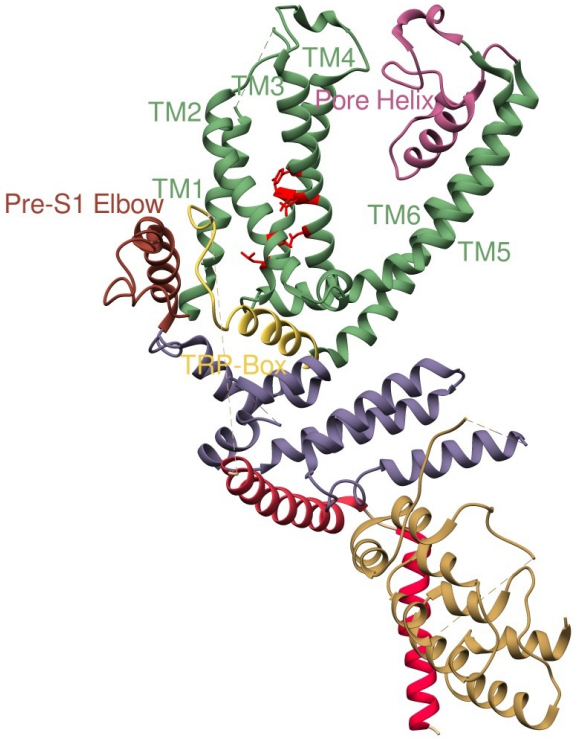

(a) Overview of the amino acids potentially involved in binding of riluzole in cavity I, their respective orientation and position (red residues).

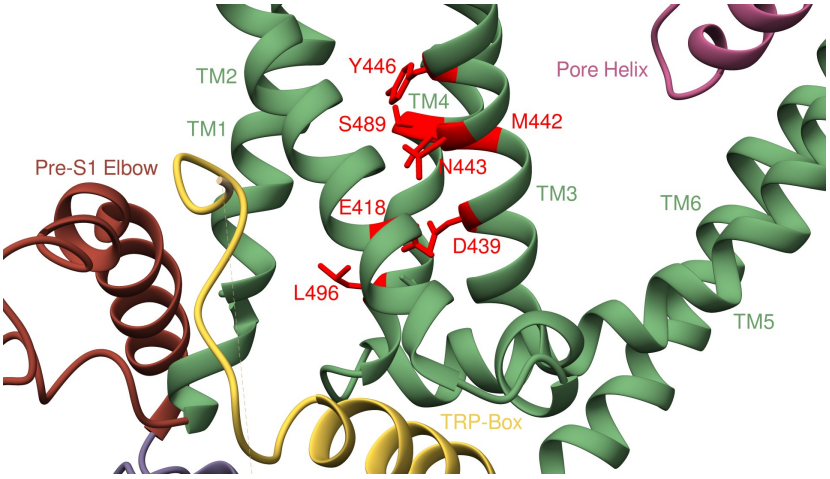

(b) Detailed view of the amino acids potentially involved in binding of riluzole in cavity I, their respective orientation and position (red residues).

Figure 3.32.: **Potential ligand binding amino acids of cavity I.** In this figure, TRPC5 (PDB: 6AEI) and amino acids which are potentially involved in binding of riluzole in cavity I are displayed with their respective orientation and position (red residues). Channel elements are colored according to Figure 1.1.

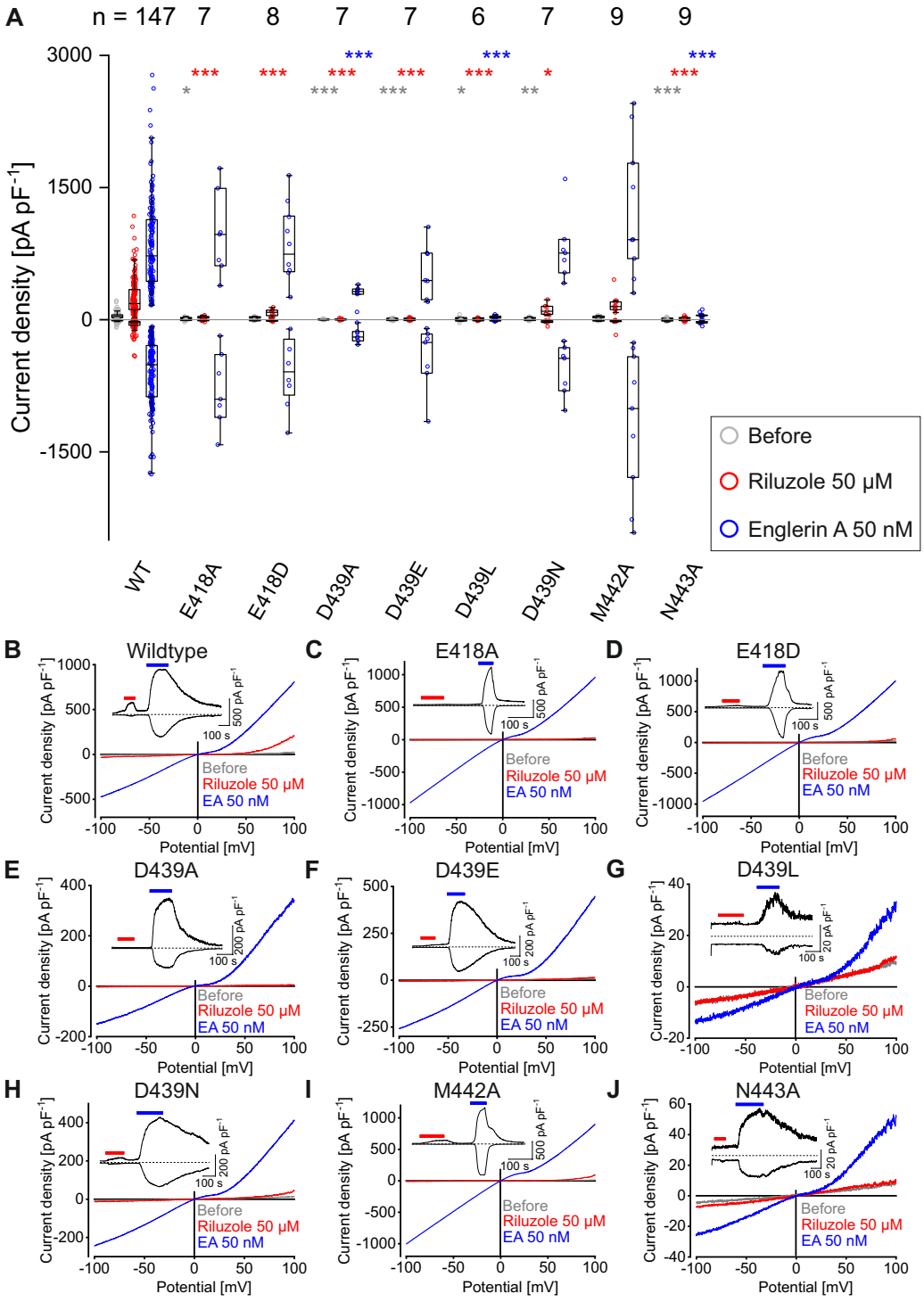

Figure 3.33.: **Whole-cell measurements of potential ligand binding amino acids in cavity I. (A)** shows the maximal and minimal current density at the potentials 100 mV and −100 mV evoked by the given treatment, respectively. Their respective distribution is indicated by the median (horizontal line) and 50 % of the data points (box) as well as the 1.5 × IQR (whiskers). The number of independent experiments is indicated by numbers over the plot. * $P < 0.05$, ** $P < 0.01$, *** $P < 0.001$ (Tested against Wildtype (WT); Mann-Whitney-U). **(B-J)** show representative single CDV curves during the given treatments selected at maximal current responses. The insets show the corresponding current density time course of the same measurement.

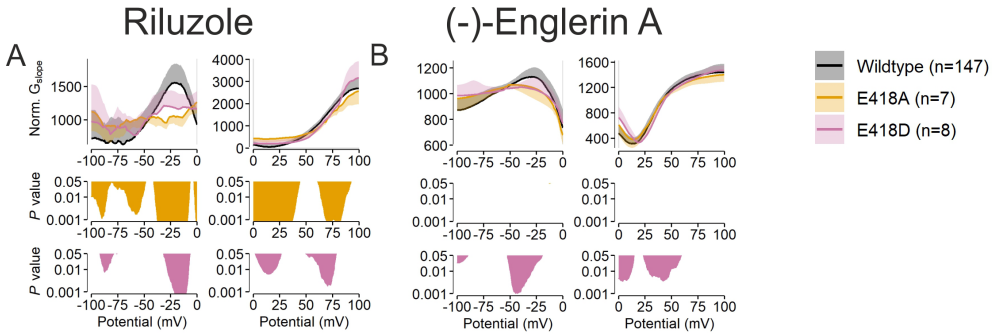

Figure 3.34.: **NSC of potential ligand binding amino acids in cavity I.** This figure shows the calculated NSC (Hermann et al., 2022) of the given mutation (top) $\pm SD$ compared to the wildtype NSC during the given treatment (bottom). Statistical significance was analyzed using the Mann-Whitney-U-test. n indicates the number of independent experiments.

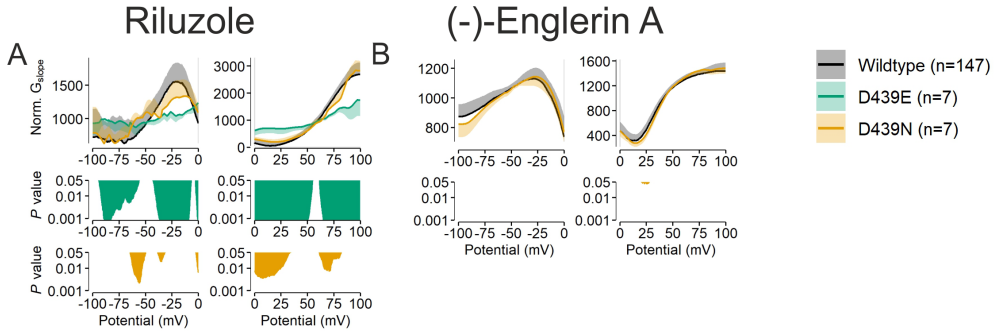

Figure 3.35.: **NSC of potential ligand binding amino acids in cavity I.** This figure shows the calculated NSC (Hermann et al., 2022) of the given mutation (top) $\pm SD$ compared to the wildtype NSC during the given treatment (bottom). Statistical significance was analyzed using the Mann-Whitney-U-test. n indicates the number of independent experiments.

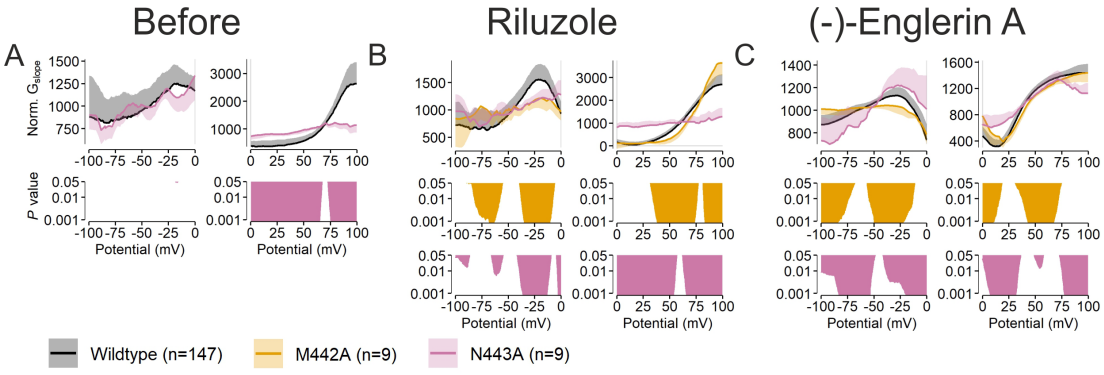

Figure 3.36.: **NSC of potential ligand binding amino acids in cavity I.** This figure shows the calculated NSC (Hermann et al., 2022) of the given mutation (top) $\pm SD$ compared to the wildtype NSC during the given treatment (bottom). Statistical significance was analyzed using the Mann-Whitney-U-test. n indicates the number of independent experiments.

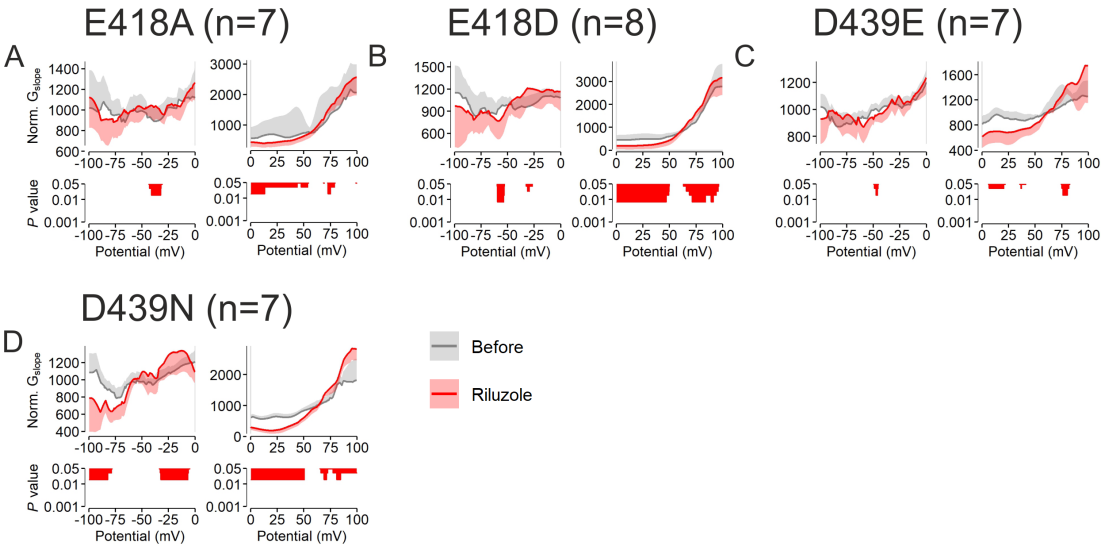

Figure 3.37.: **NSC of potential ligand binding amino acids in cavity I.** This figure shows the calculated NSC (Hermann et al., 2022) of the given mutation (top) $\pm SD$. The NSC under riluzole stimulation is compared with no treatment (bottom). Statistical significance was analyzed using the Wilcoxon signed-rank test. n indicates the number of independent experiments.

Amino acid Glu^{418} originated from the docking in cavity I from docking project II (see section 3.3 and for the location see Figure 3.32). Both mutations, glutamate at position 418 exchanged for alanine and for aspartate both cause significantly reduced riluzole evoked current densities (Figure 3.33A). The (-)-englerin A evoked current density is not changed compared to the wildtype (Figure 3.33A), indicating a riluzole specific effect. The current density time courses show no riluzole evoked peak, but a (-)-englerin A evoked peak comparable to the wildtype, respectively (Figure 3.33C, D, embedded figure).

The CDV curves before and during riluzole application (Figure 3.33C, D) are congruent, whereas the (-)-englerin A evoked CDV curve resembles the wildtype CDV curve (Figure 3.33C, D). The NSC of the riluzole evoked IV curve of E418A is very different compared with the NSC of the wildtype riluzole evoked IV curve, whereas the NSC of the (-)-englerin A evoked IV curve is not changed compared to the wildtype NSC (Figure 3.34, yellow plot). However, the NSC of the riluzole evoked IV curve of E418A is significantly changed in the outward current compared with before the activator application (Figure 3.37). Mutant E418D on the contrary shows a lesser significantly changed NSC of the riluzole evoked IV curve compared with the wildtype NSC (Figure 3.34A, magenta plot). But at the same time E418D shows to some extent a significantly changed NSC of the (-)-englerin A evoked IV curve (Figure 3.34B, magenta plot). However, the NSC of the IV curve before application of riluzole compared with the NSC during application of riluzole is significantly changed, especially in the outward current (Figure 3.37B). Regarding the inward current the riluzole stimulation has nearly no effect on the NSC (Figure 3.37B, left plot).

Taken together, mutant E418A shows a less wildtype similar riluzole evoked NSC and very low residual current response to riluzole, whereas the (-)-englerin A response is wildtype-similar. However, mutant E418D shows more wildtype specific characteristics in the NSC of the riluzole evoked IV curve, but lesser wildtype specific characteristics in the NSC of the (-)-englerin A evoked IV curve compared with E418A. Nonetheless, both mutations show low riluzole responses overall.

Therefore, the current density time courses as well as the CDV curves and their corresponding NSC confirm the results obtained by just the current densities. Even decreasing the chain length by just one carbon atom and replacing Glu^{418} with aspartate, the effect of reducing the riluzole evoked current densities is specific and highly significant. Because of the highly specific effects that mutations of Glu^{418} have on the riluzole evoked current densities, a binding of riluzole to this amino acid is likely.

The amino acid Asp^{439} appears in docking project II (Figure B.9) and was meanwhile published as a binding partner of GFB-9289, a selective TRPC4/5 inhibitor (Vinayagam et al., 2020). Because of the close proximity to already existing, electrophysiologically confirmed potential riluzole binding partners, this amino acid might also be involved in riluzole binding. The amino acid exchange aspartate at position 439 for alanine results in a very strong effect, significantly reducing the current densities before and during consecutive application of both activators (Figure 3.33A). Nonetheless, riluzole was not able to evoke any current density responses (Figure 3.33E and E, embedded figure), whereas (-)-englerin A was still able to produce a visual, although significantly reduced, current increase (Figure 3.33E and E, embedded figure).

To further investigate the potential binding of riluzole to Asp^{439}, the amino acid was substituted by other residues. Glutamate represents the least severe exchange in functionality due to the conservation of the charge and the elongation of the chain by one carbon atom. Surprisingly, the exchange of aspartate at position 439 with glutamate produces significantly reduced current densities before and during riluzole application (Figure 3.33A) but no changes in the (-)-englerin A evoked current densities (Figure 3.33A). The current density time course (Figure 3.33F, embedded figure) and CDV curve (Figure 3.33F) show a similar result, with no visual riluzole peak in the current density time course, but an unchanged (-)-englerin A evoked current and a congruent CDV curve before and during riluzole application. The NSC of the riluzole evoked IV curve of the mutant D439E shows significant differences compared with the wildtype over the whole course, therefore showing no wildtype specific characteristics at all (Figure 3.35A, green plot).

Similarly, nearly no differences can be observed when comparing the NSC before application of riluzole with the NSC during application of riluzole of the mutant D439E, suggesting no riluzole induced change of the IV curve (Figure 3.37C). Therefore, even by slightest exchanges the channel responds with a highly significant reduction of the riluzole evoked current densities. This result supports the notion that Asp^{439} might be involved in the riluzole binding.

The exchange of aspartate at position 439 for leucine is especially interesting, because the chain length is identical, but the charged residue is eliminated. But mutation D439L significantly reduces current density responses overall during consecutive application of riluzole and (-)-englerin A (Figure 3.33A). Due to the very small current amplitude overall, it is difficult to determine if the riluzole evoked current is reduced because of a specific effect or just because of a limited channel functionality or low surface expression (Figure 3.33G and G, embedded figure).

The exchange of aspartate at position 439 for asparagine conserves the chain length as well and also eliminates the charge of the carboxyl group by replacing it with a carbamoyl group. In this case, the exchange results in a significant reduction of the riluzole evoked current densities (Figure 3.33A), but not of the (-)-englerin A evoked current densities (Figure 3.33A). In the current density time course (Figure 3.33H, embedded figure) and in the IV curves a similar result can be observed. The riluzole evoked peak is still visible, but significantly reduced, whereas the (-)-englerin A evoked peak is comparable to the wildtype (Figure 3.33H, embedded figure). The riluzole IV curve on the other hand is not congruent with the IV curve before application, but significantly lower compared to the wildtype (Figure 3.33H, red), but the IV during (-)-englerin A application is comparable to the wildtype(Figure 3.33H, blue). Mutant D439N shows only some significant differences in the NSC of the riluzole evoked IV curve and no changes in the NSC of the (-)-englerin A evoked IV curve, when compared with the wildtype (Figure 3.35, yellow plot). The NSC of the IV curve before riluzole and during riluzole application are to the most part significantly different, indicating some residual riluzole evoked current response (Figure 3.37D).

Taken together, these results suggest that the amino acid Asp^{439} might be important for the riluzole interaction in general. Different exchanges cause a significant reduction of the riluzole induced current densities. By exchanging aspartate for asparagine and thus eliminating the negatively charged carboxyl

group, the riluzole evoked current responses are significantly reduced, suggesting that the carboxyl group might directly interact with riluzole. Mutation D439E, which preserves the charge of the carboxyl group, but exhibits an elongated chain might push riluzole out of its binding position and thus completely abolishes riluzole-induced currents.

The amino acid exchange of methionine at position 442 for alanine does not change the current densities in the presence and absence of the channel activators compared to the wildtype (Figure 3.33A). The current density time course (Figure 3.33I, embedded figure) and the CDV curves (Figure 3.33I) similarly show no changes when compared to the wildtype. However, analysis of the NSC of the riluzole and the (-)-englerin A evoked IV curve show significant differences when compared with the wildtype, respectively (Figure 3.36B, C, yellow plot). This may indicate some alterations of the channel functionality.

Replacement of asparagine at position 443 by alanine causes a phenotype with significantly reduced current densities before and during consecutive riluzole and (-)-englerin A application(Figure 3.33A). The riluzole evoked peak in the current density time course is not visible and the (-)-englerin A evoked peak is strongly reduced compared to the wildtype (Figure 3.33J, embedded figure). The CDV curves show small amplitudes as well (Figure 3.33J), underlining the notion that the mutation N443A results in a non functional phenotype with low overall channel functionality or surface expression. The NSC of the IV curve before activator application and during riluzole and (-)-englerin A application show significant differences when compared with the wildtype, respectively (Figure 3.36, magenta plot). Especially the NSC before and during riluzole application exhibit a slope with a high variance in the inward current and a linear slope in the outward current and therefore no wildtype-similar characteristics (Figure 3.36A, B, magenta plot). Because of the generally impaired channel function, it is not clear whether Asn^{443} is involved in a potential riluzole binding.

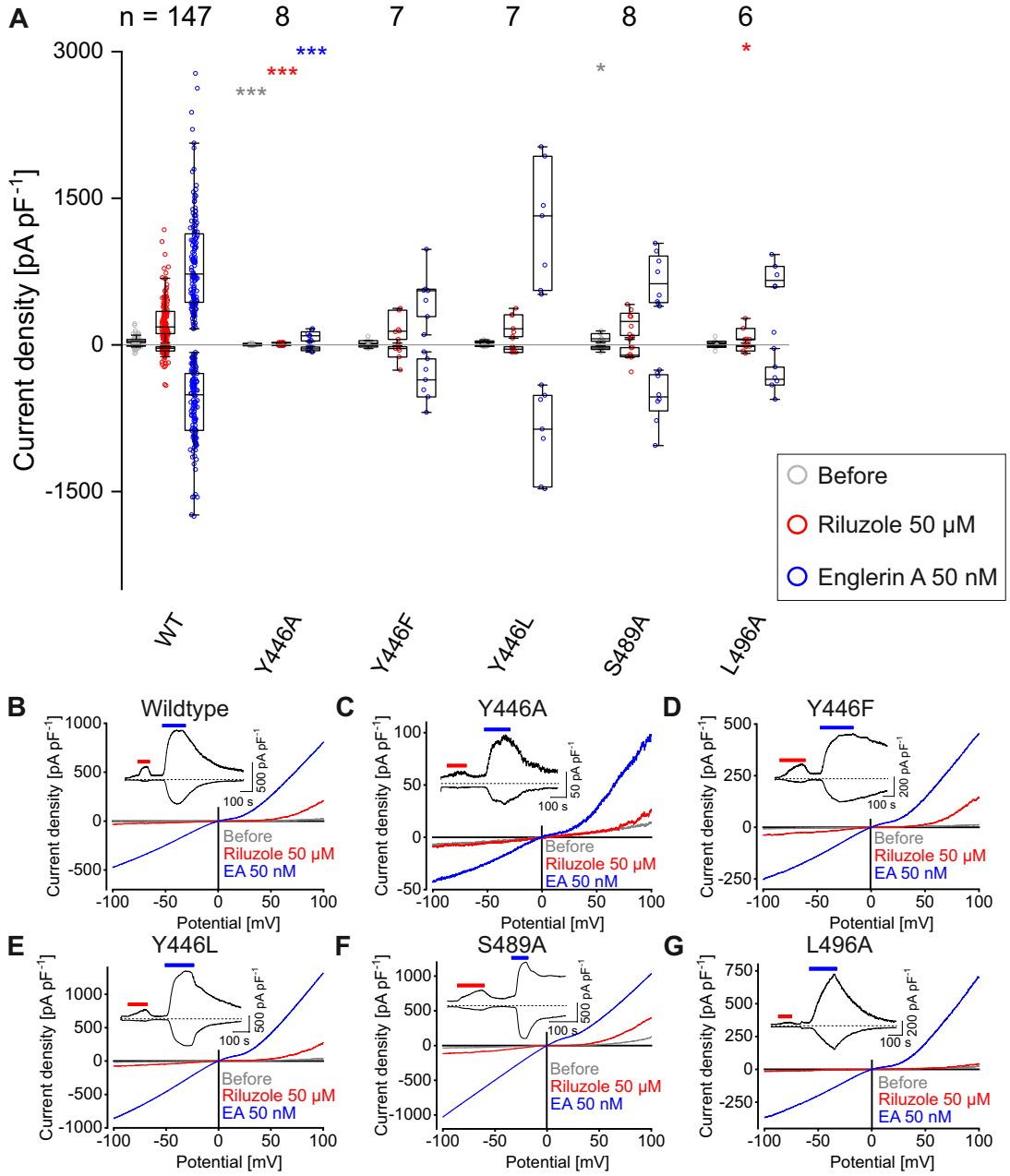

Figure 3.38.: **Whole-cell measurements of potential ligand binding amino acids in cavity I. (A)** shows the maximal and minimal current density at the potentials 100 mV and −100 mV evoked by the given treatment, respectively. Their respective distribution is indicated by the median (horizontal line) and 50 % of the data points (box) as well as the 1.5 × IQR (whiskers). The number of independent experiments is indicated by numbers over the plot. * $P < 0.05$, ** $P < 0.01$, *** $P < 0.001$ (Tested against Wildtype (WT); Mann-Whitney-U). **(B-G)** show representative single CDV curves during the given treatments selected at maximal current responses. The insets show the corresponding current density time course of the same measurement.

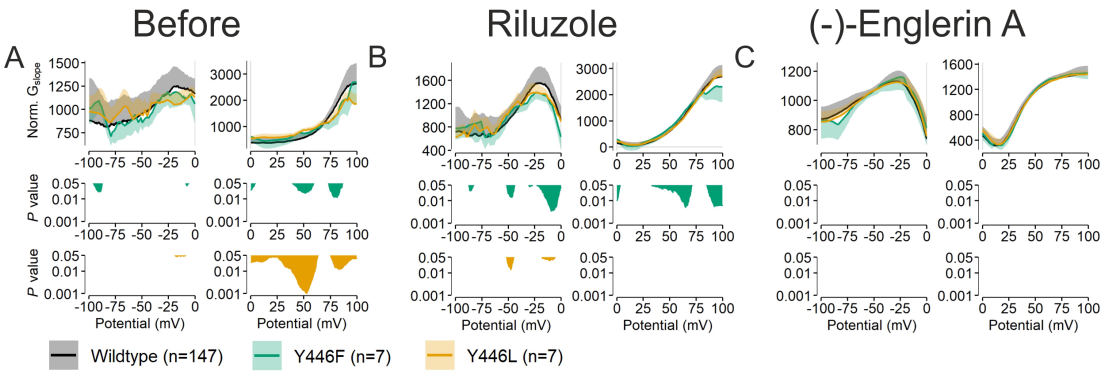

Figure 3.39.: **NSC of potential ligand binding amino acids in cavity I.** This figure shows the calculated NSC (Hermann et al., 2022) of the given mutation (top) $\pm SD$ compared to the wildtype NSC during the given treatment (bottom). Statistical significance was analyzed using the Mann-Whitney-U-test. n indicates the number of independent experiments.

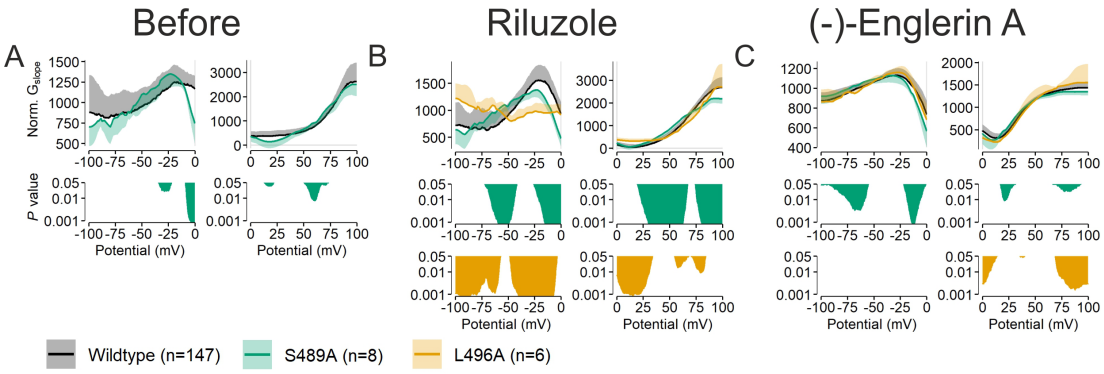

Figure 3.40.: **NSC of potential ligand binding amino acids in cavity I.** This figure shows the calculated NSC (Hermann et al., 2022) of the given mutation (top) $\pm SD$ compared to the wildtype NSC during the given treatment (bottom). Statistical significance was analyzed using the Mann-Whitney-U-test. n indicates the number of independent experiments.

Amino acids Tyr^{446}, Ser^{489} and Leu^{496} are part of the binding site of the selective TRPC4/5 inhibitor GFB-9289 which was co-crystallized with TRPC4 Vinayagam et al. (2020). Because of their proximity to previously found amino acids that are possibly involved in the riluzole binding, these amino acids were analyzed regarding their potential involvement in the riluzole binding as well. Their respective position and orientation is highlighted in Figure 3.32.

The amino acid exchange tyrosine at position 446 for alanine produces a mutant channel with significantly reduced current densities before and during consecutive riluzole and (-)-englerin A application (Figure 3.38), suggesting low overall functionality and/or a low surface expression. Therefore, additional functional amino acid exchanges for phenylalanine to maintain the benzyl group and to reduce the polarity and to leucine to eliminate the polarity and the benzene group were performed.

The mutations Y446F and Y446L neither produce a significant reduction in current densities during riluzole nor (-)-englerin A application (Figure 3.38A). The current density time courses (Figure 3.38D, E, embedded figures) as well as the CDV curves (Figure 3.38D, E) do not show any divergence compared to the wildtype, respectively. The NSCs of the IV curves before and during consecutive riluzole and (-)-englerin A application similarly shows some significant changes, but not over the whole course, when comparing the mutants Y446F and Y446L with the wildtype, respectively (Figure 3.39).

The mutation serine at position 489 to alanine similarly shows no current density reductions of the riluzole and (-)-englerin A evoked currents, respectively (Figure 3.38A, F). However, the NSC of the mutation S489A shows some significant differences when compared with the wildtype, especially in the riluzole evoked NSC (Figure 3.40 green plots). This may be caused by the close proximity to other important amino acids which are potentially involved in the binding of riluzole.

These results suggest, that the above mentioned amino acids Tyr^{446} and Ser^{489} are probably not involved in a riluzole binding.

The amino acid exchange leucine at position 496 for alanine results in a significant reduction of the riluzole evoked current densities (Figure 3.38A). The

current density time course likewise shows a significantly reduced riluzole evoked peak, but the (-)-englerin A induced current density peak was unchanged (Figure 3.38G, embedded figure). The riluzole elicited CDV curve shows a nearly congruent course compared to the basal CDV curve before the application of riluzole, whereas the (-)-englerin A elicited CDV curve (Figure 3.38G) is consistent with the wildtype CDV curve. The NSC similarly shows significant differences in the riluzole evoked IV curve and to a lesser extent in the (-)-englerin A evoked IV curve (Figure 3.40, yellow plot).

Taken together, this gives evidence for a riluzole specific effect of mutant L496A. Specifying the role of the amino acid Leu^{496} in the binding of riluzole is challenging, because the functional group of leucine is hydrophobic and uncharged. Therefore only hydrophobic interactions are possible between leucine and the potential ligand. Keeping that in mind, the drastic effect of an exchange that does not target a strong functionality but rather eliminates weak interactions suggests, that the amino acid Leu^{496} is pivotal for riluzole binding.

3.4. Surface Expression of Potential Riluzole Mutants

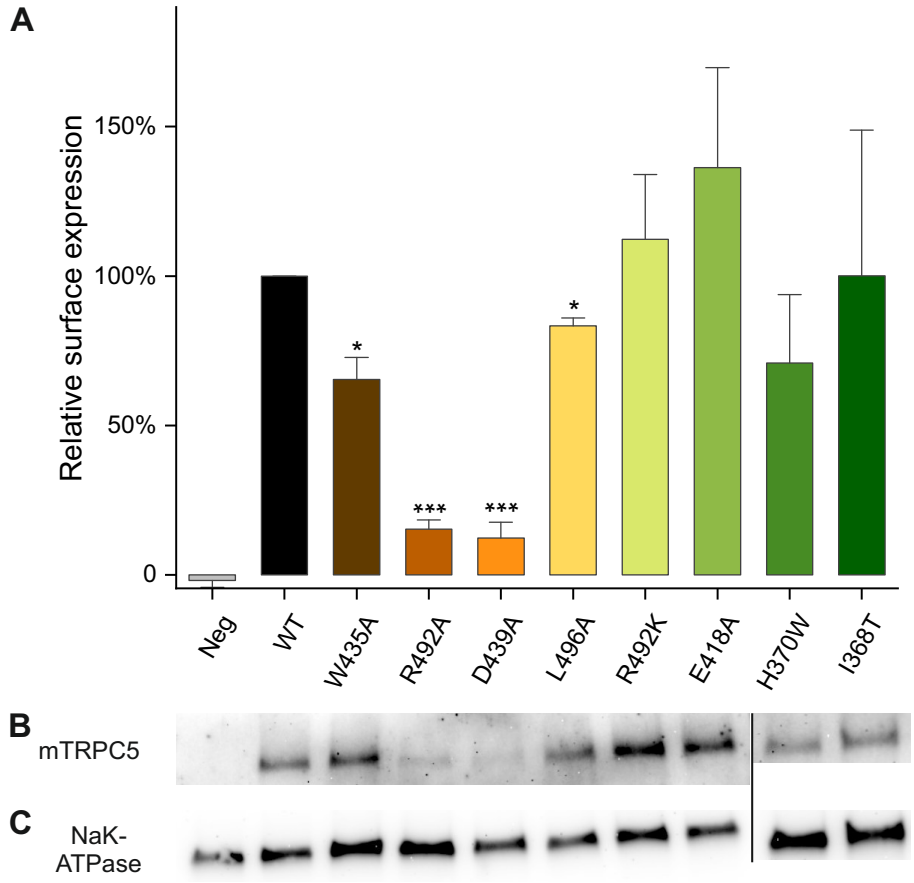

Figure 3.41.: **Surface expression of possible riluzole binding mutants.** This figure shows the surface expression of possible riluzole binding mutants. **(A)** represents the results of 3 individual western blot experiments (+ SD). The statistical significance was calculated using a two sided t-test and tested against the wildtype expression (WT) (* $p < 0.05$, ** $p < 0.01$, *** $p < 0.001$). **(B)** shows a representative western blot of the respective mutant TRPC5 channel expression. The image displays an automatically contrast optimized image using the integrated BioRad software. The vertical line represents an additional blot membrane. **(C)** represents the same blot as **(B)** after stripping and incubation with the anti-NaK-ATPase antibody.

To validate the membrane expression of the TRPC5 mutants that might specifically interfere with the riluzole binding, their surface expression was quantified by performing surface biotinylation and western blot experiments. As demonstrated in Figure 3.41, the relative surface expression of the mutants fluctuates between 136 % suggesting a slight overexpression and 12 % indicating a low expression.

3.4.1. Surface Expression Profile of Potential Riluzole Binding Mutants

The mutant W435A shows a significantly lower surface expression of 65 % compared with the wildtype (Figure 3.41A). This data fits well to the data obtained by electrophysiological whole-cell measurements (Figure 3.15). W435A produces a highly significant reduction of maximal riluzole-induced current densities. The (-)-englerin A-induced current densities were also significantly reduced but to a lesser extent (Figure 3.15). The data obtained via western blot confirm these results by indicating a slightly, but significantly lower surface expression compared to the wildtype (Figure 3.41A).

The mutant R492A did not show any current increases during application of riluzole and (-)-englerin A (Figure 3.4A, E). Therefore, the surface expression of this mutant was analyzed. In line with the electrophysiological data, the surface expression is significantly reduced (around 15 % of the wildtype TRPC5 channel), indicating that the abolished current responses are correlated with a strongly reduced surface expression (Figure 3.4A, E). But the low surface expression alone cannot explain why mutant the R492A has no current signal, because the mutant D439A is expressed at roughly the same level (12 % Figure 3.41A), but does not result in a complete loss of the channel function (Figure 3.33A, E). Therefore, R492A does not only have a low surface expression but also an impaired channel function.

The channel mutation D439A produces a significantly reduced (-)-englerin A evoked current response and the riluzole-induced currents are completely suppressed (Figure 3.33A, E). The surface expression is likewise significantly reduced (Reduced to 12 %, Figure 3.41A). But in contrast to R492A, D439A produces a functional channel even though the surface expression is very low.

The mutation L496A results in a slightly lower (83 %), but significantly reduced surface expression compared to the wildtype (Figure 3.41A). However, the (-)-englerin A-induced maximal current densities are unchanged, whereas the riluzole current densities are significantly reduced (Figure 3.38A, G). Therefore, it is not clear if the riluzole evoked current densities are just reduced because of the slightly lowered surface expression.

The mutations R492K, E418A, H370W and I368T show no significant changes in the surface expression (Figure 3.41A). This corresponds very well to the electrophysiological data. None of the four previously mentioned mutations show any significant changes in the (-)-englerin A evoked current densities (which served as an expression estimation, see Figure 3.22, Figure 3.26 and Figure 3.33), but a strong reduction in riluzole evoked current densities. Thus, these amino acids are well expressed at the cell membrane and might be involved in direct interaction with the ligand riluzole.

(-)-Englerin A as an Expression Control for Riluzole Mutants

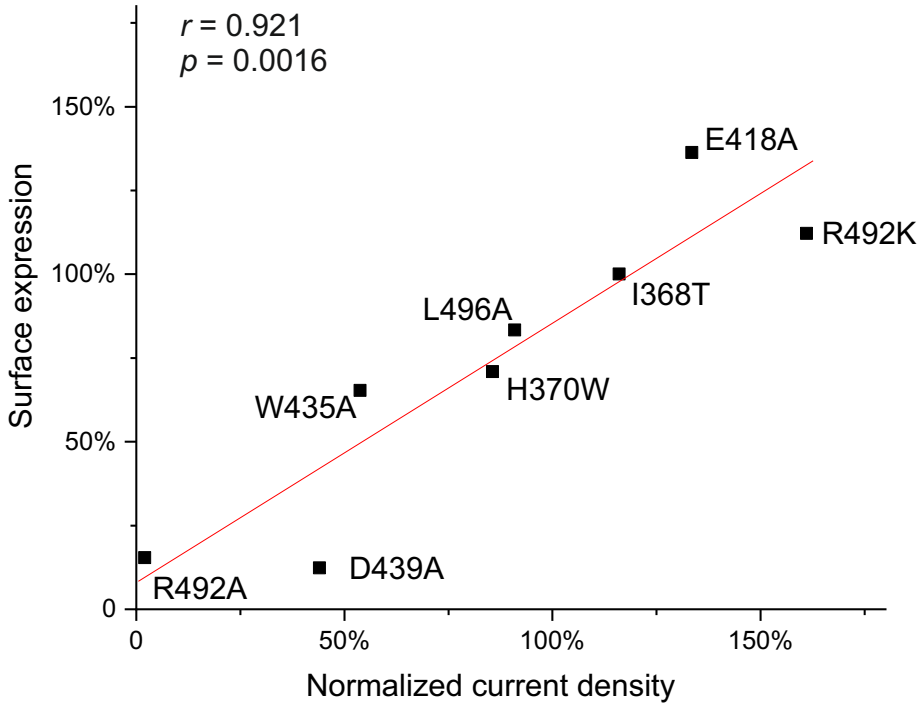

Figure 3.42.: **Correlation between surface expression of riluzole mutants measured via western blot and estimated via patch clamp experiments.** This figure shows the correlation analysis between the surface expression of riluzole mutants determined by western blot and the normalized maximal (-)-englerin A induced current densities determined by patch clamp experiments. Analysis of the linear regression yields a pearson $r = 0.912$ with $p = 0.0016$.

Figure 3.42 illustrates the correlation between the measured surface expression based on western blot experiments and the corresponding (-)-englerin A evoked current densities. With the exception of the mutant L496A all tested mutants show the same significance levels for the surface expression obtained by western blot experiments and the surface expression estimation based on (-)-englerin A evoked current densities. Taken together, (-)-englerin A evoked current densities serve well as an expression control for possible riluzole binding mutants and correlate well with the real surface expression measurements obtained via western blot (Pearson $r = 0.912$ with $P = 0.0016$).

3.5. Docking Project III

3.5.1. Extracellular and Pore Neighbouring Regions

For pentameric ligand-gated ion channels it is known that ligands bind to the extracellular side of the channel (Sauguet et al., 2015) like for example ben-

zodiazepines bind to GABA receptors (Spurny et al., 2012) or glutamate binds to glutamate-gated chloride channels (Hibbs & Gouaux, 2011). Regarding extracellular binding sites in TRPC channels, only the extracellular binding site for lanthanum-ions and protons is known so far.

Jung et al. (2003) showed that the glutamate residues Glu^{543}, Glu^{595} and Glu^{598} are important for the potentiation of TRPC5 by lanthanides, but no ion was co-crystallized at extracellular sites so far. The proton binding site of TRPC5 is thought to be similar to the lanthanide binding site (Semtner et al., 2007). Later Jeong et al. (2019) proposed that (-)-englerin A might also bind to TRPC5 in the aforementioned extracellular region by interacting with similar amino acids including Lys^{554}, His^{594} and Glu^{598}.

Therefore two additional docking runs were carried out in this region (docking project III). One docking cube was aimed to the postulated (-)-englerin A binding site (cavity IIIa), the other docking was done in close proximity but including the region on top of the pore helix (IIIb). Because both dockings are overlapping and the cavities are not clearly separated, the region is regarded as one cavity as illustrated in Figure 3.43. In the whole docking project, (-)-englerin A was used as a ligand because of its suggested binding in this area (Jeong et al., 2019). The ligand positions and potential interacting amino acids can be looked up in Appendix B, whereas the amino acid positions of potential binding residues are presented in Figure 3.44.

The cavity between pore helix and TM6 is known to play an important role in TRPC channels as suggested by recent publications. In 2013 Lichtenegger et al. suggested a coupling between the selectivity filter which is built by the pore loop and the lower gate. This phenomenon of a transduction link between lower gate and selectivity filter is already known from p-loop channels (Capes et al., 2012; Liu & Siegelbaum, 2000; Zhen et al., 2005). Lichtenegger et al. (2018) stated that amino acid residue G^{652} located in TM6 is involved in a fenestration mechanism of the photoswitchable DAG analogue OptoDArG mediated TRPC3 activation. This leads to first assumptions of a ligand binding in this cavity and its general importance for channel regulation. To further investigate the role of this part of the channel for ligand binding, an additional docking was carried out at this site (see Figure 3.43).

The docking revealed residue F^{576} as a very important potential binding candidate (see Appendix B). In 2019 Duan et al. showed that F^{576} and W^{577} render the affinity to (-)-englerin A activation of TRPC5, but much rather stayed with the hypothesis of Strübing et al. (2003), claiming that the so called LFW motif is important for general channel functionality and not so much for a specific ligand interaction. Later, Wright et al. (2020) stated that this site might be a xanthine binding site which was confirmed by co-crystallization of the xanthine-based TRPC5 inhibitor Pico-145. One year later, Song et al. (2021) further confirmed this ligand binding site by co-crystallization of HC-070, another xanthine-based inhibitor of TRPC5. They also made first assumptions that (-)-englerin A might bind there. With the knowledge of the data of Wright et al. (2020) and the general importance of the given site in TRPC channels, more mutations were conducted, which are described and discussed in the following sections.

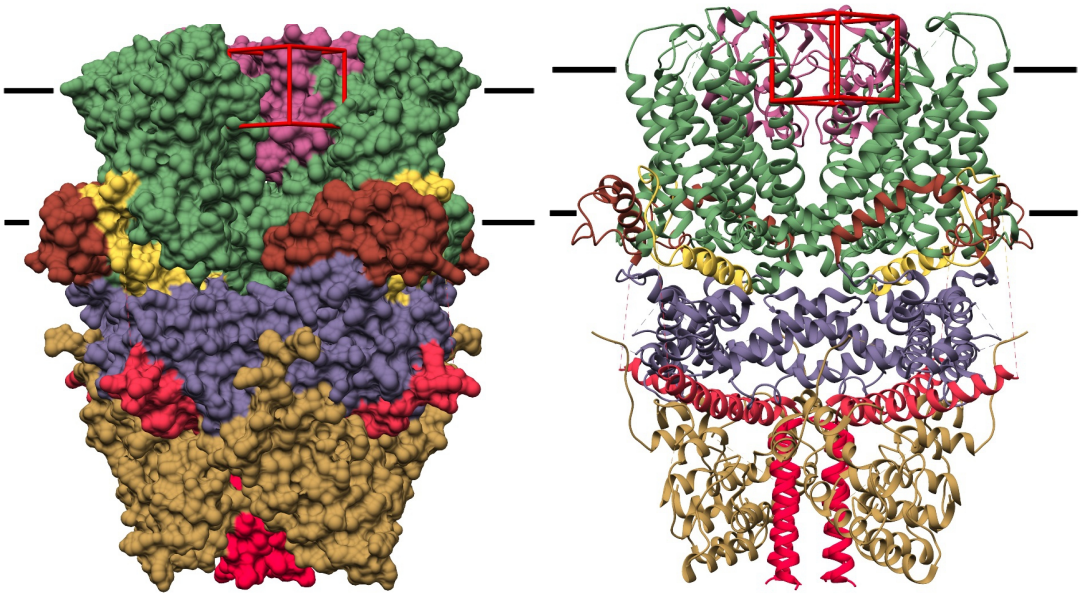

(a) TRPC5 surface structure with docking cube at position III.

(b) TRPC5 ribbon structure with docking cube at position III.

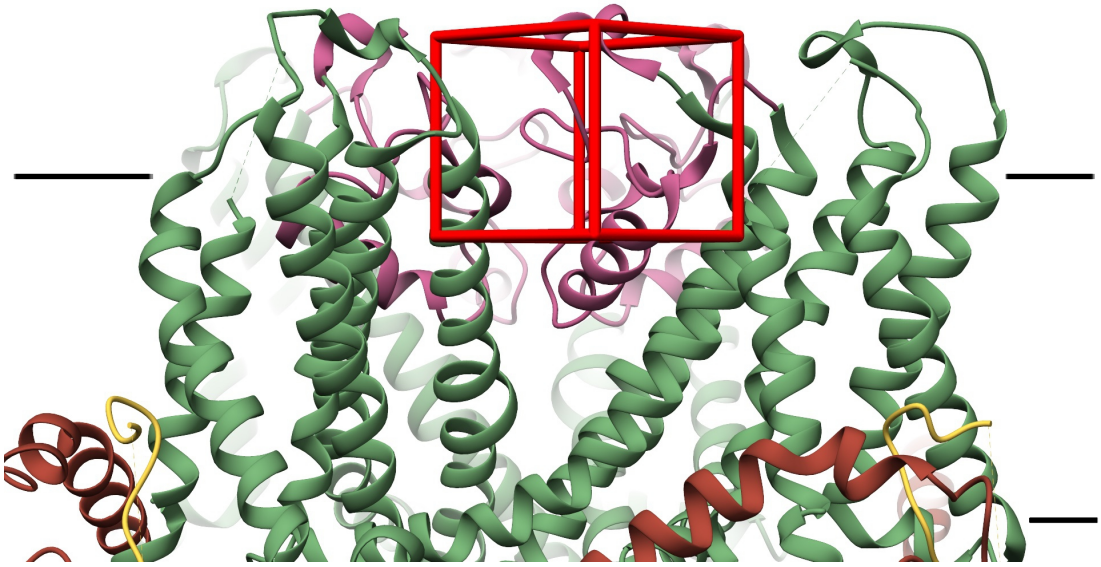

(c) TRPC5 ribbon structure with a detailed view of docking cube III.

Figure 3.43.: **Docking area in cavity III.** In this figure, docking position III is shown. TRPC5 (PDB: 6AEI, Duan et al. (2018a)) is presented either with its surface structure (a), or ribbon structure (b) and colored according to Figure 1.1. Subfigure c is a closeup of (b) for better visualization of the cube.

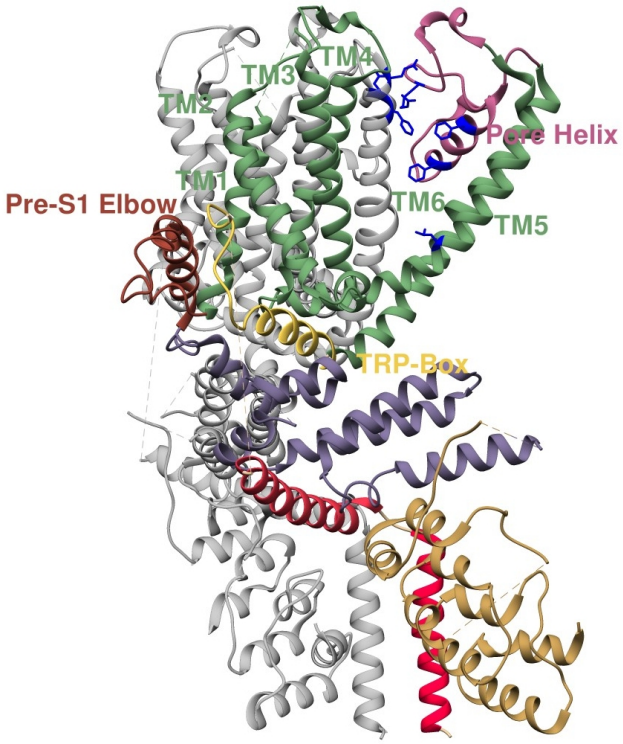

(a) Overview of the amino acids potentially involved in binding of (-)-englerin A and their respective orientation and position (blue residues).

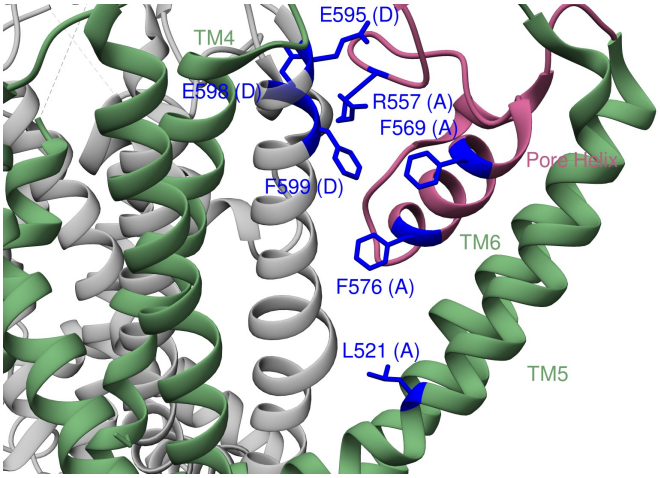

(b) Detailed view of the amino acids potentially involved in binding of (-)-englerin A and their respective orientation and position (blue residues).

Figure 3.44.: **Potential Ligand Binding Amino Acids of Cavity III/IV.** In this figure, TRPC5 (PDB: 6AEI) and amino acids which are potentially involved in binding of riluzole or (-)-englerin A are displayed with their respective orientation and position (red residues). Channel elements are colored according to Figure 1.1.

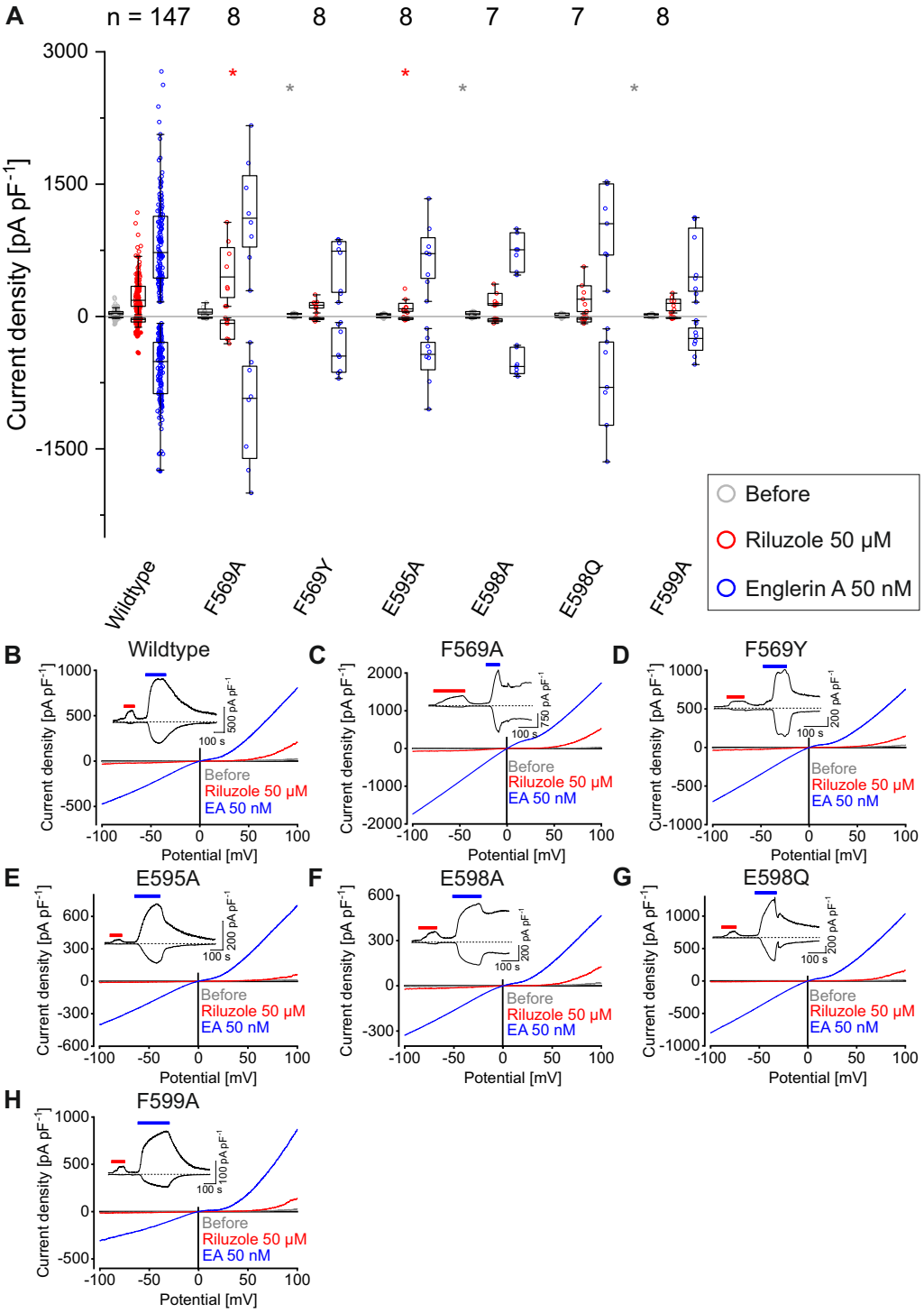

Figure 3.45.: **Whole-cell measurements of potential ligand binding amino acids in cavity III. (A)** shows the maximal and minimal current density at the potentials 100 mV and −100 mV evoked by the given treatment, respectively. Their respective distribution is indicated by the median (horizontal line) and 50 % of the data points (box) as well as the 1.5 × IQR (whiskers). The number of independent experiments is indicated by numbers over the plot. * $P < 0.05$, ** $P < 0.01$, *** $P < 0.001$ (Tested against Wildtype (WT); Mann-Whitney-U). **(B-H)** show representative single CDV curves during the given treatments selected at maximal current responses. The insets show the corresponding current density time course of the same measurement.

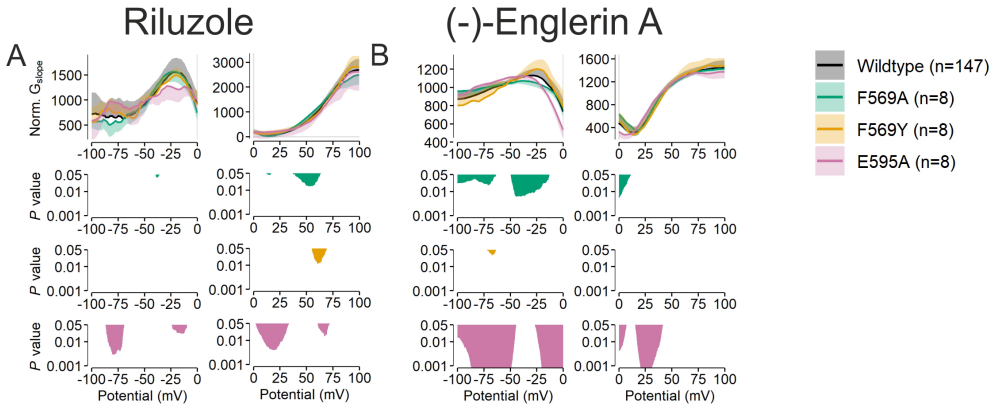

Figure 3.46.: **NSC of potential ligand binding amino acids in cavity III** This figure shows the calculated NSC (Hermann et al., 2022) of the given mutation (top) $\pm SD$ compared to the wildtype NSC during the given treatment (bottom). Statistical significance was analyzed using the Mann-Whitney-U-test. n indicates the number of independent experiments.

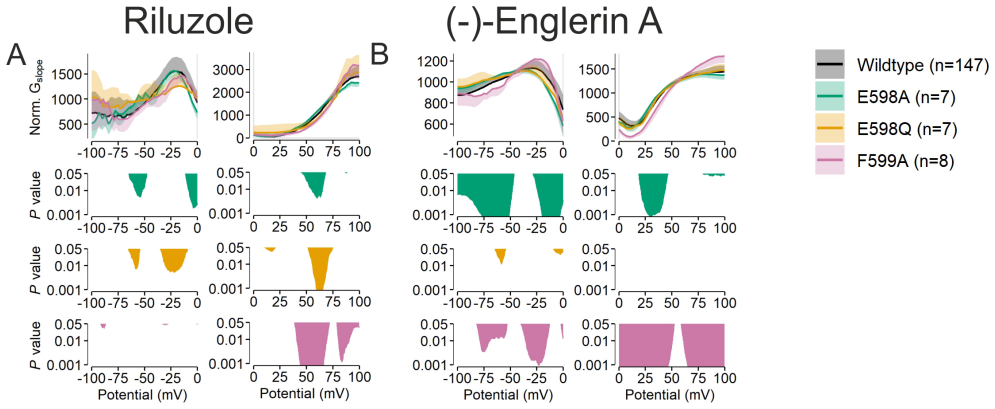

Figure 3.47.: **NSC of potential ligand binding amino acids in cavity III.** This figure shows the calculated NSC (Hermann et al., 2022) of the given mutation (top) $\pm SD$ compared to the wildtype NSC during the given treatment (bottom). Statistical significance was analyzed using the Mann-Whitney-U-test. n indicates the number of independent experiments.

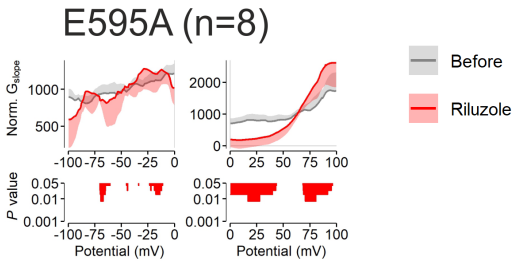

Figure 3.48.: **NSC of potential ligand binding amino acids in cavity III.** This figure shows the calculated NSC (Hermann et al., 2022) of the given mutation (top) $\pm SD$. The NSC under riluzole stimulation is compared with the basal NSC before any treatment (bottom). Statistical significance was analyzed using the Wilcoxon signed-rank test. n indicates the number of independent experiments.

In the dockings (see Appendix B) two amino acids were identified that might play a crucial role in potential (-)-englerin A binding in cavity IIIa, namely Gln^{595} and Phe^{599}. Their respective location and orientation is shown in Figure 3.44.

Phe^{569} emerged in docking III and was selected because of its contribution to many binding positions. Amino acid Glu^{598} is already described to play a role in the potentiation of TRPC5 by lanthanides and protons and might as well play a role for the (-)-englerin A binding, as mentioned above. Therefore glutamate at position 598 was substituted by glutamine, aspartate and alanine. Due to the overlapping of subcavities IIIa and IIIb as well as partly cavity IV, some amino acids show up in all dockings, therefore the three cavities are presented together.

As illustrated in Figure 3.45 all tested mutant channels are still functional and produce a current signal with both activators.

The riluzole evoked current densities of phenylalanine at position 569 substituted by alanine are significantly increased (Figure 3.45A). The (-)-englerin A induced current densities are also increased, however, the increase was not significantly different to the wildtype current densities and might be due to a slightly increased surface expression. Phe^{569} is located in the pore helix and close to the selectivity filter which might change ion selectivity or conductance. However, the NSC of the riluzole and (-)-englerin A evoked IV curves show only a few significant differences when compared to the wildtype, respectively (Figure 3.46, green plots).

Mutation of glutamate at position 595 to alanine shows significantly reduced riluzole evoked current densities, but unchanged (-)-englerin A evoked current densities compared to the wildtype (Figure 3.45A). The current density time course shows only a small riluzole evoked peak as well (Figure 3.45E, embedded figure). The CDV curves show a nearly congruent course before and after riluzole application. Interestingly, this may suggests a riluzole specific effect. Possible causes for this are discussed in the discussion section in more detail. However, the NSC suggests mainly significant differences in the (-)-englerin A evoked IV, especially in the inward current (Figure 3.46B, magenta plot).

All other mutations (F569Y, E598A, E598Q, F599A) of the dockings in cavity III show no significant changes in the current densities during the consecutively applied activators riluzole and (-)-englerin A (Figure 3.45A). The CDV curves (Figure 3.45) still show a typical TRPC5 course with a double rectification and a reversal potential at 0 mV. However, the NSC of the (-)-englerin A evoked IV curves of the mutations E598A and F599A show highly significant differences compared with the wildtype, respectively (Figure 3.47). Mutations in this region may destabilize the pore helix or indirectly destabilize the (-)-englerin A binding, but nonentheless a (-)-englerin A binding at this specific extracellular site is unlikely because no mutation chosen from the given docking is able to specifically reduce the (-)-englerin A evoked current density.

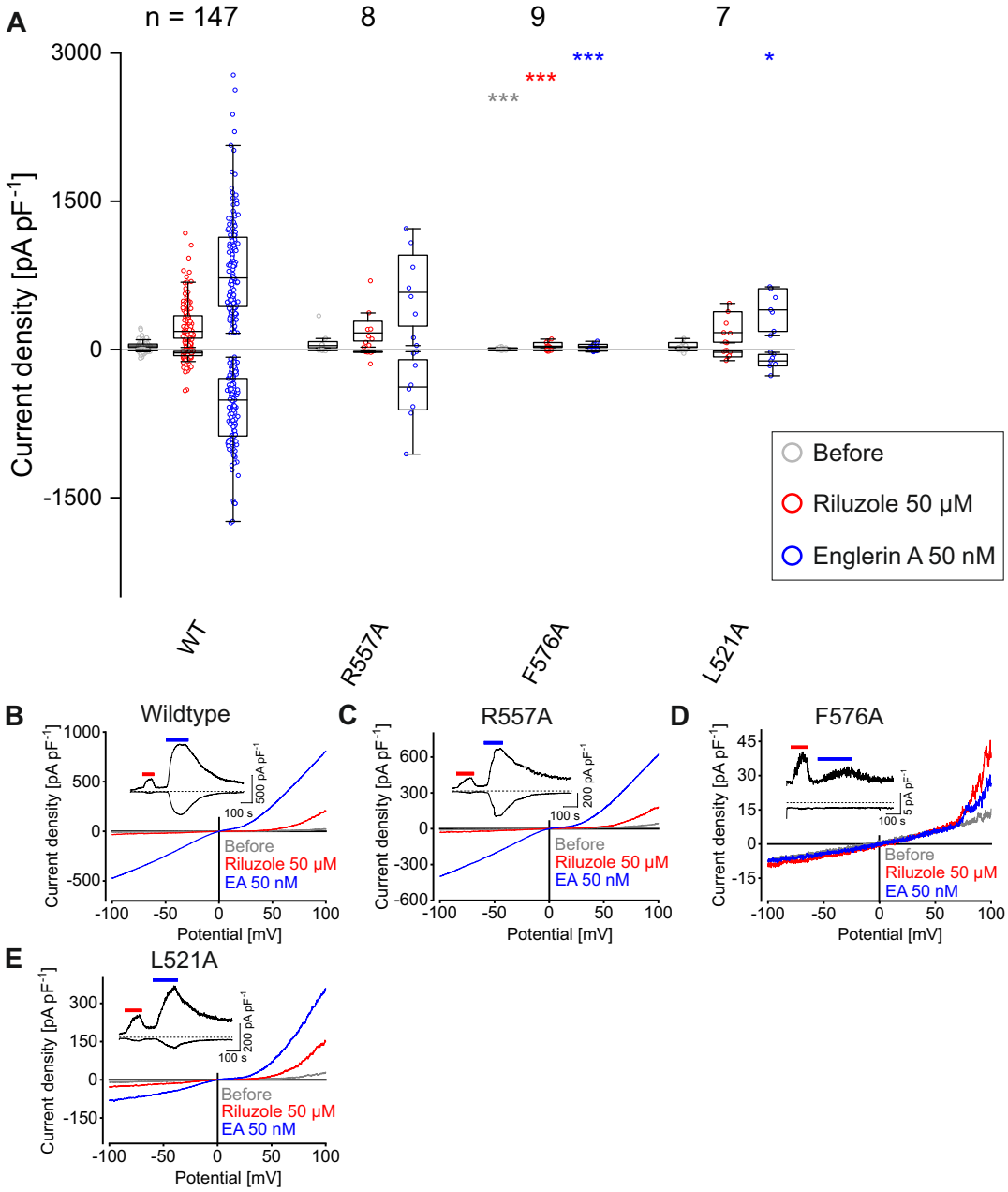

Figure 3.49.: **Whole-cell measurements of potential ligand binding amino acids in cavity III/IV. (A)** shows the maximal and minimal current density at the potentials 100 mV and −100 mV evoked by the given treatment, respectively. Their respective distribution is indicated by the median (horizontal line) and 50 % of the data points (box) as well as the 1.5 × IQR (whiskers). The number of independent experiments is indicated by numbers over the plot. * $P < 0.05$, ** $P < 0.01$, *** $P < 0.001$ (Tested against Wildtype (WT); Mann-Whitney-U). **(B-E)** show representative single CDV curves during the given treatments selected at maximal current responses. The insets show the corresponding current density time course of the same measurement.

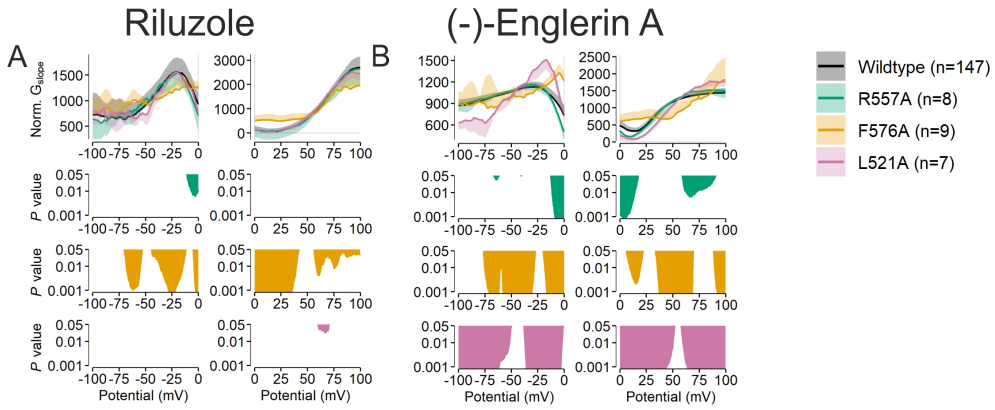

Figure 3.50.: **NSC of potential ligand binding amino acids in cavity III/IV.** This figure shows the calculated NSC (Hermann et al., 2022) of the given mutation (top) $\pm SD$ compared to the wildtype NSC during the given treatment (bottom). Statistical significance was analyzed using the Mann-Whitney-U-test. n indicates the number of independent experiments.

Phe^{576} and Leu^{521} were the only amino acids chosen from the docking in cavity IV and Arg^{557} was chosen from the docking in cavity IIIb. The amino acid Arg^{557} is located at the edge between the two binding pockets IIIa and b (Figure 3.44) and therefore contributes to a potential interaction in both pockets (further see Appendix B).

The mutation R557A does not produce any significant changes in neither the current densities (Figure 3.49A) nor the current density time course (Figure 3.49C, embedded figure) and CDV curves (Figure 3.49C). The NSC of the riluzole and (-)-englerin A evoked IV curve only shows small significant differences between R557A and the wildtype, respectively (Figure 3.50).

However, the amino acid phenylalanine at position 576 exchanged for alanine causes a strong and significant reduction of the riluzole and (-)-englerin A induced current densities (Figure 3.49A). Strikingly, the riluzole evoked responses were higher than the (-)-englerin A induced current densities (Figure 3.49D, embedded figure). The CDV curves show a similar phenomenon, where the riluzole evoked CDV curve shows a higher amplitude than the CDV curve during (-)-englerin A application. The NSC of the riluzole and (-)-englerin A evoked IV curves similarly show significant differences in nearly the whole course when compared to the wildtype, respectively (Figure 3.50, yellow plot). This suggests an (-)-englerin A specific effect and supports the notion that the amino acid Phe^{576} might be involved in (-)-englerin A binding, even though the overall channel functionality or the surface expression might be decreased.

The amino acid exchange leucine at position 521 for alanine shows significantly lower current densities after (-)-englerin A application, whereas the riluzole evoked current densities are unchanged compared to the wildtype (Figure 3.49A). The current density time course, as well as the CDV curves show a similar result, where the evoked peak and corresponding CDV curve during (-)-englerin A application is lowered compared to the wildtype and the riluzole evoked peak and corresponding CDV curve are comparable to the wildtype, respectively (Figure 3.49E and embedded figure). The NSC of the riluzole evoked IV curves indicate nearly no significant differences compared to the wildtype (Figure 3.50A, magenta plot), whereas the NSC of the (-)-englerin A evoked IV curve shows significant differences nearly over the whole course. Therefore, these results suggest a similar impression as obtained by analyzing the current densities of the mutant F521A. This may indicate a (-)-englerin A specific effect and therefore a possible binding of (-)-englerin A to Leu^{521}.

With the knowledge of amino acids Phe^{576} and L^{521} being possible (-)-englerin A binding partners, dockings in the region were reevaluated and surrounding amino acids were also mutated. This relates especially to the docking in cavity IV (see Figure 3.51).

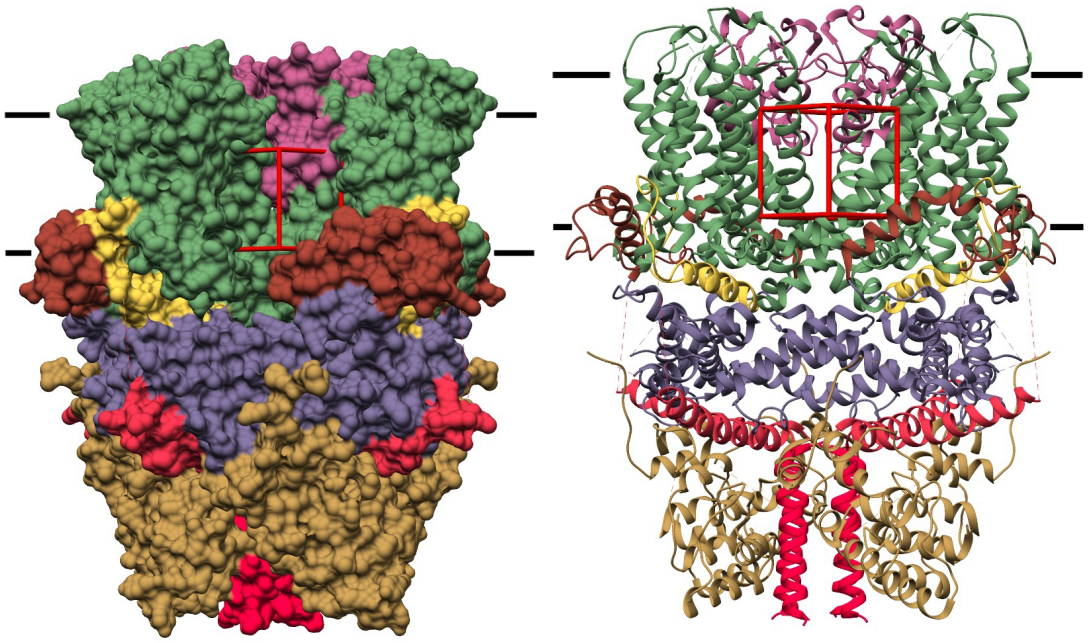

(a) TRPC5 surface structure with docking cube at position IV.

(b) TRPC5 ribbon structure with docking cube at position IV.

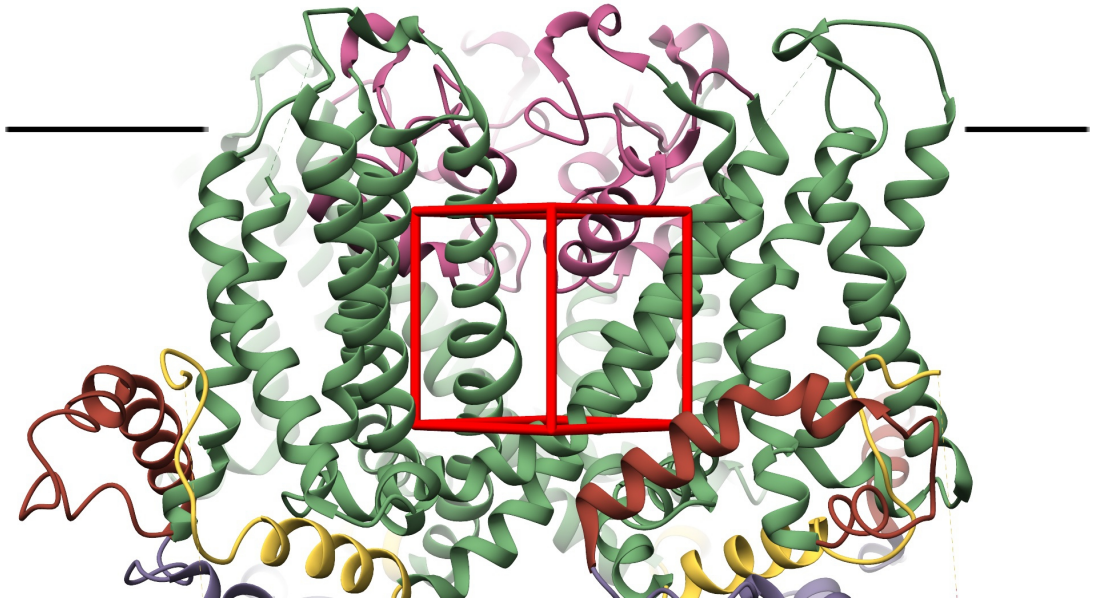

(c) TRPC5 ribbon structure with a detailed view of docking cube IV.

Figure 3.51.: **Docking Area in Cavity IV.** In this figure, docking position IV is shown. TRPC5 (PDB: 6AEI, Duan et al. (2018a)) is presented either with its surface structure (a), or ribbon structure (b) and colored according to Figure 1.1 but independently of their related protein chain. Subfigure c is a closeup of (b) for better visualization of the cube.

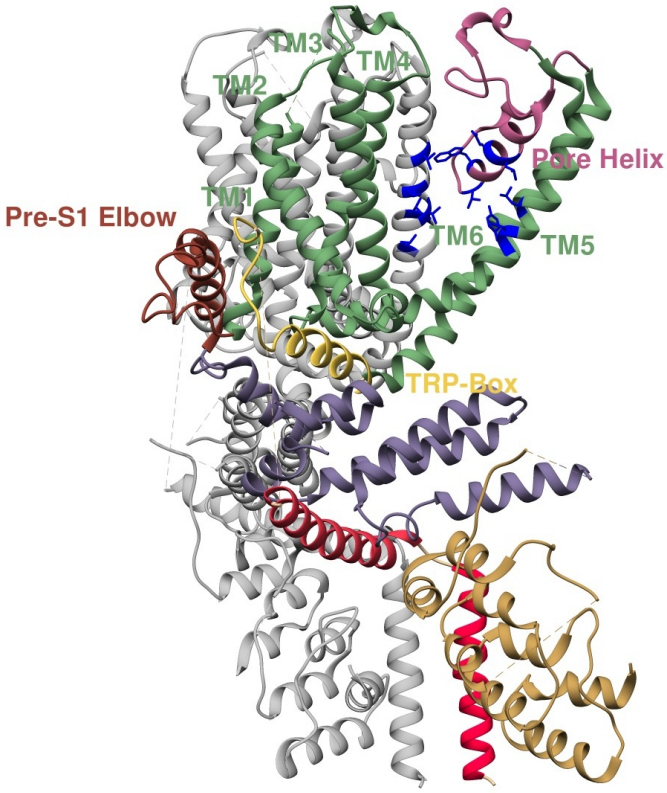

(a) Overview of the amino acids potentially involved in binding of (-)-englerin A and their respective orientation and position (blue residues).

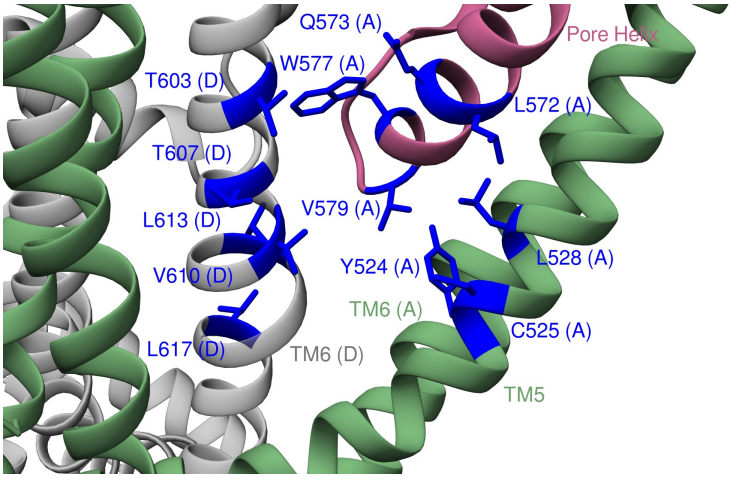

(b) Detailed view of the amino acids potentially involved in binding of (-)-englerin A and their respective orientation and position (blue residues).

Figure 3.52.: **Potential ligand binding amino acids of cavity IV.** In this figure, TRPC5 (PDB: 6AEI) and amino acids which are potentially involved in binding of (-)-englerin A are displayed with their respective orientation and position (blue residues). Channel elements are colored according to Figure 1.1.

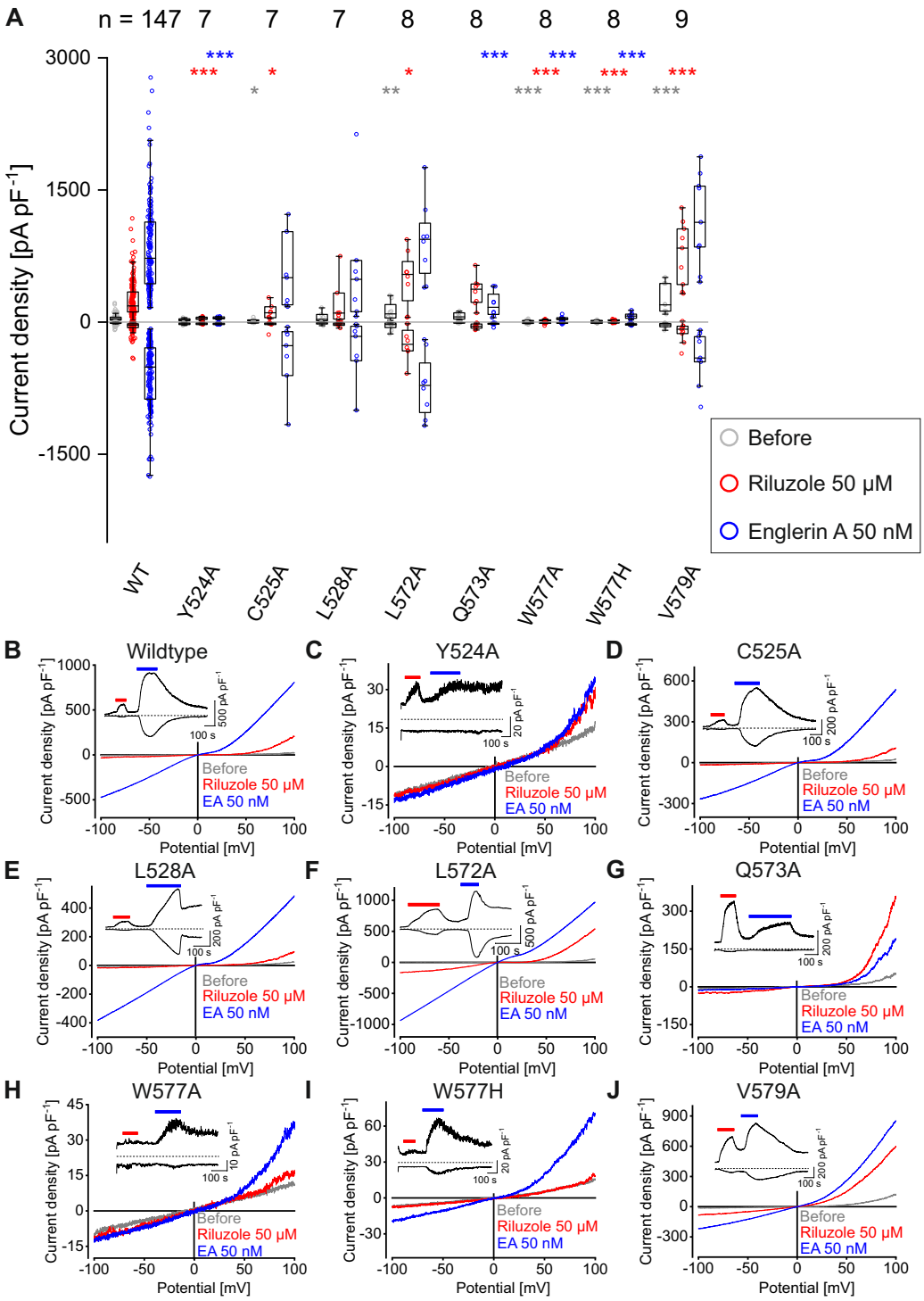

Figure 3.53.: **Whole-cell measurements of potential ligand binding amino acids in cavity IV. (A)** shows the maximal and minimal current density at the potentials 100 mV and −100 mV evoked by the given treatment, respectively. Their respective distribution is indicated by the median (horizontal line) and 50 % of the data points (box) as well as the 1.5 × IQR (whiskers). The number of independent experiments is indicated by numbers over the plot. * $P < 0.05$, ** $P < 0.01$, *** $P < 0.001$ (Tested against Wildtype (WT); Mann-Whitney-U). **(B-J)** show representative single CDV curves during the given treatments selected at maximal current responses. The insets show the corresponding current density time course of the same measurement.

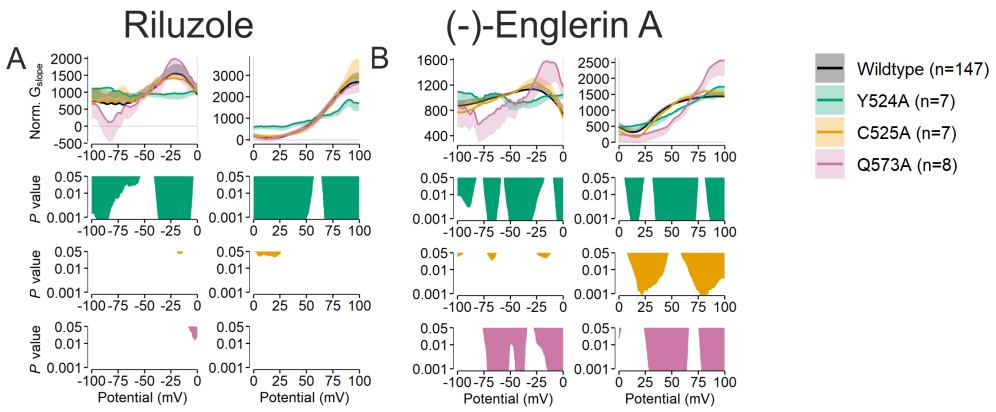

Figure 3.54.: **NSC of potential ligand binding amino acids in cavity IV.** This figure shows the calculated NSC (Hermann et al., 2022) of the given mutation (top) $\pm SD$ compared to the wildtype NSC during the given treatment (bottom). Statistical significance was analyzed using the Mann-Whitney-U-test. n indicates the number of independent experiments.

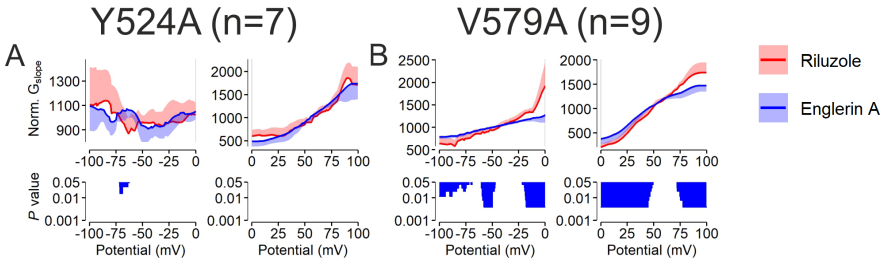

Figure 3.55.: **NSC of potential ligand binding amino acids in cavity IV.** This figure shows the calculated NSC (Hermann et al., 2022) of the given mutation (top) $\pm SD$. The NSC under (-)-englerin A stimulation is compared with the NSC under riluzole treatment (bottom). Statistical significance was analyzed using the Wilcoxon signed-rank test. n indicates the number of independent experiments.

The exchange tyrosine at position 524 for alanine produces a phenotype that is similar to the phenotype of mutation F576A. The riluzole and (-)-englerin A evoked current densities are significantly reduced, therefore the overall currents are low (Figure 3.53A). This result is confirmed by the current density time course and the CDV plots. The CDV relations of the riluzole and the (-)-englerin A evoked currents show a nearly congruent course(Figure 3.53C). The current density time course shows only low current density increases by application of riluzole or (-)-englerin A (Figure 3.53C, embedded figure). But nonetheless, the riluzole evoked current density peak has the same height as the (-)-englerin A evoked current density peak (Figure 3.53C, embedded figure). The NSC of the riluzole and (-)-englerin A evoked IV curves show significant differences over nearly the whole course when compared with the wildtype, respectively (Figure 3.54, green plot). Interestingly, when comparing the NSC of the riluzole and (-)-englerin A evoked IV curve of the mutant Y524A with each other, no significant differences can be observed, meaning that the IV relation during the riluzole stimulation is very similar to the IV relation during the (-)-englerin A stimulation (Figure 3.55A). Taken together, this may suggest an (-)-englerin A specific effect and consequently a possible binding of (-)-englerin A to Tyr^{524}.

The amino acid exchange cysteine at position 525 for alanine shows a significant reduction of the riluzole evoked current densities (Figure 3.53A) and no significant reductions of the (-)-englerin A evoked current densities. The current density time course and the CDV relations both are not distinguishable from the wildtype (Figure 3.53D). The NSC of the riluzole evoked IV curves however indicate only a few significant differences compared to the wildtype, whereas the NSC of the (-)-englerin A evoked IV curve shows highly significant differences in the outward current (Figure 3.54, yellow plot). The riluzole specific current density reduction is hardly explainable. Maybe Cys^{525} has influence on the lower gate as well, as it has been shown for other amino acids in TM5 (like Gly^{511} or Asn^{500}) or it has stabilizing effects on TM6, which influences the riluzole mediated activation.

The mutation of leucine at position 528 to alanine results in no significant reduction of the current densities, neither before nor during consecutive riluzole and (-)-englerin A application (Figure 3.53A).

The amino acid exchange leucine at position 572 for alanine produces a phenotype with significantly higher riluzole evoked current densities and no significant changes in the (-)-englerin A induced current densities (Figure 3.53A).

The mutation glutamine at position 573 exchanged for alanine causes a particularly interesting phenotype: The riluzole evoked current densities are not changed compared to the wildtype, but the (-)-englerin A evoked current densities are significantly reduced (Figure 3.53A). The current density time course shows a higher riluzole elicited peak than the consecutive (-)-englerin A evoked peak (Figure 3.53G, embedded figure). The CDV curve during riluzole application has a greater amplitude than during (-)-englerin A application (Figure 3.53G). Remarkably, the inward current densities are not increasing during (-)-englerin A application. This may has something to do with the location of the amino acid Gln^{573}, being in the pore helix, which is pointing to an effect on the pore and/or on the selectivity filter. By manipulating the pore helix structure, effects on the selectivity filter are likely. Similarly, the NSC shows highly significant differences in the (-)-englerin A evoked current but nearly no differences in the NSC of the riluzole evoked current compared with the wildtype, respectively (Figure 3.54

magenta plot). Taken together, the mutation Q573A results in the most obvious effect on the (-)-englerin A evoked current densities. Therefore Gln^{573} might be involved in direct (-)-englerin A binding.

The mutation valine at 579 replaced by alanine results in a mutant channel with a significant increase in the riluzole evoked current densities, whereas the (-)-englerin A elicited current densities are unchanged compared to the wildtype channel (Figure 3.53A). In the current density time course (Figure 3.53J, embedded figure), as well as in the CDV curve (Figure 3.53J), the riluzole evoked peak amplitude is nearly as high as the (-)-englerin A evoked current amplitude. Nonetheless, the NSC of the riluzole and (-)-englerin A evoked IV curves are significantly different (Figure 3.55B). Val^{579} is in very close proximity to the selectivity filter (the restriction point is Gly^{581}) and the last amino acid of the pore helix. Therefore amino acid exchanges in the pore helix are likely to affect the current amplitudes.

Mutations of Trp^{577}, namely to alanine and histidine result in a phenotype with strong overall current density reductions before and during consecutive riluzole and (-)-englerin A application (Figure 3.53A). Therefore either the channel functionality or the surface expression are low. Interestingly, both mutations show hardly any riluzole evoked current (Figure 3.53H, I, embedded figures). It is hard to tell if the overall current is too low to see any riluzole evoked current density peaks, because riluzole inherently shows lower current densities than (-)-englerin A. Other mutations around or directly in the pore helix like F569A (Figure 3.45), L572A and V579A (Figure 3.53) show a similar effect. However, these mutations all increase the riluzole induced current amplitude compared to the wildtype. Taken together, this may suggests a riluzole specific effect of W577A and W577H but the overall channel functionality or expression is reduced, therefore a specific effect is hard to determine.

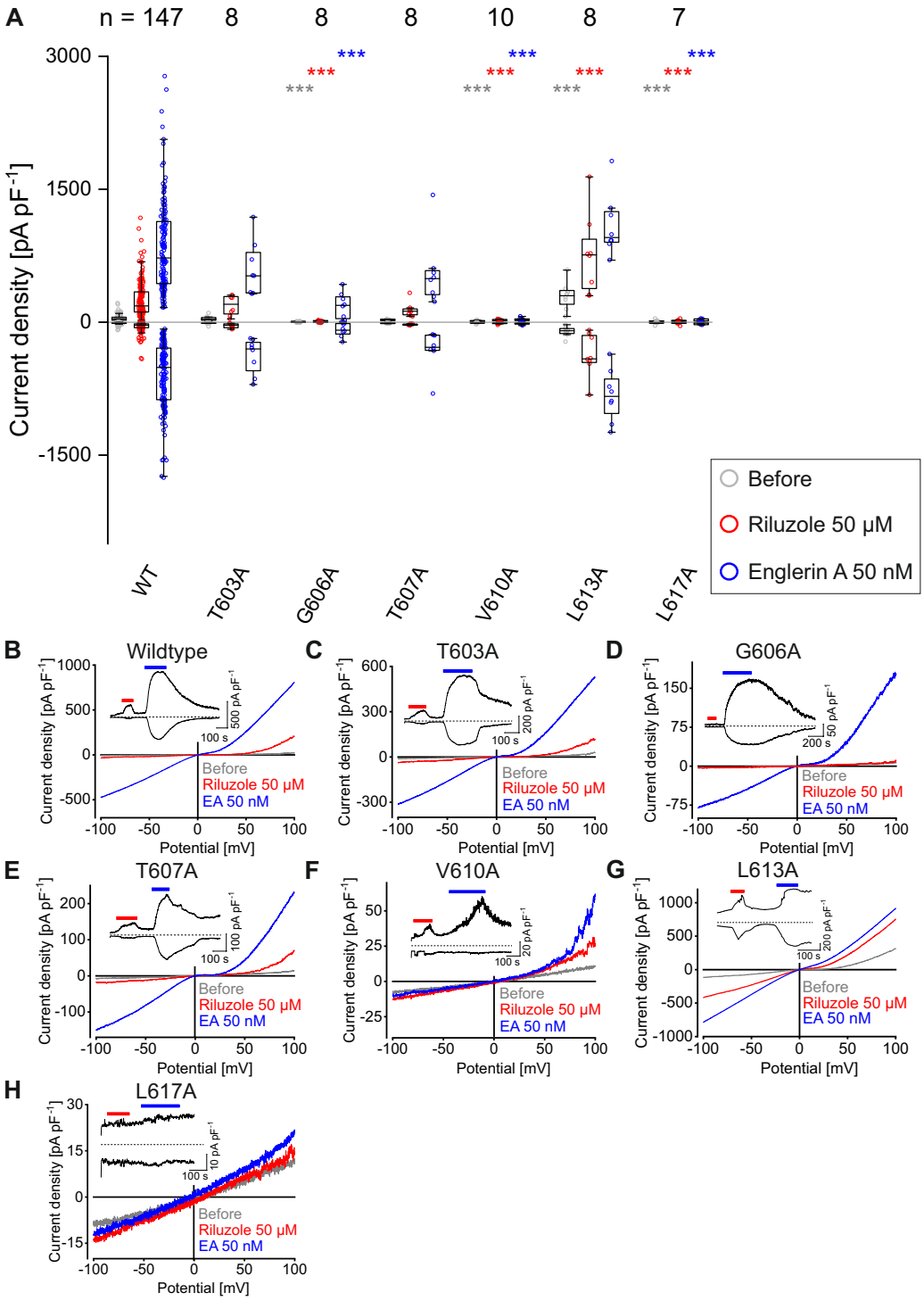

Figure 3.56.: **Whole-cell measurements of potential ligand binding amino acids in cavity IV. (A)** shows the maximal and minimal current density at the potentials 100 mV and −100 mV evoked by the given treatment, respectively. Their respective distribution is indicated by the median (horizontal line) and 50 % of the data points (box) as well as the 1.5 × IQR (whiskers). The number of independent experiments is indicated by numbers over the plot. * $P < 0.05$, ** $P < 0.01$, *** $P < 0.001$ (Tested against Wildtype (WT); Mann-Whitney-U). **(B-H)** show representative single CDV curves during the given treatments selected at maximal current responses. The insets show the corresponding current density time course of the same measurement.

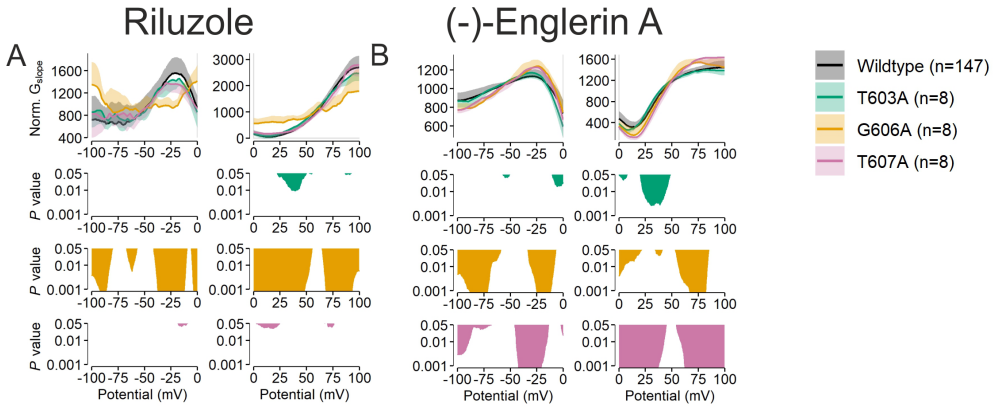

Figure 3.57.: **NSC of potential ligand binding amino acids in cavity IV.** This figure shows the calculated NSC (Hermann et al., 2022) of the given mutation (top) $\pm SD$ compared to the wildtype NSC during the given treatment (bottom). Statistical significance was analyzed using the Mann-Whitney-U-test. n indicates the number of independent experiments.

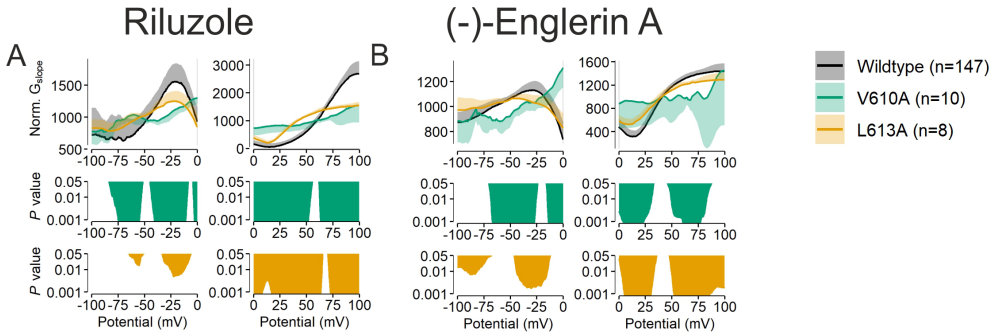

Figure 3.58.: **NSC of potential ligand binding amino acids in cavity IV.** This figure shows the calculated NSC (Hermann et al., 2022) of the given mutation (top) $\pm SD$ compared to the wildtype NSC during the given treatment (bottom). Statistical significance was analyzed using the Mann-Whitney-U-test. n indicates the number of independent experiments.

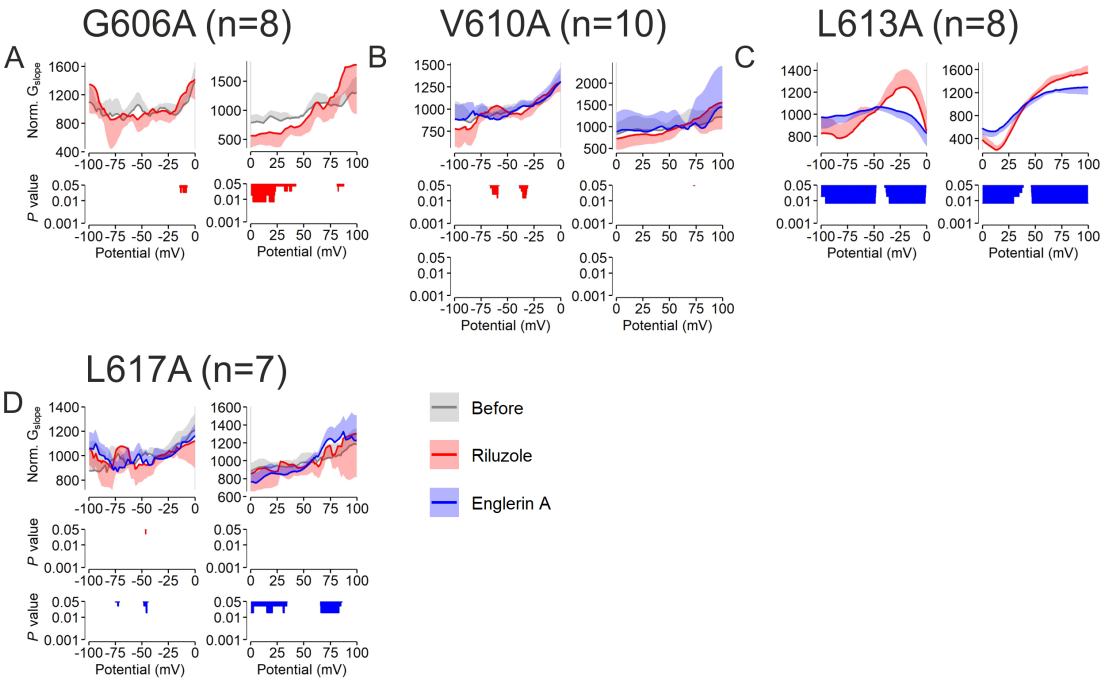

Figure 3.59.: **NSC of potential ligand binding amino acids in cavity IV.** This figure shows the calculated NSC (Hermann et al., 2022) of the given mutation (top) $\pm SD$. **(A,B,D)** The given treatment is compared with the basal NSC before any treatment (bottom) or **(C)** with the NSC under riluzole stimulation. Statistical significance was analyzed using the Wilcoxon signed-rank test. n indicates the number of independent experiments.

The amino acids Thr^{603}, Gly^{606}, Thr^{607}, Val^{610}, Leu^{613} and Leu^{617} are all located in TM6 and are building the side wall of cavity IV (see Figure 3.52). The mutation of threonine at position 603 substituted by alanine and threonine at position 607 replaced by alanine had no effect on the riluzole and the (-)-englerin A induced current densities (Figure 3.56A). The current density time courses (Figure 3.56C, E, embedded figures) and CDV relations do not show any significant changes compared to the wildtype. However, the NSC suggests only minor significant differences in the riluzole and in the (-)-englerin A evoked IV of mutant T603A compared to the wildtype (Figure 3.57 green plot). The NSC of the riluzole induced IV curve of the mutant T607A shows nearly no significant differences when compared to the wildtype, whereas the NSC of the (-)-englerin A evoked IV curve shows highly significant differences compared with the wildtype (Figure 3.57 magenta plot). Nonetheless, a binding of (-)-englerin A to Thr^{607} is unlikely because the current densities are not significantly reduced. An indirect effect of T607A on the (-)-englerin A binding or the conductivity however is not excluded.

The amino acid exchange of glycine at position 606 to alanine causes reduced current density responses before and during consecutive application of riluzole and (-)-englerin A. The current density time course shows no riluzole evoked peak, whereas the (-)-englerin A induced peak is still prominent(Figure 3.56D, embedded figure). The CDV curve further supports this finding by a congruent course before and during application of riluzole (Figure 3.56D). Therefore, the effect seems to be riluzole specific. The NSC of the riluzole and (-)-englerin A evoked IV of mutant G606A show highly significant differences when compared with the wildtype, respectively (Figure 3.57 yellow plot).

The amino acid exchange valine at position 610 for alanine results in a mutant channel with reduced current densities before and during consecutive riluzole and (-)-englerin A application (Figure 3.56A). The current density time course (Figure 3.56F, embedded figure) and CDV curve (Figure 3.56F) show very low current amplitudes as well, making it hard to derive specific effects. The NSC of the riluzole and (-)-englerin A evoked IV curve similarly show a relatively linear outward current slope and overall a high significantly different slope when compared with the wildtype, respectively (Figure 3.58 green plot). By comparing the CDV curves during riluzole and (-)-englerin A application with each other, it gets obvious that the maximum outward current equals roughly $50\,\mathrm{pA\,pF^{-1}}$ for the (-)-englerin A evoked current and roughly $25\,\mathrm{pA\,pF^{-1}}$ for the riluzole evoked one, resulting in a ratio of 2. Comparing this value to the wildtype, it equals roughly 4. This could suggest a (-)-englerin A specific effect for V610A. The NSC of the riluzole and (-)-englerin A evoked IV curves of the mutant V610A show nearly no significant differences, meaning their shape is very similar (Figure 3.59B). Typically their IV shapes differ drastically and as a result their similarity could be another evidence for either an (-)-englerin A specific effect or a manipulation of the selectivity of the channel.

The amino acid exchange leucine at position 613 for alanine results in significantly higher current densities before and during application of riluzole (Figure 3.56A). The riluzole evoked peak and the riluzole evoked CDV curves show that the riluzole induced currents are nearly as high as the (-)-englerin A induced currents. The riluzole evoked IV curve not only approximates the (-)-englerin A evoked outward current, but also the (-)-englerin A elicited inward current. No other mutation shows such a drastic increase in the riluzole evoked inward current

(Figure 3.56A). However, the NSCs of the riluzole and the (-)-englerin A evoked IV curves suggest no approximation in shape (Figure 3.59C). But the NSC of the riluzole and (-)-englerin A evoked IV curves also differ compared with the NSC of the wildtype riluzole and (-)-englerin A activation, respectively (Figure 3.58 yellow plot). Leu^{613} is part of TM6 and facing towards the ion conducting pore. The exchange to alanine probably changes the ion selectivity and generates an (-)-englerin A-like activation with a strong inward current.

The mutation of leucine at position 617 to alanine results in a channel with significantly reduced current densities before and during consecutive application of riluzole and (-)-englerin A (Figure 3.56A). The current density time course as well as the CDV curves both show no current density responses to either of the two activators(Figure 3.56H and Figure 3.56H, embedded figure). The NSCs before and curing consecutive application of riluzole and (-)-englerin A also shows only minor significant differences when compared with each other, meaning riluzole and (-)-englerin A are not able to evoke any changes in the IV course during stimulation (Figure 3.59). Therefore Leu^{617} seems to be important for the general channel functionality and/or for the expression of the channel.

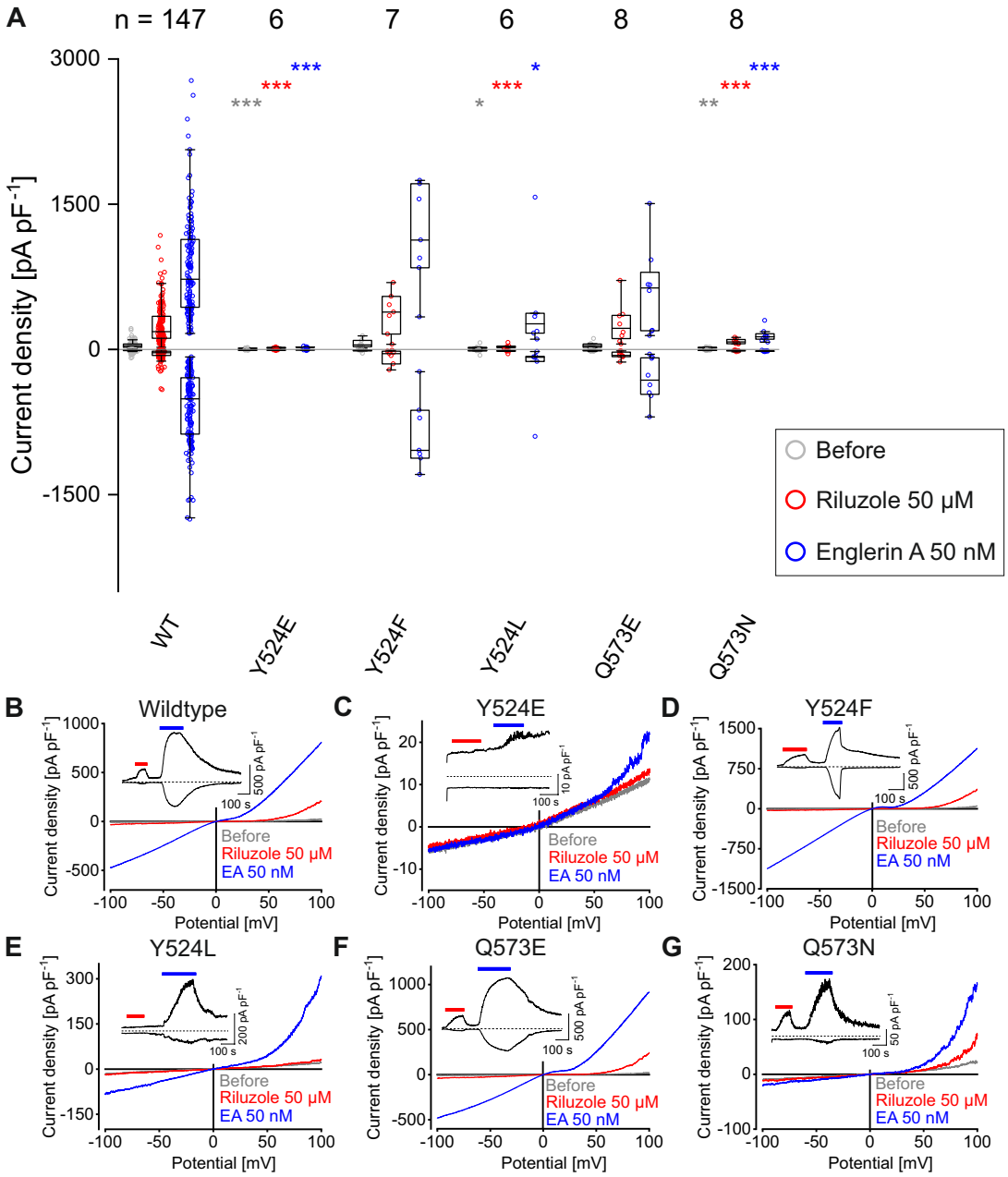

Figure 3.60.: **Whole-cell measurements of potential ligand binding amino acids in cavity IV. (A)** shows the maximal and minimal current density at the potentials 100 mV and −100 mV evoked by the given treatment, respectively. Their respective distribution is indicated by the median (horizontal line) and 50 % of the data points (box) as well as the 1.5 × IQR (whiskers). The number of independent experiments is indicated by numbers over the plot. * $P < 0.05$, ** $P < 0.01$, *** $P < 0.001$ (Tested against Wildtype (WT); Mann-Whitney-U). **(B-G)** show representative single CDV curves during the given treatments selected at maximal current responses. The insets show the corresponding current density time course of the same measurement.

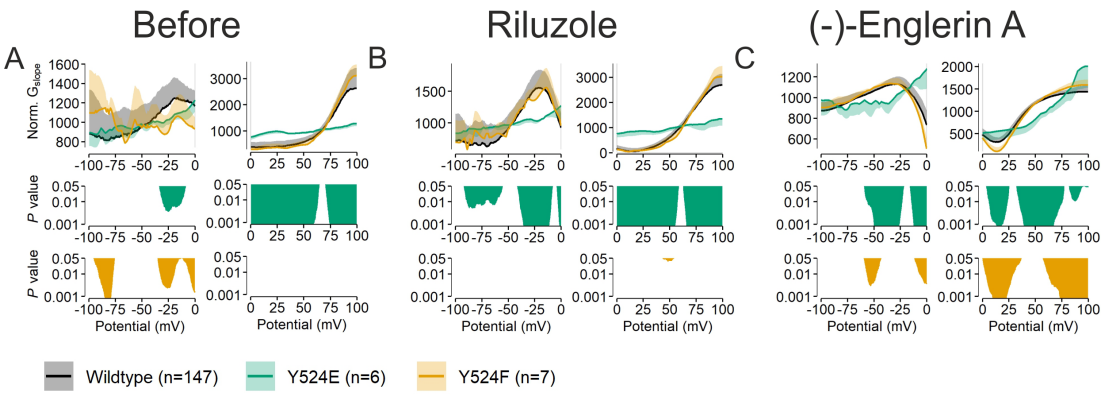

Figure 3.61.: **NSC of potential ligand binding amino acids in cavity IV.** This figure shows the calculated NSC (Hermann et al., 2022) of the given mutation (top) $\pm SD$ compared to the wildtype NSC during the given treatment (bottom). Statistical significance was analyzed using the Mann-Whitney-U-test. n indicates the number of independent experiments.

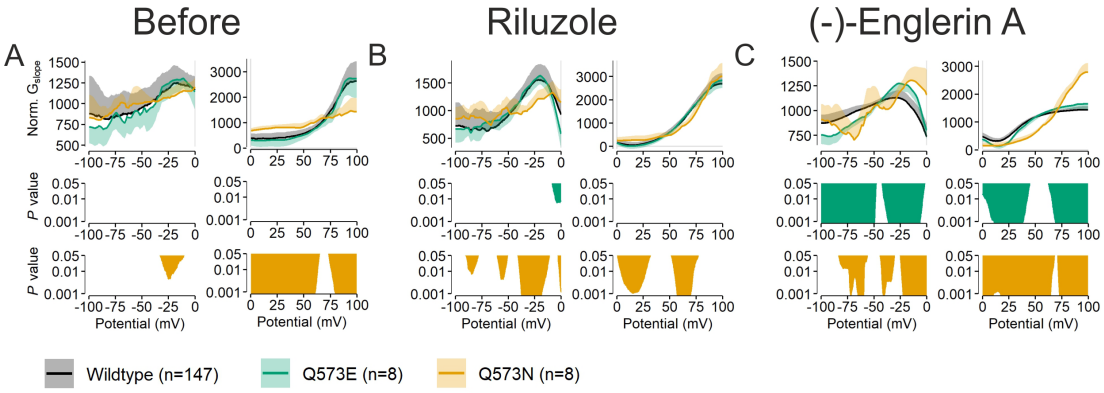

Figure 3.62.: **NSC of potential ligand binding amino acids in cavity IV.** This figure shows the calculated NSC (Hermann et al., 2022) of the given mutation (top) $\pm SD$ compared to the wildtype NSC during the given treatment (bottom). Statistical significance was analyzed using the Mann-Whitney-U-test. n indicates the number of independent experiments.

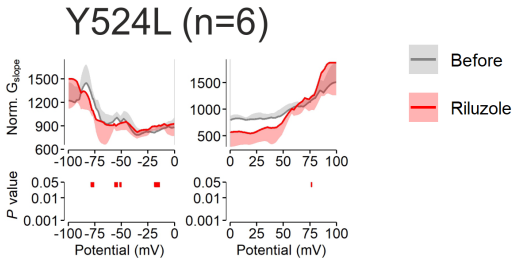

Figure 3.63.: **NSC of potential ligand binding amino acids in cavity IV.** This figure shows the calculated NSC (Hermann et al., 2022) of the given mutation (top) $\pm SD$. The given treatment is compared with the basal NSC before any treatment (bottom). Statistical significance was analyzed using the Wilcoxon signed-rank test. n indicates the number of independent experiments.

Since the mutations Y524A and Q573A significantly reduce the (-)-englerin A induced current responses concomitant with riluzole induced current density increases that are higher or as high as the (-)-englerin A induced currents, these amino acids might be involved in a potential (-)-englerin A binding. Therefore, they are further analyzed by performing additional functional amino acid exchanges.

The mutation Y524E results in a nonfunctional or non-expressed channel, as the mutation produces a channel with significant reductions in current density values before and during consecutive riluzole and (-)-englerin A application (Figure 3.60A). The current density time course and the extracted CDV curve likewise show very small current density amplitudes (Figure 3.60C and embedded figure). Probably the exchange from an aromatic to a polar amino acid is too severe in the given position. The NSCs before and during a riluzole and during a (-)-englerin A stimulation similarly depict highly significant changes when compared with the wildtype NSC, respectively (Figure 3.61 green plot). The NSCs before and during riluzole application even show no typical characteristics at all, indicated by a linear slope (Figure 3.61A, B green plot).

The more conservative amino acid exchange tyrosine at position 524 for phenylalanine results in no significantly changed current densities and no change in the current density time course compared to the wildtype (Figure 3.60A, D, embedded figure). The CDV curves show no noticeable differences compared to the wildtype (Figure 3.60D). The NSC before riluzole activation shows some significant differences in the inward current compared with the wildtype, but the NSC has a high variance in this part of the plot, which may lead to artifacts (Figure 3.61A left yellow plot). The NSC of the riluzole evoked IV curves shows no significant differences when compared to the wildtype (Figure 3.61B yellow plot). However, the NSC during the (-)-englerin A activation exhibits some significant differences compared with the wildtype, underlining a potential role of Tyr^{524} in the (-)-englerin A binding (Figure 3.61C yellow plot). Therefore, Y524F to some extent rescues the functionality of the wildtype Tyr^{524}.

Mutating Tyr^{524} to leucine results in small significant differences before and during (-)-englerin A application and a highly significant reduction in the riluzole evoked current densities (Figure 3.60A). The same effect can be observed in the current density time course ((Figure 3.60E, embedded figure). The riluzole elicited peak is not visible, whereas the (-)-englerin A evoked peak is still prominent. The CDV shows a similar result with a congruent course before and during application of riluzole (Figure 3.60E). Even the NSC exhibits only minor significant differences when comparing the NSC before and the NSC during a riluzole application, suggesting a specific effect on the riluzole mediated activation of mutation Y524L (Figure 3.63).

Therefore, Y524L results in the opposite effect of the originate Y524A mutation. Aromatic amino acids are often heavily involved in stabilizing tertiary structures by π-π interactions. Additionally, Tyr^{524} is located in TM5, which seems to have an impact on the riluzole specific activation of the channel, as other mutations like G511A and N500Y suggest. TM5 may be involved in a coupling, which is further discussed in chapter 4 and may be a pivotal region linking the (-)-englerin A and riluzole mediated activation pathway, respectively.

The amino acid exchange glutamine at position 573 for glutamate shows no significant changes in the current densities compared to the wildtype (Figure 3.60A).

The CDV curve and current density time course are not noticeable different from the wildtype, respectively (Figure 3.60F and embedded figure). Surprisingly, the NSC reveals highly significant differences especially in the (-)-englerin A evoked IV course (Figure 3.62C green plot). This also points towards an effect specifically targeting the (-)-englerin A mediated activation.

The amino acid exchange glutamine at position 573 for asparagine greatly reduces the overall channel functionality and/or expression, as indicated by significant reductions of the current densities before and during consecutive application of riluzole and of (-)-englerin A (Figure 3.60A). Nonetheless, the current density time course and the CDV curves show a greater reduction in the (-)-englerin A evoked current density than in the riluzole evoked current densities compared with the wildtype, respectively (Figure 3.60G and embedded figure). This implies a specific effect of Q573N on the (-)-englerin A mediated channel activation. The NSCs similarly exhibits highly significant differences before and during riluzole and (-)-englerin A application when compared with the wildtype, respectively (Figure 3.62 yellow plot). But the least significant differences are observed when comparing the riluzole evoked IV curve and their corresponding NSC of mutant Q573N with the wildtype (Figure 3.63B yellow plot).

The introduction of a negative charge and the conservation of the chain length at the same time (Q573E) seems to be less effective on the (-)-englerin A mediated activation than the conservation of the functionality and concomitant reduction of the chain length (Q573N). Therefore either the exact shape of the whole cavity surface area created by the residue of Gln^{573} is very important, or the exact position of the carbonyl-oxygen for a possible (-)-englerin A interaction is essential.

3.6. Surface Expression of Potential (-)-Englerin A Mutants

The amino acids displayed in Figure 3.64 were selected as the most important potential binding partners in the (-)-englerin A mediated activation of TRPC5. Therefore the surface expression was quantified using a surface biotinylation kit and compared with the wildtype.

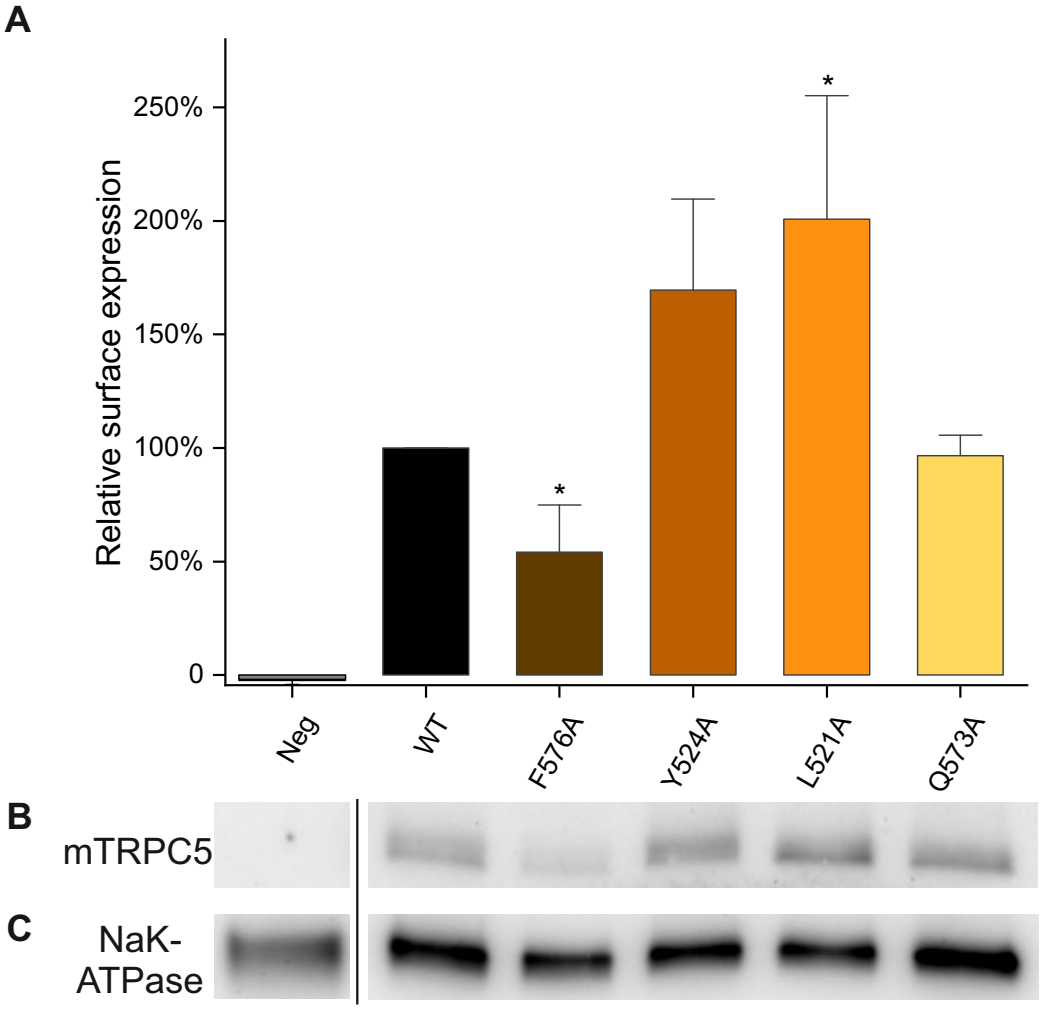

Figure 3.64.: **Surface expression of possible (-)-englerin A binding mutants.** This figure shows the surface expression of possible (-)-englerin A binding mutants. **(A)** represents the results of 3 individual western blot experiments. The statistical significance was calculated using a two sided t-test and tested against the wildtype expression (WT) (* $p < 0.05$, ** $p < 0.01$, *** $p < 0.001$). **(B)** shows a representative western blot of the respective mutant TRPC5 channel expression. The image displays an automatically contrast optimized image using the integrated BioRad software. The vertical line represents a different, additional blot membrane. **(C)** represents the same blot as **(B)** after stripping and incubation with the anti-NaK-ATPase antibody.

3.6.1. Surface Expression Profile of Potential (-)-Englerin A Binding Mutants

The mutation F576A shows a significantly reduced surface expression of 54 % compared to the wildtype (Figure 3.64). The riluzole as well as the (-)-englerin A evoked current densities are both greatly reduced. This cannot be explained just by the lower surface expression, as the riluzole evoked current densities suggest an even lower surface expression than 54 %. Therefore, the overall channel functionality seems to be greatly impaired (Figure 3.49). This result can be explained by the fact that Phe^{576} is located in the pore helix and therefore represents a part of a very delicate channel feature in the context of channel functionality.

The surface expression of Y524A is not significantly changed. In electrophysiological experiments however, Y524A shows greatly reduced current density responses to a riluzole stimulation as well as to an (-)-englerin A stimulation (Figure 3.53A, C) suggesting that the reduced current responses are not due to an decreased surface expression, but rather to a loss of channel functionality.

Elimination of the aromatic moiety causes a (-)-englerin A specific reduction of the elicited current densities as well as a general loss of the channel functionality, as observed with the mutations Y524A and Y524E. However, re-introducion of an aromatic residue as in the case of Y524F completely rescues the channel functionality. Surprisingly, the introduction of a non-aromatic but non-polar and smaller amino acid as in the case of Y524L reverts the effect of Y524A and causes a riluzole specific current density reduction (Figure 3.60). Taken together, Tyr^{524} which is located in TM5 seems to have a multi-functional role in the channel physiology in general, not only for the potential (-)-englerin A binding.

The mutation L521A shows a significantly increased surface expression (Figure 3.49). Electrophysiological data shows that (Figure 3.49) the riluzole elicited current densities are unchanged, whereas the (-)-englerin A evoked current densities are significantly reduced. It can be speculated that this effect is (-)-englerin A specific and that Leu^{521} might be involved in an (-)-englerin A binding. In the case of the L521A mutant, the riluzole stimulation can serve as an estimation of the surface expression.

The mutation Q573A however shows no changes in the surface expression which is in line with electrophysiological data showing that only the (-)-englerin A induced current densities are reduced while the riluzole induced current responses are unchanged (Figure 3.64 and Figure 3.53). These findings suggest that the riluzole stimulation might serve as a control for the estimation of the surface expression and it can be speculated that the amino acid Gln^{573} might participate in an (-)-englerin A binding.

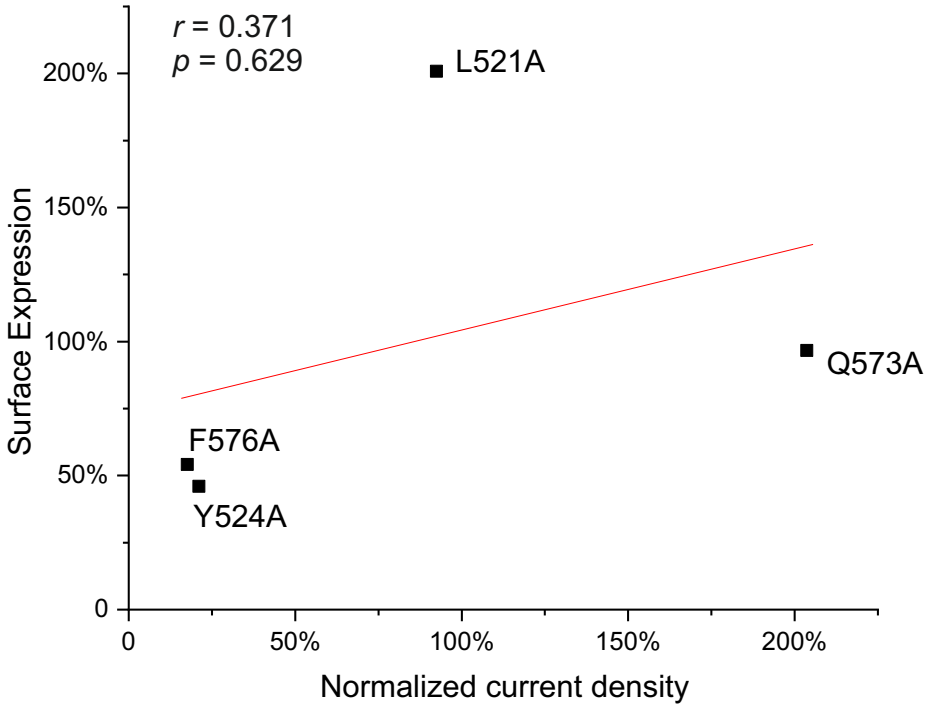

Figure 3.65.: **Correlation between surface expression of (-)-englerin A mutants measured via western blot and estimated via patch clamp experiments.** This figure shows the correlation analysis between surface expression of (-)-englerin A mutants determined by western blot and the normalized maximal riluzole induced current densities determined by patch clamp experiments. Analysis of the linear regression yields a pearson $r = 0.371$ with $p = 0.629$.

The Pearson Correlation Coefficient for the normalized current densities and the surface expression determined by western blot analysis amounts to 0.371 and thus showing no correlation (Figure 3.65). Therefore riluzole evoked current densities serve less well as a surface expression estimation for potential (-)-englerin A binding mutants than vice versa (Figure 3.42). A possible cause might be the importance of the potential (-)-englerin A binding mutants for the channel functionality in general. Most of the mutants are located either in the pore helix, which is directly involved in ion selectivity or they are located in helices like TM5 which stabilizes the pore complex and therefore potentially mediate channel activation.

4. Discussion

4.1. Two Distinct Binding Pockets of (-)-Englerin A and Riluzole

Summarizing the results of the whole-cell patch clamp measurements as well as the surface expression data, it becomes obvious, that (-)-englerin A and riluzole can bind to two distinct cavities in the TRPC5 channel. The most important amino acids involved in the riluzole binding are Ile^{368}, His^{370}, Glu^{418}, Trp^{435}, Asp^{439}, Arg^{492} and Leu^{496}. Whereas the most important amino acids for the (-)-englerin A binding are Leu^{521}, Tyr^{524}, Gln^{573} and Phe^{576}.

The two distinct binding sites are depicted in Figure 4.1 which shows amino acids that might be important for the binding of the two activators riluzole and (-)-englerin A, respectively. The colors represent the ratios between maximal (-)-englerin A and riluzole induced currents at 100 mV. The mean (-)-englerin A evoked current densities of wildtype TRPC5 were five times higher than the mean riluzole evoked current densities. Thus, a lower current ratio of < 5 indicates higher riluzole induced currents compared to (-)-englerin A induced currents and vice versa. Consequently, a lower current density ratio points towards a mutant with impaired (-)-englerin A mediated activation and vice versa.

The color scale is based on the assumption that a ratio change of either half or double the wildtype ratio are noticeable effects. Half the wildtype value translates to < 2.5 (blue) and represents a possible (-)-englerin A current reduction compared to the riluzole-evoked current. Whereas double the wildtype ratio translates to > 10 (red) and represents a possible riluzole current reduction compared to (-)-englerin A.

As Figure 4.1 indicates, red colored amino acids cluster in one region, whereas blue colored amino acids cluster in a distinct region. Red colored amino acids gather near the VSLD and blue colored amino acids are grouping around the pore helix, TM5 and 6, respectively. Interestingly, in the red cluster are a few blue colored amino acids and vice versa. This could suggest either indirect effects on the binding pockets (as demonstrated using the example of Phe^{497}, Figure 4.7) or effects on the signal transduction, as described in more detail in (section 4.2).

In the following, the docking poses were re-evaluated to find the actual binding pose of both ligands. Therefore ligand poses with the most amino acid interactions with the ligand, which were electrophysiologically confirmed, were considered.

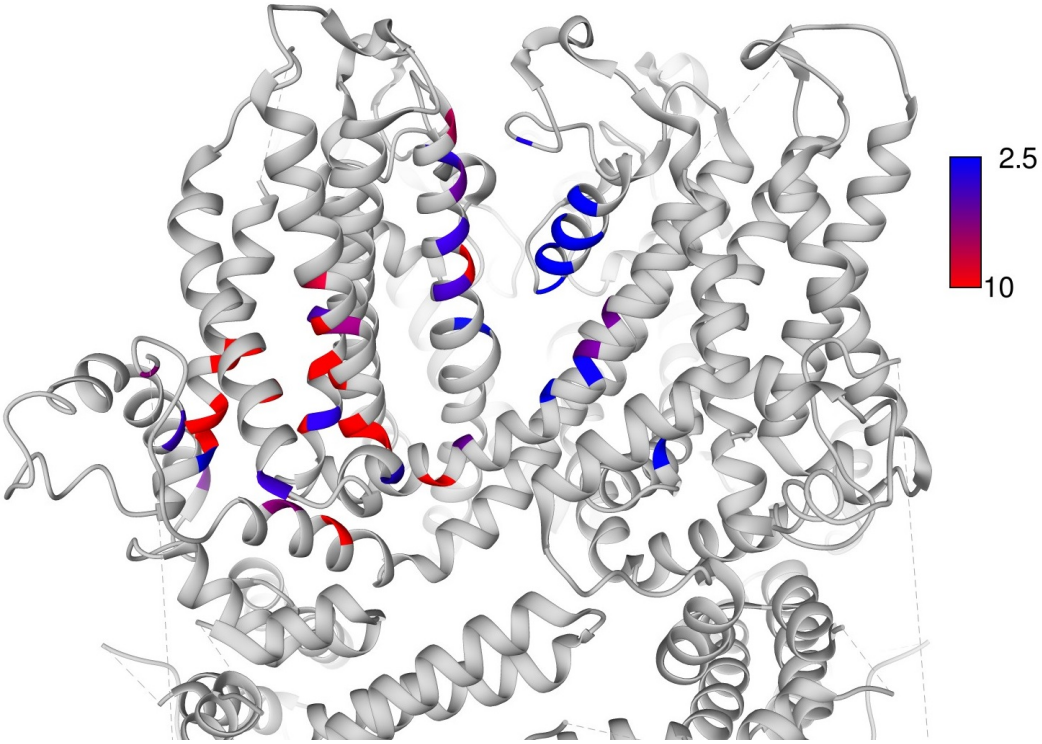

Figure 4.1.: **(-)-Englerin A and riluzole evoked current density ratios.** This figure represents TRPC5 (PDB: 6AEI, Duan et al. (2019)) with a ratio calculation between the maximal (-)-englerin A and the maximal riluzole evoked current densities. Blue indicates a low current density ratio resulting from lower (-)-englerin A induced maximal current densities at 100 mV compared to the maximal riluzole induced current densities at 100 mV. Red indicates a high current density ratio resulting from higher maximal (-)-englerin A induced current densities at 100 mV compared to the maximal riluzole induced current densities at 100 mV. The wildtype ratio of the maximal (-)-englerin A evoked current densities compared to themaximal riluzole evoked current densities equals the middle of the scale (violet). If the amino acids were exchanged for other amino acids than alanine, the most severe exchange was depicted, respectively. The raw data is shown in Appendix D.

4.1.1. The (-)-Englerin A Binding Site

The most important amino acids for the (-)-englerin A binding, according to the results of the patch clamp measurements, are Gln^{573}, Phe^{576}, Tyr^{524} and Leu^{521} (see Figure 3.49 and Figure 3.53). In Figure 4.2 all amino acids which were electrophysiologically analyzed and were part of the most probable docking result are shown. Namely, the most promising (-)-englerin A pose is position 1 of the docking in cavity IV as a part of docking project III (see Figure 4.2 and Figure B.8a). Amino acids with either significant results in the electrophysiological measurements or very close contact to the predicted ligand position got distance-measured and possible interactions are displayed in Figure 4.2.

Leu^{521} seems to play a major role by potentially stabilizing the cavity surface and forming hydrophobic interactions with the phenolic residue of (-)-englerin A (as indicated by Figure 3.49 and Figure 4.2).

Tyr^{524} may stabilize the phenolic part of (-)-englerin A as well (as indicated in Figure 4.2), probably via aromatic interactions. The centroids of both aromatic rings are displayed as black spheres in Figure 4.2 with a distance of 5.3 Å between each other. This may suggest a π-π interaction between both aromatic rings, which typically occurs between 4.5 to 7 Å distance of both centroids to one another (Anjana et al., 2012).

Even though Leu^{572} appears in the docking result, the electrophysiological data of mutant L572A show a significantly higher riluzole response compared to the wildtype but an unchanged (-)-englerin A response. Therefore, Leu^{572} might rather has a stabilizing effect on (-)-englerin A with only weak interactions suggesting a minor role of Leu^{572} for the binding of (-)-englerin A.

Gln^{573} on the other hand plays a central role in the (-)-englerin A binding. The mutation Q573A is the only exchange being able to strongly reduce the (-)-englerin A evoked current while retaining a wildtype similar riluzole activation (Figure 3.53). Depending on the rotation of the glutamic acid portion of (-)-englerin A, Gln^{573} is either able to interact with the hydroxyl-oxygen or -hydrogen. One possibility is a glutamic acid HO···H_2N glutamine hydrogen bond (illustrated in Figure 4.2) or a glutamic acid OH···O=R glutamine hydrogen bond. Due to no significant changes in the current density of the mutation Q573E (lacking the H_2N-R group) the latter case seems more reasonable.

Phe^{576} may also stabilize the phenolic portion of (-)-englerin A as indicated by both centroids and a distance of 5.6 Å (Figure 4.2). Another possible interaction side is the guaine-sesquiterpene backbone of (-)-englerin A. As indicated by the centroids the average distance between the backbone and Phe^{576} is 6.2 Å and a lot of hydrophobic interactions are possible. Another function of Phe^{576} is the stabilization of the cavity surface and back-wall. It has a central role in stabilizing the whole pore region, especially the pore helix by interacting with Trp^{577} (Duan et al., 2019).

Interestingly, Trp^{577} shows no (-)-englerin A specific effect (Figure 3.20). In the docking on the other hand Trp^{577} has very interesting possible interactions, including the possible NH···OH hydrogen bond with the glycolic acid part of (-)-englerin A as indicated in Figure 4.2. Probably by eliminating the Trp^{577} functional moiety the pore helix and the close selectivity filter get destabilized and therefore the channel functionality overall gets restricted. If a ligand binding site is in a very delicate region of the channel, as it is the case for (-)-englerin A, it is very likely that the overall channel functionality gets impaired by introducing

mutations which might interfere with specific effects.

Ala^{602} appears in the docking but was not mutated due to very less possible interactions of the sidechain.

Thr^{603} does not seem to play a major role in the (-)-englerin A binding as indicated by no significant changes in the current density values for the mutant T603A (Figure 3.56).

V610A has a strongly reduced overall channel functionality, with a slightly stronger reduction of the (-)-englerin A evoked current densities than of the riluzole evoked current densities (Figure 3.56). Nonetheless, the influence on the binding seems to be minor.

Val^{610} could potentially stabilize the phenolic part of (-)-englerin A or builds the pocket surface with minor hydrophobic interaction with (-)-englerin A as indicated in Figure 4.2 and Appendix B.

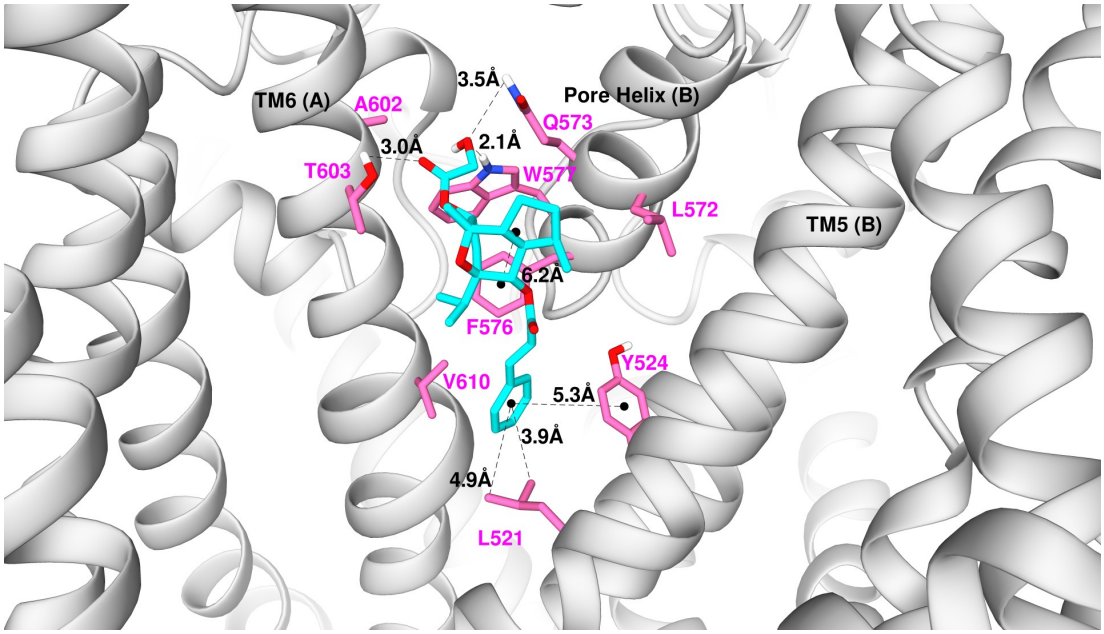

Figure 4.2.: **Predicted (-)-englerin A binding site.** This figure shows a representation of TRPC5 (PDB: 6AEI, Duan et al. (2019)) and (-)-englerin A (cyan) in the most probable binding position calculated via molecular docking (see Figure B.8). Amino acids possibly contribute to a (-)-englerin A binding which were either confirmed via patch clamp measurements or were part of the docking result are shown in magenta. Possible interactions are indicated with dotted lines and the measured distance is given in Å. Centroids of aromatic rings are indicated with black dots. Two TRPC5 monomers are contributing to the binding pocket (indicated by (A) or (B).

The proposed (-)-englerin A binding site is quite similar to the DAG (Song et al., 2021) and xanthine binding site (Wright et al., 2020) of TRPC5 as well as to the AM-0883 binding site of TRPC6 (Bai et al., 2020) which were all identified via cryo-EM.

Interestingly, Pico-145 and HC-070 which are both inhibitors of TRPC5, belong to the xanthine based class of inhibitors and both bind to the same cavity (Wright et al., 2020; Song et al., 2021). As previously mentioned, AM-0883 binds to the same site while being a TRPC6 activator that is structurally distinct

from the xanthines and (-)-englerin A and related to SAR7334, an aminoindanol that was characterized as an inhibitor of TRPC3/6/7 (Maier et al., 2015). AM237 is a selective TRPC5 activator also belonging to the xanthine class. However, AM237 has not being co-crystallized, yet (Minard et al., 2019; Song et al., 2021). It is assumed that AM-237 binds to the same cavity as HC-070 and Pico-145 because of its chemical similarity. In addition, AM-237 is a selective TRPC5 activator that inhibits (-)-englerin A induced currents, whereas HC-070 and Pico-145 are both strict inhibitors. This makes AM-237 a very versatile and interesting compound.

In Figure 4.3 the possible (-)-englerin A binding site is compared to the HC-070, Pico-145 and DAG binding sites of TRPC5. Gln^{573} plays a key role in all the compared structures by stabilizing the propanolic part (in the case of the xanthine derivatives), the glutamic acid part (in the case of (-)-englerin A) and the hydroxyl head group of DAG, respectively.

In all cases, Phe^{576} stabilizes the backbone of the compound and builds the cavity back-wall.

Tyr^{524} seems to play a major role in the binding of (-)-englerin A and Pico-145. It stabilizes the phenolic portion especially if it is rotated towards the inside of the channel, like in the case of (-)-englerin A and Pico-145.

The actual role of DAG in this binding pocket still remains elusive. It was co-crystallized when Song et al. (2021) tried to co-crystallize (-)-englerin A. The authors reported that DAG (see Figure 4.3d) occupies this pocket in the apo-state of the channel. However, their claimed apo-state represents a channel that was previously treated with (-)-englerin A. Because no (-)-englerin A density was found, this state was labeled as apo-state. Maybe this cavity is occupied by a phospholipid in the closed state, which then gets displaced by for example (-)-englerin A to transfer the channel in an open state, which then gets again displaced by DAG during channel deactivation.

At present, it is unclear if DAG is permanently bound in this pocket and stabilizes the whole upper channel. Residual parts of DAG still co-crystallize in the HC-070 bound channel state suggesting that DAG is still present when inhibitors are bound. Maybe ligands such as (-)-englerin A or HC-070 need the presence of DAG for binding to the pore region. However, if DAG would always be bound or at least when the cavity is occupied by a ligand, it is still confusing why other groups did not manage to co-crystallize DAG as well.

Wright et al. (2020) were able to co-crystallize Pico145 (a derivative of HC-070) with TRPC5, but instead of DAG they found a phospholipid density in the same pocket of the apo-state of the channel. The phospholipid partly stayed in the position even when Pico145 was bound, thus being very similar to the DAG density found by Song et al. (2021). Previous publications of TRPC4 and TRPC5 3D structures always reported a phospholipid density in this pocket of the un-liganded TRPC4 and 5 channels in their apo-states (Duan et al., 2018a,b, 2019; Vinayagam et al., 2018, 2020). Other TRPC channel structures like TRPC3 and TRPC6 show the same phospholipid density in the given binding pocket of the apo-channel state (Fan et al., 2018; Bai et al., 2020; Tang et al., 2018). Altogether, Song et al. (2021) are the only ones who identified DAG instead of a phospholipid in the pore region.

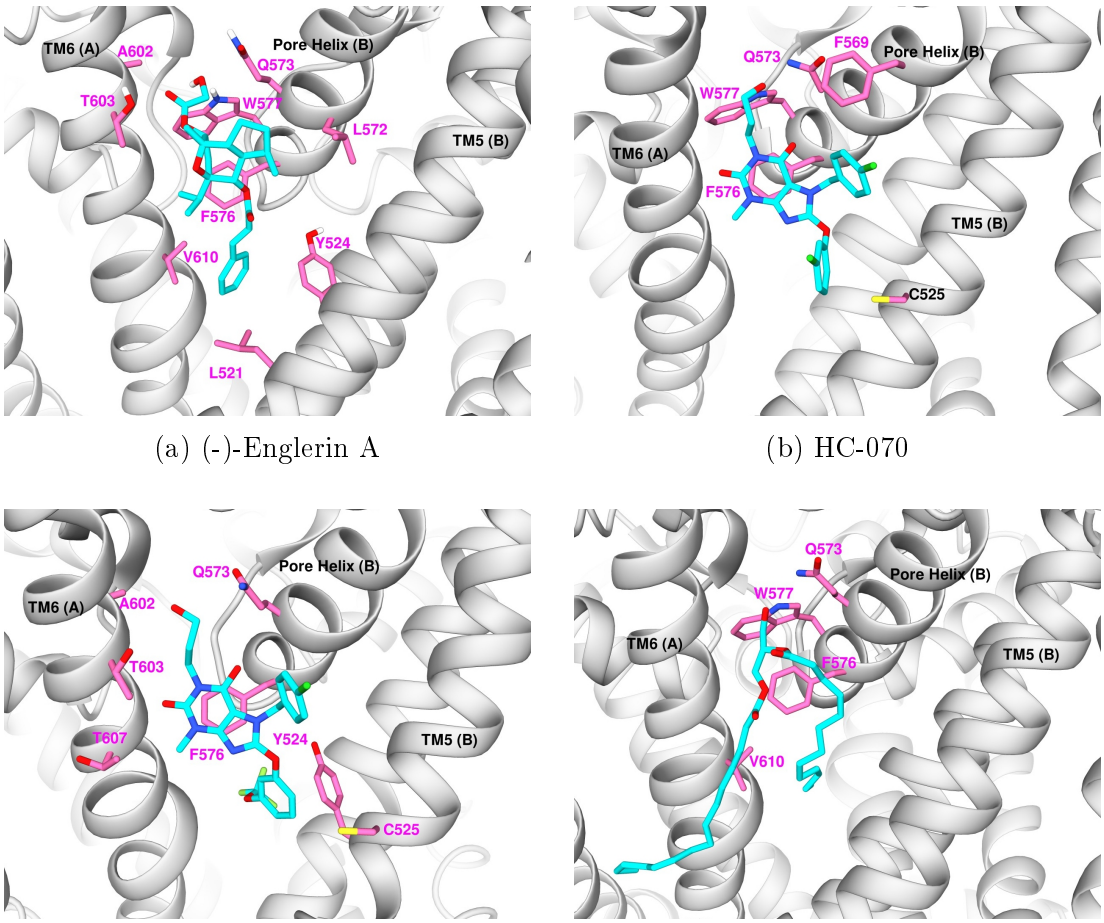

(a) (-)-Englerin A (b) HC-070

(c) Pico-145 (d) DAG

Figure 4.3.: **Comparison of ligands binding to the (-)-englerin A binding site.** This figure compares different ligands binding to the same binding site in TRPC5. The potential (-)-englerin A binding site **(a)** is presented in this thesis (TRPC5 was used as a template (PDB: 6AEI, Duan et al. (2019))), whereas HC-070 **(b)** (PDB: 7D4Q, Song et al. (2021)), DAG **(d)** (PDB: 7E4T, Song et al. (2021)) and Pico-145 **(c)** (PDB: 6YSN, Wright et al. (2020)) were resolved in complex with a TRPC5 structure. The ligand is colored in cyan, whereas amino acids participating in a binding are colored in magenta. Because two monomers are building the binding pocket, (A) and (B) mark their respective structural elements.

Nontheless, there is increasing evidence that the cavity plays a role in lipid-sensing and especially in DAG mediated channel activation. In the TRPC3 channel Lichtenegger et al. (2018) reported a fenestration mechanism of Gly^{652}, which is the homologous amino acid to Gly^{606} in TRPC5, that has the ability to distinguish between DAG derivatives.

Two years later, Bai et al. (2020) exchanged amino acids in TRPC6 in the same region, with the result of reducing the DAG mediated Ca^{2+} signal. They showed that amino acid exchanges to alanine at positions Glu^{672}, Phe^{675} and Trp^{680} result in a decreased calcium signal. Interestingly, Trp^{680} in TRPC6 (corresponding to Trp^{577} in TRPC5) is the only amino acid, which Bai et al. (2020) as well as Song et al. (2021) both claim to participate in the DAG binding. All other amino acids both authors suggest to be involved in the DAG binding are different and not conserved between TRPC5 and 6. Strikingly, Gln^{573}, which seems to play a major role in the TRPC5 ligand binding to this pocket (as illustrated in Figure 4.3) is not conserved in TRPC6. This would mean that the DAG binding site between both channels is not conserved and slightly different which might be the reason for the observed differences in the DAG sensitivity of TRPC4, 5 and TRPC3, 6, 7 channels (Storch et al., 2017; Hofmann et al., 1999).

Altogether, the proposed (-)-englerin A binding site is located between TM5 and the pore helix of one monomer and TM6 of the adjacent monomer. TM6 seems to play a minor role in ligand binding, as mutations show hardly any effects. The site partially overlaps with the xanthine binding site of Pico-145, HC-070 and probably AM-237, as well as with the DAG binding site (Figure 4.3).

Gln^{573} and Phe^{576} seem to play a major role in ligand binding as they are conserved between the binding sites in TRPC5. Additionally, both amino acids are located in the pore helix and thus might easily influence the selectivity filter. Interestingly, the binding pocket seems to transduce various signals, as channel inhibitors like Pico-145 and HC-070 bind there as well as channel activators like (-)-englerin A. AM-237 highlights the versatility of the pocket due to its unique role as a channel activator as well as a competitive antagonist of the (-)-englerin A induced channel activation (Minard et al., 2019).

Another similarity between the ligands is that they all have an EC_{50} in the pico- to nanomolar range, except for DAG. But the role of DAG in the given binding pocket is not finally understood and more research is needed.

4.1.2. The Riluzole Binding Site

Regarding the electrophysiological data, mutations of Ile^{368}, His^{370}, Glu^{418} and Asp^{439} have the most pronounced effects on the riluzole induced currents. These amino acids are displayed in Figure 4.4 with distance measurements of the possible interactions with riluzole.

Ile^{368} may play a major role in riluzole binding, as described in section 3.3. Mutation I368T shows a significant current density reduction in the electrophysiological measurements. The mutant channel is still expressed at the cell surface similarly to the wildtype (Figure 3.41) making it a striking candidate for riluzole binding. However, the 3D-structure reveals a bend in the helix structure of TM1 at the position of Ile^{368} as indicated in Figure 4.4. Either the structure was miscalculated at the given position, or Ile^{368} does not play a direct role in the riluzole

binding.

The His^{370} residue on the other hand is rotated towards riluzole and the binding pocket. Depending on local pH value changes the protonation state of histidine can change. In neutral pH, two neutral charged tautomers exist, thus the hydrogen can either be located at the δ1-N (named π tautomer) or at the ε2-N (as indicated in Figure 4.4, named τ tautomer) (Li & Hong, 2011). In a low pH milieu, histidine can even be positively charged. The distance from the δ1-N to the nearest fluorine of riluzole amounts to 3.1 Å. If His^{370} is then present in the π tautomer, this enables a suitable distance for a polar interaction between a possible δ1-N hydrogen of His^{370} and the tri-fluorine group of riluzole.

Phe^{414} possibly interacts with the benzothiazole π-electron system of riluzole. In the given docking position the Phe^{414} benzene centroid is 4.9 Å away from the benzene centroid of riluzole enabling a proper distance for a π-π interaction (Figure 4.4).

The Glu^{418} exchanges show significant, riluzole specific effects in electrophysiological measurements (as described in section 3.3) as well as a surface expression that is similar to the wildtype in the case of the mutant E418A (Figure 3.41). The deprotonated carboxylate group might interact with the amino hydrogen of riluzole to form a hydrogen bond over 2.8 Å. This interaction seems to play a major role in the riluzole binding, due to significant reductions in the current response with minimal changes in the functionality of Glu^{418} (section 3.3) and likewise appears in the docking result.

Trp^{435} is too far away from riluzole in the given docking pose to show any direct interactions. Although W435A shows a very specific effect on the riluzole evoked current densities (Figure 3.15) the surface expression is significantly reduced (Figure 3.41) supposing a more indirect effect on the riluzole binding. Trp^{435} may stabilizes Arg^{492} through a cation-π-interaction. Hence, by exchanging Trp^{435}, the Arg^{492} position gets slightly changed, resulting in a weakened riluzole binding.

Asp^{439} is probably involved in a riluzole binding as already discussed in section 3.3. It may, similar to Glu^{418}, forms a hydrogen bond with the amino hydrogen of riluzole (distance: 2.8 Å). If exchanged to asparagine the delocalized charge gets removed leading to a weaker riluzole binding (see section 3.3). An exchange to glutamate on the other hand moves the charge further inward into the binding pocket, moving past the riluzole amino hydrogen.

Arg^{492} might as well play an important role, as described in subsection 3.2.3 and section 3.4. Due to a positive charge delocalized between the amino groups of Arg^{492} it may interact with the π electron-system of riluzole's benzothiazole moiety to form a cation-π-interaction. The distance between the benzene centroid and the arginine's delocalized charge amounts to 5 Å, representing a good distance for an interaction (Ferreira de Freitas & Schapira, 2017).

Strikingly, the riluzole binding site was published during the thesis. Yang et al. (2022) report that riluzole binds to the VSLD nearly identical to the binding site propagated in this thesis. They report the interacting amino acids are Tyr^{374} and Phe^{414} with a π-π stacking interaction, Arg^{492} with a cation-π interaction and Asp^{439} and Ser^{495} with a hydrogen bond. Asn^{443} forms a hydrophobic interaction with riluzole whereas Met^{442}, Leu^{493} and Leu^{496} may form van der Waals interactions with riluzole. This overlaps partly with the here presented data, as Phe^{414}, Asp^{439}, Arg^{492} and Leu^{496} show the same possible interactions, but Tyr^{374}, Ser^{495}, Asn^{443}, Met^{442} and Leu^{493} were evaluated differently regarding

a possible binding in this thesis.

Tyr^{374} and Asn^{443} showed a rather non functional phenotype when exchanged for alanine, respectively and were therefore not further tested as other amino acids showed more obvious effects (Figure 3.26 and Figure 3.33).

The exchanges of Ser^{495} and Met^{442} for alanine showed no significant reductions in the current densities, respectively and were therefore not further analyzed (Figure 3.4 and Figure 3.4).

Leu^{493} was not considered and not tested in the electrophysiological measurements because of the very rare appearance in the dockings.

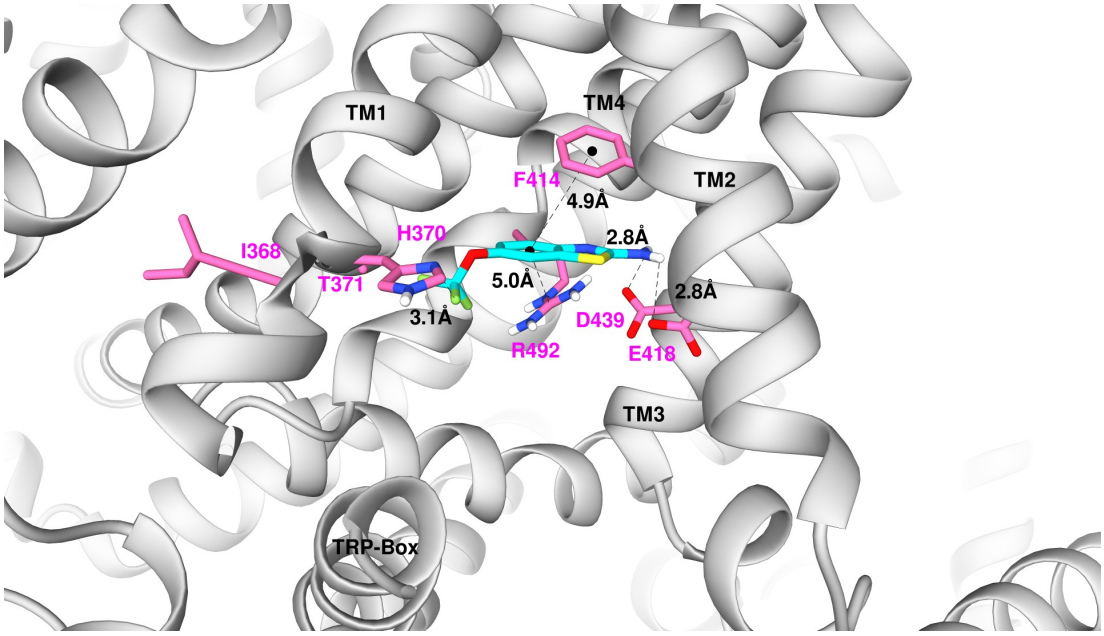

Figure 4.4.: **Predicted riluzole binding site.** This figure shows a representation of TRPC5 (PDB: 6AEI, Duan et al. (2019)) with riluzole (cyan) in the a probable binding position calculated via molecular docking. Amino acids that possibly contribute to a riluzole binding which were either confirmed via patch clamp measurements or were part of the docking result are shown in magenta. Possible interactions are indicated with dotted lines and the measured distance is given in Å. Centroids of aromatic rings are indicated with black dots. The riluzole pose was part of the docking in cavity I during docking project II and represents pose 10 (Figure 4.4 and Figure B.9j).

Comparison with Other Inhibitors Binding to the Same Site

In the presented riluzole binding pocket of TRPC5, other ligands like clemizole, GFB-8438, GFB-8749 and GFB-9289 have already been co-resolved (GFB-8438, GFB-8749 and GFB-9289 with TRPC4 and clemizole with TRPC5). Nonetheless, all of these ligands except for riluzole are channel inhibitors. Therefore, riluzole is the first channel activator, which is thought to bind at the presented ligand binding site between TM1, 2, 3, 4 and the TRP helix. The amino acids participating in the ligand binding seem to be partly conserved, but there are slight variations between the particular ligand binding sites, even between the very similar piperazinone/pyridazinone-based GFB compounds.

The only amino acids which are present is all five ligand binding sites are Arg^{492} (corresponds to Arg^{491} in TRPC4) and Asp^{439} (corresponds to Asp^{438} in TRPC4). Interestingly, the chemical structures of the inhibitors are much larger than that of riluzole. However, they still bind the same ligand binding pocket. This suggests a flexibility in the binding pocket. Eventually, water molecules or ions are additionally involved in the ligand binding. Vinayagam et al. (2020) accordingly suggest a possible involvement of the Ca^{2+} ion in ligand binding, or the stabilization of the ion by a ligand. They further suggest an induced fit mechanism enabling the ligand binding, were residues flip and rotate towards the ligand during binding. This could explain why the ligands that differ in size still bind to the same cavity and why amino acids like Ile^{368} have an effect on the riluzole binding even if they are rotated away from the binding site.

Taken together, the riluole binding site is monomeric and located in the VSLD, between TM1, TM2, TM3, TM4 and the TRP-helix. Mutations of Ile^{368} among others show the strongest effects, but it is unclear if the amino acid plays a role in direct ligand binding or if it has an indirect effect. Other amino acids which show strong effects are His^{370}, Glu^{418} and Asp^{439}. Interestingly, Glu^{418} and Asp^{439} are were also shown to be involved in Ca_2^+-ion binding (Duan et al., 2019; Vinayagam et al., 2018, 2020; Song et al., 2021). The Ca^{2+} binding site seems to be at least conserved between TRPC4 and TRPC5, but its role is not discovered yet. Especially the importance of the Ca^{2+} ion for activator and inhibitor binding in the VSLD is an interesting topic where more research is needed.

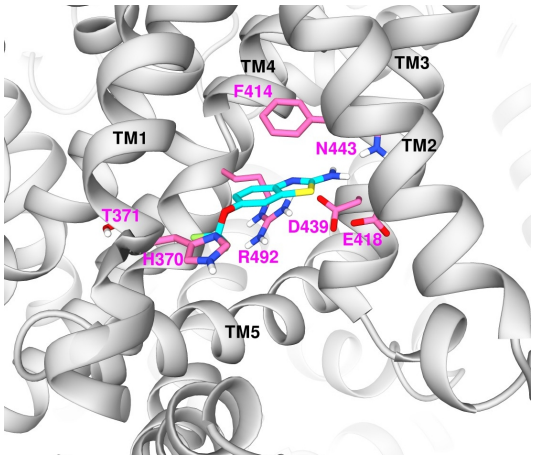

(a) Riluzole

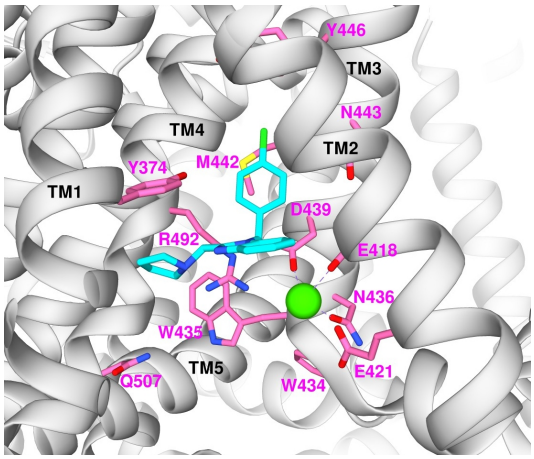

(b) Clemizole

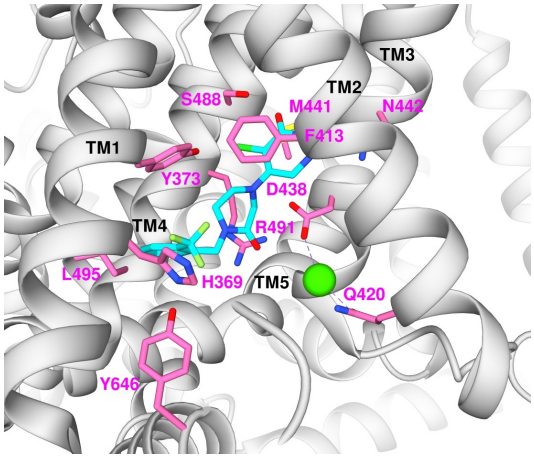

(c) GFB-8438

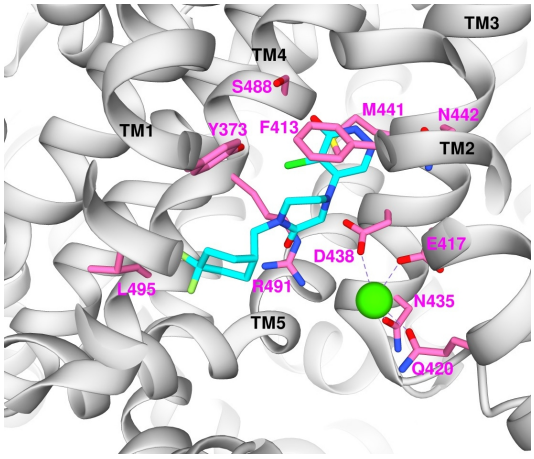

(d) GFB-8749

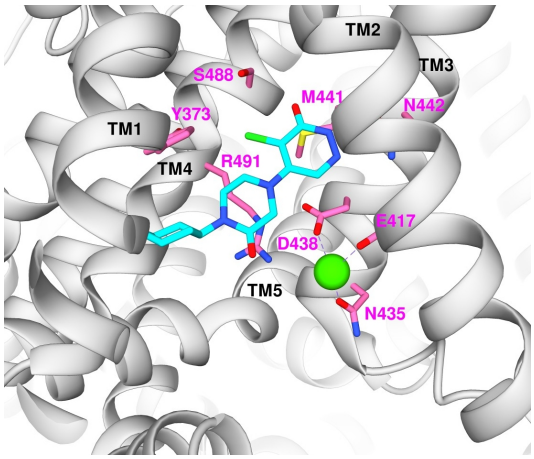

(e) GFB-9289

Figure 4.5.: **Comparison of ligands binding to the proposed riluzole binding site.** The riluzole binding site **(a)** which was identified in this theses is presented with TRPC5 (PDB: 6AEI, Duan et al. (2019)). Clemizole **(b)** was resolved in complex with TRPC5 (PDB: 7D4P, Song et al. (2021)). GFB-8438 **(c)** (PDB: 7B0S), GFB-8749 **(d)** (PDB: 7B05) and GFB-9289 **(e)** (PDB: 7B16) were resolved in complex with TRPC4 (Vinayagam et al., 2020). The ligand is colored in cyan, whereas amino acids participating in a binding are colored in magenta.

Cation binding site

Vinayagam et al. (2020) state, that the cation density in their electron map of TRPC4 represents a Ca^{2+} ion. They found the Ca^{2+} ion to be present in the ligand bound state, as well as in the apo-state of the channel. They further suggest that this ion may be stabilized by the ligand through a bridging water molecule and vice versa. Other authors similarly found a cation density in TRPC4 and TRPC5 at this location but they were not sure about the exact ion because the buffer used for the cryo-EM experiments only contained sodium ions (Duan et al., 2018b, 2019). Nevertheless, Song et al. (2021) assumed a Ca^{2+} ion density to be present in the membrane bound channel. The Ca^{2+} binding site seems to be conserved with small deviations among other TRP channels as well, including TRPM4, TRPM2 and TRPM8 (Autzen et al., 2018; Zhang et al., 2018; Diver et al., 2019).

Even though TRPC5 can be activated by extracellular Ca^{2+}, which is abolished by deleting the Ca^{2+} binding site (Song et al., 2021), (-)-englerin A seems to still activate the channel when deleting this site in TRPC5 (Duan et al., 2019). Clemizol still inhibits (-)-englerin A evoked currents in these Ca^{2+} non-binding mutants (Song et al., 2021). Therefore the role of this bound Ca^{2+} remains still elusive and needs to be investigated. In particular, its involvement in channel modulation and ligand binding is not fully understood.

Strikingly, Yang et al. (2022) suggest a regulatory role of Ca^{2+} for the riluzole binding, as they found synergistic effects of riluzole and Ca^{2+}. In contrast, they show that riluzole is able to activate TRPC5 when the Ca^{2+} binding site is deleted (so called EED-Mutant) and no extracellular Ca^{2+} is present. However, in 2 µM Ca^{2+} conditions riluzole is not able to evoke any TRPC5 current in the EED mutant. Therefore, due to the complex role of Ca^{2+} in TRPC channel modulation experimental design is challenging. Ca^{2+} is involved in many regulatory processes and in binding of different PKC-subtypes, CaM and other TRPC channel regulatory proteins.

4.2. Possible Transduction Mechanisms of the (-)-Englerin A and Riluzole Acitivation

Bai et al. (2020) co-crystallized TRPC6 with a channel activator as well as with a channel inhibitor thereby revealing some channel movements between both structures. Although they did not manage to present the channel in an open state, they observed significant structural changes between the activator and the inhibitor-bound channel. They could show movements in the lower part of TM5 and in the extracellular part of TM3. Vinayagam et al. (2020) suggest, the channel opening is mediated by the TRP-box and radial movements towards or away from the channel pore. The TRP-box is also directly connected to TM6 which stays in close contact to TM5. Beck et al. (2013) already suggested a very crucial role of the TM4-TM5 linker region in the gating process of TRPC5, as mutations of Gly^{503} and Gly^{504} resulted in permantently open channels.

The results of this thesis likewise suggest a very prominent role of the amino acids located in TM5 and in the TM4-5 linker region for the transduction and thereby indirectly influencing the gating process. The amino acids Leu^{496}, Phe^{497},

Asn^{500}, Gly^{511} are located in the same area, either in the lower part of TM4, the lower part of TM5 or in the intracellular loop between these two TM domains.

The Intracellular Loop Between TM4 and TM5 as a Critical Transduction Domain

Leu^{496} might play an indirect role for the riluzole binding, because the residue is rotated slightly away from the riluzole pocket and it is located around 5.7 Å away from the tri-flourine group of riluzole in the given docking pose. Therefore a direct involvement of Leu^{496} in riluzole binding in the given pose is unlikely. Due to its close proximity to other amino acids which might be involved in transduction, like Asn^{500}, Leu^{496} may also play a role for the transduction. However, in the actual co-crystallized riluzole pose, Leu^{496} may forms van der Waals interactions and therefore also plays a minor role in riluzole binding (Yang et al., 2022).

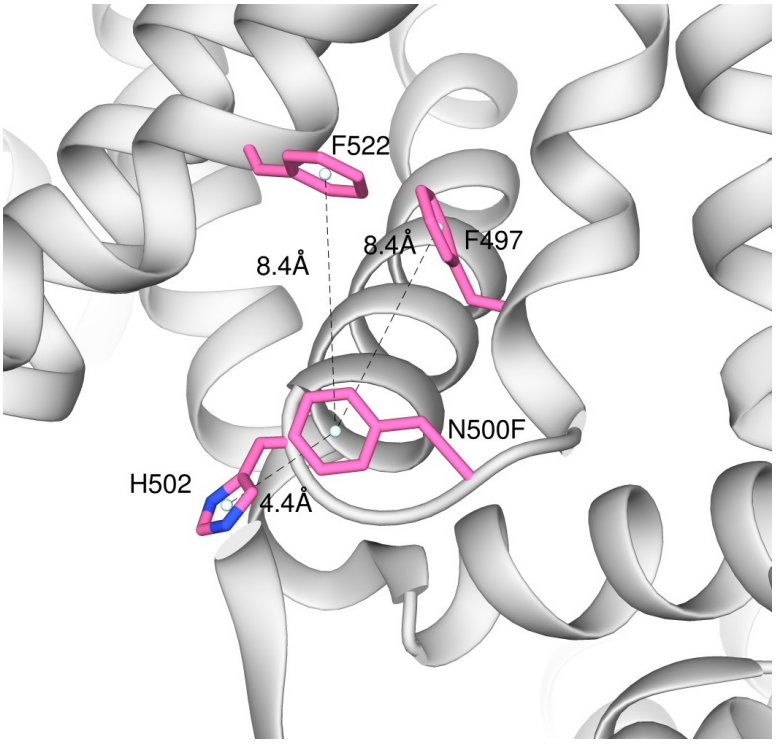

Figure 4.6.: **Possible interactions of mutation N500F.** In this figure a representation of TRPC5 (PDB: 6AEI, Duan et al. (2019)) and possible interactions of mutation N500F are shown. Amino acid residues are colored in magenta, whereas centroids are depicted as white spheres and distances are indicated via dotted lines and measurements are given in Å.

The amino acid Asn^{500} is located even more down-stream in the intracellular loop between TM4 and TM5. The mutation N500A is already described and published by Duan et al. (2019). They found that Asn^{500} interacts with cholesteryl hemisuccinate (CHS) leading to the hypothesis that cholesterol might be important for channel activation via GPCRs. They showed that N500A is still responding to (-)-englerin A, but not to a receptor stimulation. This may indicate a different signal transduction of both activation mechanisms, the (-)-englerin A and the receptor-mediated activation of TRPC5).

CHS is often used as a detergent to stabilize membrane proteins for cryo-EM thereby mimicking the role of cholesterol in the membrane, especially in the case of GPCRs (Kulig et al., 2014). However, the physical properties of cholesterol and CHS differ in molecular dynamics simulations and the role as a mimicking compound is controversially discussed (Kulig et al., 2014; Augustyn et al., 2019).

Another possibility is depicted in Figure 4.6. The region around Asn^{500} eventually needs to be flexible during the riluzole activation. By exchanging asparagine for phenylalanine (N500F), the intracellular loop between TM4 and 5 gets more stabilized by an increased possibility for π-π-interactions between N500F, His^{502}, Phe^{522} and Phe^{497}. Depending on the actual rotation angle of the N500F residues, the distances between aromatic centroids could be viable (typically: 4.5–7 Å (Ferreira de Freitas & Schapira, 2017)).

Another possible interacting residue is His^{502}. Histidine is one of the most versatile interaction partners in protein structures, because the residue properties depend on the protonation state, i. e. the local pH value. Histidine can be neutral or positively charged and therefore can serve as a hydrogen bond donor, acceptor or π-π as well as π-cation interaction partner (Gallivan & Dougherty, 1999; Liao et al., 2013b). Due to the low distance of 4.4 Å from the His^{502} centroid to the N500F centroid, an interaction may be possible.

4.2.1. TM5 is Fixed Through a Hinge Region

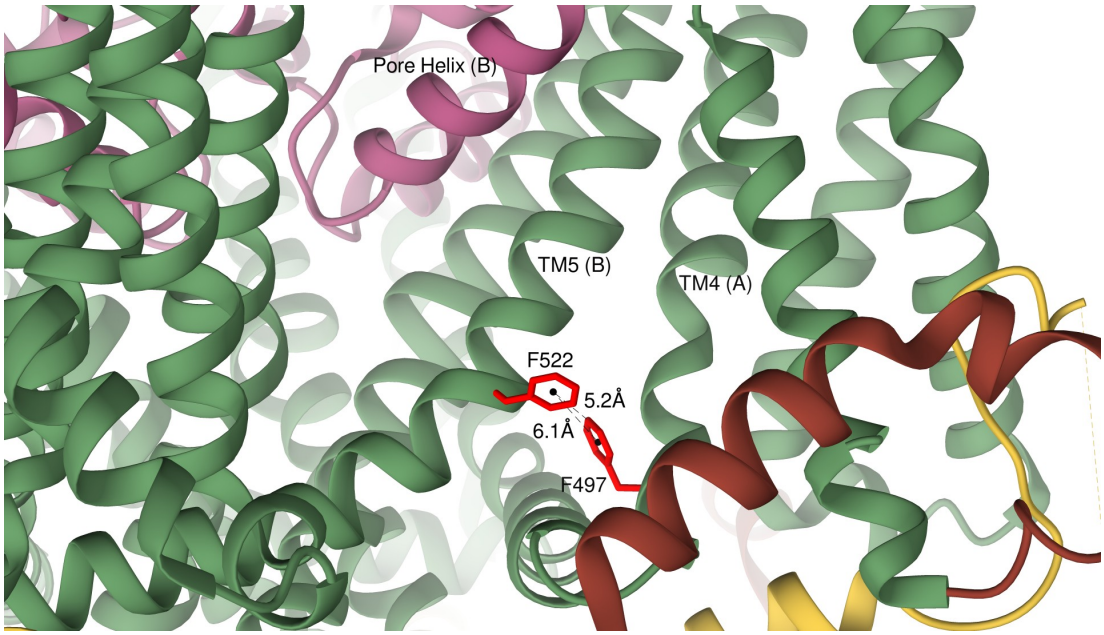

Figure 4.7.: **Possible interactions of amino acid Phe^{497}.** In this figure a representation of TRPC5 (PDB: 6AEI, Duan et al. (2019)) and possible interactions of amino acid Phe^{497} are shown. Amino acid residues are colored in red, whereas centroids are depicted as black spheres and distances are indicated via dotted lines and measured in Å. Channel structural elements are colored according to Figure 1.1.

Strikingly, mutations of the amino acid Phe^{497} significantly reduces the (-)-englerin A evoked current density significantly, while the mutations of the neigh-

boring residue Asn^{500} reduce the riluzole evoked current densities. Two scenarios are imaginable.

Either Phe^{497} is involved in the transduction of the (-)-englerin A mediated activation, or Phe^{497} indirectly stabilizes the (-)-englerin A binding site.

Figure 4.7 illustrates the position of Phe^{497} which might explain why F497Y reduces the (-)-englerin A evoked current densities (subsection 3.2.2). Amino acid Phe^{497} which is located in the lower part of TM4, may interact with Phe^{522}, located in TM5 of the other monomer though a π-π interaction. Both benzene centroids are 6.1 Å apart from each other and the closest distance between both benzene rings is 5.2 Å (see Figure 4.7).

The amino acid exchange F497Y seems to already loosen the interaction between both helices. A study with synthetic peptides and inter-chain interactions in β-hairpins suggests the following contribution to folding free energy: Trp-Phe > Phe-Phe > Phe-Tyr. Therefore the given Tyr-Phe interation represents the lowest interaction energy of the three possible π-π interactions (Makwana & Mahalakshmi, 2014). The amino acid exchange F497Y seems to result in binding energy loss between Phe^{497} and Phe^{522}.

Phe^{522} might stabilize the closeby (-)-englerin A binding site. The exchange F497Y disturbs the interaction with Phe^{522} in the previously described manner, thereby reshaping the (-)-englerin A binding site.

The other possibility might be, that through the Phe^{497}-Phe^{522} interaction the connection between both helices may act like a hinge, stabilizing this exact part of the helices and making it rigid. The lower part of TM5 on the other hand is flexible, allowing a signal transduction through the helix.

Further down of Phe^{522} in TM5, Gly^{511} and Gly^{504} are located. Mutations of Gly^{511} are presented in this thesis (see Figure 3.8). The mutation G511A results in a specific reduction of the riluzole current densities. Whereas G504S is a mutation that was published by Beck et al. (2013). The mutation G504S results in a permanently open channel which has lost any gating ability suggesting that Gly^{504} stands in contact with the gate.

By making the exchange F497Y, this hinge might gets disrupted, resulting in a loose TM5 which is unable to make specific movements or to communicate with the gate through the (-)-englerin A binding site. Interestingly, the riluzole mediated channel activation remains unaffected as the exchange F497Y results in riluzole evoked current densities that are similar to the wildtype current densities (Figure 3.20). Therefore the top part of TM5 seems to be important for the (-)-englerin A mediated channel activation and the lower part for the riluzole mediated channel activation.

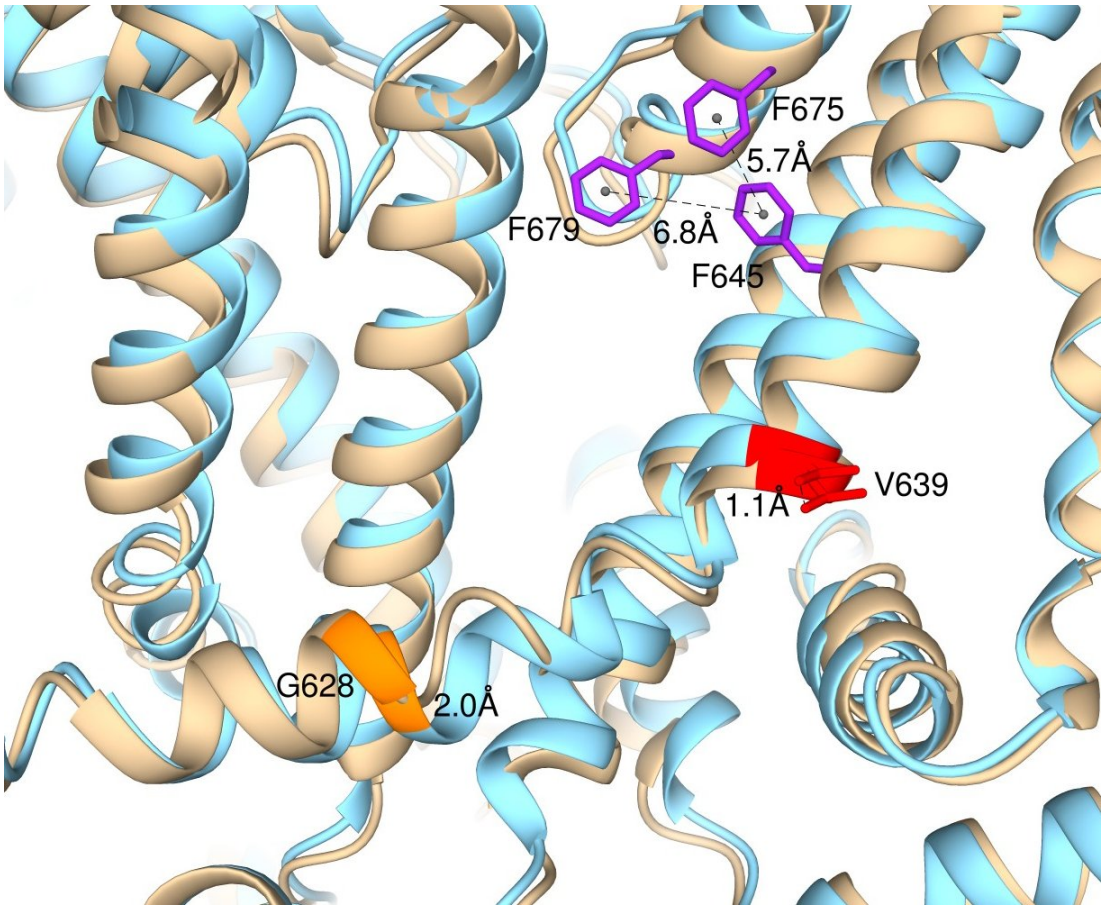

Figure 4.8.: **Alignment of AM-0883 and AM-1473 bound TRPC6.** This figure shows an alignment of the agonist AM-0883 (cyan, PDB: 6UZ8, Bai et al. (2020)) and the antagonist AM-1473 (ochre, PDB: 6UZA, Bai et al. (2020)) bound TRPC6 structure. Amino acid residues are colored in violet, whereas centroids are depicted as black spheres and distances are indicated via dotted lines and measured in Å. In orange and red the protein backbone and residues of Gly^{628} and Val^{639} are colored, respectively (homologous to Gly^{511} and Phe^{522} in TRPC5). The measurements indicates the distance between the residues in the agonist and antagonist bound structure.

A similar mechanism can be observed in TRPC6 (Figure 4.8). Because of the movements which were resolved comparing the inhibitor bound channel structure and the apo-state of the channel (Bai et al., 2020), some insights in a possible activation mechanism can be gained.

Phe^{522} is missing in TRPC6 and the homologous amino acid is Val^{639} (depicted in Figure 4.8). Phe^{645}, Phe^{679} as well as Phe^{675} are stabilizing the pore helix and TM5 by interaction with each other, resulting in a similar hinge region as residue Phe^{522} in TRPC5.

The activator and inhibitor bound structures are nearly congruent at Phe^{645}, whereas Gly^{628} which is homologous to Gly^{511} in TRPC5 displays a flexible region with a 2 Å difference between the backbone carbonyl-carbon atoms of the activator and inhibitor bound structures, respectively. Therefore in TRPC6 the movement in TM5 takes place downstream of Phe^{645} and a similar movement might occur downstream of Phe^{522} in TRPC5 as well.

Consequently, TM6 could follow this movement at the crossing of TM5 and 6 thereby opening the gate. Additionally, we have to keep in mind that the given structure is not the channel in its open state, but it displays a closed state with a bound activator. Therefore even greater movements between the open and the closed state of the channel might take place.

4.3. Comparison of Transduction Mechanisms

So far, TRPC channels seem to have 3 conserved ligand binding sites. Two of them are presented in this thesis (see Figure 4.3 and Figure 4.5) and the third binding site is a binding site for the inhibitor (2-(benzo[d][1,3]dioxol-5-ylamino)thiazol-4-yl)((3S,5R)-3,5-dimethylpiperidin-1-yl)methanone (BTDM) that was identified in the TRPC6 channel (Tang et al., 2018). This binding site is also conserved in TRPM8, where it was found to be a binding site for the inhibitor resiniferatoxin (RTX) (Diver et al., 2019). However, a role of the pocket in other TRPC channels except for TRPC6 has not been discovered yet.

The first two mentioned binding sites can either be occupied by channel inhibitors or channel activators. Therefore these two channel regions seem to be regulatory hotspots. Interestingly, some ligands act as channel activators or channel inhibitors depending on the channel state, respectively. AM-237 can either act as an activator for TRPC5, or act as an inhibitor when the channel is prestimulated by (-)-englerin A (Minard et al., 2019). Similarly, A54 is a competitive antagonist of the (-)-englerin A mediated TRPC5 activation, but in contrast to that A54 potentiates the Gd^{3+} mediated TRPC5 activation.

Due to the structural similarity of AM-237, Pico-145 and HC-070, it can be speculated that AM-237 binds to a similar site. (-)-Englerin A also seems to bind to this site, as presented in Figure 4.3. Due to the derivative structure of A54 and (-)-englerin A it is likely that both ligands bind to the same cavity.

Lanthanides might also bind in close proximity to the xanthine/(-)-englerin A binding site (Jung et al., 2003). Therefore it is likely that ligands binding in this channel region might interact and interfere with each other.

Additionally, the selectivity filter plays a key role in ligand binding to this pocket. For potassium channels a model is established and discussed where the channel activation can not only occur at the lower gate, but also at the selectivity filter by coupling with the lower gate (Heer et al., 2017; Kopec et al., 2019; Schewe et al., 2019). In the described model the selectivity filter would represent a second activation gate distinct from the intracellular lower gate.

Huffer et al. (2020) suggests a key role of the selectivity filter in the gating process of the ion permeation by comparing selectivity filter constriction points of different published TRP channel 3D-structures and determining great variations. This is in line with previous suggestions that the selectivity filter in TRPV1 might act as a second gate (Cao et al., 2013; Gao et al., 2016).

Altogether, the role of the selectivity filter in TRP channels is only poorly understood until now. However, the two gates might both serve as activation gates that split the possibilities for channel activation into two segments. One part of the ligands interacts with the upper gate (selectivity filter) and mediates the channel regulation like the xanthines, (-)-englerin A and DAG, while other ligands mainly interact with the lower gate like riluzole, clemizole, GFB-8749, GFB-8438 and GFB-9289.

Schewe et al. (2019) denote the opening of a potassium channel at the selectivity filter gate as a "pharmacological master key". The (-)-englerin A activation also offers unique features compared to other channel activators like a non-selective cation inward current. Additionally, a triple mutant where all lower gate amino acids are exchanged for alanine did result in a loss of potentiation by Gd^{3+} but in a non affected (-)-englerin A current response (Duan et al., 2019).

This supports the uniqueness of the (-)-englerin A activation and it can be speculated that (-)-englerin A might act in a similar fashion. This further highlights the sensitive channel regulation and shows that the regulation mechanism of TRPC channels is still poorly understood.

Another possible interaction link for both binding sites to control the lower gate is TM6 and the TRP-box. TM6 is directly involved in the binding site of (-)-englerin A. Therefore, (-)-englerin A can gain access to the lower gate by counterclockwise rotation and unwinding of TM6 (Bai et al., 2020). Interestingly, mutations in TM6 have no specific effects on the (-)-englerin A current densities. A significant reduction of (-)-englerin A induced currents by mutations located in TM6 always occurs together with a significant reduction of riluzole evoked currents. This indicates a decrease of the overall channel functionality rather than an (-)-englerin A specific effect Figure 3.56. An (-)-englerin A specific effect would be expected if TM6 is the main structural element involved in the transduction of the (-)-englerin A mediated TRPC5 activation.

Riluzole could gain access to the lower gate through the TRP-box. If the proposed mechanism of Vinayagam et al. (2020) is correct, the TRP-box which is located right beneath the riluzole binding site can slide towards and away from the ion conducting pathway thereby opening and closing the lower gate.

Taken together, riluzole and (-)-englerin A possess distinct binding sites and it can be speculated that their transduction mechanisms are also different. The functional link between both pockets and the gate are either TM5 or TM6 and the TRP-box.

4.4. Outlook

The two presented distinct activator binding sites for riluzole and (-)-englerin A suggest a tight regulation of TRPC5 channels. Interestingly, activators as well as inhibitors bind the same binding pockets, indicating that these regions are key regulatory sites of the channel. It is still obscure if the two binding pockets interact with each other and how they influence the channel gate. The two activator binding sites might act together and have a synergistic effect on the channel current which needs to be analyzed in further studies. Hereby, a detailed analysis of the IV curves by applying the NSC (Hermann et al., 2022) could also be very helpful.

Furthermore, it is not clear whether channel inhibitors and activators that bind at the same or at a different binding site can interfere with each other and have competitive effects.

In addition, the signal transduction mechanism of the channel inhibitors is not fully understood since they do not directly block the channel pore as it is described for some toxins like tetrodotoxin, a potent neurotoxin which blocks voltage-gated sodium channels.

Another still unanswered question is the endogenous activation mechanism of TRPC5 channels. An example to illustrate this topic is the discussion about DAG in the context of TRPC5. Song et al. (2021) managed to resolve a DAG molecule that is bound in the pore region of TRPC5, but the role of DAG in this binding site is still not fully understood. Although it was shown that DAG can inhibit TRPC5 channels, under certain circumstances that involve the dissociation of the C-terminal bound scaffolding protein NHERF, DAG was able to directly activate TRPC5 channels (Storch et al., 2017). However, in the 3D-structure of TRPC5 a DAG molecule is bound in an inactive channel state in the presence as well as in the absence of an inhibitor, suggesting that DAG alone is not sufficient to cause an open channel state. Thus, the role of DAG for TRPC5 channel activation needs to be analyzed in future studies.

Taken together, the concepts of strict inhibitors and activators at least for TRPC5 channels should be rethought as some ligands can act as either inhibitor or activator depending on the channel state.

Furthermore, the role of Ca^{2+} for the TRPC5 channel regulation is also incompletely understood. Recently, a Ca^{2+} ion was found in the ligand binding site of riluzole. Interestingly, Song et al. (2021) show that high Ca^{2+} concentrations are not important for the clemizole binding in TRPC4.

However, Zimova et al. (2022) recently showed for the TRPC5 inhibitor duloxetine which binds roughly at the same site as clemizole and riluzole, that Ca^{2+} may influences the duloxetine induced channel inhibition as Ca^{2+} free conditions change the duloxetine induced inhibition kinetics. Molecular dynamic simulations similarly suggest a better duloxetine binding when the Ca^{2+} ion is present in the binding site (Zimova et al., 2022).

Interestingly, duloxetine is an antidepressant drug which raises the assumption that the TRPC5 channel inhibition might play a role for the antidepressant effect. The role of Ca^{2+} for the riluzole binding is also still obscure. Notably, the Ca^{2+} binding messenger protein CaM is also important for the regulation of the TRPC5 activity. Therefore, both mechanisms might interfere with each other.

To address the mechanisms that regulate TRPC5 channel activation very precisely, planar lipid bilayers are an option (Zakharian, 2019). In the case of TRP channels the technique was already used to discover the role of PIP_2 in TRPM8 channels (Zakharian et al., 2009, 2010). The advantage of using reconstituted channels in artificial membranes is, that an involvement of other interacting proteins and signal transduction pathways can be excluded.

Another tool to further characterize the pathways leading to TRPC5 channel activation are single channel patch-clamp experiments. For example, specific ligand binding mutants can be used, like the TRPC5 channel mutant Q573A in the case of (-)-englerin A or the mutants E418A or R492K in the case of riluzole. Performing single-channel measurements, differences in the single-channel properties like the mean open time, the single-channel conductance and the current kinetics can be investigated. This method might also allow to analyze whether distinct amino acids are involved in ligand binding or rather in signal transduction. Because the structure of a TRPC channel in its open state is still missing, a systematic biophysical characterization of the channel properties is still indispensable to unravel the complex regulation of the activation mechanism of TRPC channels.

Bibliography

Akbulut, Y., Gaunt, H. J., Muraki, K., Ludlow, M. J., Amer, M. S., Bruns, A., Vasudev, N. S., Radtke, L., Willot, M., Hahn, S., Seitz, T., Ziegler, S., Christmann, M., Beech, D. J. & Waldmann, H. (2015): *(-)-Englerin A is a potent and selective activator of TRPC4 and TRPC5 calcium channels.* In: Angewandte Chemie (International ed. in English), **54**, 12: 3787–3791.

Akee, R. K., Ransom, T., Ratnayake, R., McMahon, J. B. & Beutler, J. A. (2012): *Chlorinated englerins with selective inhibition of renal cancer cell growth.* In: Journal of natural products, **75**, 3: 459–463.

Albert, A. P., Saleh, S. N. & Large, W. A. (2008): *Inhibition of native TRPC6 channel activity by phosphatidylinositol 4,5-bisphosphate in mesenteric artery myocytes.* In: The Journal of physiology, **586**, 13: 3087–3095.

Alessandri-Haber, N., Dina, O. A., Chen, X. & Levine, J. D. (2009): *TRPC1 and TRPC6 channels cooperate with TRPV4 to mediate mechanical hyperalgesia and nociceptor sensitization.* In: The Journal of neuroscience : the official journal of the Society for Neuroscience, **29**, 19: 6217–6228.

Alley, M. C., Scudiero, D. A., Monks, A., Hursey, M. L., Czerwinski, M. J., Fine, D. L., Abbott, B. J., Mayo, J. G., Shoemaker, R. H. & Boyd, M. R. (1988): *Feasibility of drug screening with panels of human tumor cell lines using a microculture tetrazolium assay.* In: Cancer research, **48**, 3: 589–601.

Ambudkar, I. S., de Souza, L. B. & Ong, H. L. (2017): *TRPC1, Orai1, and STIM1 in SOCE: Friends in tight spaces.* In: Cell calcium, **63**: 33–39.

Anjana, R., Vaishnavi, M. K., Sherlin, D., Kumar, S. P., Naveen, K., Kanth, P. S. & Sekar, K. (2012): *Aromatic-aromatic interactions in structures of proteins and protein-DNA complexes: a study based on orientation and distance.* In: Bioinformation, **8**, 24: 1220–1224.

Antigny, F., Girardin, N. & Frieden, M. (2012): *Transient receptor potential canonical channels are required for in vitro endothelial tube formation.* In: The Journal of biological chemistry, **287**, 8: 5917–5927.

Arniges, M., Fernández-Fernández, J. M., Albrecht, N., Schaefer, M. & Valverde, M. A. (2006): *Human TRPV4 channel splice variants revealed a key role of ankyrin domains in multimerization and trafficking.* In: The Journal of biological chemistry, **281**, 3: 1580–1586.

Augustyn, B., Stepien, P., Poojari, C., Mobarak, E., Polit, A., Wisniewska-Becker, A. & Róg, T. (2019): *Cholesteryl Hemisuccinate Is*

Not a Good Replacement for Cholesterol in Lipid Nanodiscs. In: The journal of physical chemistry. B, **123**, 46: 9839–9845.

Autzen, H. E., Myasnikov, A. G., Campbell, M. G., Asarnow, D., Julius, D. & Cheng, Y. (2018): *Structure of the human TRPM4 ion channel in a lipid nanodisc.* In: Science (New York, N.Y.), **359**, 6372: 228–232.

Bai, C.-X., Giamarchi, A., Rodat-Despoix, L., Padilla, F., Downs, T., Tsiokas, L. & Delmas, P. (2008): *Formation of a new receptor-operated channel by heteromeric assembly of TRPP2 and TRPC1 subunits.* In: EMBO reports, **9**, 5: 472–479.

Bai, Y., Yu, X., Chen, H., Horne, D., White, R., Wu, X., Lee, P., Gu, Y., Ghimire-Rijal, S., Lin, D. C.-H. & Huang, X. (2020): *Structural basis for pharmacological modulation of the TRPC6 channel.* In: eLife, **9**.

Beck, A., Speicher, T., Stoerger, C., Sell, T., Dettmer, V., Jusoh, S. A., Abdulmughni, A., Cavalié, A., Philipp, S. E., Zhu, M. X., Helms, V., Wissenbach, U. & Flockerzi, V. (2013): *Conserved gating elements in TRPC4 and TRPC5 channels.* In: The Journal of biological chemistry, **288**, 27: 19471–19483.

Beckmann, H., Richter, J., Hill, K., Urban, N., Lemoine, H. & Schaefer, M. (2017): *A benzothiadiazine derivative and methylprednisolone are novel and selective activators of transient receptor potential canonical 5 (TRPC5) channels.* In: Cell calcium, **66**: 10–18.

Bell, D. R., Gerlach, J. H., Kartner, N., Buick, R. N. & Ling, V. (1985): *Detection of P-glycoprotein in ovarian cancer: a molecular marker associated with multidrug resistance.* In: Journal of clinical oncology : official journal of the American Society of Clinical Oncology, **3**, 3: 311–315.

Bensimon, G., Lacomblez, L. & Meininger, V. (1994): *A controlled trial of riluzole in amyotrophic lateral sclerosis. ALS/Riluzole Study Group.* In: The New England journal of medicine, **330**, 9: 585–591.

Berridge, M. (2004): *Conformational coupling: a physiological calcium entry mechanism.* In: Science's STKE : signal transduction knowledge environment, **2004**, 243: pe33.

Bird, G. S. & Putney, J. W. (2018): *Calcium Entry Channels in Non-Excitable Cells: Pharmacology of Store-Operated Calcium Entry Channels.* Boca Raton (FL).

Bork, P. (1993): *Hundreds of ankyrin-like repeats in functionally diverse proteins: mobile modules that cross phyla horizontally?* In: Proteins, **17**, 4: 363–374.

Boulay, G., Zhu, X., Peyton, M., Jiang, M., Hurst, R., Stefani, E. & Birnbaumer, L. (1997): *Cloning and expression of a novel mammalian homolog of Drosophila transient receptor potential (Trp) involved in calcium entry secondary to activation of receptors coupled by the Gq class of G protein.* In: The Journal of biological chemistry, **272**, 47: 29672–29680.

Breeden, L. & Nasmyth, K. (1987): *Similarity between cell-cycle genes of budding yeast and fission yeast and the Notch gene of Drosophila.* In: Nature, **329**, 6140: 651–654.

Bush, E. W., Hood, D. B., Papst, P. J., Chapo, J. A., Minobe, W., Bristow, M. R., Olson, E. N. & McKinsey, T. A. (2006): *Canonical transient receptor potential channels promote cardiomyocyte hypertrophy through activation of calcineurin signaling.* In: The Journal of biological chemistry, **281**, 44: 33487–33496.

Cao, E., Liao, M., Cheng, Y. & Julius, D. (2013): *TRPV1 structures in distinct conformations reveal activation mechanisms.* In: Nature, **504**, 7478: 113–118.

Capes, D. L., Arcisio-Miranda, M., Jarecki, B. W., French, R. J. & Chanda, B. (2012): *Gating transitions in the selectivity filter region of a sodium channel are coupled to the domain IV voltage sensor.* In: Proceedings of the National Academy of Sciences, **109**, 7: 2648–2653.

Carafoli, E. & Krebs, J. (2016): *Why Calcium? How Calcium Became the Best Communicator.* In: The Journal of biological chemistry, **291**, 40: 20849–20857.

Carson, C., Raman, P., Tullai, J., Xu, L., Henault, M., Thomas, E., Yeola, S., Lao, J., McPate, M., Verkuyl, J. M., Marsh, G., Sarber, J., Amaral, A., Bailey, S., Lubicka, D., Pham, H., Miranda, N., Ding, J., Tang, H.-M., Ju, H., Tranter, P., Ji, N., Krastel, P., Jain, R. K., Schumacher, A. M., Loureiro, J. J., George, E., Berellini, G., Ross, N. T., Bushell, S. M., Erdemli, G. & Solomon, J. M. (2015): *Englerin A Agonizes the TRPC4/C5 Cation Channels to Inhibit Tumor Cell Line Proliferation.* In: PloS one, **10**, 6: e0127498.

Chang, A. S., Chang, S. M., Garcia, R. L. & Schilling, W. P. (1997): *Concomitant and hormonally regulated expression of trp genes in bovine aortic endothelial cells.* In: FEBS Letters, **415**, 3: 335–340. URL `https://pubmed.ncbi.nlm.nih.gov/9357995/`.

Chang, Q., Gyftogianni, E., van de Graaf, S. F. J., Hoefs, S., Weidema, F. A., Bindels, R. J. M. & Hoenderop, J. G. J. (2004): *Molecular determinants in TRPV5 channel assembly.* In: The Journal of biological chemistry, **279**, 52: 54304–54311.

Chen, X., Li, W., Riley, A. M., Soliman, M., Chakraborty, S., Stamatkin, C. W. & Obukhov, A. G. (2017): *Molecular Determinants of the Sensitivity to Gq/11-Phospholipase C-dependent Gating, Gd3+ Potentiation, and Ca2+ Permeability in the Transient Receptor Potential Canonical Type 5 (TRPC5) Channel.* In: The Journal of biological chemistry, **292**, 3: 898–911.

Chen, X., Sooch, G., Demaree, I. S., White, F. A. & Obukhov, A. G. (2020): *Transient Receptor Potential Canonical (TRPC) Channels: Then and Now.* In: Cells, **9**, 9.

Chenard, B. L. & Gallaschun, R. (2014): *Substituted Xanthines and Methods of Use Thereof.*

Clapham, D. E. (2007): *Calcium signaling.* In: Cell, **131**, 6: 1047–1058.

Clapham, D. E., Runnels, L. W. & Strübing, C. (2001): *The TRP ion channel family.* In: Nature reviews. Neuroscience, **2**, 6: 387–396.

Constantin, B. (2016): *Role of Scaffolding Proteins in the Regulation of TRPC-Dependent Calcium Entry.* In: Advances in experimental medicine and biology, **898**: 379–403.

Cosens, D. J. & Manning, A. (1969): *Abnormal electroretinogram from a Drosophila mutant.* In: Nature, **224**, 5216: 285–287.

DiNitto, J. P., Cronin, T. C. & Lambright, D. G. (2003): *Membrane recognition and targeting by lipid-binding domains.* In: Science's STKE : signal transduction knowledge environment, **2003**, 213: re16.

Diver, M. M., Cheng, Y. & Julius, D. (2019): *Structural insights into TRPM8 inhibition and desensitization.* In: Science (New York, N.Y.), **365**, 6460: 1434–1440.

Dong, Y., Pan, Q., Jiang, L., Chen, Z., Zhang, F., Liu, Y., Xing, H., Shi, M., Li, J., Li, X., Zhu, Y., Chen, Y., Bruce, I. C., Jin, J. & Ma, X. (2014): *Tumor endothelial expression of P-glycoprotein upon microvesicular transfer of TrpC5 derived from adriamycin-resistant breast cancer cells.* In: Biochemical and biophysical research communications, **446**, 1: 85–90.

Du, J., Ma, X., Shen, B., Huang, Y., Birnbaumer, L. & Yao, X. (2014): *TRPV4, TRPC1, and TRPP2 assemble to form a flow-sensitive heteromeric channel.* In: FASEB journal : official publication of the Federation of American Societies for Experimental Biology, **28**, 11: 4677–4685.

Duan, J., Li, J., Chen, G.-L., Ge, Y., Liu, J., Xie, K., Peng, X., Zhou, W., Zhong, J., Zhang, Y., Xu, J., Xue, C., Liang, B., Zhu, L., Liu, W., Zhang, C., Tian, X.-L., Wang, J., Clapham, D. E., Zeng, B., Li, Z. & Zhang, J. (2019): *Cryo-EM structure of TRPC5 at 2.8-Å resolution reveals unique and conserved structural elements essential for channel function.* In: Science advances, **5**, 7: eaaw7935.

Duan, J., Li, J., Chen, G.-L., Zeng, B., Xie, K., Peng, X., Zhou, W., Zhong, J., Zhang, Y., Xu, J., Xue, C., Zhu, L., Liu, W., Tian, X.-L., Wang, J., Clapham, D. E., Li, Z. & Zhang, J. (2018a): *Cryo-EM structure of the receptor-activated TRPC5 ion channel at 2.9 angstrom resolution.* In: , **7**.

Duan, J., Li, J., Zeng, B., Chen, G.-L., Peng, X., Zhang, Y., Wang, J., Clapham, D. E., Li, Z. & Zhang, J. (2018b): *Structure of the mouse TRPC4 ion channel.* In: Nature communications, **9**, 1: 3102.

Eder, P., Schindl, R., Romanin, C. & Groschner, K. (2007): *Chapter 24: TRP Ion Channel Function in Sensory Transduction and Cellular Signaling Cascades: Protein–Protein Interactions in TRPC Channel Complexes.* In: TRP Ion Channel Function in Sensory Transduction and Cellular Signaling Cascades.

Engelke, M., Friedrich, O., Budde, P., Schäfer, C., Niemann, U., Zitt, C., Jüngling, E., Rocks, O., Lückhoff, A. & Frey, J. (2002): *Structural domains required for channel function of the mouse transient receptor potential protein homologue TRP1b.* In: FEBS Letters, **523**, 1-3: 193–199.

Erler, I., Hirnet, D., Wissenbach, U., Flockerzi, V. & Niemeyer, B. A. (2004): *Ca2+-selective transient receptor potential V channel architecture and function require a specific ankyrin repeat.* In: The Journal of biological chemistry, **279**, 33: 34456–34463.

Fan, C., Choi, W., Sun, W., Du, J. & Lü, W. (2018): *Structure of the human lipid-gated cation channel TRPC3.* In: eLife, **7**.

Fash, D. M., Peer, C. J., Li, Z., Talisman, I. J., Hayavi, S., Sulzmaier, F. J., Ramos, J. W., Sourbier, C., Neckers, L., Figg, W. D., Beutler, J. A. & Chain, W. J. (2016): *Synthesis of a Stable and Orally Bioavailable Englerin Analogue.* In: Bioorganic & medicinal chemistry letters, **26**, 11: 2641–2644.

Ferreira de Freitas, R. & Schapira, M. (2017): *A systematic analysis of atomic protein-ligand interactions in the PDB.* In: MedChemComm, **8**, 10: 1970–1981.

Fischer, M. J. M. & Edwardson, J. M. (2014): *V2A2lidating TRP channel heteromers.* In: Temperature: Multidisciplinary Biomedical Journal, **1**, 1: 26–27.

Folkman, J. (2002): *Role of angiogenesis in tumor growth and metastasis.* In: Seminars in Oncology, **29**, 6: 15–18. URL `https://www.sciencedirect.com/science/article/pii/S0093775402700651`.

Freichel, M., Suh, S. H., Pfeifer, A., Schweig, U., Trost, C., Weissgerber, P., Biel, M., Philipp, S., Freise, D., Droogmans, G., Hofmann, F., Flockerzi, V. & Nilius, B. (2001): *Lack of an endothelial store-operated Ca2+ current impairs agonist-dependent vasorelaxation in TRP4-/- mice.* In: Nature cell biology, **3**, 2: 121–127.

Freichel, M., Tsvilovskyy, V. & Camacho-Londoño, J. E. (2014): *TRPC4- and TRPC4-containing channels.* In: Handbook of experimental pharmacology, **222**: 85–128.

Gallivan, J. P. & Dougherty, D. A. (1999): *Cation-pi interactions in structural biology.* In: Proceedings of the National Academy of Sciences, **96**, 17: 9459–9464.

Gao, Y., Cao, E., Julius, D. & Cheng, Y. (2016): *TRPV1 structures in nanodiscs reveal mechanisms of ligand and lipid action.* In: Nature, **534**, 7607: 347–351.

Garcia, R. L. & Schilling, W. P. (1997): *Differential expression of mammalian TRP homologues across tissues and cell lines.* In: Biochemical and biophysical research communications, **239**, 1: 279–283.

García-Sanz, N., Valente, P., Gomis, A., Fernández-Carvajal, A., Fernández-Ballester, G., Viana, F., Belmonte, C. & Ferrer-Montiel, A. (2007): *A role of the transient receptor potential domain of vanilloid receptor I in channel gating.* In: The Journal of neuroscience : the official journal of the Society for Neuroscience, **27**, 43: 11641–11650.

Grant, P., Song, J. Y. & Swedo, S. E. (2010): *Review of the use of the glutamate antagonist riluzole in psychiatric disorders and a description of recent use in childhood obsessive-compulsive disorder.* In: Journal of child and adolescent psychopharmacology, **20**, 4: 309–315.

Gregorio-Teruel, L., Valente, P., González-Ros, J. M., Fernández-Ballester, G. & Ferrer-Montiel, A. (2014): *Mutation of I696 and W697 in the TRP box of vanilloid receptor subtype I modulates allosteric channel activation.* In: The Journal of general physiology, **143**, 3: 361–375.

Gregorio-Teruel, L., Valente, P., Liu, B., Fernández-Ballester, G., Qin, F. & Ferrer-Montiel, A. (2015): *The Integrity of the TRP Domain Is Pivotal for Correct TRPV1 Channel Gating.* In: Biophysical journal, **109**, 3: 529–541.

Greka, A., Navarro, B., Oancea, E., Duggan, A. & Clapham, D. E. (2003): *TRPC5 is a regulator of hippocampal neurite length and growth cone morphology.* In: Nature neuroscience, **6**, 8: 837–845.

Groschner, K., Hingel, S., Lintschinger, B., Balzer, M., Romanin, C., Zhu, X. & Schreibmayer, W. (1998): *Trp proteins form store-operated cation channels in human vascular endothelial cells.* In: FEBS Letters, **437**, 1-2: 101–106.

Guéguinou, M., Harnois, T., Crottes, D., Uguen, A., Deliot, N., Gambade, A., Chantôme, A., Haelters, J. P., Jaffrès, P. A., Jourdan, M. L., Weber, G., Soriani, O., Bougnoux, P., Mignen, O., Bourmeyster, N., Constantin, B., Lecomte, T., Vandier, C. & Potier-Cartereau, M. (2016): *SK3/TRPC1/Orai1 complex regulates SOCE-dependent colon cancer cell migration: a novel opportunity to modulate anti-EGFR mAb action by the alkyl-lipid Ohmline.* In: Oncotarget, **7**, 24: 36168–36184.

Haan, C. & Behrmann, I. (2007): *A cost effective non-commercial ECL-solution for Western blot detections yielding strong signals and low background.* In: Journal of immunological methods, **318**, 1-2: 11–19.

Hanahan, D. & Weinberg, R. A. (2000): *The Hallmarks of Cancer*, Bd. 100.

Hanahan, D. & Weinberg, R. A. (2011): *Hallmarks of cancer: the next generation*, Bd. 144.

Hardie, R. C. & Minke, B. (1992): *The trp gene is essential for a light-activated Ca2+ channel in Drosophila photoreceptors.* In: Neuron, **8**, 4: 643–651.

He, D.-x. & Ma, X. (2016): *Transient receptor potential channel C5 in cancer chemoresistance.* In: Acta pharmacologica Sinica, **37**, 1: 19–24.

Heer, F. T., Posson, D. J., Wojtas-Niziurski, W., Nimigean, C. M. & Bernèche, S. (2017): *Mechanism of activation at the selectivity filter of the KcsA K+ channel.* In: eLife, **6**.

Hermann, C., Treder, A., Näher, M., Geiseler, R., Gudermann, T., Mederos Y Schnitzler, M. & Storch, U. (2022): *The normalized slope conductance as a tool for quantitative analysis of current-voltage relations.* In: Biophysical journal, **121**, 8: 1435–1448.

Hibbs, R. E. & Gouaux, E. (2011): *Principles of activation and permeation in an anion-selective Cys-loop receptor.* In: Nature, **474**, 7349: 54–60.

Hilgemann, D. W. & Ball, R. (1996): *Regulation of cardiac Na+,Ca2+ exchange and KATP potassium channels by PIP2.* In: Science (New York, N.Y.), **273**, 5277: 956–959.

Hille, B. (2001): *Ion channels of excitable membranes.* 3. ed. Aufl. Sinauer, Sunderland, Mass.

Hofmann, T., Obukhov, A. G., Schaefer, M., Harteneck, C., Gudermann, T. & Schultz, G. (1999): *Direct activation of human TRPC6 and TRPC3 channels by diacylglycerol.* In: Nature, **397**, 6716: 259–263.

Hoth, M. & Penner, R. (1992): *Depletion of intracellular calcium stores activates a calcium current in mast cells.* In: Nature, **355**, 6358: 353–356.

House, S. J., Potier, M., Bisaillon, J., Singer, H. A. & Trebak, M. (2008): *The non-excitable smooth muscle: calcium signaling and phenotypic switching during vascular disease.* In: Pflugers Archiv : European journal of physiology, **456**, 5: 769–785.

Huffer, K. E., Aleksandrova, A. A., Jara-Oseguera, A., Forrest, L. R. & Swartz, K. J. (2020): *Global alignment and assessment of TRP channel transmembrane domain structures to explore functional mechanisms.* In: eLife, **9**.

Inoue, H., Nojima, H. & Okayama, H. (1990): *High efficiency transformation of Escherichia coli with plasmids.* In: Gene, **96**, 1: 23–28.

Inoue, R., Jensen, L. J., Shi, J., Morita, H., Nishida, M., Honda, A. & Ito, Y. (2006): *Transient receptor potential channels in cardiovascular function and disease.* In: Circulation research, **99**, 2: 119–131.

Inoue, R., Okada, T., Onoue, H., Hara, Y., Shimizu, S., Naitoh, S., Ito, Y. & Mori, Y. (2001): *The transient receptor potential protein homologue TRP6 is the essential component of vascular alpha(1)-adrenoceptor-activated Ca(2+)-permeable cation channel.* In: Circulation research, **88**, 3: 325–332.

Jardin, I., Lopez, J. J., Salido, G. M. & Rosado, J. A. (2008): *Orai1 mediates the interaction between STIM1 and hTRPC1 and regulates the mode of activation of hTRPC1-forming Ca2+ channels.* In: The Journal of biological chemistry, **283**, 37: 25296–25304.

Jeon, J.-P., Hong, C., Park, E. J., Jeon, J.-H., Cho, N.-H., Kim, I.-G., Choe, H., Muallem, S., Kim, H. J. & So, I. (2012): *Selective Gai subunits as novel direct activators of transient receptor potential canonical (TRPC)4 and TRPC5 channels.* In: The Journal of biological chemistry, **287**, 21: 17029–17039.

Jeon, J.-P., Lee, K. P., Park, E. J., Sung, T. S., Kim, B. J., Jeon, J.-H. & So, I. (2008): *The specific activation of TRPC4 by Gi protein subtype.* In: Biochemical and biophysical research communications, **377**, 2: 538–543.

Jeong, S., Ko, J., Kim, M., Park, K. C., Park, E. Y. J., Kim, J., Baik, Y., Wie, J., Cho, A. E., Jeon, J.-H. & So, I. (2019): *Englerin A-sensing charged residues for transient receptor potential canonical 5 channel activation.* In: The Korean journal of physiology & pharmacology : official journal of the Korean Physiological Society and the Korean Society of Pharmacology, **23**, 3: 191–201.

Ju, M., Shi, J., Saleh, S. N., Albert, A. P. & Large, W. A. (2010): *Ins(1,4,5)P3 interacts with PIP2 to regulate activation of TRPC6/C7 channels by diacylglycerol in native vascular myocytes.* In: The Journal of physiology, **588**, Pt 9: 1419–1433.

Jung, S., Mühle, A., Schaefer, M., Strotmann, R., Schultz, G. & Plant, T. D. (2003): *Lanthanides potentiate TRPC5 currents by an action at extracellular sites close to the pore mouth.* In: The Journal of biological chemistry, **278**, 6: 3562–3571.

Junho, C. V. C., Caio-Silva, W., Trentin-Sonoda, M. & Carneiro-Ramos, M. S. (2020): *An Overview of the Role of Calcium/Calmodulin-Dependent Protein Kinase in Cardiorenal Syndrome.* In: Frontiers in physiology, **11**: 735.

Just, S., Chenard, B. L., Ceci, A., Strassmaier, T., Chong, J. A., Blair, N. T., Gallaschun, R. J., Del Camino, D., Cantin, S., D'Amours, M., Eickmeier, C., Fanger, C. M., Hecker, C., Hessler, D. P., Hengerer, B., Kroker, K. S., Malekiani, S., Mihalek, R., McLaughlin, J., Rast, G., Witek, J., Sauer, A., Pryce, C. R. & Moran, M. M. (2018): *Treatment with HC-070, a potent inhibitor of TRPC4 and TRPC5, leads to anxiolytic and antidepressant effects in mice.* In: PloS one, **13**, 1: e0191225.

Kaczmarek, J. S., Riccio, A. & Clapham, D. E. (2012): *Calpain cleaves and activates the TRPC5 channel to participate in semaphorin 3A-induced neuronal growth cone collapse.* In: Proceedings of the National Academy of Sciences, **109**, 20: 7888–7892.

Kahr, H., Schindl, R., Fritsch, R., Heinze, B., Hofbauer, M., Hack, M. E., Mörtelmaier, M. A., Groschner, K., Peng, J.-B., Takanaga, H., Hediger, M. A. & Romanin, C. (2004): *CaT1 knock-down strategies fail to affect CRAC channels in mucosal-type mast cells.* In: The Journal of physiology, **557**, Pt 1: 121–132.

Kakiuchi, S. & Yamazaki, R. (1970): *Calcium dependent phosphodiesterase activity and its activating factor (PAF) from brain.* In: Biochemical and biophysical research communications, **41**, 5: 1104–1110.

Kanki, H., Kinoshita, M., Akaike, A., Satoh, M., Mori, Y. & Kaneko, S. (2001): *Activation of inositol 1,4,5-trisphosphate receptor is essential for the opening of mouse TRP5 channels.* In: Molecular pharmacology, **60**, 5: 989–998.

Kim, B. J., Kim, M. T., Jeon, J.-H., Kim, S. J. & So, I. (2008): *Involvement of phosphatidylinositol 4,5-bisphosphate in the desensitization of canonical transient receptor potential 5.* In: Biological & pharmaceutical bulletin, **31**, 9: 1733–1738.

Kim, M. S., Zeng, W., Yuan, J. P., Shin, D. M., Worley, P. F. & Muallem, S. (2009): *Native Store-operated Ca2+ Influx Requires the Channel Function of Orai1 and TRPC1.* In: The Journal of biological chemistry, **284**, 15: 9733–9741.

Kiselyov, K., Mignery, G. A., Zhu, M. X. & Muallem, S. (1999): *The N-Terminal Domain of the IP3 Receptor Gates Store-Operated hTrp3 Channels.* In: Molecular cell, **4**, 3: 423–429.

Kiselyov, K., Xu, X., Mozhayeva, G., Kuo, T., Pessah, I., Mignery, G., Zhu, X., Birnbaumer, L. & Muallem, S. (1998): *Functional interaction between InsP3 receptors and store-operated Htrp3 channels.* In: Nature, **396**, 6710: 478–482.

Kobori, T., Smith, G. D., Sandford, R. & Edwardson, J. M. (2009): *The transient receptor potential channels TRPP2 and TRPC1 form a heterotetramer with a 2:2 stoichiometry and an alternating subunit arrangement.* In: The Journal of biological chemistry, **284**, 51: 35507–35513.

Kopec, W., Rothberg, B. S. & de Groot, B. L. (2019): *Molecular mechanism of a potassium channel gating through activation gate-selectivity filter coupling.* In: Nature communications, **10**, 1: 5366.

Köttgen, M., Buchholz, B., Garcia-Gonzalez, M. A., Kotsis, F., Fu, X., Doerken, M., Boehlke, C., Steffl, D., Tauber, R., Wegierski, T., Nitschke, R., Suzuki, M., Kramer-Zucker, A., Germino, G. G., Watnick, T., Prenen, J., Nilius, B., Kuehn, E. W. & Walz, G. (2008): *TRPP2 and TRPV4 form a polymodal sensory channel complex.* In: The Journal of cell biology, **182**, 3: 437–447.

Krause, E., Pfeiffer, F., Schmid, A. & Schulz, I. (1996): *Depletion of intracellular calcium stores activates a calcium conducting nonselective cation*

current in mouse pancreatic acinar cells. In: The Journal of biological chemistry, **271**, 51: 32523–32528.

Kricka, L. J., Cooper, M. & Ji, X. (1996): *Synthesis and characterization of 4-iodophenylboronic acid: a new enhancer for the horseradish peroxidase-catalyzed chemiluminescent oxidation of luminol.* In: Analytical biochemistry, **240**, 1: 119–125.

Kulig, W., Tynkkynen, J., Javanainen, M., Manna, M., Rog, T., Vattulainen, I. & Jungwirth, P. (2014): *How well does cholesteryl hemisuccinate mimic cholesterol in saturated phospholipid bilayers?* In: Journal of molecular modeling, **20**, 2: 2121.

Lacomblez, L., Bensimon, G., Leigh, P. N., Guillet, P., Powe, L., Durrleman, S., Delumeau, J. C. & Meininger, V. (1996): *A confirmatory dose-ranging study of riluzole in ALS. ALS/Riluzole Study Group-II.* In: Neurology, **47**, 6 Suppl 4: S242–50.

Laemmli, U. K. (1970): *Cleavage of structural proteins during the assembly of the head of bacteriophage T4.* In: Nature, **227**, 5259: 680–685.

Laskowski, R. A. & Swindells, M. B. (2011): *LigPlot+: multiple ligand-protein interaction diagrams for drug discovery.* In: Journal of chemical information and modeling, **51**, 10: 2778–2786.

Lee, K. P., Yuan, J. P., So, I., Worley, P. F. & Muallem, S. (2010): *STIM1-dependent and STIM1-independent function of transient receptor potential canonical (TRPC) channels tunes their store-operated mode.* In: The Journal of biological chemistry, **285**, 49: 38666–38673.

Lemonnier, L., Trebak, M. & Putney, J. W. (2008): *Complex regulation of the TRPC3, 6 and 7 channel subfamily by diacylglycerol and phosphatidylinositol-4,5-bisphosphate.* In: Cell calcium, **43**, 5: 506–514.

Li, S. & Hong, M. (2011): *Protonation, Tautomerization, and Rotameric Structure of Histidine: A Comprehensive Study by Magic-Angle-Spinning Solid-State NMR.* In: Journal of the American Chemical Society, **133**, 5: 1534–1544.

Liao, M., Cao, E., Julius, D. & Cheng, Y. (2013a): *Structure of the TRPV1 ion channel determined by electron cryo-microscopy.* In: Nature, **504**, 7478: 107–112.

Liao, S.-M., Du, Q.-S., Meng, J.-Z., Pang, Z.-W. & Huang, R.-B. (2013b): *The multiple roles of histidine in protein interactions.* In: Chemistry Central Journal, **7**: 44.

Lichtenegger, M., Stockner, T., Poteser, M., Schleifer, H., Platzer, D., Romanin, C. & Groschner, K. (2013): *A novel homology model of TRPC3 reveals allosteric coupling between gate and selectivity filter.* In: Cell calcium, **54**, 3: 175–185.

Lichtenegger, M., Tiapko, O., Svobodova, B., Stockner, T., Glasnov, T. N., Schreibmayer, W., Platzer, D., de La Cruz, G. G., Krenn, S.,

Schober, R., Shrestha, N., Schindl, R., Romanin, C. & Groschner, K. (2018): *An optically controlled probe identifies lipid-gating fenestrations within the TRPC3 channel.* In: Nature chemical biology, **14**, 4: 396–404.

Liou, J., Kim, M. L., Heo, W. D., Jones, J. T., Myers, J. W., Ferrell, J. E. & Meyer, T. (2005): *STIM is a Ca2+ sensor essential for Ca2+-store-depletion-triggered Ca2+ influx.* In: Current biology : CB, **15**, 13: 1235–1241.

Liu, J. & Siegelbaum, S. A. (2000): *Change of Pore Helix Conformational State upon Opening of Cyclic Nucleotide-Gated Channels.* In: Neuron, **28**, 3: 899–909.

Liu, X., Bandyopadhyay, B. C., Singh, B. B., Groschner, K. & Ambudkar, I. S. (2005): *Molecular analysis of a store-operated and 2-acetyl-sn-glycerol-sensitive non-selective cation channel. Heteromeric assembly of TRPC1-TRPC3.* In: The Journal of biological chemistry, **280**, 22: 21600–21606.

Logothetis, D. E., Petrou, V. I., Zhang, M., Mahajan, R., Meng, X.-Y., Adney, S. K., Cui, M. & Baki, L. (2015): *Phosphoinositide control of membrane protein function: a frontier led by studies on ion channels.* In: Annual review of physiology, **77**: 81–104.

Ludlow, M. J., Gaunt, H. J., Rubaiy, H. N., Musialowski, K. E., Blythe, N. M., Vasudev, N. S., Muraki, K. & Beech, D. J. (2017): *(-)-Englerin A-evoked Cytotoxicity Is Mediated by Na+ Influx and Counteracted by Na+/K+-ATPase.* In: The Journal of biological chemistry, **292**, 2: 723–731.

Luik, R. M., Wu, M. M., Buchanan, J. & Lewis, R. S. (2006): *The elementary unit of store-operated Ca2+ entry: local activation of CRAC channels by STIM1 at ER-plasma membrane junctions.* In: The Journal of cell biology, **174**, 6: 815–825.

Lux, S. E., John, K. M. & Bennett, V. (1990): *Analysis of cDNA for human erythrocyte ankyrin indicates a repeated structure with homology to tissue-differentiation and cell-cycle control proteins.* In: Nature, **344**, 6261: 36–42.

Ma, H. T., Venkatachalam, K., Li, H. S., Montell, C., Kurosaki, T., Patterson, R. L. & Gill, D. L. (2001): *Assessment of the role of the inositol 1,4,5-trisphosphate receptor in the activation of transient receptor potential channels and store-operated Ca2+ entry channels.* In: The Journal of biological chemistry, **276**, 22: 18888–18896.

Ma, X., Cai, Y., He, D., Zou, C., Zhang, P., Lo, C. Y., Xu, Z., Chan, F. L., Yu, S., Chen, Y., Zhu, R., Lei, J., Jin, J. & Yao, X. (2012): *Transient receptor potential channel TRPC5 is essential for P-glycoprotein induction in drug-resistant cancer cells.* In: Proceedings of the National Academy of Sciences, **109**, 40: 16282–16287.

Ma, X., Chen, Z., Hua, D., He, D., Wang, L., Zhang, P., Wang, J., Cai, Y., Gao, C., Zhang, X., Zhang, F., Wang, T., Hong, T., Jin, L., Qi, X., Chen, S., Gu, X., Yang, D., Pan, Q., Zhu, Y., Chen, Y., Chen, D.,

Jiang, L., Han, X., Zhang, Y., Jin, J. & Yao, X. (2014): *Essential role for TrpC5-containing extracellular vesicles in breast cancer with chemotherapeutic resistance.* In: Proceedings of the National Academy of Sciences, **111**, 17: 6389–6394.

Maier, T., Follmann, M., Hessler, G., Kleemann, H.-W., Hachtel, S., Fuchs, B., Weissmann, N., Linz, W., Schmidt, T., Löhn, M., Schroeter, K., Wang, L., Rütten, H. & Strübing, C. (2015): *Discovery and pharmacological characterization of a novel potent inhibitor of diacylglycerol-sensitive TRPC cation channels.* In: British journal of pharmacology, **172**, 14: 3650–3660.

Majeed, Y., Bahnasi, Y., Seymour, V. A. L., Wilson, L. A., Milligan, C. J., Agarwal, A. K., Sukumar, P., Naylor, J. & Beech, D. J. (2011): *Rapid and contrasting effects of rosiglitazone on transient receptor potential TRPM3 and TRPC5 channels.* In: Molecular pharmacology, **79**, 6: 1023–1030.

Makwana, K. M. & Mahalakshmi, R. (2014): *Comparative analysis of cross strand aromatic-Phe interactions in designed peptide β-hairpins.* In: Organic & biomolecular chemistry, **12**, 13: 2053–2061.

Marcotte, E. M., Pellegrini, M., Yeates, T. O. & Eisenberg, D. (1999): *A census of protein repeats.* In: Journal of molecular biology, **293**, 1: 151–160.

Marshall, C. B., Nishikawa, T., Osawa, M., Stathopulos, P. B. & Ikura, M. (2015): *Calmodulin and STIM proteins: Two major calcium sensors in the cytoplasm and endoplasmic reticulum.* In: Biochemical and biophysical research communications, **460**, 1: 5–21.

McDaniel, S. S., Platoshyn, O., Wang, J., Yu, Y., Sweeney, M., Krick, S., Rubin, L. J. & Yuan, J. X. (2001): *Capacitative Ca(2+) entry in agonist-induced pulmonary vasoconstriction.* In: American journal of physiology. Lung cellular and molecular physiology, **280**, 5: L870–80.

Miehe, S., Bieberstein, A., Arnould, I., Ihdene, O., Rütten, H. & Strübing, C. (2010): *The phospholipid-binding protein SESTD1 is a novel regulator of the transient receptor potential channels TRPC4 and TRPC5.* In: The Journal of biological chemistry, **285**, 16: 12426–12434.

Mignen, O., Thompson, J. L. & Shuttleworth, T. J. (2008): *Both Orai1 and Orai3 are essential components of the arachidonate-regulated Ca2+-selective (ARC) channels.* In: The Journal of physiology, **586**, 1: 185–195.

Miller, M., Shi, J., Zhu, Y., Kustov, M., Tian, J.-b., Stevens, A., Wu, M., Xu, J., Long, S., Yang, P., Zholos, A. V., Salovich, J. M., Weaver, C. D., Hopkins, C. R., Lindsley, C. W., McManus, O., Li, M. & Zhu, M. X. (2011): *Identification of ML204, a novel potent antagonist that selectively modulates native TRPC4/C5 ion channels.* In: The Journal of biological chemistry, **286**, 38: 33436–33446.

Minard, A., Bauer, C. C., Chuntharpursat-Bon, E., Pickles, I. B., Wright, D. J., Ludlow, M. J., Burnham, M. P., Warriner, S. L., Beech, D. J., Muraki, K. & Bon, R. S. (2019): *Potent, selective, and*

subunit-dependent activation of TRPC5 channels by a xanthine derivative. In: British journal of pharmacology, **176**, 20: 3924–3938.

Minard, A., Bauer, C. C., Wright, D. J., Rubaiy, H. N., Muraki, K., Beech, D. J. & Bon, R. S. (2018): *Remarkable Progress with Small-Molecule Modulation of TRPC1/4/5 Channels: Implications for Understanding the Channels in Health and Disease.* In: Cells, **7**, 6.

Minke, B., Wu, C. & Pak, W. L. (1975): *Induction of photoreceptor voltage noise in the dark in Drosophila mutant.* In: Nature, **258**, 5530: 84–87.

Molawi, K., Delpont, N. & Echavarren, A. M. (2010): *Enantioselective synthesis of (-)-englerins A and B.* In: Angewandte Chemie (International ed. in English), **49**, 20: 3517–3519.

Montell, C. (2005): *The TRP superfamily of cation channels.* In: Science's STKE : signal transduction knowledge environment, **2005**, 272: re3.

Morelli, M. B., Amantini, C., Liberati, S., Santoni, M. & Nabissi, M. (2013): *TRP channels: new potential therapeutic approaches in CNS neuropathies.* In: CNS & neurological disorders drug targets, **12**, 2: 274–293.

Mosavi, L. K., Cammett, T. J., Desrosiers, D. C. & Peng, Z.-Y. (2004): *The ankyrin repeat as molecular architecture for protein recognition.* In: Protein science : a publication of the Protein Society, **13**, 6: 1435–1448.

Müller, M., Niemeyer, K., Urban, N., Ojha, N. K., Zufall, F., Leinders-Zufall, T., Schaefer, M. & Thorn-Seshold, O. (2022): *BTDAzo - A Photoswitchable TRPC5 Channel Activator.* In: Angewandte Chemie (International ed. in English).

Murthy, A., Gonzalez-Agosti, C., Cordero, E., Pinney, D., Candia, C., Solomon, F., Gusella, J. & Ramesh, V. (1998): *NHE-RF, a regulatory cofactor for Na(+)-H+ exchange, is a common interactor for merlin and ERM (MERM) proteins.* In: The Journal of biological chemistry, **273**, 3: 1273–1276.

Naylor, J., Minard, A., Gaunt, H. J., Amer, M. S., Wilson, L. A., Migliore, M., Cheung, S. Y., Rubaiy, H. N., Blythe, N. M., Musialowski, K. E., Ludlow, M. J., Evans, W. D., Green, B. L., Yang, H., You, Y., Li, J., Fishwick, C. W. G., Muraki, K., Beech, D. J. & Bon, R. S. (2016): *Natural and synthetic flavonoid modulation of TRPC5 channels.* In: British journal of pharmacology, **173**, 3: 562–574.

Nicolaou, K. C., Kang, Q., Ng, S. Y. & Chen, D. Y.-K. (2010): *Total synthesis of englerin A.* In: Journal of the American Chemical Society, **132**, 23: 8219–8222.

Nilius, B. & Owsianik, G. (2011): *The transient receptor potential family of ion channels.* In: Genome biology, **12**, 3: 218.

Ningoo, M., Plant, L. D., Greka, A. & Logothetis, D. E. (2021): *PIP2 regulation of TRPC5 channel activation and desensitization.* In: The Journal of biological chemistry, 100726.

Obukhov, A. G. & Nowycky, M. C. (2004): *TRPC5 activation kinetics are modulated by the scaffolding protein ezrin/radixin/moesin-binding phosphoprotein-50 (EBP50).* In: Journal of cellular physiology, **201**, 2: 227–235.

Okada, T., Shimizu, S., Wakamori, M., Maeda, A., Kurosaki, T., Takada, N., Imoto, K. & Mori, Y. (1998): *Molecular cloning and functional characterization of a novel receptor-activated TRP Ca2+ channel from mouse brain.* In: The Journal of biological chemistry, **273**, 17: 10279–10287.

Otsuguro, K.-i., Tang, J., Tang, Y., Xiao, R., Freichel, M., Tsvilovskyy, V., Ito, S., Flockerzi, V., Zhu, M. X. & Zholos, A. V. (2008): *Isoform-specific inhibition of TRPC4 channel by phosphatidylinositol 4,5-bisphosphate.* In: The Journal of biological chemistry, **283**, 15: 10026–10036.

Pettersen, E. F., Goddard, T. D., Huang, C. C., Couch, G. S., Greenblatt, D. M., Meng, E. C. & Ferrin, T. E. (2004): *UCSF Chimera–a visualization system for exploratory research and analysis.* In: Journal of computational chemistry, **25**, 13: 1605–1612.

Phelan, K. D., Shwe, U. T., Abramowitz, J., Wu, H., Rhee, S. W., Howell, M. D., Gottschall, P. E., Freichel, M., Flockerzi, V., Birnbaumer, L. & Zheng, F. (2013): *Canonical transient receptor channel 5 (TRPC5) and TRPC1/4 contribute to seizure and excitotoxicity by distinct cellular mechanisms.* In: Molecular pharmacology, **83**, 2: 429–438.

Philipp, S., Cavalié, A., Freichel, M., Wissenbach, U., Zimmer, S., Trost, C., Marquart, A., Murakami, M. & Flockerzi, V. (1996): *A mammalian capacitative calcium entry channel homologous to Drosophila TRP and TRPL.* In: The EMBO Journal, **15**, 22: 6166–6171.

Philipp, S., Hambrecht, J., Braslavski, L., Schroth, G., Freichel, M., Murakami, M., Cavalié, A. & Flockerzi, V. (1998): *A novel capacitative calcium entry channel expressed in excitable cells.* In: The EMBO Journal, **17**, 15: 4274–4282.

Plant, T. D. & Schaefer, M. (2005): *Receptor-operated cation channels formed by TRPC4 and TRPC5.* In: Naunyn-Schmiedeberg's archives of pharmacology, **371**, 4: 266–276.

Polat, O. K., Isaeva, E., Zhu, K., Noben, M., Sudhini, Y., Samelko, B., Kumar, V. S., Wei, C., Altintas, M. M., Dryer, S. E., Sever, S., Staruschenko, A. & Reiser, J. (2021): *Evaluation of podocyte Rac-1 induced kidney disease by modulation of TRPC5.*

Poteser, M., Graziani, A., Rosker, C., Eder, P., Derler, I., Kahr, H., Zhu, M. X., Romanin, C. & Groschner, K. (2006): *TRPC3 and TRPC4 associate to form a redox-sensitive cation channel. Evidence for expression of native TRPC3-TRPC4 heteromeric channels in endothelial cells.* In: The Journal of biological chemistry, **281**, 19: 13588–13595.

Puram, S. V., Riccio, A., Koirala, S., Ikeuchi, Y., Kim, A. H., Corfas, G. & Bonni, A. (2011): *A TRPC5-regulated calcium signaling pathway controls dendrite patterning in the mammalian brain.* In: Genes & development, **25**, 24: 2659–2673.

Putney, J. W. (1986): *A model for receptor-regulated calcium entry.* In: Cell calcium, **7**, 1: 1–12.

Radtke, L., Willot, M., Sun, H., Ziegler, S., Sauerland, S., Strohmann, C., Fröhlich, R., Habenberger, P., Waldmann, H. & Christmann, M. (2011): *Total synthesis and biological evaluation of (-)-englerin A and B: synthesis of analogues with improved activity profile.* In: Angewandte Chemie (International ed. in English), **50**, 17: 3998–4002.

Ratnayake, R., Covell, D., Ransom, T. T., Gustafson, K. R. & Beutler, J. A. (2009): *Englerin A, a selective inhibitor of renal cancer cell growth, from Phyllanthus engleri.* In: Organic letters, **11**, 1: 57–60.

Riccio, A., Li, Y., Moon, J., Kim, K.-S., Smith, K. S., Rudolph, U., Gapon, S., Yao, G. L., Tsvetkov, E., Rodig, S. J., Van't Veer, A., Meloni, E. G., Carlezon, W. A., Bolshakov, V. Y. & Clapham, D. E. (2009): *Essential role for TRPC5 in amygdala function and fear-related behavior.* In: Cell, **137**, 4: 761–772.

Riccio, A., Li, Y., Tsvetkov, E., Gapon, S., Yao, G. L., Smith, K. S., Engin, E., Rudolph, U., Bolshakov, V. Y. & Clapham, D. E. (2014): *Decreased anxiety-like behavior and Gαq/11-dependent responses in the amygdala of mice lacking TRPC4 channels.* In: The Journal of neuroscience : the official journal of the Society for Neuroscience, **34**, 10: 3653–3667.

Riccio, A., Mattei, C., Kelsell, R. E., Medhurst, A. D., Calver, A. R., Randall, A. D., Davis, J. B., Benham, C. D. & Pangalos, M. N. (2002): *Cloning and functional expression of human short TRP7, a candidate protein for store-operated Ca2+ influx.* In: The Journal of biological chemistry, **277**, 14: 12302–12309.

Richter, J. M., Schaefer, M. & Hill, K. (2014a): *Clemizole hydrochloride is a novel and potent inhibitor of transient receptor potential channel TRPC5.* In: Molecular pharmacology, **86**, 5: 514–521.

Richter, J. M., Schaefer, M. & Hill, K. (2014b): *Riluzole activates TRPC5 channels independently of PLC activity.* In: British journal of pharmacology, **171**, 1: 158–170.

Rodrigues, T., Sieglitz, F., Somovilla, V. J., Cal, P. M. S. D., Galione, A., Corzana, F. & Bernardes, G. J. L. (2016): *Unveiling (-)-Englerin A as a Modulator of L-Type Calcium Channels.* In: Angewandte Chemie (International ed. in English), **55**, 37: 11077–11081.

Rohacs, T. (2009): *Phosphoinositide regulation of non-canonical transient receptor potential channels.* In: Cell calcium, **45**, 6: 554–565.

Rohács, T., Lopes, C. M. B., Michailidis, I. & Logothetis, D. E. (2005): *PI(4,5)P2 regulates the activation and desensitization of TRPM8 channels through the TRP domain.* In: Nature neuroscience, **8**, 5: 626–634.

Roos, J., DiGregorio, P. J., Yeromin, A. V., Ohlsen, K., Lioudyno, M., Zhang, S., Safrina, O., Kozak, J. A., Wagner, S. L., Cahalan, M. D., Veliçelebi, G. & Stauderman, K. A. (2005): *STIM1, an essential and conserved component of store-operated Ca2+ channel function.* In: The Journal of cell biology, **169**, 3: 435–445.

Rubaiy, H. N., Ludlow, M. J., Henrot, M., Gaunt, H. J., Miteva, K., Cheung, S. Y., Tanahashi, Y., Hamzah, N., Musialowski, K. E., Blythe, N. M., Appleby, H. L., Bailey, M. A., McKeown, L., Taylor, R., Foster, R., Waldmann, H., Nussbaumer, P., Christmann, M., Bon, R. S., Muraki, K. & Beech, D. J. (2017): *Picomolar, selective, and subtype-specific small-molecule inhibition of TRPC1/4/5 channels.* In: The Journal of biological chemistry, **292**, 20: 8158–8173.

Rubaiy, H. N., Ludlow, M. J., Siems, K., Norman, K., Foster, R., Wolf, D., Beutler, J. A. & Beech, D. J. (2018a): *Tonantzitlolone is a nanomolar potency activator of transient receptor potential canonical 1/4/5 channels.* In: British journal of pharmacology, **175**, 16: 3361–3368.

Rubaiy, H. N., Seitz, T., Hahn, S., Choidas, A., Habenberger, P., Klebl, B., Dinkel, K., Nussbaumer, P., Waldmann, H., Christmann, M. & Beech, D. J. (2018b): *Identification of an (-)-englerin A analogue, which antagonizes (-)-englerin A at TRPC1/4/5 channels.* In: British journal of pharmacology, **175**, 5: 830–839.

Saarikangas, J., Zhao, H. & Lappalainen, P. (2010): *Regulation of the actin cytoskeleton-plasma membrane interplay by phosphoinositides.* In: Physiological reviews, **90**, 1: 259–289.

Salas, M. M., Hargreaves, K. M. & Akopian, A. N. (2009): *TRPA1-mediated responses in trigeminal sensory neurons: interaction between TRPA1 and TRPV1.* In: The European journal of neuroscience, **29**, 8: 1568–1578.

Sauguet, L., Shahsavar, A. & Delarue, M. (2015): *Crystallographic studies of pharmacological sites in pentameric ligand-gated ion channels.* In: Biochimica et biophysica acta, **1850**, 3: 511–523.

Schaefer, M. (2005): *Homo- and heteromeric assembly of TRP channel subunits.* In: Pflugers Archiv : European journal of physiology, **451**, 1: 35–42.

Schaefer, M., Plant, T. D., Obukhov, A. G., Hofmann, T., Gudermann, T. & Schultz, G. (2000): *Receptor-mediated regulation of the nonselective cation channels TRPC4 and TRPC5.* In: The Journal of biological chemistry, **275**, 23: 17517–17526.

Schaldecker, T., Kim, S., Tarabanis, C., Tian, D., Hakroush, S., Castonguay, P., Ahn, W., Wallentin, H., Heid, H., Hopkins, C. R., Lindsley, C. W., Riccio, A., Buvall, L., Weins, A. & Greka, A. (2013): *Inhibition of the TRPC5 ion channel protects the kidney filter.* In: The Journal of clinical investigation, **123**, 12: 5298–5309.

Schewe, M., Sun, H., Mert, Ü., Mackenzie, A., Pike, A. C. W., Schulz, F., Constantin, C., Vowinkel, K. S., Conrad, L. J., Kiper, A. K., Gonzalez, W., Musinszki, M., Tegtmeier, M., Pryde, D. C., Belabed, H., Nazare, M., de Groot, B. L., Decher, N., Fakler, B., Carpenter, E. P., Tucker, S. J. & Baukrowitz, T. (2019): *A pharmacological master key mechanism that unlocks the selectivity filter gate in K+ channels.* In: Science (New York, N.Y.), **363**, 6429: 875–880.

Schindl, R., Frischauf, I., Kahr, H., Fritsch, R., Krenn, M., Derndl, A., Vales, E., Muik, M., Derler, I., Groschner, K. & Romanin, C. (2008): *The first ankyrin-like repeat is the minimum indispensable key structure for functional assembly of homo- and heteromeric TRPC4/TRPC5 channels.* In: Cell calcium, **43**, 3: 260–269.

Semtner, M., Schaefer, M., Pinkenburg, O. & Plant, T. D. (2007): *Potentiation of TRPC5 by protons.* In: The Journal of biological chemistry, **282**, 46: 33868–33878.

Sharma, S. H., Pablo, J. L., Montesinos, M. S., Greka, A. & Hopkins, C. R. (2019): *Design, synthesis and characterization of novel N-heterocyclic-1-benzyl-1H-benzodimidazole-2-amines as selective TRPC5 inhibitors leading to the identification of the selective compound, AC1903.* In: Bioorganic & medicinal chemistry letters, **29**, 2: 155–159.

Shewan, A., Eastburn, D. J. & Mostov, K. (2011): *Phosphoinositides in cell architecture.* In: Cold Spring Harbor perspectives in biology, **3**, 8: a004796.

Shi, J., Ju, M., Abramowitz, J., Large, W. A., Birnbaumer, L. & Albert, A. P. (2012): *TRPC1 proteins confer PKC and phosphoinositol activation on native heteromeric TRPC1/C5 channels in vascular smooth muscle: comparative study of wild-type and TRPC1-/- mice.* In: FASEB journal : official publication of the Federation of American Societies for Experimental Biology, **26**, 1: 409–419.

Shi, J., Miralles, F., Birnbaumer, L., Large, W. A. & Albert, A. P. (2016): *Store depletion induces Gaq-mediated PLCβ1 activity to stimulate TRPC1 channels in vascular smooth muscle cells.* In: FASEB journal : official publication of the Federation of American Societies for Experimental Biology, **30**, 2: 702–715.

Shi, J., Miralles, F., Kinet, J.-P., Birnbaumer, L., Large, W. A. & Albert, A. P. (2017): *Evidence that Orai1 does not contribute to store-operated TRPC1 channels in vascular smooth muscle cells.* In: Channels (Austin, Tex.), **11**, 4: 329–339.

Shibata, S., Nagase, M., Yoshida, S., Kawarazaki, W., Kurihara, H., Tanaka, H., Miyoshi, J., Takai, Y. & Fujita, T. (2008): *Modification of mineralocorticoid receptor function by Rac1 GTPase: implication in proteinuric kidney disease.* In: Nature medicine, **14**, 12: 1370–1376.

Shoemaker, R. H. (2006): *The NCI60 human tumour cell line anticancer drug screen.* In: Nature reviews. Cancer, **6**, 10: 813–823.

Smani, T., Domínguez-Rodriguez, A., Callejo-García, P., Rosado, J. A. & Avila-Medina, J. (2016): *Phospholipase A2 as a Molecular Determinant of Store-Operated Calcium Entry.* In: Advances in experimental medicine and biology, **898**: 111–131.

Song, K., Wei, M., Guo, W., Quan, L., Kang, Y., Wu, J.-X. & Chen, L. (2021): *Structural basis for human TRPC5 channel inhibition by two distinct inhibitors.* In: eLife, **10**.

Sourbier, C., Scroggins, B. T., Ratnayake, R., Prince, T. L., Lee, S., Lee, M.-J., Nagy, P. L., Lee, Y. H., Trepel, J. B., Beutler, J. A., Linehan, W. M. & Neckers, L. (2013): *Englerin A stimulates PKCθto inhibit insulin signaling and to simultaneously activate HSF1: pharmacologically induced synthetic lethality.* In: Cancer cell, **23**, 2: 228–237.

Spurny, R., Ramerstorfer, J., Price, K., Brams, M., Ernst, M., Nury, H., Verheij, M., Legrand, P., Bertrand, D., Bertrand, S., Dougherty, D. A., de Esch, I. J. P., Corringer, P.-J., Sieghart, W., Lummis, S. C. R. & Ulens, C. (2012): *Pentameric ligand-gated ion channel ELIC is activated by GABA and modulated by benzodiazepines.* In: Proceedings of the National Academy of Sciences, **109**, 44: E3028–34.

Stanzione, R., Forte, M., Cotugno, M., Bianchi, F., Marchitti, S. & Rubattu, S. (2022): *Relevance of stromal interaction molecule 1 (STIM1) in experimental and human stroke.* In: Pflugers Archiv : European journal of physiology, **474**, 1: 141–153.

Stewart, A. P., Smith, G. D., Sandford, R. N. & Edwardson, J. M. (2010): *Atomic force microscopy reveals the alternating subunit arrangement of the TRPP2-TRPV4 heterotetramer.* In: Biophysical journal, **99**, 3: 790–797.

Storch, U., Forst, A.-L., Pardatscher, F., Erdogmus, S., Philipp, M., Gregoritza, M., Mederos Y Schnitzler, M. & Gudermann, T. (2017): *Dynamic NHERF interaction with TRPC4/5 proteins is required for channel gating by diacylglycerol.* In: Proceedings of the National Academy of Sciences of the United States of America, **114**, 1: E37–E46.

Storch, U., Forst, A.-L., Philipp, M., Gudermann, T. & Mederos Y Schnitzler, M. (2012): *Transient receptor potential channel 1 (TRPC1) reduces calcium permeability in heteromeric channel complexes.* In: The Journal of biological chemistry, **287**, 5: 3530–3540.

Strübing, C., Krapivinsky, G., Krapivinsky, L. & Clapham, D. E. (2001): *TRPC1 and TRPC5 Form a Novel Cation Channel in Mammalian Brain.* In: Neuron, **29**, 3: 645–655.

Strübing, C., Krapivinsky, G., Krapivinsky, L. & Clapham, D. E. (2003): *Formation of novel TRPC channels by complex subunit interactions in embryonic brain.* In: The Journal of biological chemistry, **278**, 40: 39014–39019.

Sunggip, C., Shimoda, K., Oda, S., Tanaka, T., Nishiyama, K., Mangmool, S., Nishimura, A., Numaga-Tomita, T. & Nishida, M. (2018): *TRPC5-eNOS Axis Negatively Regulates ATP-Induced Cardiomyocyte Hypertrophy.* In: Frontiers in pharmacology, **9**: 523.

Tang, J., Lin, Y., Zhang, Z., Tikunova, S., Birnbaumer, L. & Zhu, M. X. (2001): *Identification of common binding sites for calmodulin and inositol 1,4,5-trisphosphate receptors on the carboxyl termini of trp channels.* In: The Journal of biological chemistry, **276**, 24: 21303–21310.

Tang, Q., Guo, W., Zheng, L., Wu, J.-X., Liu, M., Zhou, X., Zhang, X. & Chen, L. (2018): *Structure of the receptor-activated human TRPC6 and TRPC3 ion channels.* In: Cell research, **28**, 7: 746–755.

Tang, Y., Tang, J., Chen, Z., Trost, C., Flockerzi, V., Li, M., Ramesh, V. & Zhu, M. X. (2000): *Association of mammalian trp4 and phospholipase C isozymes with a PDZ domain-containing protein, NHERF.* In: The Journal of biological chemistry, **275**, 48: 37559–37564.

Tao, X., Lee, A., Limapichat, W., Dougherty, D. A. & MacKinnon, R. (2010): *A gating charge transfer center in voltage sensors.* In: Science (New York, N.Y.), **328**, 5974: 67–73.

Terawaki, S.-i., Maesaki, R. & Hakoshima, T. (2006): *Structural basis for NHERF recognition by ERM proteins.* In: Structure (London, England : 1993), **14**, 4: 777–789.

Thakur, D. P., Tian, J.-b., Jeon, J., Xiong, J., Huang, Y., Flockerzi, V. & Zhu, M. X. (2016): *Critical roles of Gi/o proteins and phospholipase C-δ1 in the activation of receptor-operated TRPC4 channels.* In: Proceedings of the National Academy of Sciences, **113**, 4: 1092–1097.

Thompson, J. L., Mignen, O. & Shuttleworth, T. J. (2013): *The ARC channel–an endogenous store-independent Orai channel.* In: Current topics in membranes, **71**: 125–148.

Tian, D., Jacobo, S. M. P., Billing, D., Rozkalne, A., Gage, S. D., Anagnostou, T., Pavenstädt, H., Pavenstaedt, H., Hsu, H.-H., Schlondorff, J., Ramos, A. & Greka, A. (2010): *Antagonistic regulation of actin dynamics and cell motility by TRPC5 and TRPC6 channels.* In: Science signaling, **3**, 145: ra77.

Traynor, B. J., Alexander, M., Corr, B., Frost, E. & Hardiman, O. (2003): *An outcome study of riluzole in amyotrophic lateral sclerosis–a population-based study in Ireland, 1996-2000.* In: Journal of neurology, **250**, 4: 473–479.

Trebak, M., Lemonnier, L., DeHaven, W. I., Wedel, B. J., Bird, G. S. & Putney, J. W. (2009): *Complex functions of phosphatidylinositol 4,5-bisphosphate in regulation of TRPC5 cation channels.* In: Pflugers Archiv : European journal of physiology, **457**, 4: 757–769.

Trott, O. & Olson, A. J. (2010): *AutoDock Vina: improving the speed and accuracy of docking with a new scoring function, efficient optimization, and multithreading.* In: Journal of computational chemistry, **31**, 2: 455–461.

Uhlén, M., Björling, E., Agaton, C., Szigyarto, C. A.-K., Amini, B., Andersen, E., Andersson, A.-C., Angelidou, P., Asplund, A., Asplund, C., Berglund, L., Bergström, K., Brumer, H., Cerjan, D., Ekström, M., Elobeid, A., Eriksson, C., Fagerberg, L., Falk, R., Fall, J., Forsberg, M., Björklund, M. G., Gumbel, K., Halimi, A., Hallin, I., Hamsten, C., Hansson, M., Hedhammar, M., Hercules, G., Kampf, C., Larsson, K., Lindskog, M., Lodewyckx, W., Lund, J., Lundeberg, J., Magnusson, K., Malm, E., Nilsson, P., Odling, J., Oksvold, P., Olsson, I., Oster, E., Ottosson, J., Paavilainen, L., Persson, A., Rimini, R., Rockberg, J., Runeson, M., Sivertsson, A., Sköllermo, A., Steen, J., Stenvall, M., Sterky, F., Strömberg, S., Sundberg, M., Tegel, H., Tourle, S., Wahlund, E., Waldén, A., Wan, J., Wernérus, H., Westberg, J., Wester, K., Wrethagen, U., Xu, L. L., Hober, S. & Pontén, F. (2005): *A human protein atlas for normal and cancer tissues based on antibody proteomics.* In: Molecular & cellular proteomics : MCP, **4**, 12: 1920–1932.

Uhlén, M., Fagerberg, L., Hallström, B. M., Lindskog, C., Oksvold, P., Mardinoglu, A., Sivertsson, Å., Kampf, C., Sjöstedt, E., Asplund, A., Olsson, I., Edlund, K., Lundberg, E., Navani, S., Szigyarto, C. A.-K., Odeberg, J., Djureinovic, D., Takanen, J. O., Hober, S., Alm, T., Edqvist, P.-H., Berling, H., Tegel, H., Mulder, J., Rockberg, J., Nilsson, P., Schwenk, J. M., Hamsten, M., von Feilitzen, K., Forsberg, M., Persson, L., Johansson, F., Zwahlen, M., von Heijne, G., Nielsen, J. & Pontén, F. (2015): *Proteomics. Tissue-based map of the human proteome.* In: Science (New York, N.Y.), **347**, 6220: 1260419.

Vaca, L. & Kunze, D. L. (1994): *Depletion of intracellular Ca2+ stores activates a Ca(2+)-selective channel in vascular endothelium.* In: The American journal of physiology, **267**, 4 Pt 1: C920–5.

Valente, P., García-Sanz, N., Gomis, A., Fernández-Carvajal, A., Fernández-Ballester, G., Viana, F., Belmonte, C. & Ferrer-Montiel, A. (2008): *Identification of molecular determinants of channel gating in the transient receptor potential box of vanilloid receptor I.* In: FASEB journal : official publication of the Federation of American Societies for Experimental Biology, **22**, 9: 3298–3309.

Vannier, B., Peyton, M., Boulay, G., Brown, D., Qin, N., Jiang, M., Zhu, X. & Birnbaumer, L. (1999): *Mouse trp2, the homologue of the human trpc2 pseudogene, encodes mTrp2, a store depletion-activated capacitative Ca2+ entry channel.* In: Proceedings of the National Academy of Sciences, **96**, 5: 2060–2064.

Vazquez, G., Lievremont, J. P., St J Bird, G. & Putney, J. W. (2001): *Human Trp3 forms both inositol trisphosphate receptor-dependent and receptor-*

independent store-operated cation channels in DT40 avian B lymphocytes. In: Proceedings of the National Academy of Sciences, **98**, 20: 11777–11782.

Venkatachalam, K., Ma, H. T., Ford, D. L. & Gill, D. L. (2001): *Expression of functional receptor-coupled TRPC3 channels in DT40 triple receptor InsP3 knockout cells.* In: The Journal of biological chemistry, **276**, 36: 33980–33985.

Venkatachalam, K. & Montell, C. (2007): *TRP channels.* In: Annual review of biochemistry, **76**: 387–417.

Venkatachalam, K., Zheng, F. & Gill, D. L. (2003): *Regulation of canonical transient receptor potential (TRPC) channel function by diacylglycerol and protein kinase C.* In: The Journal of biological chemistry, **278**, 31: 29031–29040.

Verkhratsky, A. & Parpura, V. (2014): *Store-operated calcium entry in neuroglia.* In: Neuroscience bulletin, **30**, 1: 125–133.

Vig, M., Beck, A., Billingsley, J. M., Lis, A., Parvez, S., Peinelt, C., Koomoa, D. L., Soboloff, J., Gill, D. L., Fleig, A., Kinet, J.-P. & Penner, R. (2006): *CRACM1 multimers form the ion-selective pore of the CRAC channel.* In: Current biology : CB, **16**, 20: 2073–2079.

Vinayagam, D., Mager, T., Apelbaum, A., Bothe, A., Merino, F., Hofnagel, O., Gatsogiannis, C. & Raunser, S. (2018): *Electron cryomicroscopy structure of the canonical TRPC4 ion channel.* In: eLife, **7**.

Vinayagam, D., Quentin, D., Yu-Strzelczyk, J., Sitsel, O., Merino, F., Stabrin, M., Hofnagel, O., Yu, M., Ledeboer, M. W., Nagel, G., Malojcic, G. & Raunser, S. (2020): *Structural basis of TRPC4 regulation by calmodulin and pharmacological agents.* In: eLife, **9**.

Walker, R. L., Hume, J. R. & Horowitz, B. (2001): *Differential expression and alternative splicing of TRP channel genes in smooth muscles.* In: American journal of physiology. Cell physiology, **280**, 5: C1184–92.

Wallace, A. C., Laskowski, R. A. & Thornton, J. M. (1995): *LIGPLOT: a program to generate schematic diagrams of protein-ligand interactions.* In: Protein engineering, **8**, 2: 127–134.

Walsh, L., Reilly, J. F., Cornwall, C., Gaich, G. A., Gipson, D. S., Heerspink, H. J. L., Johnson, L., Trachtman, H., Tuttle, K. R., Farag, Y. M. K., Padmanabhan, K., Pan-Zhou, X.-R., Woodworth, J. R. & Czerwiec, F. S. (2021): *Safety and Efficacy of GFB-887, a TRPC5 Channel Inhibitor, in Patients With Focal Segmental Glomerulosclerosis, Treatment-Resistant Minimal Change Disease, or Diabetic Nephropathy: TRACTION-2 Trial Design.* In: Kidney international reports, **6**, 10: 2575–2584.

Wang, M., Ji, S., Shao, G., Zhang, J., Zhao, K., Wang, Z. & Wu, A. (2018a): *Effect of exosome biomarkers for diagnosis and prognosis of breast cancer patients.* In: Clinical & translational oncology : official publication

of the Federation of Spanish Oncology Societies and of the National Cancer Institute of Mexico, **20**, 7: 906–911.

Wang, T., Chen, Z., Zhu, Y., Pan, Q., Liu, Y., Qi, X., Jin, L., Jin, J., Ma, X. & Hua, D. (2015): *Inhibition of transient receptor potential channel 5 reverses 5-Fluorouracil resistance in human colorectal cancer cells.* In: The Journal of biological chemistry, **290**, 1: 448–456.

Wang, T., Ning, K., Lu, T.-X., Sun, X., Jin, L., Qi, X., Jin, J. & Hua, D. (2017): *Increasing circulating exosomes-carrying TRPC5 predicts chemoresistance in metastatic breast cancer patients.* In: Cancer Science, **108**, 3: 448–454.

Wang, X., Dande, R. R., Yu, H., Samelko, B., Miller, R. E., Altintas, M. M. & Reiser, J. (2018b): *TRPC5 Does Not Cause or Aggravate Glomerular Disease.* In: Journal of the American Society of Nephrology : JASN, **29**, 2: 409–415.

Wen, W., Yao, Q., Chen, Y., Li, Z., Maitikuerban, B., Zhang, Y., Zhang, J., Simayi, Z., Xu, X. & Zhang, X. (2020): *Transient receptor potential canonical 5 channel is involved in the cardiac damage related to obstructive sleep apnea-hypopnea syndrome in rats.* In: Annals of palliative medicine, **9**, 3: 895–902.

Wes, P. D., Chevesich, J., Jeromin, A., Rosenberg, C., Stetten, G. & Montell, C. (1995): *TRPC1, a human homolog of a Drosophila store-operated channel.* In: Proceedings of the National Academy of Sciences, **92**, 21: 9652–9656.

Wildeman, A. G. (1988): *Regulation of SV40 early gene expression.* In: Biochemistry and Cell Biology, **66**, 6: 567–577.

Willot, M., Radtke, L., Könning, D., Fröhlich, R., Gessner, V. H., Strohmann, C. & Christmann, M. (2009): *Total synthesis and absolute configuration of the guaiane sesquiterpene englerin A.* In: Angewandte Chemie (International ed. in English), **48**, 48: 9105–9108.

Wong, C.-O., Huang, Y. & Yao, X. (2010): *Genistein potentiates activity of the cation channel TRPC5 independently of tyrosine kinases.* In: British journal of pharmacology, **159**, 7: 1486–1496.

Wong, F., Hokanson, K. M. & Chang, L. T. (1985): *Molecular basis of an inherited retinal defect in Drosophila.* In: Investigative ophthalmology & visual science, **26**, 2: 243–246.

Wright, D. J., Simmons, K. J., Johnson, R. M., Beech, D. J., Muench, S. P. & Bon, R. S. (2020): *Human TRPC5 structures reveal interaction of a xanthine-based TRPC1/4/5 inhibitor with a conserved lipid binding site.* In: Communications biology, **3**, 1: 704.

Wu, Z., Zhao, S., Fash, D. M., Li, Z., Chain, W. J. & Beutler, J. A. (2017): *Englerins: A Comprehensive Review.* In: Journal of natural products, **80**, 3: 771–781.

Xu, S. Z. & Beech, D. J. (2001): *TrpC1 is a membrane-spanning subunit of store-operated Ca(2+) channels in native vascular smooth muscle cells.* In: Circulation research, **88**, 1: 84–87.

Yang, F., Xiao, X., Cheng, W., Yang, W., Yu, P., Song, Z., Yarov-Yarovoy, V. & Zheng, J. (2015a): *Structural mechanism underlying capsaicin binding and activation of the TRPV1 ion channel.* In: Nature chemical biology, **11**, 7: 518–524.

Yang, L.-P., Jiang, F.-J., Wu, G.-S., Deng, K., Wen, M., Zhou, X., Hong, X., Zhu, M. X. & Luo, H.-R. (2015b): *Acute Treatment with a Novel TRPC4/C5 Channel Inhibitor Produces Antidepressant and Anxiolytic-Like Effects in Mice.* In: PloS one, **10**, 8: e0136255.

Yang, Y., Wei, M. & Chen, L. (2022): *Structural identification of riluzole-binding site on human TRPC5.* In: Cell discovery, **8**, 1: 67.

Yeromin, A. V., Zhang, S. L., Jiang, W., Yu, Y., Safrina, O. & Cahalan, M. D. (2006): *Molecular identification of the CRAC channel by altered ion selectivity in a mutant of Orai.* In: Nature, **443**, 7108: 226–229.

Yin, Y., Le, S. C., Hsu, A. L., Borgnia, M. J., Yang, H. & Lee, S.-Y. (2019): *Structural basis of cooling agent and lipid sensing by the cold-activated TRPM8 channel.* In: Science (New York, N.Y.), **363**, 6430.

Yin, Y., Wu, M., Zubcevic, L., Borschel, W. F., Lander, G. C. & Lee, S.-Y. (2018): *Structure of the cold- and menthol-sensing ion channel TRPM8.* In: Science (New York, N.Y.), **359**, 6372: 237–241.

Yip, H., Chan, W.-Y., Leung, P.-C., Kwan, H.-Y., Liu, C., Huang, Y., Michel, V., Yew, D. T.-W. & Yao, X. (2004): *Expression of TRPC homologs in endothelial cells and smooth muscle layers of human arteries.* In: Histochemistry and cell biology, **122**, 6: 553–561.

Yip, K. M., Fischer, N., Paknia, E., Chari, A. & Stark, H. (2020): *Atomic-resolution protein structure determination by cryo-EM.* In: Nature, **587**, 7832: 157–161. URL `https://www.nature.com/articles/s41586-020-2833-4`.

Yoshida, T., Inoue, R., Morii, T., Takahashi, N., Yamamoto, S., Hara, Y., Tominaga, M., Shimizu, S., Sato, Y. & Mori, Y. (2006): *Nitric oxide activates TRP channels by cysteine S-nitrosylation.* In: Nature chemical biology, **2**, 11: 596–607.

Yu, H., Suleiman, H., Kim, A. H. J., Miner, J. H., Dani, A., Shaw, A. S. & Akilesh, S. (2013): *Rac1 activation in podocytes induces rapid foot process effacement and proteinuria.* In: Molecular and Cellular Biology, **33**, 23: 4755–4764.

Yu, M., Ledeboer, M. W., Daniels, M., Malojcic, G., Tibbitts, T. T., Coeffet-Le Gal, M., Pan-Zhou, X.-R., Westerling-Bui, A., Beconi, M., Reilly, J. F., Mundel, P. & Harmange, J.-C. (2019): *Discovery of a Potent and Selective TRPC5 Inhibitor, Efficacious in a Focal Segmental*

Glomerulosclerosis Model. In: ACS medicinal chemistry letters, **10**, 11: 1579–1585.

Yuan, J. P., Kiselyov, K., Shin, D. M., Chen, J., Shcheynikov, N., Kang, S. H., Dehoff, M. H., Schwarz, M. K., Seeburg, P. H., Muallem, S. & Worley, P. F. (2003): *Homer Binds TRPC Family Channels and Is Required for Gating of TRPC1 by IP3 Receptors.* In: Cell, **114**, 6: 777–789.

Yun, C. H., Lamprecht, G., Forster, D. V. & Sidor, A. (1998): *NHE3 kinase A regulatory protein E3KARP binds the epithelial brush border Na+/H+ exchanger NHE3 and the cytoskeletal protein ezrin.* In: The Journal of biological chemistry, **273**, 40: 25856–25863.

Zakharian, E. (2019): *TRP Channel Reconstitution in Lipid Bilayers.* In: Methods in molecular biology (Clifton, N.J.), **1987**: 143–166.

Zakharian, E., Cao, C. & Rohacs, T. (2010): *Gating of transient receptor potential melastatin 8 (TRPM8) channels activated by cold and chemical agonists in planar lipid bilayers.* In: The Journal of neuroscience : the official journal of the Society for Neuroscience, **30**, 37: 12526–12534.

Zakharian, E., Thyagarajan, B., French, R. J., Pavlov, E. & Rohacs, T. (2009): *Inorganic polyphosphate modulates TRPM8 channels.* In: PloS one, **4**, 4: e5404.

Zeng, W., Yuan, J. P., Kim, M. S., Choi, Y. J., Huang, G. N., Worley, P. F. & Muallem, S. (2008): *STIM1 gates TRPC channels, but not Orai1, by electrostatic interaction.* In: Molecular cell, **32**, 3: 439–448.

Zergane, M., Kuebler, W. M. & Michalick, L. (2021): *Heteromeric TRP Channels in Lung Inflammation.* In: Cells, **10**, 7.

Zhang, P., Liu, X., Li, H., Chen, Z., Yao, X., Jin, J. & Ma, X. (2017): *TRPC5-induced autophagy promotes drug resistance in breast carcinoma via CaMKKβ/AMPKa/mTOR pathway.* In: Scientific reports, **7**, 1: 3158.

Zhang, Z., Tang, J., Tikunova, S., Johnson, J. D., Chen, Z., Qin, N., Dietrich, A., Stefani, E., Birnbaumer, L. & Zhu, M. X. (2001): *Activation of Trp3 by inositol 1,4,5-trisphosphate receptors through displacement of inhibitory calmodulin from a common binding domain.* In: Proceedings of the National Academy of Sciences, **98**, 6: 3168–3173.

Zhang, Z., Tóth, B., Szollosi, A., Chen, J. & Csanády, L. (2018): *Structure of a TRPM2 channel in complex with Ca2+ explains unique gating regulation.* In: eLife, **7**.

Zhen, X.-G., Xie, C., Fitzmaurice, A., Schoonover, C. E., Orenstein, E. T. & Yang, J. (2005): *Functional architecture of the inner pore of a voltage-gated Ca2+ channel.* In: The Journal of general physiology, **126**, 3: 193–204.

Zholos, A. V. (2014): *TRPC5.* In: Handbook of experimental pharmacology, **222**: 129–156.

Zhou, Q., Chen, X. & Ma, D. (2010): *Asymmetric, protecting-group-free total synthesis of (-)-englerin A.* In: Angewandte Chemie (International ed. in English), **49**, 20: 3513–3516.

Zhou, Y., Castonguay, P., Sidhom, E.-H., Clark, A. R., Dvela-Levitt, M., Kim, S., Sieber, J., Wieder, N., Jung, J. Y., Andreeva, S., Reichardt, J., Dubois, F., Hoffmann, S. C., Basgen, J. M., Montesinos, M. S., Weins, A., Johnson, A. C., Lander, E. S., Garrett, M. R., Hopkins, C. R. & Greka, A. (2017): *A small-molecule inhibitor of TRPC5 ion channels suppresses progressive kidney disease in animal models.* In: Science (New York, N.Y.), **358**, 6368: 1332–1336.

Zhou, Y., Kim, C., Pablo, J. L. B., Zhang, F., Jung, J. Y., Xiao, L., Bazua-Valenti, S., Emani, M., Hopkins, C. R., Weins, A. & Greka, A. (2021): *TRPC5 Channel Inhibition Protects Podocytes in Puromycin-Aminonucleoside Induced Nephrosis Models.* In: Frontiers in medicine, **8**: 721865.

Zhu, M. H., Chae, M., Kim, H. J., Lee, Y. M., Kim, M. J., Jin, N. G., Yang, D. K., So, I. & Kim, K. W. (2005): *Desensitization of canonical transient receptor potential channel 5 by protein kinase C.* In: American journal of physiology. Cell physiology, **289**, 3: C591–600.

Zhu, M. X. (2005): *Multiple roles of calmodulin and other Ca(2+)-binding proteins in the functional regulation of TRP channels.* In: Pflugers Archiv : European journal of physiology, **451**, 1: 105–115.

Zhu, M. X. & Tang, J. (2004): *TRPC channel interactions with calmodulin and IP3 receptors.* In: Novartis Foundation symposium, **258**: 44–58; discussion 58–62, 98–102, 263–6.

Zhu, X., Chu, P. B., Peyton, M. & Birnbaumer, L. (1995): *Molecular cloning of a widely expressed human homologue for the Drosophila trp gene.* In: FEBS Letters, **373**, 3: 193–198.

Zhu, X., Jiang, M., Peyton, M., Boulay, G., Hurst, R., Stefani, E. & Birnbaumer, L. (1996): *trp, a Novel Mammalian Gene Family Essential for Agonist-Activated Capacitative Ca2+ Entry.* In: Cell, **85**, 5: 661–671.

Zhu, Y., Lu, Y., Qu, C., Miller, M., Tian, J., Thakur, D. P., Zhu, J., Deng, Z., Hu, X., Wu, M., McManus, O. B., Li, M., Hong, X., Zhu, M. X. & Luo, H.-R. (2015a): *Identification and optimization of 2-aminobenzimidazole derivatives as novel inhibitors of TRPC4 and TRPC5 channels.* In: British journal of pharmacology, **172**, 14: 3495–3509.

Zhu, Y., Pan, Q., Meng, H., Jiang, Y., Mao, A., Wang, T., Hua, D., Yao, X., Jin, J. & Ma, X. (2015b): *Enhancement of vascular endothelial growth factor release in long-term drug-treated breast cancer via transient receptor potential channel 5-Ca(2+)-hypoxia-inducible factor 1a pathway.* In: Pharmacological research, **93**: 36–42.

Zimova, L., Ptakova, A., Mitro, M., Krusek, J. & Vlachova, V. (2022): *Activity dependent inhibition of TRPC1/4/5 channels by duloxetine involves voltage sensor-like domain.* In: Biomedicine & pharmacotherapy = Biomedecine & pharmacotherapie, **152**: 113262.

Zitt, C., Obukhov, A. G., Strübing, C., Zobel, A., Kalkbrenner, F., Lückhoff, A. & Schultz, G. (1997): *Expression of TRPC3 in Chinese hamster ovary cells results in calcium-activated cation currents not related to store depletion.* In: The Journal of cell biology, **138**, 6: 1333–1341.

Zitt, C., Zobel, A., Obukhov, A. G., Harteneck, C., Kalkbrenner, F., Lückhoff, A. & Schultz, G. (1996): *Cloning and Functional Expression of a Human Ca2+-Permeable Cation Channel Activated by Calcium Store Depletion.* In: Neuron, **16**, 6: 1189–1196.

Zou, Y., Liu, Z., Zhou, Y., Wang, J., Xu, Q., Zhao, X. & Miao, Z. (2021): *TRPC5 mediates TMZ resistance in TMZ-resistant glioblastoma cells via NFATc3-P-gp pathway.* In: Translational oncology, **14**, 12: 101214.

A. Mutagenesis Primer

Table A.1.: **Mutagenesis primers and their corresponding annealing temperatures.** Mutagenesis primers and their corresponding annealing temperatures. The mutation site is indicated by lower case letters. The codon-usage was optimized for the human translation machinery.

Mutation	Primer name	Primer sequence (5'-3')	Annealing temperature [°C]
I294A	mTRPC5-I294A-Forw	GAAGGTGGCAgccAAATATCACCAGAAAG	62
	mTRPC5-I294A-Rev	AGCTTGGCCAGGTCATGA	
I294V	mTRPC5_I294V_F	GAAGGTGGCAgtgAAATATCACCAGAAAG	64
	mTRPC5_I294V_R	AGCTTGGCCAGGTCATGA	
W327A	mTRPC5-W327A-Forw	GAGAAAACACgcgGTAGTCAAGCTTCTGACCTGC	68
	mTRPC5-W327A-Rev	CGCCATCCAGGGAAGCCA	
C334A	mTRPC5-C334A-F	GCTTCTGACCgccATGACCATTG	57
	mTRPC5-C334A-R	TTGACTACCCAGTGTTTTC	
F367A	mTRPC5-F367A-fw	CTTTATTAAGgccATCTGCCACAC	56
	mTRPC5-F367A-rev	GGTTTCTTGATGAAAAGC	
I368A	mTRPC5-I368A-F	TATTAAGTTCgccTGCCACACAGC	58
	mTRPC5-I368A-R	AAGGGTTTCTTGATGAAAAG	
I368T	mTRPC5_I368T_F	TATTAAGTTCaccTGCCACACAG	58
	mTRPC5_I368T_R	AAGGGTTTCTTGATGAAAAG	
I368V	mTRPC5_I368V_F	TATTAAGTTCgtgTGCCACACAG	58
	mTRPC5_I368V_R	AAGGGTTTCTTGATGAAAAG	
H370A	mTRPC5-H370A-Forw	GTTCATCTGCgcaACAGCATCCTATCTG	56
	mTRPC5-H370A-Rev	TTAATAAAGGGTTTCTTGATG	
H370F	mTRPC5_H370F_F	GTTCATCTGCttcACAGCATCCTATC	56
	mTRPC5_H370F_R	TTAATAAAGGGTTTCTTGATG	
H370K	mTRPC5-H370K-fw	GTTCATCTGCaagACAGCATCCTATC	60
	mTRPC5-H370K-rev	TTAATAAAGGGTTTCTTGATGAAAAG	

Mutation	Primer name	Primer sequence (5'-3')	Annealing temperature [°C]
H370N	mTRPC5_H370N_F	GTTCATCTGCaacACAGCATCCT	63
	mTRPC5_H370N_R	TTAATAAAGGGTTTCTTGATGAAAAGC	
H370W	mTRPC5_H370W_F	GTTCATCTGCtggACAGCATCCTATC	56
	mTRPC5_H370W_R	TTAATAAAGGGTTTCTTGATG	
T371A	mTRPC5_T371A_F	CATCTGCCACgccGCATCCTATC	60
	mTRPC5_T371A_R	AACTTAATAAAGGGTTTCTTGATG	
T371I	mTRPC5-T371I-fw	CATCTGCCACatcGCATCCTATCTG	56
	mTRPC5-T371I-rev	AACTTAATAAAGGGTTTCTTG	
T371L	mTRPC5-T371L-fw	CATCTGCCACctgGCATCCTATCTG	56
	mTRPC5-T371L-rev	AACTTAATAAAGGGTTTCTTG	
T371Y	mTRPC5-T371Y-Forw	CATCTGCCACtacGCATCCTATCTGAC	56
	mTRPC5-T371Y-Rev	AACTTAATAAAGGGTTTCTTG	
Y374A	mTRPC5-Y374A-fw	CACAGCATCCgccCTGACCTTCC	58
	mTRPC5-Y374A-rev	TGGCAGATGAACTTAATAAAG	
L375A	mTRPC5-F375A-F	AGCATCCTATgccACCTTCCTCTTC	59
	mTRPC5-F375A-R	GTGTGGCAGATGAACTTAATAAAG	
F379A	mTRPC5-F379A-F	GACCTTCCTCgccATGCTTCTCC	60
	mTRPC5-F379A-R	AGATAGGATGCTGTGTGG	
F414A	mTRPC5-F414A-Forw	GGTTCTAGGTgccATTTGGGGGG	61
	mTRPC5-F414A-Rev	CAAGGCAGTATCATCCATTC	
F414Y	mTRPC5_F414Y_F	GGTTCTAGGTtacATTTGGGGGG	61
	mTRPC5_F414Y_R	CAAGGCAGTATCATCCATTC	

Mutation	Primer name	Primer sequence (5'-3')	Annealing temperature [°C]
E418A	mTRPC5-E418A-F	CATTTGGGGGgccATAAAGGAAATG	60
	mTRPC5-E418A-R	AAACCTAGAACCCAAGGC	
E418D	mTRPC5_E418D_F	CATTTGGGGGgacATAAAGGAAATG	61
	mTRPC5_E418D_R	AAACCTAGAACCCAAGGC	
E418K	mTRPC5_E418K_F	CATTTGGGGGaagATAAAGGAAATG	61
	mTRPC5_E418K_R	AAACCTAGAACCCAAGGC	
E418N	mTRPC5-E418N-fw	CATTTGGGGGaacATAAAGGAAATGTGG	61
	mTRPC5-E418N-rev	AAACCTAGAACCCAAGGC	
E418Q	mTRPC5_E418Q_F	CATTTGGGGGcagATAAAGGAAATG	62
	mTRPC5_E418Q_R	AAACCTAGAACCCAAGGC	
E421A	mTRPC5_E421A_F	GGAGATAAAGgccATGTGGGATG	57
	mTRPC5_E421A_R	CCCCAAATGAAACCTAGAAC	
D424Q	mTRPC5-D424Q-Forw	GGAAATGTGGcaaGGTGGATTCAC	59
	mTRPC5-D424Q-Rev	TTTATCTCCCCCCAAATG	
H432A	mTRPC5-H432A-Forw	GGAATACATCgcgGATTGGTGGAACCTGATGG	60
	mTRPC5-H432A-Rev	GTGAATCCACCATCCCAC	
N436A	mTRPC5-R436A-Forw	TGATTGGTGGgccCTGATGGATTTTG	60
	mTRPC5-R436A-Rev	TGGATGTATTCCGTGAATC	
N436D	mTRPC5_N436D_F	TGATTGGTGGgacCTGATGGATT	56
	mTRPC5_N436D_R	TGGATGTATTCCGTGAATCC	
N436L	mTRPC5_N436L_F	TGATTGGTGGttgCTGATGGATTTTG	56
	mTRPC5_N436L_R	TGGATGTATTCCGTGAATC	

Mutation	Primer name	Primer sequence (5'-3')	Annealing temperature [°C]
D439A	mTRPC5-D439A-fw	GAACCTGATGgccTTTGCAATGAAC	57
	mTRPC5-D439A-rev	CACCAATCATGGATGTATTC	
D439E	mTRPC5_D439E_F	GAACCTGATGgagTTTGCAATGAAC	62
	mTRPC5_D439E_R	CACCAATCATGGATGTATTCC	
D439L	mTRPC5_D439L_F	GAACCTGATGttgTTTGCAATGAACTCC	56
	mTRPC5_D439L_R	CACCAATCATGGATGTATTC	
D439N	mTRPC5_D439N_F	GAACCTGATGaacTTTGCAATGAAC	59
	mTRPC5_D439N_R	CACCAATCATGGATGTATTC	
D439Q	mTRPC5-D439Q-fw	GAACCTGATGcagTTTGCAATGAAC	59
	mTRPC5-D439Q-rev	CACCAATCATGGATGTATTC	
M442A	mTRPC5-N442A-fw	GGATTTTGCAgccAACTCCCTCTACC	59
	mTRPC5-N442A-rev	ATCAGGTTCCACCAATCATG	
N443A	mTRPC5-N443A-fw	TTTTGCAATGgccTCCCTCTACCTG	59
	mTRPC5-N443A-rev	TCCATCAGGTTCCACCAA	
N443D	mTRPC5_N443D_F	TTTTGCAATGgacTCCCTCTACC	64
	mTRPC5_N443D_R	TCCATCAGGTTCCACCAAT	
N443L	mTRPC5_N443L_F	TTTTGCAATGttgTCCCTCTACCTGGC	59
	mTRPC5_N443L_R	TCCATCAGGTTCCACCAA	
Y446A	mTRPC5-Y446A-fw	GAACTCCCTCgccCTGGCAACTATTTC	57
	mTRPC5-Y446A-rev	ATTGCAAAATCCATCAGG	
Y446F	mTRPC5_Y446F_F	GAACTCCCTCttcCTGGCAACTA	61
	mTRPC5_Y446F_R	ATTGCAAAATCCATCAGGTTC	
Y446L	mTRPC5_Y446L_F	GAACTCCCTCttgCTGGCAACTATTTC	57
	mTRPC5_Y446L_R	ATTGCAAAATCCATCAGG	

Mutation	Primer name	Primer sequence (5'-3')	Annealing temperature [°C]
S489A	mTRPC5-S489A-fw	CAACATTTTAgccTCCTTGCGTCTCATATC	57
	mTRPC5-S489A-rev	GATATTGCGAAGAGTGCTTC	
R492A	mTRPC5-R492A-Forw	AAGTTCCTTGgccCTCATATCCTTGTTC	56
	mTRPC5-R492A-Rev	AAAATGTTGGATATTGCG	
R492K	mTRPC5-F492K-F	AAGTTCCTTGaaaCTCATATCCTTGTTC	56
	mTRPC5-F492K-R	AAAATGTTGGATATTGCG	
S495A	mTRPC5-S495A-Forw	GCGTCTCATAgccTTGTTCACAG	63
	mTRPC5-S495A-Rev	AAGGAACTTAAAATGTTGGATATTGC	
L496A	mTRPC5-L496A-fw	TCTCATATCCgccTTCACAGCCAACTCC	56
	mTRPC5-L496A-rev	CGCAAGGAACTTAAAATG	
L496I	mTRPC5-L496I-fw	TCTCATATCCatcTTCACAGCCAAC	57
	mTRPC5-L496I-rev	CGCAAGGAACTTAAAATG	
L496T	mTRPC5-L496T-fw	TCTCATATCCaccTTCACAGCCAACTCC	57
	mTRPC5-L496T-rev	CGCAAGGAACTTAAAATG	
F497A	mTRPC5-F497A-F	CATATCCTTGgcgACAGCCAACTC	57
	mTRPC5-F497A-R	AGACGCAAGGAACTTAAAATG	
F497Y	mTRPC5-R497Y-Forw	CATATCCTTGtacACAGCCAACTC	61
	mTRPC5-R497Y-Rev	AGACGCAAGGAACTTAAAATG	
N500A	mTRPC5-N500A-fw	GTTCACAGCCgccTCCCATTTAG	57
	mTRPC5-N500A-rev	AAGGATATGAGACGCAAG	
N500F	mTRPC5-N500F-Forw	GTTCACAGCCttcTCCCATTTAG	57
	mTRPC5-N500F-Rev	AAGGATATGAGACGCAAG	

Mutation	Primer name	Primer sequence (5'-3')	Annealing temperature [°C]
G511A	mTRPC5-G511A-Forw	GATCTCTTTGgcaCGAATGCTGC	64
	mTRPC5-G511A-Rev	TGCAGAGGCCCTAAATGG	
R512A	mTRPC5-L512A-Forw	CTCTTTGGGAgctATGCTGCTTGATATACTC	60
	mTRPC5-L512A-Rev	ATCTGCAGAGGCCCTAAA	
R512K	mTRPC5_R512K_F	CTCTTTGGGAaagATGCTGCTTGATATACTC	61
	mTRPC5_R512K_R	ATCTGCAGAGGCCCTAAA	
L514A	mTRPC5-L514A-Forw	GGGACGAATGgcgCTTGATATACTC	59
	mTRPC5-L514A-Rev	AAAGAGATCTGCAGAGGC	
L521A	mTRPC5-L521A-fw	ACTCAAATTTgccTTTATCTACTGCC	57
	mTRPC5-L521A-rev	ATATCAAGCAGCATTCGTC	
L521I	mTRPC5-L521I-fw	ACTCAAATTTatcTTTATCTACTGC	58
	mTRPC5-L521I-rev	ATATCAAGCAGCATTCGTC	
L521T	mTRPC5-L521T-fw	ACTCAAATTTaccTTTATCTACTGCC	57
	mTRPC5-L521T-rev	ATATCAAGCAGCATTCGTC	
Y524A	mTRPC5-Y524A-fw	TCTCTTTATCgccTGCCTAGTACTAC	56
	mTRPC5-Y524A-rev	AATTTGAGTATATCAAGCAGC	
Y524E	mTRPC5_Y524E_F	TCTCTTTATCgagTGCCTAGTAC	56
	mTRPC5_Y524E_R	AATTTGAGTATATCAAGCAGC	
Y524F	mTRPC5_Y524F_F	TCTCTTTATCttcTGCCTAGTAC	58
	mTRPC5_Y524F_R	AATTTGAGTATATCAAGCAGC	
Y524L	mTRPC5_Y524L_F	TCTCTTTATCttgTGCCTAGTACTACTG	57
	mTRPC5_Y524L_R	AATTTGAGTATATCAAGCAGC	

Mutation	Primer name	Primer sequence (5'-3')	Annealing temperature [°C]
C525A	mTRPC5-C525A-fw	CTTTATCTACgccCTAGTACTACTGGC	56
	mTRPC5-C525A-rev	AGAAATTTGAGTATATCAAGC	
L528A	mTRPC5-L528A-fw	CTGCCTAGTAgccCTGGCTTTTGCC	57
	mTRPC5-L528A-rev	TAGATAAAGAGAAATTTGAGTATATC	
R557A	mTRPC5-R557A-F	CAAGGGGATCgcgTGTGAAAAACAGAAC	57
	mTRPC5-R557A-R	CAGTTGTTAGGTTCATCAATAG	
F569A	mTRPC5-F569A-fw	CTCCACGCTCgccGAAACCCTTC	57
	mTRPC5-F569A-rev	AAGGCGTTGTTCTGTTTTTC	
F569Y	mTRPC5-F569Y-fw	CTCCACGCTCtacGAAACCCTTC	61
	mTRPC5-F569Y-rev	AAGGCGTTGTTCTGTTTTTC	
L572A	mTRPC5-L572A-fw	CTTTGAAACCgccCAGTCGCTCTTCTGGTCTG	66
	mTRPC5-L572A-rev	AGCGTGGAGAAGGCGTTG	
Q573A	mTRPC5-Q573A-fw	TGAAACCCTTgccTCGCTCTTCTGGTCTGTCTTTG	65
	mTRPC5-Q573A-rev	AAGAGCGTGGAGAAGGCG	
Q573D	mTRPC5-Q573D-fw	TGAAACCCTTgacTCGCTCTTCTGGTCTG	65
	mTRPC5-Q573D-rev	AAGAGCGTGGAGAAGGCG	
Q573E	mTRPC5-Q573E-fw	TGAAACCCTTgagTCGCTCTTCTG	66
	mTRPC5-Q573E-rev	AAGAGCGTGGAGAAGGCG	
Q573N	mTRPC5-Q573N-fw	TGAAACCCTTaacTCGCTCTTCTGGTCTG	64
	mTRPC5-Q573N-rev	AAGAGCGTGGAGAAGGCG	
Q573R	mTRPC5-Q573R-fw	TGAAACCCTTagaTCGCTCTTCTGGTCTGTC	63
	mTRPC5-Q573R-rev	AAGAGCGTGGAGAAGGCG	
Q573W	mTRPC5_Q573W_F	TGAAACCCTTtggTCGCTCTTCTGG	64
	mTRPC5_Q573W_R	AAGAGCGTGGAGAAGGCG	

Mutation	Primer name	Primer sequence (5'-3')	Annealing temperature [°C]
F576A	mTRPC5-F576A-F	TCAGTCGCTCgcgTGGTCTGTCTTTGG	60
	mTRPC5-F576A-R	AGGGTTTCAAAGAGCGTG	
F576Y	mTRPC5-F576Y-fw	TCAGTCGCTCtacTGGTCTGTCT	63
	mTRPC5-F576Y-rev	AGGGTTTCAAAGAGCGTG	
W577A	mTRPC5-W577A-fw	GTCGCTCTTCgccTCTGTCTTTGGCC	57
	mTRPC5-W577A-rev	TGAAGGGTTTCAAAGAGC	
W577H	mTRPC5-W577H-fw	GTCGCTCTTCcacTCTGTCTTTGGCC	57
	mTRPC5-W577H-rev	TGAAGGGTTTCAAAGAGC	
V579A	mTRPC5-V579A-fw	CTTCTGGTCTgccTTTGGCCTCC	66
	mTRPC5-V579A-rev	AGCGACTGAAGGGTTTCAAAG	
E595Q	mTRPC5-E595Q-F	GGCCCGACATcagTTCACTGAGT	64
	mTRPC5-E595Q-R	TTCACATTGGTAACATAGAGATTTAGG	
F596A	mTRPC5-F596A-F	CCGACATGAGgcgACTGAGTTTGTG	59
	mTRPC5-F596A-R	GCCTTCACATTGGTAACATAG	
F599A	mTRPC5-F599A-F	GTTCACTGAGgcgGTGGGAGCTACGATG	64
	mTRPC5-F599A-R	TCATGTCGGGCCTTCACA	
T603A	mTRPC5-T603A-fw	TGTGGGAGCTgccATGTTTGGGAC	62
	mTRPC5-T603A-rev	AACTCAGTGAACTCATGTCG	
G606A	mTRPC5-G606A-fw	TACGATGTTTgccACATACAACGTCATC	61
	mTRPC5-G606A-rev	GCTCCCACAAACTCAGTG	
T607A	mTRPC5-T607A-fw	GATGTTTGGGgccTACAACGTCATC	61
	mTRPC5-T607A-rev	GTAGCTCCCACAAACTCAG	

Mutation	Primer name	Primer sequence (5'-3')	Annealing temperature [°C]
V610A	mTRPC5-V610A-fw	GACATACAACgccATCTCCCTGG	64
	mTRPC5-V610A-rev	CCAAACATCGTAGCTCCC	
L613A	mTRPC5-L613A-fw	CGTCATCTCCgccGTAGTGCTGC	57
	mTRPC5-L613A-rev	TTGTATGTCCCAAACATC	
V614A	mTRPC5-V614A-fw	CATCTCCCTGgccGTGCTGCTGA	61
	mTRPC5-V614A-rev	ACGTTGTATGTCCCAAAC	
L617A	mTRPC5-L617A-fw	GGTAGTGCTGgccAATATGCTCATC	57
	mTRPC5-L617A-rev	AGGGAGATGACGTTGTATG	
E638A	mTRPC5-E638A-Forw	TGCTGATATTgcgTGGAAGTTTGC	63
	mTRPC5-E638A-Rev	TGATCGGCAATGAGCTGG	
E638D	mTRPC5_E638D_F	TGCTGATATTgacTGGAAGTTTGCG	61
	mTRPC5_E638D_R	TGATCGGCAATGAGCTGG	
E638Q	mTRPC5_E638Q_F	TGCTGATATTcagTGGAAGTTTGC	62
	mTRPC5_E638Q_R	TGATCGGCAATGAGCTGG	
A642S	mTRPC5-L642S-Forw	GTGGAAGTTTtcgAGAACAAAGC	57
	mTRPC5-L642S-Rev	TCAATATCAGCATGATCG	
L646A	mTRPC5-L646A-Forw	GAGAACAAAGgccTGGATGAGTTAC	57
	mTRPC5-L646A-Rev	GCAAACTTCCACTCAATATC	
Y650A	mTRPC5-Y650A-Forw	CTGGATGAGTgccTTTGATGAAGG	57
	mTRPC5-Y650A-Rev	AGCTTTGTTCTCGCAAAC	
N662A	mTRPC5-N662A-Forw	ACCTCCTTTCgccATTATTCCCAGCCC	63
	mTRPC5-N662A-Rev	GGTAAGGTGCCACCTTCA	

B. Docking Results

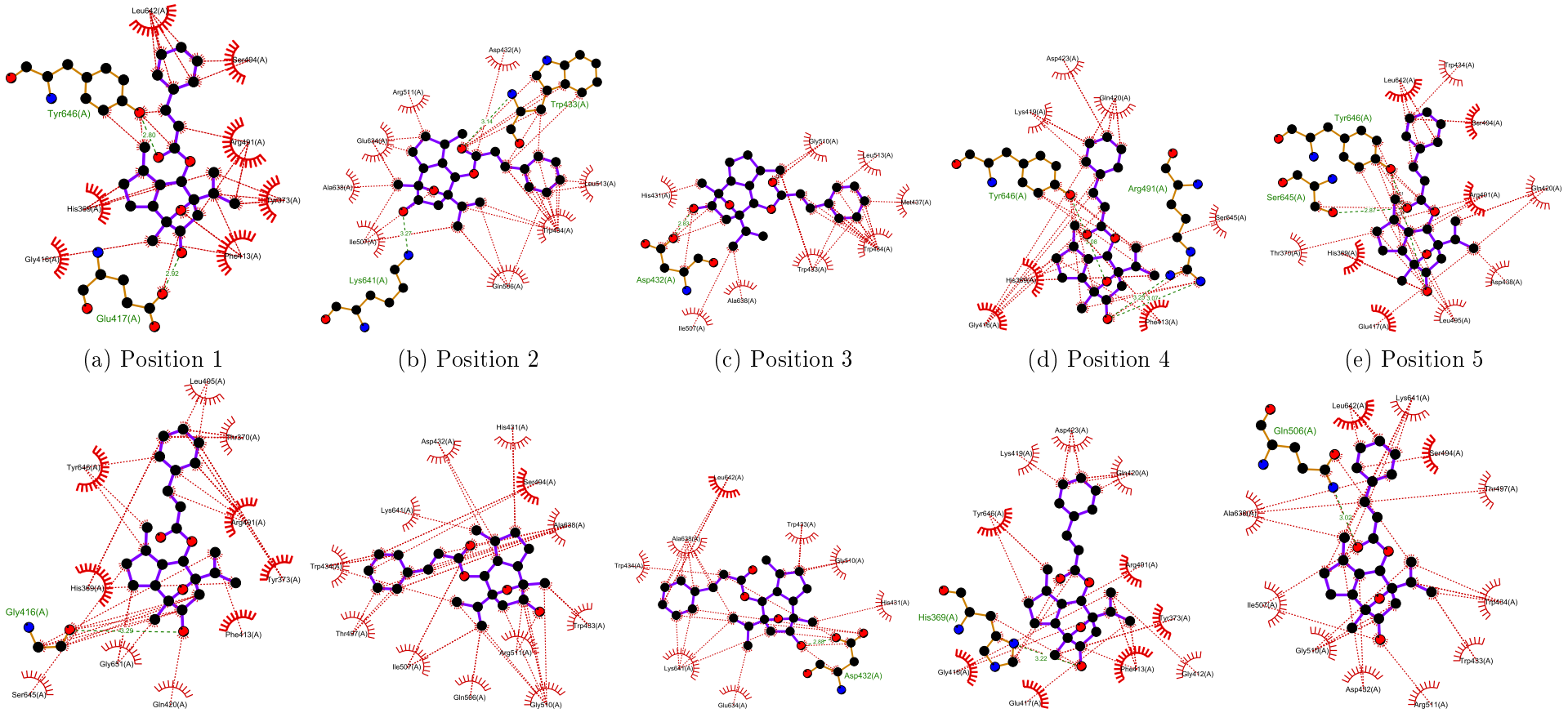

(a) Position 1 (b) Position 2 (c) Position 3 (d) Position 4 (e) Position 5

(f) Position 6 (g) Position 7 (h) Position 8 (i) Position 9 (j) Position 10

Figure B.1.: **Docking results and interacting amino acids of TRPC4 docked with englerin B in cavity I.** This figure shows the docking results and interacting amino acids (Ligand position 1 (a) to position 10 (j)) of TRPC4 (PDB: 5Z96) docked with englerin B in cavity I. Dashed green lines indicate hydrogen bonds (with their distance given in Å), dashed red lines indicate polar and non-polar interactions. Filled black circles represent carbon atoms, blue circles represent nitrogen atoms, red circles indicate oxygen atoms, yellow stands for sulphur atoms and green for fluorine. Letters in brackets behind interacting amino acids indicate the protein chain.

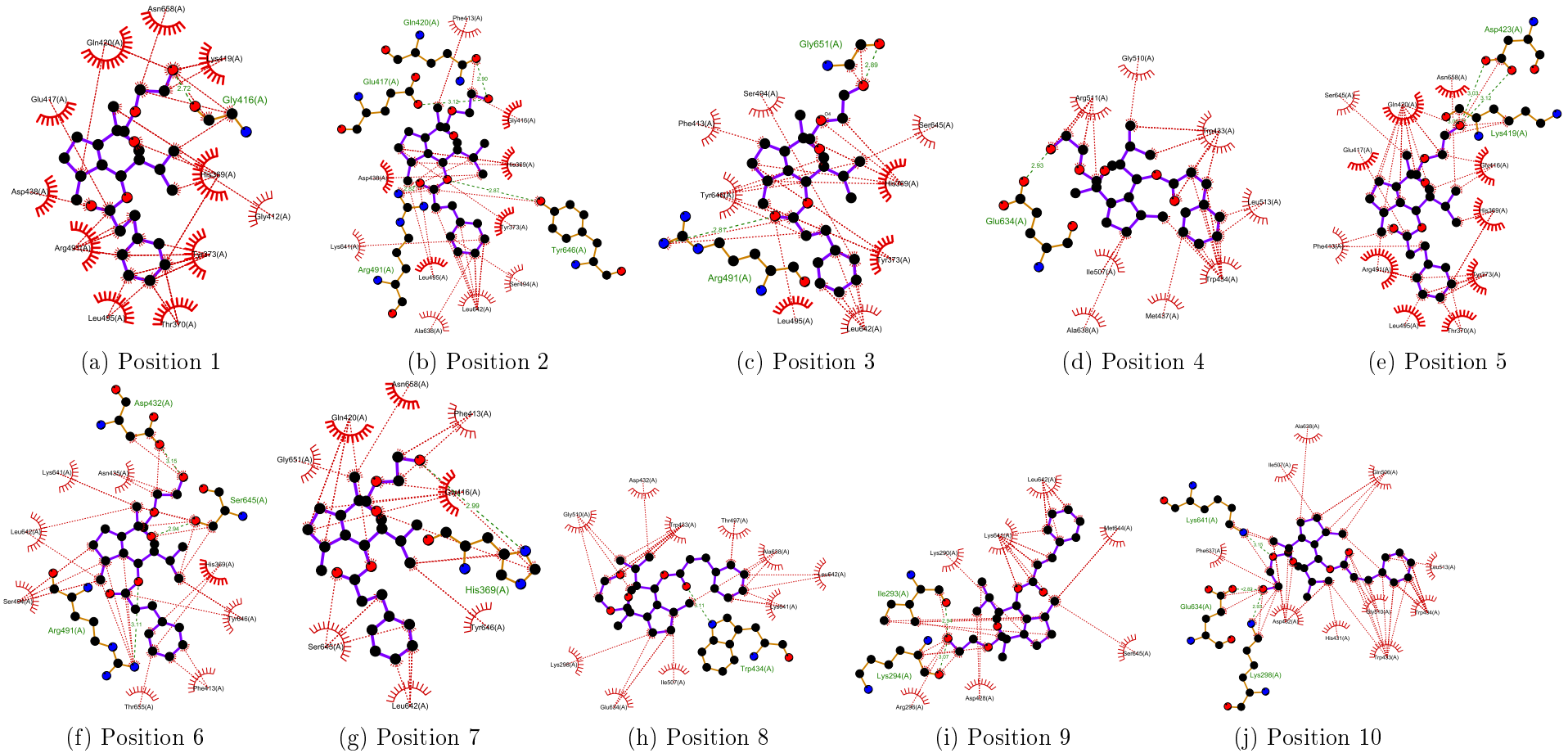

(a) Position 1 (b) Position 2 (c) Position 3 (d) Position 4 (e) Position 5

(f) Position 6 (g) Position 7 (h) Position 8 (i) Position 9 (j) Position 10

Figure B.2.: **Docking results and interacting amino acids of TRPC4 docked with A54 in cavity I.** This figure shows the docking results and interacting amino acids (Ligand position 1 (a) to position 10 (j)) of TRPC4 (PDB: 5Z96) docked with A54 in cavity I. Dashed green lines indicate hydrogen bonds (with their distance given in Å), dashed red lines indicate polar and non-polar interactions. Filled black circles represent carbon atoms, blue circles represent nitrogen atoms, red circles indicate oxygen atoms, yellow stands for sulphur atoms and green for fluorine. Letters in brackets behind interacting amino acids indicate the protein chain.

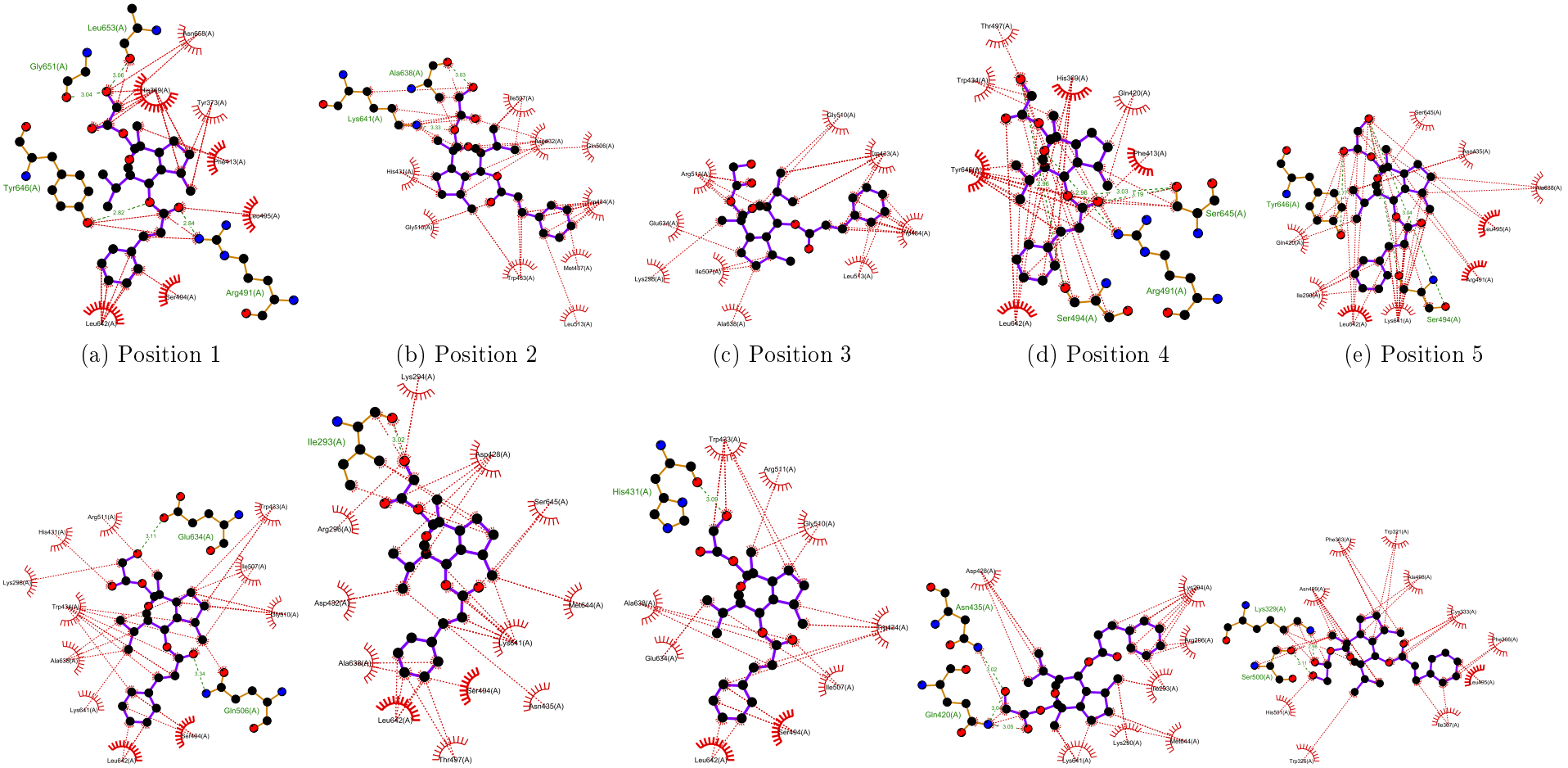

(a) Position 1 (b) Position 2 (c) Position 3 (d) Position 4 (e) Position 5

(f) Position 6 (g) Position 7 (h) Position 8 (i) Position 9 (j) Position 10

Figure B.3.: **Docking results and interacting amino acids of TRPC5 docked with (-)-englerin A in cavity I.** This figure shows the docking results and interacting amino acids (Ligand position 1 (a) to position 10 (j)) of TRPC4 (PDB: 5Z96) docked with (-)-englerin A in cavity I. Dashed green lines indicate hydrogen bonds (with their distance given in Å), dashed red lines indicate polar and non-polar interactions. Filled black circles represent carbon atoms, blue circles represent nitrogen atoms, red circles indicate oxygen atoms, yellow stands for sulphur atoms and green for fluorine. Letters in brackets behind interacting amino acids indicate the protein chain.

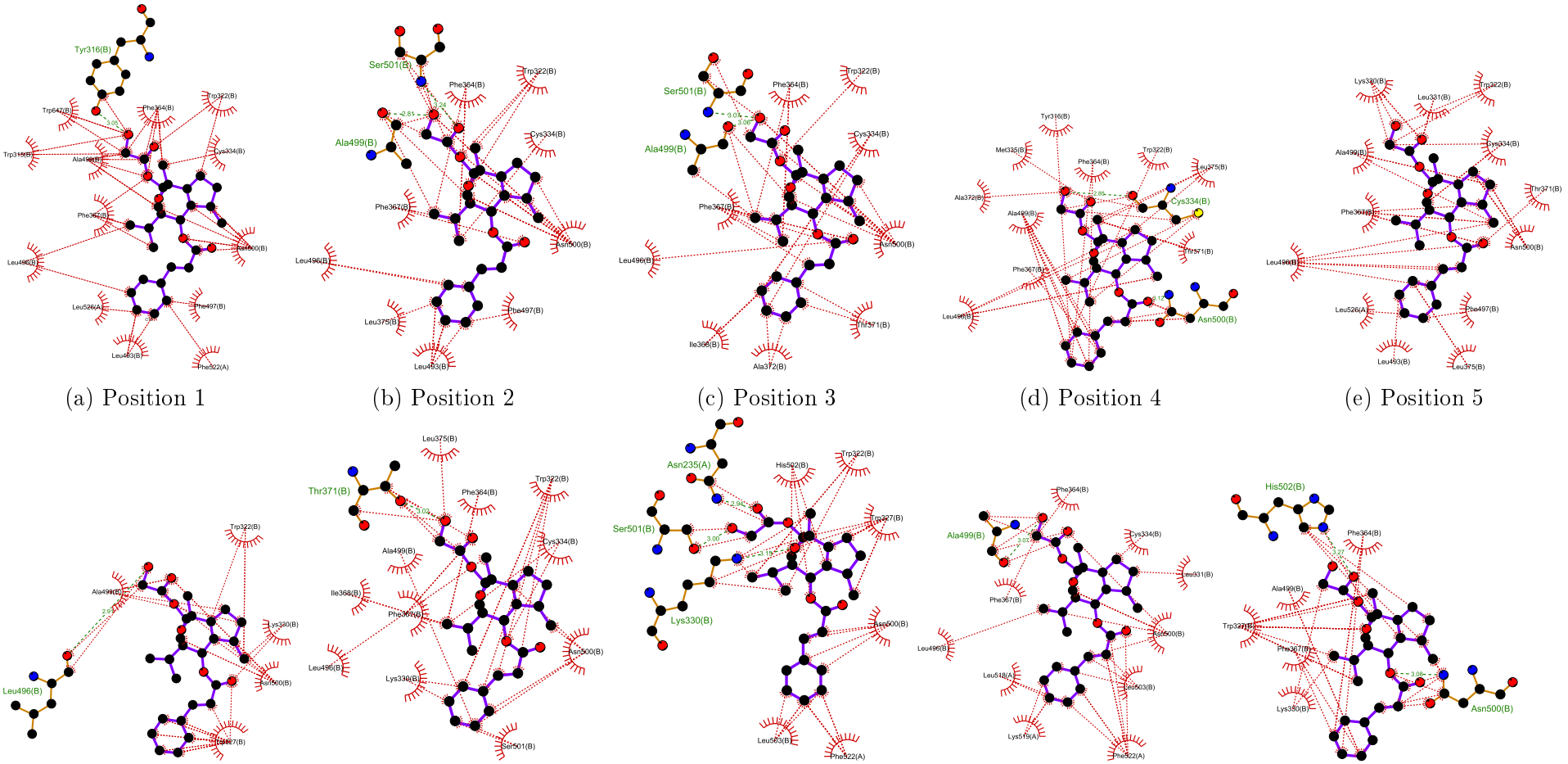

(a) Position 1 (b) Position 2 (c) Position 3 (d) Position 4 (e) Position 5

(f) Position 6 (g) Position 7 (h) Position 8 (i) Position 9 (j) Position 10

Figure B.4.: **Docking results and interacting amino acids of TRPC5 docked with (-)-englerin A in cavity IIa.** This figure shows the docking results and interacting amino acids (Ligand position 1 (a) to position 10 (j)) of TRPC5 (PDB: 6AEI) docked with (-)-englerin A in cavity IIa (lower part). Dashed green lines indicate hydrogen bonds (with their distance given in Å), dashed red lines indicate polar and non-polar interactions. Filled black circles represent carbon atoms, blue circles represent nitrogen atoms, red circles indicate oxygen atoms, yellow stands for sulphur atoms and green for fluorine. Letters in brackets behind interacting amino acids indicate the protein chain.

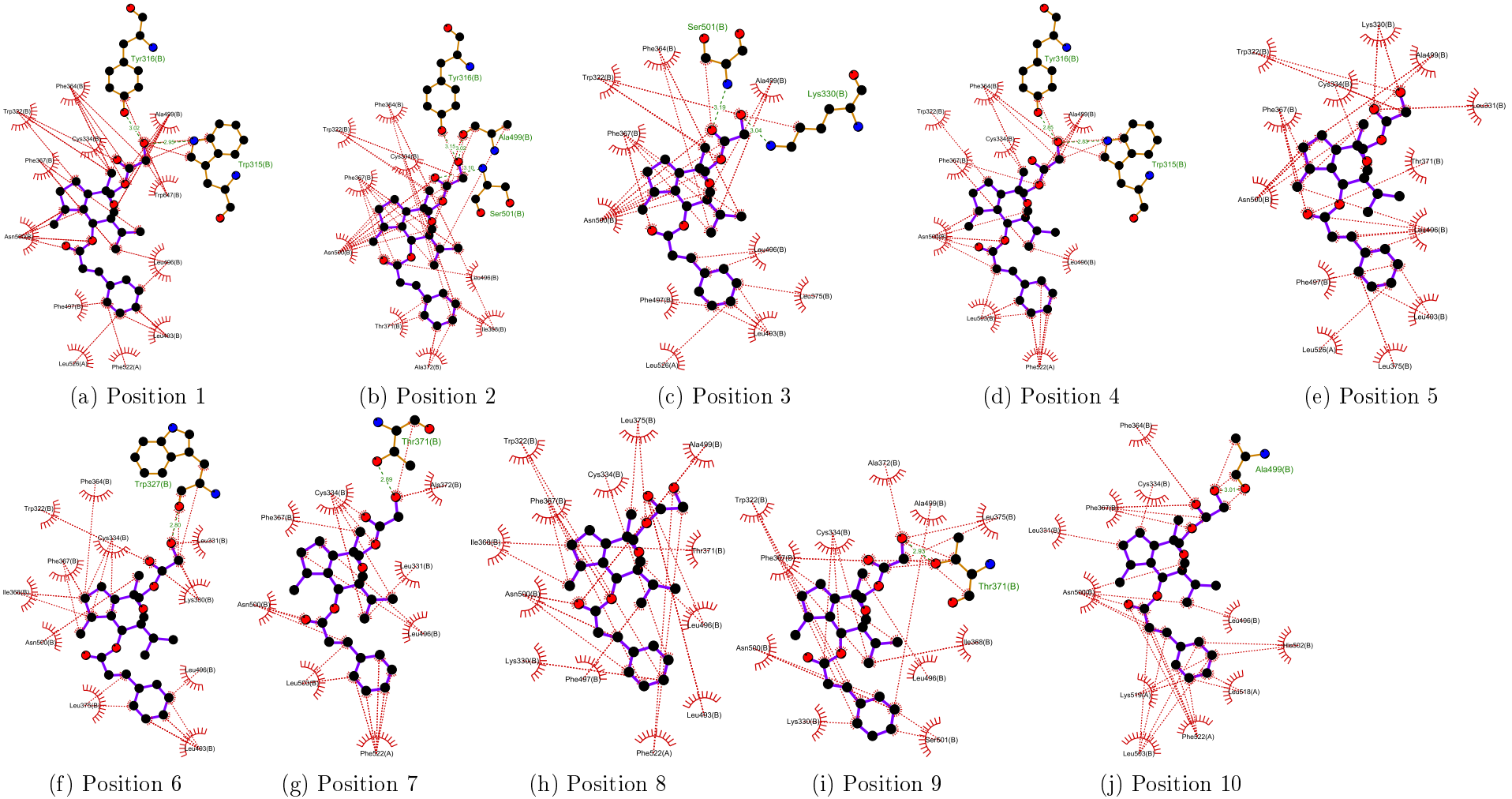

(a) Position 1 (b) Position 2 (c) Position 3 (d) Position 4 (e) Position 5

(f) Position 6 (g) Position 7 (h) Position 8 (i) Position 9 (j) Position 10

Figure B.5.: **Docking results and interacting amino acids of TRPC5 docked with (-)-englerin A in cavity IIb.** This figure shows the docking results and interacting amino acids (Ligand position 1 (a) to position 10 (j)) of TRPC5 (PDB: 6AEI) docked with (-)-englerin A in cavity IIb (upper part). Dashed green lines indicate hydrogen bonds (with their distance given in Å), dashed red lines indicate polar and non-polar interactions. Filled black circles represent carbon atoms, blue circles represent nitrogen atoms, red circles indicate oxygen atoms, yellow stands for sulphur atoms and green for fluorine. Letters in brackets behind interacting amino acids indicate the protein chain.

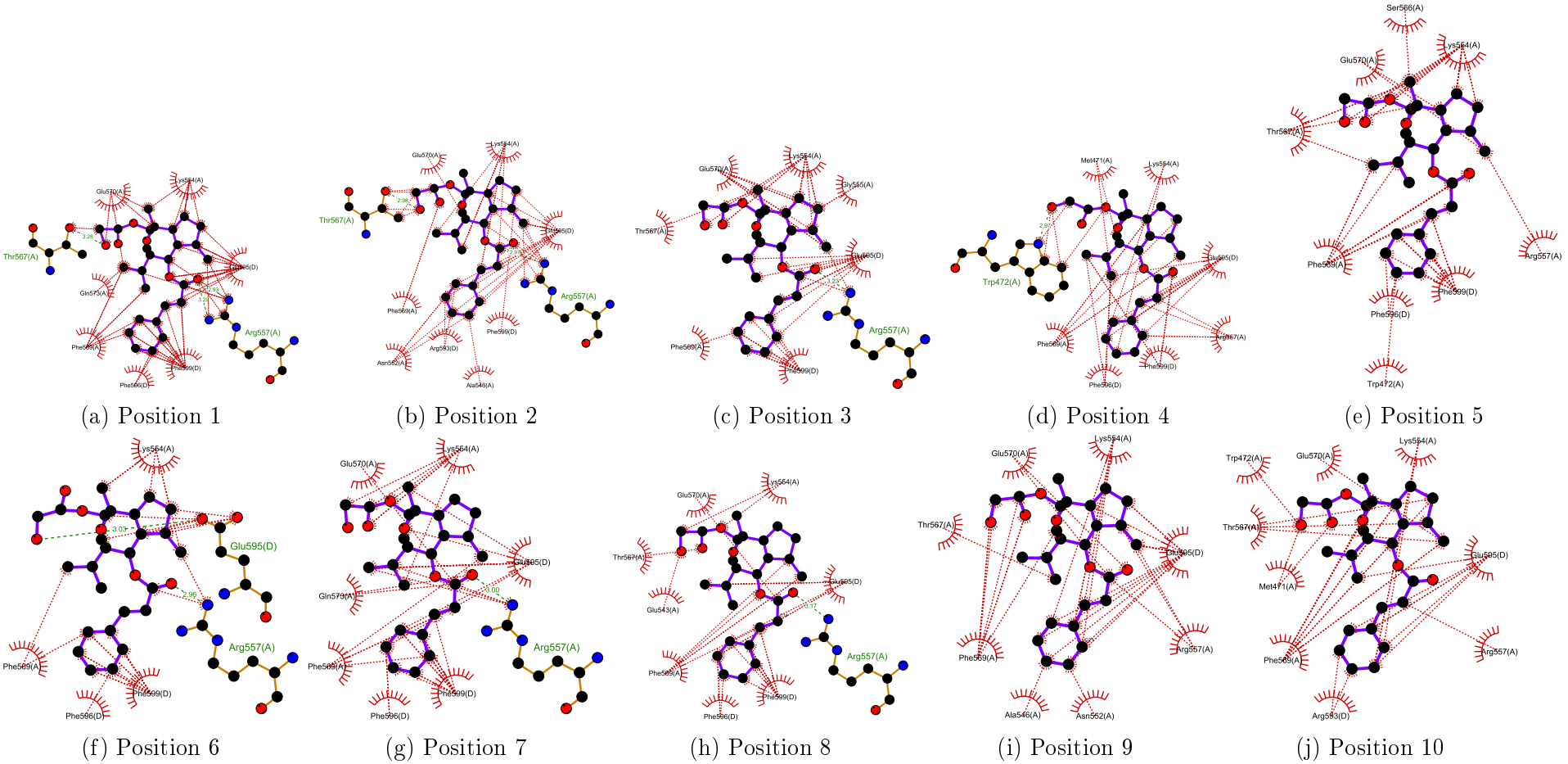

(a) Position 1 (b) Position 2 (c) Position 3 (d) Position 4 (e) Position 5

(f) Position 6 (g) Position 7 (h) Position 8 (i) Position 9 (j) Position 10

Figure B.6.: **Docking results and interacting amino acids of TRPC5 docked with (-)-englerin A in cavity IIIa.** This figure shows the docking results and interacting amino acids (Ligand position 1 (a) to position 10 (j)) of TRPC5 (PDB: 6AEI) docked with (-)-englerin A in cavity IIIa. Dashed green lines indicate hydrogen bonds (with their distance given in Å), dashed red lines indicate polar and non-polar interactions. Filled black circles represent carbon atoms, blue circles represent nitrogen atoms, red circles indicate oxygen atoms, yellow stands for sulphur atoms and green for fluorine. Letters in brackets behind interacting amino acids indicate the protein chain.

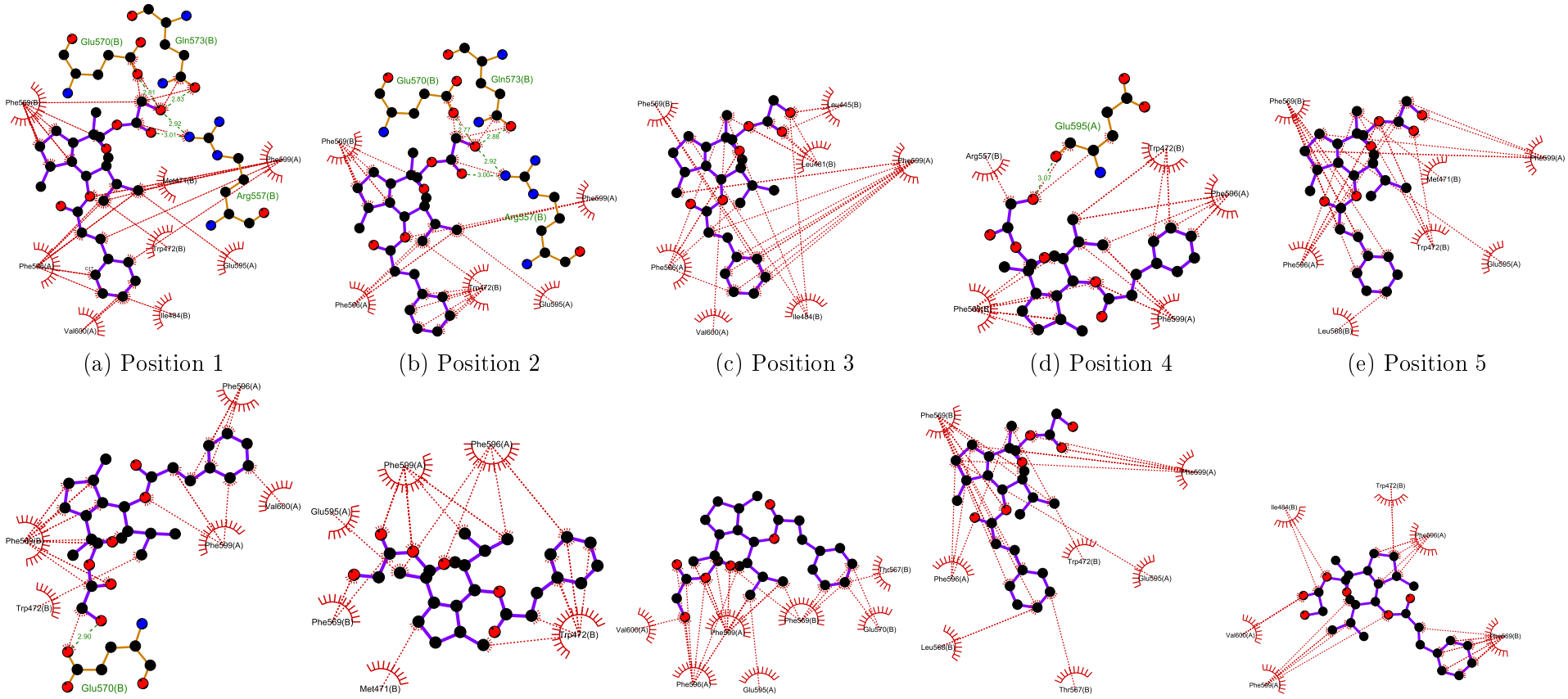

(a) Position 1 (b) Position 2 (c) Position 3 (d) Position 4 (e) Position 5

(f) Position 6 (g) Position 7 (h) Position 8 (i) Position 9 (j) Position 10

Figure B.7.: **Docking results and interacting amino acids of TRPC5 docked with (-)-englerin A in cavity IIIb.** This figure shows the docking results and interacting amino acids (Ligand position 1 (a) to position 10 (j)) of TRPC5 (PDB: 6AEI) docked with (-)-englerin A in cavity IIIb. Dashed green lines indicate hydrogen bonds (with their distance given in Å), dashed red lines indicate polar and non-polar interactions. Filled black circles represent carbon atoms, blue circles represent nitrogen atoms, red circles indicate oxygen atoms, yellow stands for sulphur atoms and green for fluorine. Letters in brackets behind interacting amino acids indicate the protein chain.

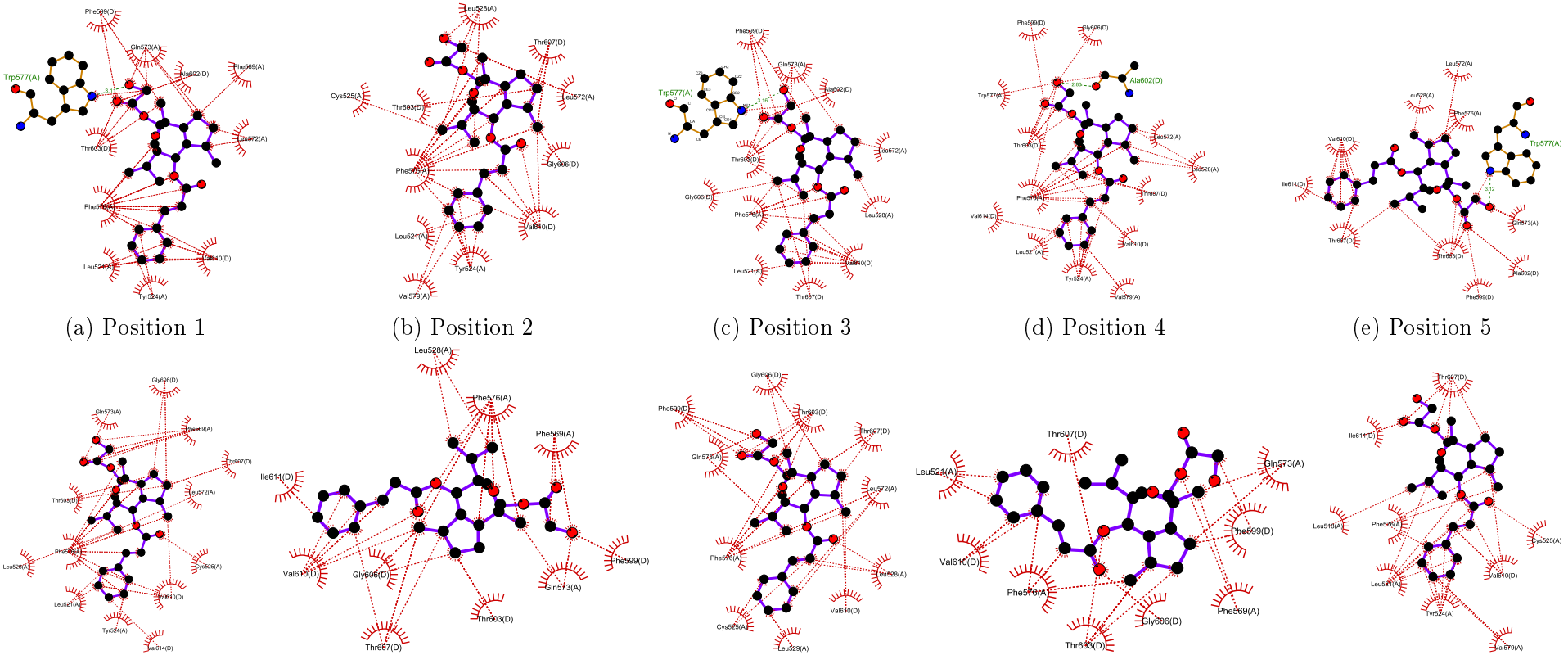

(a) Position 1 (b) Position 2 (c) Position 3 (d) Position 4 (e) Position 5

(f) Position 6 (g) Position 7 (h) Position 8 (i) Position 9 (j) Position 10

Figure B.8.: **Docking results and interacting amino acids of TRPC5 docked with (-)-englerin A in cavity IV.** This figure shows the docking results and interacting amino acids (Ligand position 1 (a) to position 10 (j)) of TRPC5 (PDB: 6AEI) docked with (-)-englerin A in cavity IV. Dashed green lines indicate hydrogen bonds (with their distance given in Å), dashed red lines indicate polar and non-polar interactions. Filled black circles represent carbon atoms, blue circles represent nitrogen atoms, red circles indicate oxygen atoms, yellow stands for sulfur atoms and green for fluorine. Letters in brackets behind interacting amino acids indicate the protein chain.

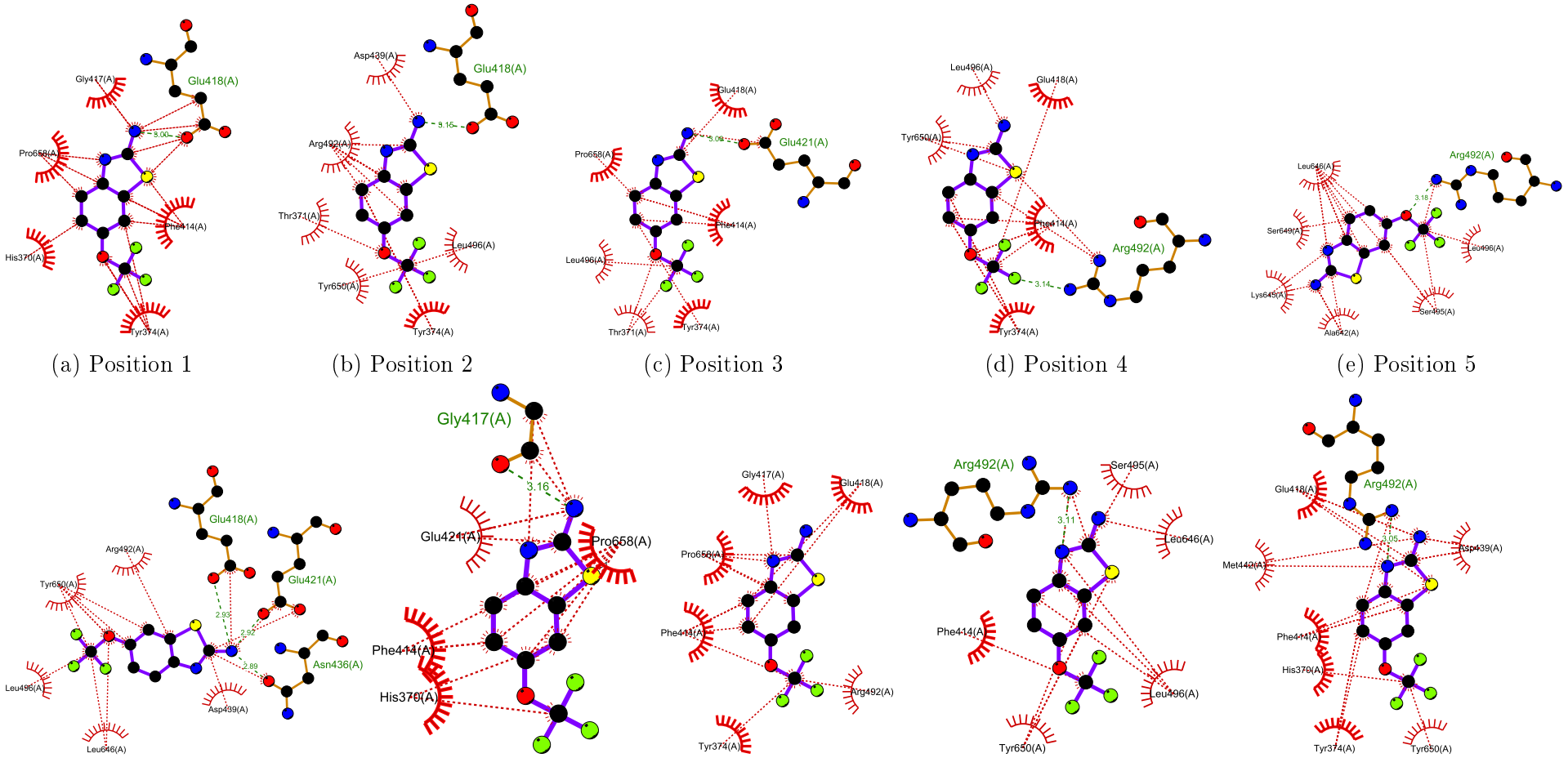

(a) Position 1 (b) Position 2 (c) Position 3 (d) Position 4 (e) Position 5

(f) Position 6 (g) Position 7 (h) Position 8 (i) Position 9 (j) Position 10

Figure B.9.: **Docking results and interacting amino acids of TRPC4 docked with riluzole in cavity I.** This figure shows the docking results and interacting amino acids (Ligand position 1 (a) to position 10 (j)) of TRPC5 (PDB: 6AEI) docked with riluzole in cavity I. Dashed green lines indicate hydrogen bonds (with their distance given in Å), dashed red lines indicate polar and non-polar interactions. Filled black circles represent carbon atoms, blue circles represent nitrogen atoms, red circles indicate oxygen atoms, yellow stands for sulphur atoms and green for fluorine. Letters in brackets behind interacting amino acids indicate the protein chain.

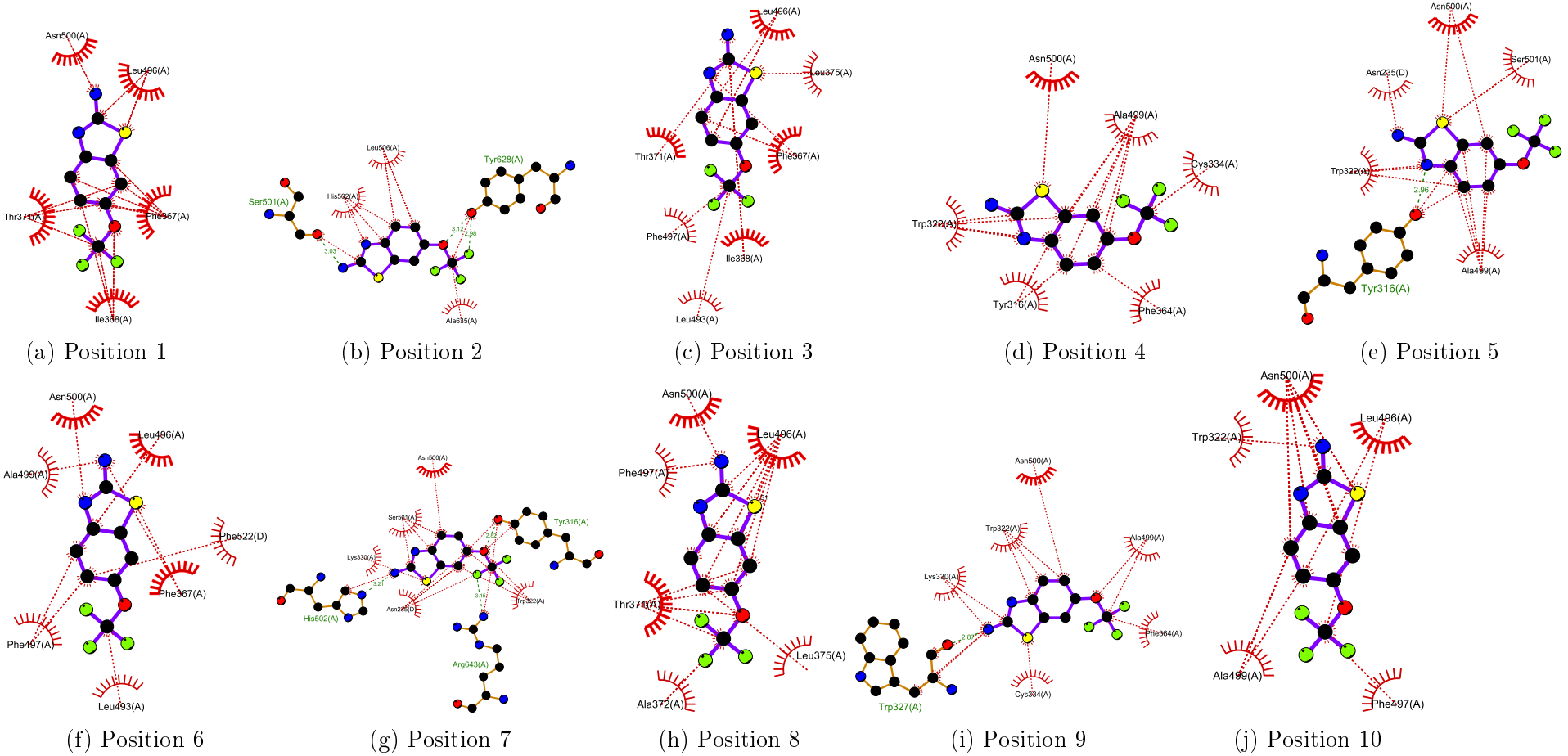

(a) Position 1 (b) Position 2 (c) Position 3 (d) Position 4 (e) Position 5

(f) Position 6 (g) Position 7 (h) Position 8 (i) Position 9 (j) Position 10

Figure B.10.: **Docking results and interacting amino acids of TRPC4 docked with riluzole in cavity II.** This figure shows the docking results and interacting amino acids (Ligand position 1 (a) to position 10 (j)) of TRPC5 (PDB: 6AEI) docked with riluzole in cavity II. Dashed green lines indicate hydrogen bonds (with their distance given in Å), dashed red lines indicate polar and non-polar interactions. Filled black circles represent carbon atoms, blue circles represent nitrogen atoms, red circles indicate oxygen atoms, yellow stands for sulphur atoms and green for fluorine. Letters in brackets behind interacting amino acids indicate the protein chain.

C. Western Blots

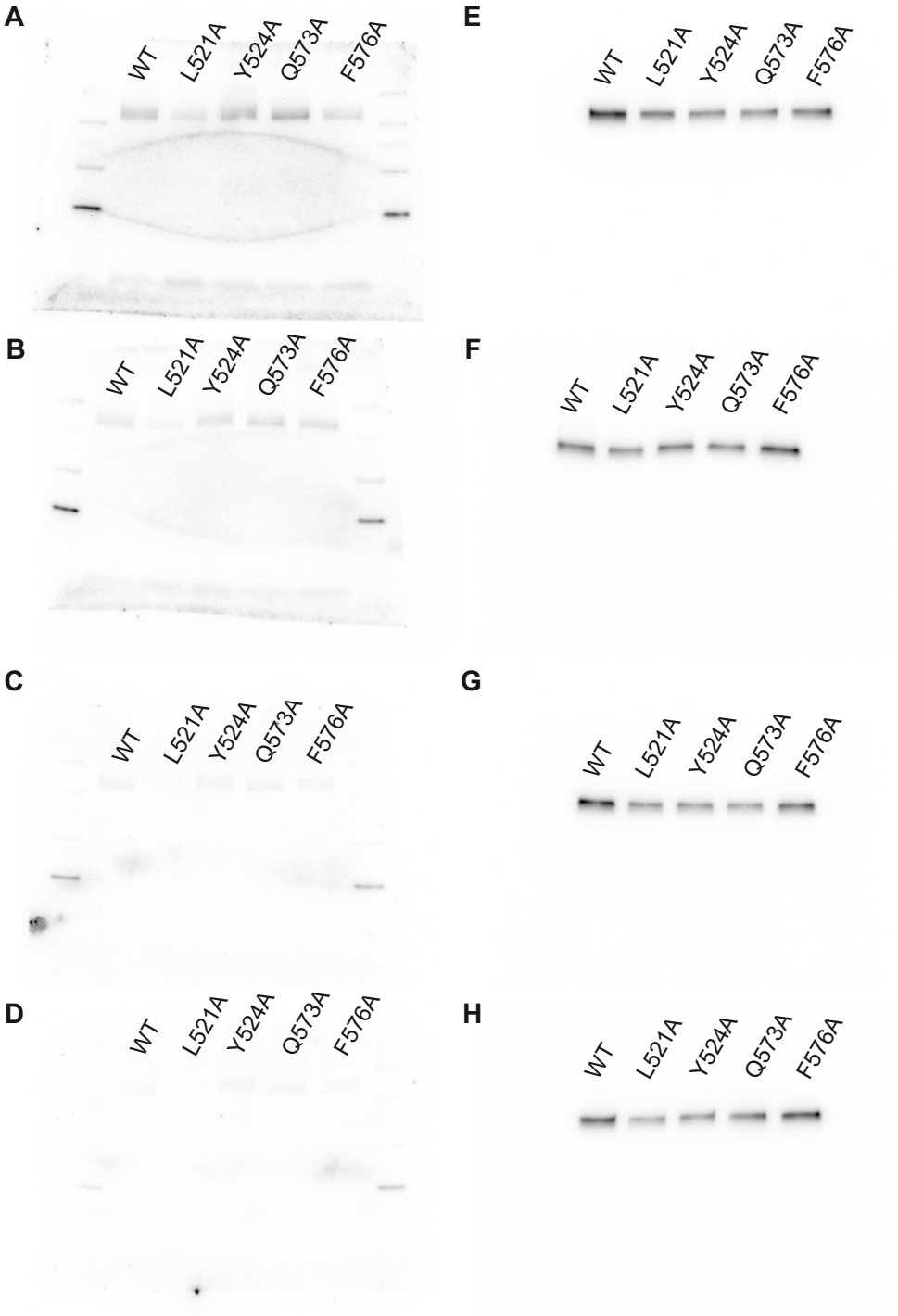

Figure C.1.: **Raw pictures of the surface expression of (-)-englerin A non-binding mutant TRPC5 channels.** This figure shows raw pictures of four (technical replicates) western blots detecting TRPC5 **(A-D)** and NaK-ATPase surface expression **(E-H)** in biotinylated samples of HEK293T cells expressing indicated mutant channels that are possibly involved in (-)-englerin A binding. **(A-D)** and **(E-H)** show the same blots after stripping and reprobing, respectively. The used antibodies and dilutions can looked up in Table 2.14.

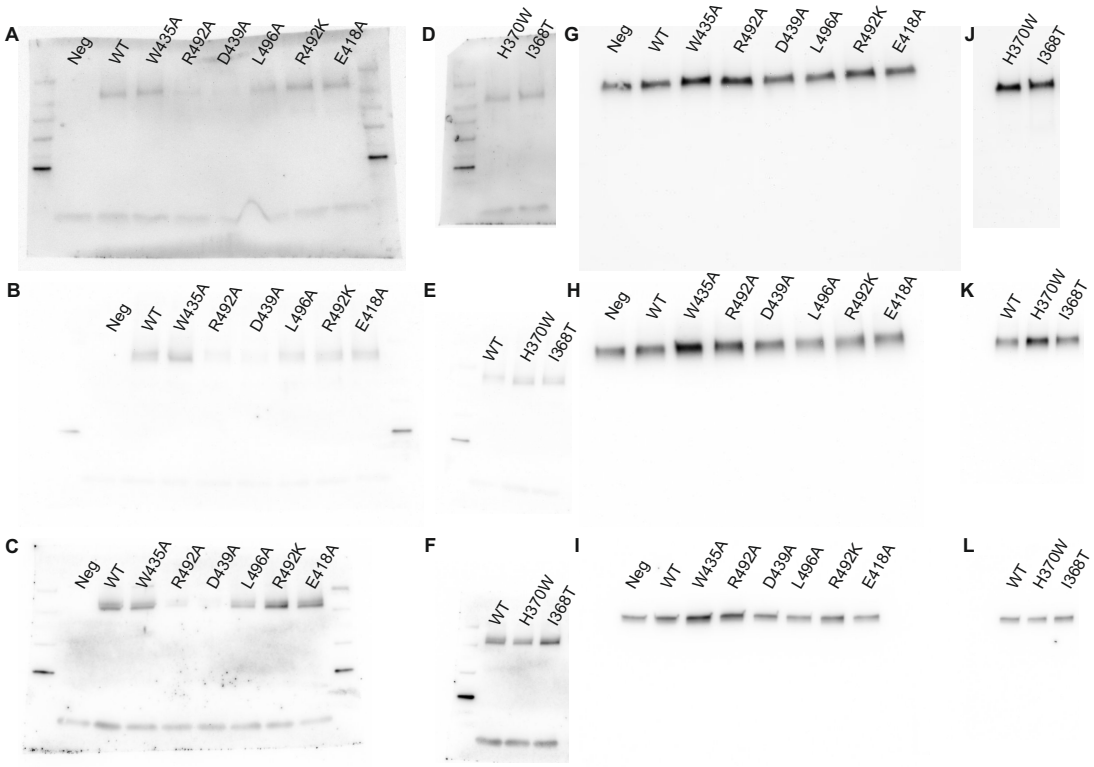

Figure C.2.: **Raw pictures of the surface expression of riluzole non-binding mutant TRPC5 channels.** This figure shows raw pictures of three (technical replicates) western blots detecting TRPC5 **(A-F)** and NaK-ATPase surface expression **(G-L)** in biotinylated samples of HEK293T cells expressing indicated mutant channels that possibly are invovled in riluzole binding. **(A-F)** and **(E-L)** show the same blots after stripping and reprobing, respectively. Because one gel could hold a maximum of ten samples, two blots were used to detect all mutants. The used antibodies and dilutions can looked up in Table 2.14.

D. (-)-Englerin A/Riluzole Ratios of All Mutants

Table D.1.: **Ratios between mean maximal (-)-englerin A and mean maximal riluzole evoked current densities of the measured mutants.** The ratios are visualized in Figure 4.1.

Mutation	Ratio
WT	5.00
I294A	1.83
W327A	5.69
C334A	4.22
F367A	2.37
I368A	111.80
I368T	60.57
I368V	15.62
H370A	32.95
H370W	23.63
H370L	4.10
H370N	2.07
T371Y	−4.52
T371A	4.13
Y374A	12.97
F414A	22.64
E418A	80.74
E418D	20.36
D424Q	4.25
H432A	3.51
W434H	12.58
W435A	143.61
N436A	26.90
N436L	23.79
D439A	36.91
D439L	7.28
D439N	10.82
D439E	122.87
M442A	6.61
N443A	13.37
Y446A	8.46
Y446L	7.34
Y446F	4.83
S489A	4.75
R492A	1.08
R492K	−175.00
S495A	3.68
L496A	15.07
F497Y	2.29
N500F	44.25
R512A	21.33
L514A	5.57

Mutation	Ratio
WT	5.00
L521A	2.23
Y524A	2.83
Y524E	2.33
Y524L	27.55
Y524F	3.48
C525A	5.71
L528A	5.75
R557A	3.31
F569Y	6.20
F569A	2.53
L572A	2.19
Q573N	1.94
Q573A	0.47
Q573E	2.20
F576A	0.72
W577H	10.67
W577A	2.78
V579A	1.73
E595A	7.69
E598A	3.74
E598Q	5.76
F599A	5.50
T603A	4.09
G606A	23.32
T607A	4.46
V610A	2.03
L613A	1.67
L617A	2.37
E638A	2.35
E638D	−3.76
A642S	15.78
L646A	6.53
Y650A	1.73
N662A	6.51

Author's Declaration

TREDER, AARON

Name, Vorname

Ich erkläre hiermit an Eides statt, dass ich die vorliegende Dissertation mit dem Titel:

Identification and Characterization of Two Distinct Activator Binding Sites in the TRPC5 Channel

selbständig verfasst, mich außer der angegebenen keiner weiteren Hilfsmittel bedient und alle Erkenntnisse, die aus dem Schrifttum ganz oder annähernd übernommen sind, als solche kenntlich gemacht und nach ihrer Herkunft unter Bezeichnung der Fundstelle einzeln nachgewiesen habe.

Ich erkläre des Weiteren, dass die hier vorgelegte Dissertation nicht in gleicher oder in ähnlicher Form bei einer anderen Stelle zur Erlangung eines akademischen Grades eingereicht wurde.

München, den 22.03.23

Ort, Datum

Aaron Treder

Unterschrift Doktorand

Acknowledgement

Zunächst möchte ich PD Dr. Ursula Storch für die Betreuung und das Ermöglichen dieser Arbeit danken. Ebenfalls danken möchte ich für die Beantwortung sämtlicher Fragen und die Hilfe bei Problemen während der Durchführung dieser Arbeit.
Außerdem gilt mein Dank Prof. Dr. Michael Mederos y Schnitzler für zahlreiche konstruktive Gespräche.
Des Weiteren möchte ich Prof. Dr. Gudermann für das Ermöglichen der Arbeit am Walther-Straub-Institut danken.
Ganz herzlich möchte ich mich auch bei meinen Kollegen bedanken, die mich nicht nur auf der Arbeit und im Laboralltag unterstützt haben, sondern auch privat immer ein offenes Ohr hatten. Mein besonderer Dank gilt Roman, Christian, Jasmin, Laura, Birte und Marius. Aber auch Neringa, Francesca, Rahel, Serap, Miyuki, Dennis und Julien möchte ich für die gemeinsame Zeit und Unterstützung danken.
Nicht zuletzt möchte ich mich auch bei meiner Familie und meiner Freundin bedanken, die mich immer unterstützt haben und auch in schwierigen Zeiten an meiner Seite stehen.

Vielen Dank euch Allen!

Publications and Congress Contributions

Publications

(1) Hermann, C.[1], **Treder, A.**[1], Näher, M., Geiseler, R., Gudermann, T., Mederos Y Schnitzler, M. and Storch, U. (2022): *The Normalized Slope Conductance as a Tool for Quantitative Analysis of Current-Voltage Relations.* In: Biophys J, **121**, (8): 1435-1448.
doi: 10.1016/j.bpj.2022.03.016

(2) Friedrich, L., Byrne, R., **Treder, A.**, Singh, I., Bauer, C., Gudermann, T., Mederos Y Schnitzler, M., Storch, U. and Schneider, G. (2020): *Shape Similarity by Fractal Dimensionality: An Application in the de novo Design of (-)-Englerin A Mimetics* In: ChemMedChem **15**, (7): 566-570.
doi: 10.1002/cmdc.202000017

(3) Krause, L., Biesgen, D., **Treder, A.**, Schweizer, S., Klumpp, E., Knief, C. and Siebers, N. (2019): *Initial Microaggregate Formation: Association of Microorganisms to Montmorillonite-Goethite Aggregates Under Wetting and Drying Cycles.* In: Geoderma, **351**: 250-260.
doi: 10.1016/j.geoderma.2019.05.001

(4) Keller, S., **Treder, A.**, von Reuss, S., H., Escalante-Semerena, J., C. and Schubert, T. (2016): *The SMUL_1544 Gene Product Governs Norcobamide Biosynthesis in the Tetrachloroethene-Respiring Bacterium Sulfurospirillum multivorans.* In: J Bacteriol, **198**, (16): 2236-43.
doi: 10.1128/JB.00289-16

Congress Contributions

(1) **Treder, A.**, Friedrich, L., Byrne, R., Singh, I., Bauer, C., Gudermann, T., Schneider, G., Mederos y Schnitzler, M. and Storch, U. (2020): *Electrophysiological Analysis of de novo Designed (-)-Englerin A Mimetics.* Poster Presentation. At: 5th German Pharm-Tox Summit, Leipzig, Germany

[1] Authors contributed equally